

LEVEL

(17)

REPORT NO. NADC-78259-60

AD A0 67287



**CERTIFICATION OF COMPOSITE AIRCRAFT STRUCTURES
UNDER IMPACT, FATIGUE AND ENVIRONMENTAL CONDITIONS**

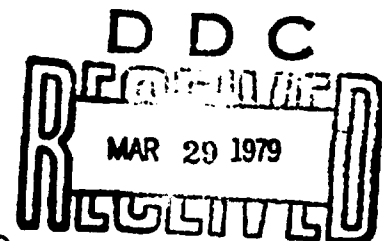
PART I

LOW SPEED IMPACT OF PLATES OF COMPOSITE MATERIALS

Pei Chi Chou, William J. Flis and Harry Miller
DREXEL UNIVERSITY
Philadelphia, Pennsylvania 19104

JANUARY 1978

FINAL CONTRACT REPORT
1 July 1976 - 31 December 1977
CONTRACT NO. N62269-76-C-0378



[Handwritten signature]

C

DDC FILE COPY

APPROVED FOR PUBLIC RELEASE; DISTRIBUTION UNLIMITED

Prepared for
NAVAL AIR DEVELOPMENT CENTER
Warminster, Pennsylvania 18974

79 03 28 008

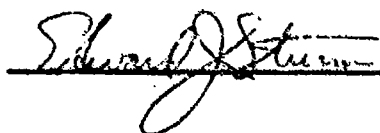
NOTICES

REPORT NUMBERING SYSTEM - The numbering of technical project reports issued by the Naval Air Development Center is arranged for specific identification purposes. Each number consists of the Center acronym, the calendar year in which the number was assigned, the sequence number of the report within the specific calendar year, and the official 2-digit correspondence code of the Command Office or the Functional Directorate responsible for the report. For example: Report No. NADC-78015-20 indicates the fifteenth Center report for the year 1978, and prepared by the Systems Directorate. The numerical codes are as follows:

CODE	OFFICE OR DIRECTORATE
00	Commander, Naval Air Development Center
01	Technical Director, Naval Air Development Center
02	Comptroller
10	Directorate Command Projects
20	Systems Directorate
30	Sensors & Avionics Technology Directorate
40	Communication & Navigation Technology Directorate
50	Software Computer Directorate
60	Aircraft & Crew Systems Technology Directorate
70	Planning Assessment Resources
80	Engineering Support Group

PRODUCT ENDORSEMENT - The discussion or instructions concerning commercial products herein do not constitute an endorsement by the Government nor do they convey or imply the license or right to use such products.

APPROVED BY:



DATE

17 November 1978

12

UNCLASSIFIED

19

REPORT NO.

NADC

78259-60-PT-1

18

6

CERTIFICATION OF COMPOSITE AIRCRAFT STRUCTURES
UNDER IMPACT, FATIGUE AND ENVIRONMENTAL CONDITIONS.

PART I.

LOW SPEED IMPACT OF PLATES OF COMPOSITE MATERIALS.

9 Final rept. 1 Jul 76 - 31 Dec 77,

10

Pei Chi/Chou,
William J./Flis
Harry/Miller

DREXEL UNIVERSITY

Philadelphia, Pennsylvania.

REC'D
MAR 1979

11

Jan 1978

12

233p.

Prepared for
NAVAL AIR DEVELOPMENT CENTER
Warminster, Pennsylvania 18974

15 N62269-76-C-0378

UNCLASSIFIED

405 723

79 03 28 008

at

UNCLASSIFIED

SECURITY CLASSIFICATION OF THIS PAGE (When Data Entered)

REPORT DOCUMENTATION PAGE		READ INSTRUCTIONS BEFORE COMPLETING FORM
1. REPORT NUMBER NADC-78259-60	2. GOVT ACCESSION NO.	3. RECIPIENT'S CATALOG NUMBER
4. TITLE (and Subtitle) Certification of Composite Aircraft Structures Under Impact, Fatigue and Environmental Conditions. Part I-Low Speed Impact of Plates of Composite Materials		5. TYPE OF REPORT & PERIOD COVERED • Final Contract Report July 1 1976 - Dec. 31 1977
		6. PERFORMING ORG. REPORT NUMBER
7. AUTHOR(s) Pei Chi Chou William J. Flis Harry Miller		8. CONTRACT OR GRANT NUMBER(s) N62269-76-C-0378
9. PERFORMING ORGANIZATION NAME AND ADDRESS Drexel University Philadelphia, PA 19104		10. PROGRAM ELEMENT, PROJECT, TASK AREA & WORK UNIT NUMBERS
11. CONTROLLING OFFICE NAME AND ADDRESS Aircraft and Crew Systems Technology Directorate Naval Air Development Center Warminster, PA 18974		12. REPORT DATE January 1978
14. MONITORING AGENCY NAME & ADDRESS (if different from Controlling Office)		13. NUMBER OF PAGES 219
		15. SECURITY CLASS. (of this report) UNCLASSIFIED
		15a. DECLASSIFICATION/DOWNGRADING SCHEDULE
16. DISTRIBUTION STATEMENT (of this Report) Approved for Public Release; distribution unlimited		
17. DISTRIBUTION STATEMENT (of the abstract entered in Block 20, if different from Report)		
18. SUPPLEMENTARY NOTES		
19. KEY WORDS (Continue on reverse side if necessary and identify by block number) Composites Structural Response Plates Impact Experiments		
20. ABSTRACT (Continue on reverse side if necessary and identify by block number) This report presents a series of design curves which give the peak strain in several types of simple structures (beams and plates) due to low velocity impact. These curves have been developed based on both analytical solutions of impact and numerous impact experiments. It is shown that all impact problems may be divided into two regimes based on the ratio of the mass of the structure to the mass of the impactor. For large impactors multiple impacts occur and the structural response depends chiefly on the kinetic energy of the impactor. For small impactors only a single impact occurs. Its force and duration determined chiefly by contact effects and the		

DD FORM 1 JAN 73 1473

UNCLASSIFIED

SECURITY CLASSIFICATION OF THIS PAGE (When Data Entered)

20. impactor momentum governs the response. Thus different forms of design curves are required for each regime.

ACCESSION for

White Section	<input checked="" type="checkbox"/>
Buff Section	<input type="checkbox"/>

NOTES
PMS
UNANNOUNCED
JUSTIFICATION

BY
DISTRIBUTION/AVAILABILITY CODES

Dist	Gen	Spec
A		

TABLE OF CONTENTS

	Page
List of Figures	
List of Tables	
I. INTRODUCTION	1
II. DESIGN CURVE FOR IMPACTS BY LARGE IMPACTORS	7
A. Generalized One-Degree-of-Freedom Model	7
1. Simply Supported Beam	10
2. Simply Supported Plate	11
3. Clamped Plate	12
4. Comprehensive Impact Strain Curve	13
5. Critical Impact Velocity Curve	15
B. Timoshenko Solution of Transverse Plate Impact	17
1. Description of Solution Method	18
2. Dimensionless Form of Timoshenko Solutions	20
a. Plate Impact	20
b. Beam Impact	22
3. Parametric Study for Large Impactors	24
C. Impact Experiments	27
1. Specimens	28
2. Strain-Measurement Impact Experiments	32
3. Impact-to-Failure Experiments	39
D. Design Curves for Shear Failure Due to Impact	40
1. Simply Supported Beam	46
a. Relative Importance of Shear and Bending	47
b. Critical Impact Velocity Curve	49
2. Simply Supported Plate	50
III. IMPACTS BY SMALL IMPACTORS	56
A. Simply Supported Beam	56
1. Approximate Analysis	56
2. Timoshenko Solution	60
B. Simply Supported Plate	63
1. Approximate Analysis	63
2. Comparison with Experimental Results	69
IV. DESIGN PROCEDURE	70
A. Use of Design Curves in This Report	70
B. Construction of New Design Curves by Experiments	80
C. Construction of New Design Curves by Analytical Tools	82

NADC-78259-60

V. SUMMARY	84
VI. REFERENCES	85
VII. APPENDICES	
APPENDIX A STATIC SOLUTION OF A SIMPLY SUPPORTED ORTHOTROPIC PLATE	87
APPENDIX B STATIC DEFLECTION OF A CLAMPED RECTANGULAR ORTHOTROPIC PLATE DUE TO A CENTRAL POINT LOAD	91
APPENDIX C COMPUTER PROGRAM FOR CALCULATING TIMOSHENKO SOLUTION OF PLATE IMPACT	100
APPENDIX D SIMPLY SUPPORTED BEAM CENTRALLY LOADED BY HALF-SINE PULSE	105
APPENDIX E DETAILED RESULTS OF IMPACT EXPERIMENTS	110
APPENDIX F THE EFFECT OF THE APPROXIMATION $H = \sqrt{D_{11}D_{22}}$ ON THE PREDICTED IMPACT RESPONSE OF AN ORTHOTROPIC PLATE	215

NADC-78259-60

List of Figures

Figure	Page
1. Comparison of large and small impactor cases	3
2. One-degree-of freedom model, momentum conserved	8
3. One-degree-of-freedom model, energy conserved	8
4. Functions of aspect-orthotropy parameter η for constructing impact design curves	14
5. Comprehensive impact strain curve for simply supported and clamped rectangular plates	16
6. Generalized strain curves	26
7. Exploded view of plate clamping device	33
8. Typical $\bar{\epsilon}_x$ vs. M curve for clamped orthotropic plate	35
9. Typical $\bar{\epsilon}_x$ vs. M curve for simply supported orthotropic plate	36
10. Strain curve for clamped plates impacted by large masses	37
11. Strain curve for simply supported plates impacted by large masses	38
12. Typical critical velocity curve for clamped plates	41
13. Critical velocity curve for clamped and simply supported plates	42
14. Typical reflectoscope trace of plate specimen	43
15. Typical reflectoscope trace of plate specimen	44
16. Typical reflectoscope trace of plate specimen	45
17. Shear stress curve for simply supported beam	48
18. Critical impact velocity for shear and bending failure	51
19. Edge shear stress curve for simply supported rectangular orthotropic plates	54
20. Function of aspect-orthotropy ratio η for shear stress curve of simply supported plate	55
21. Generalized strain ϵ^* vs. mass ratio M for impacts of simply supported beams by small impactors	62
22. Plot of $g(\delta, \eta)$ showing weak dependence on δ	67
23. Strain curve for impact of simply supported rectangular plate by a small mass	68
24. Selected design curve for impacts of simply supported beams by large impactors	71
25. Selected design curve for impacts of simply supported beams by small impactors	72

I-III

.NADC-78259-60

- | | | |
|-----|--|----|
| 26. | Selected design curve for impacts of simply supported plates impacted by large impactors | 76 |
| 27. | Selected design curve for clamped plate impacted by large impactors | 77 |
| 28. | Selected design curve for impact of simply supported rectangular plate by a small impactor | 78 |

NADC-78259-60

List of Tables

Table		Page
I.	Parametric Study: Plate Impact Cases Calculated by the Timoshenko Solution	25
II.	Graphite/Epoxy Plate Specimens	29
III.	Shear and Flexural Stiffnesses of Graphite/Epoxy Plate Specimens	30
IV.	Design Curve Parameters for Graphite/Epoxy Plate Specimens	31
V.	Computer-Calculated Values of $f(\beta)$	59
VI.	Calculations Using Timoshenko Solution for Large Mass Ratio M	61

Foreword

This is part I of the final technical report for Contract No. N62269-76-C-0378, which is sponsored by the Naval Air Development Center, Warminster, Pa. The work was performed during the period of July 1, 1976 through December 30, 1977. Mr. Lee W. Gause was the contract monitor.

The contracted study is under the title "Certification of Composite Aircraft Structures under Impact, Fatigue and Environmental Conditions"; parts I and II of the study are under the supervision of Dr. P.C. Chou, while part III is under Dr. A.S.D. Wang, both of Drexel University.

This report concerns part I of the contract, low speed impact of plates of composite materials. It is a self-contained report, including definitions of all nomenclature used, and its own introduction and conclusions.

The authors would like to thank Dr. Edward J. McQuillen, Dr. James L. Huang and Mr. Lee W. Gause for the frequent technical discussions. They would also like to thank Mr. Frank Patota and Mr. George Chou who helped conducting part of the experiments.

I. INTRODUCTION

Aerospace structures frequently undergo impacts by blunt objects, including dropped tools, hail, and runway stones impinging on exposed aircraft components, and foreign objects entering jet engines. The failure of a component subject to such an impact is often of the structural type, rather than due to local penetration or indentation. A number of numerical techniques (e.g., finite-element method, lumped-parameter models) are available for calculating structural response to impact, but these are typically complicated, time-consuming, and usable only on a problem-by-problem basis. Designers need a quick, convenient, widely applicable method for this purpose.

In a previous report [1], a method was developed for constructing a design curve which predicts the response of a given type of structure to impact loading. This curve gives the maximum strain in the structure, which may have various dimensions and material properties, due to impacts involving a certain range of impact masses and velocities. An example of the bending response of a simply supported beam under central impact was presented in detail. Both experimental results and numerical calculations involving several solutions of beam impact were used in establishing the design curve. The impact cases studied in [1] were limited to large impactor mass, where the impactor has mass roughly equal to or greater than that of the beam.

In the present report, the design-curve approach is extended to anisotropic plates, and impacts by small impactors. Shear failures are also studied. The elementary model of impact on beams presented in [1] is generalized to embrace all structures. This model is then applied to the cases of clamped and

simply supported anisotropic rectangular plates and to predicting impact failure due to shear effects in both beams and plates. Design curves are also developed for predicting the response of beams and plates to impact by small impactors. In each instance, both analytical methods and impact experiments are employed in generating the design curves.

In dealing with low-velocity impact problems, it is convenient to divide them into two domains, based on the ratio M of the mass of the structure to the mass of the impactor (see Fig. 1). The motion of the impactor and the response of the structure for a large impactor differ greatly from those for a small impactor. The two domains will be treated separately; the assumptions and final design curves are also different for the two domains.

In impacts where the mass ratio M is small (large impactor), it has been observed that multiple collisions occur and that the general motion of the impactor follows the path of the structure at the impact point (Fig. 1a). The final rebound of the impactor takes place after the structure has reached its maximum deflection. Further, the entire event is generally more prolonged than the fundamental period of structural vibration.

On the other hand, when M is large (small impactor), only a single, sudden collision occurs, after which the impactor rebounds and the structure continues to vibrate freely, reaching its maximum deflection at a later time (Fig. 1b). The duration of actual contact is characteristically much shorter than the fundamental period of vibration. The sudden rebound of the impactor is due chiefly to the elastic resistance of the structure and the impactor to local indentation, i.e., contact effects between the two bodies.

IMPACT REGIMES

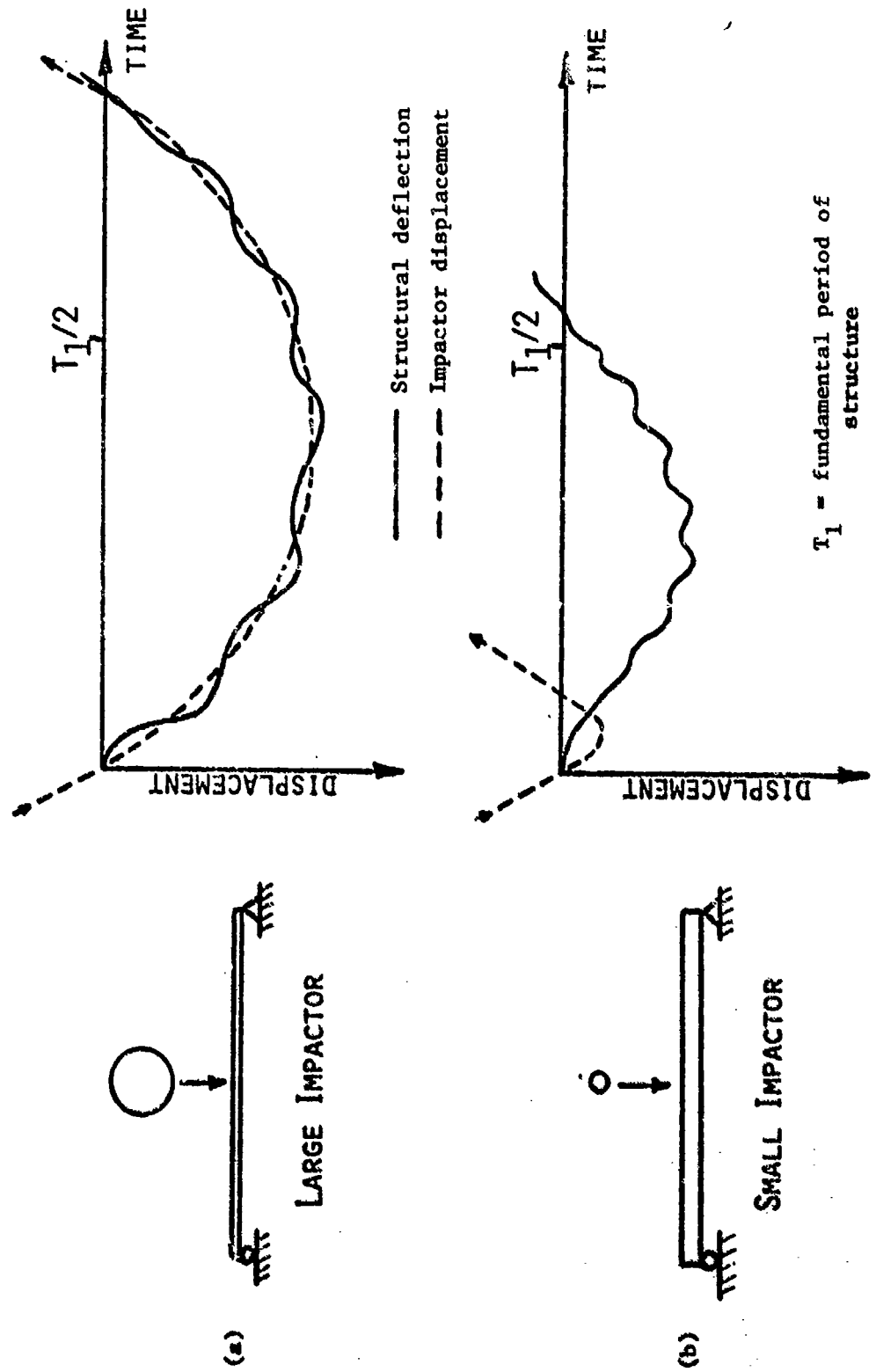


Figure 1. Comparison of large- and small-impactor cases.

In [1], six analytical models of impact were examined, including two classical one-degree-of-freedom models; a two-degrees-of-freedom model which accounts for contact effects; a solution by Clebsch [2], which assumes plastic impact and treats the beam with attached impactor as a free-vibration problem; a modified Clebsch solution due to McQuillen et al. [3]; and Timoshenko's solution [4], which couples the impactor displacement with the beam deflection using Hertz's law for contact deformations. The dimensionless parameters which determine the peak impact response according to each solution method were derived.

It was shown in [1] that, for those models which neglect contact effects, the maximum strain due to impact, when properly normalized to $\bar{\epsilon}$, is a function of the mass ratio M only and is independent of any other parameters. These solution methods, however, are generally not suited for treating problems involving small impactors. Conversely, the two models that include contact effects indicate a dependence of $\bar{\epsilon}$ on M and another parameter, and are useful over the entire range of M . For large impactors, it was demonstrated that the dependence on the other parameter is weak, so that a single $\bar{\epsilon}$ vs. M curve approximately represents all impact situations. In addition, when data from assorted impact experiments were plotted in coordinates of $\bar{\epsilon}$ and M , a single curve could be drawn through all data points, with about $\pm 30\%$ variation, for large impactors.

In this report, several approaches are taken in extending the design-curve concept to impacts of other structures by large impactors (Section II). First, the one-degree-of-freedom model described in [1] is generalized to encompass all structures and is then applied to anisotropic laminated rectangular plates with clamped and simply supported boundary conditions. Then, in order to identify additional significant parameters, the structural impact equations of Timoshenko are cast in a dimensionless form; the influence of each of these parameters is appraised by a series of calculations using Timoshenko's solution in which the values of the parameters are systematically varied. Next, we discuss two series of impact experiments performed on laminated graphite/epoxy plates; in one series, the bending strains in the plates were measured, and in the other, the plates were repeatedly impacted at gradually increasing velocities until failure occurred. The purpose of these experiments is twofold: to verify the analytically constructed design curves, and to demonstrate how design curves may also be constructed experimentally. Finally, design curves for predicting shear failure due to impact are developed, and the relative importance of shear and bending effects in impact failure is discussed.

For cases in which the mass of the impactor is small with respect to the mass of the structure (large M), the dependence of the generalized strain $\bar{\epsilon}$ on the mass ratio M is not exclusive; another dimensionless parameter which involves the geometric and material properties governing the contact effects between the two bodies can also be shown to be significant. This contact parameter, denoted λ , and the mass ratio M together determine the duration of contact between the structure and impactor (relative to the fundamental period of vibration), which is typically quite short. Clearly, the duration of contact is important in determining the response of the structure.

The most sophisticated solution method applicable to problems involving small impactors, the Timoshenko solution, involves a nonlinear integral equation which can only be solved numerically on a problem-by-problem basis, and is thus not convenient for developing a design curve. However, by making the simplifying assumption that the structure does not appreciably deflect during the short period of actual contact, the problem uncouples into two parts - the elastic Hertzian impact of a sphere on a semi-infinite body, and the vibration response of the structure to a dynamic load (i.e., the contact force). This leads to an approximate relationship (for each type of structure) between the parameters \bar{e} , M , and λ , which may be further simplified to a simple equation in the mass ratio M and a new generalized strain for small impactors ϵ^* (Section III). By comparison with experimental data and with calculations involving the complete Timoshenko solution, the form of this relationship is shown to be useful as a design guide.

In Section IV, procedures for using the design curves presented in this report are described, and a few examples are given. Also included are methods for constructing new design curves for structures not treated in this report, based on either analytical tools or impact experiments.

II. DESIGN CURVE FOR IMPACTS BY LARGE IMPACTORS

For impact cases where the mass of the structure is small compared to the mass of the impactor, the structure may be assumed to behave as a simple spring, or as a one-degree-of-freedom mass-spring system. Details of this approach as applied to simply supported beams were presented in Ref.[1]; in this section, this impact model is briefly reviewed, because it will be useful in the development of parameters in plate impact problems. These parameters are employed in constructing a design curve for predicting the response of plates to impacts by large masses. Finally, by examining data from a large number of experiments and by studying impact solutions using more sophisticated analytical techniques, the validity of the design curve is established and the range of its usefulness is demonstrated.

A. Generalized One-Degree-of-Freedom Model

In this model, the impactor and the structure are considered attached together after contact and move together as a single mass m , and the motion of the structure is governed by an equivalent spring. The initial velocity of the combined mass, v_0 , may be determined by two methods: One is based on the conservation of momentum (Fig. 2), the other on the conservation of energy (Fig. 3). In the first case.

$$m = m_2 + em_1 \quad (1)$$

where m_2 is the impactor mass, and em_1 is an "equivalent" mass of the structure. The equivalent mass may be obtained by matching the total kinetic energy of the structure with the kinetic energy of the unknown equivalent mass traveling at the velocity of the impact point in the structure, assuming that the deflection mode shape is the static deflection curve. For simply supported beams,

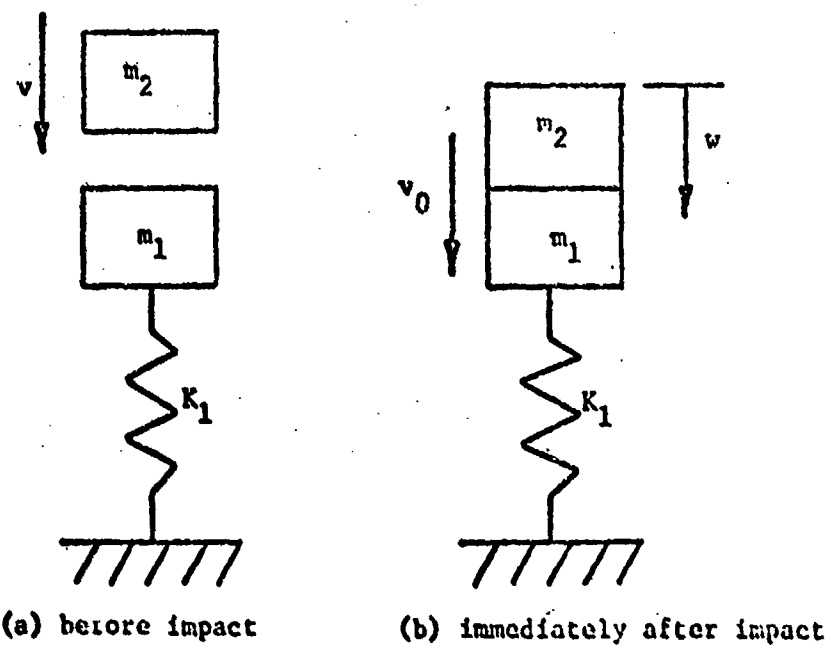


Figure 2. One-degree-of-freedom model of impact, momentum conserved.

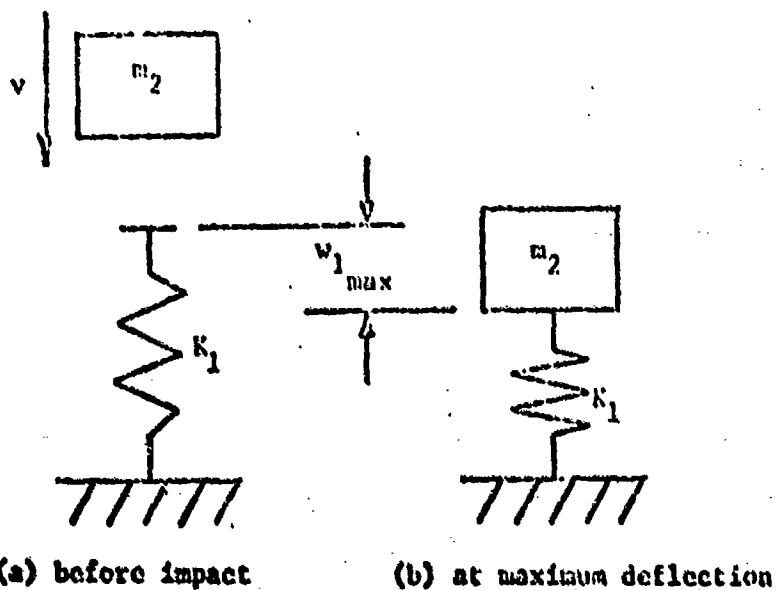


Figure 3. One-degree-of-freedom model of impact, energy conserved.

$e = 17/35$. By equating the momentum of the impactor before impact, $m_2 v$, with the momentum of the combined mass m , we have

$$v_0 = v/(1 + eM). \quad (2)$$

where

$$M = m_1/m_2. \quad (3)$$

Note that according to Eq. (2), the energy before and after impact is not conserved, i.e., $mv_0^2 < m_2 v^2$.

In the energy conserved case, we assume $e = 0$, so that

$$\begin{aligned} m &= m_2 \\ v_0 &= v \end{aligned} \quad (4)$$

As a result, the kinetic energy in the impactor is conserved, and will be entirely converted to strain energy in the structure. For small values of M , the difference between these two approaches is small.

The spring constant K_1 is the force per unit deflection, with respect to a force acting at the impact point in the direction of the impactor velocity, or

$$P = K_1 w_1$$

After acquiring the initial velocity v_0 , the mass-spring system is assumed to perform a free vibration. The maximum deflection is then

$$w_{1,max} = v_0 \sqrt{\frac{m}{K_1}} \quad (5)$$

In modeling the structure by a mass-spring system, it is implied that only the first mode of vibration is retained and that its mode shape is the same as the static deflection distribution under a concentrated force.

Next, we shall consider the most critical strain ϵ_2 in the structure which occurs at a known point 2. Assume that a proportional relation between ϵ_2 and w_1 can be found,

$$\epsilon_2 = \left(\frac{1}{d_{12}} \right) w_1 \quad (6)$$

where d_{12} can be determined from the static deflection distribution, or from experimental static measurements. Combining Eqs. (5) and (6), we obtain the maximum strain as

$$\epsilon_{2_{\max}} = \frac{v_0}{d_{12}} \sqrt{\frac{m}{K_1}} \quad (7)$$

or, combining Eqs. (1), (2), and (7),

$$\epsilon_{2_{\max}} = \frac{v}{d_{12}} \sqrt{\frac{m_2}{(1+eM)K_1}} \quad (8)$$

1. Simply Supported Beam

The next step of defining a generalized strain $\bar{\epsilon}$ is best illustrated by considering a specific type of structure. For a simply supported beam of length L and depth h , impacted at middle span, we have

$$d_{12} = L^2/6h \quad (9)$$

and

$$K_1 = 48EI/L^3. \quad (10)$$

Therefore,

$$\epsilon_{\max} = \frac{v}{c_b} \frac{h}{k} \sqrt{\frac{3}{4} \frac{1}{M(1+eM)}} \quad (11)$$

where $c_b = \sqrt{E/\rho}$, the velocity of longitudinal waves in a bar.

Defining the generalized strain as

$$\bar{\epsilon} = \epsilon_{\max} \frac{c_b}{v} \frac{k}{h} \quad (12)$$

we obtain finally,

$$\bar{\epsilon} = \sqrt{\frac{3}{4} \frac{1}{M(1+eM)}} \quad (13)$$

which is the equation of the design curve for simply supported beams impacted by large masses, as given in [1].

The corresponding expressions for d_{12} , K_1 and \bar{c} for simply supported and clamped orthotropic plates will be given in the following sections.

2. Simply Supported Plate

The impact design curve for simply supported, rectangular, orthotropic plates may be generated by applying the generalized one-degree-of-freedom model. For transverse impacts at the center of the plate, we first consider the corresponding static problem involving a centrally applied concentrated load. In this case, the maximum deflection occurs at the center of the plate, and the maximum strain on the surface opposite the applied load. It is shown in Appendix A that subject to a mild approximation, the spring constant of a plate so loaded may be expressed as

$$K_1 = \frac{P}{w_{\max}} = \frac{\pi^4 D_{11}}{4ab \left(\frac{a}{b}\right)^2 f_1(n)} \quad (14)$$

where

$$f_1(n) = \sum_{m=1,3,5}^{\infty} \sum_{n=1,3,5}^{\infty} \frac{1}{C_{mn}} \quad (15)$$

$$n = \left(\frac{a}{b}\right)^2 \sqrt{\frac{D_{22}}{D_{11}}} \quad (16)$$

$$C_{mn} = m^4 + 2m^2 n^2 + n^4 \eta^2 \quad (17)$$

The strain-deflection constant d_{12} relating the strain due to bending in the x-direction to the maximum deflection w_1 is

$$\frac{e_x}{w_1} = \frac{1}{d_{12}} = \frac{w^2 h f_2(n)}{2ab \left(\frac{a}{b}\right) f_1(n)} \quad (18)$$

where

$$f_2(n) = \sum_{m=1,3,5}^{\infty} \sum_{n=1,3,5}^{\infty} \frac{m^2}{C_{mn}} \quad (19)$$

By combining Eqs. (14) and (18) with Eq. (8), and assuming that $e = 0$ (conservation of energy), we obtain

$$\epsilon_{x_{\max}} = f_2(n) h v \left[\frac{\rho h}{D_{11} M f_1(n)} \right]^{1/2} = \frac{h v}{c_p k} \frac{f_2(n)}{[M f_1(n)]^{1/2}} \quad (20)$$

If we define the generalized strain $\bar{\epsilon}_x$ as

$$\bar{\epsilon}_x = \epsilon_{x_{\max}} \left(\frac{c_p}{v} \right) \left(\frac{k}{h} \right) \quad (21)$$

where $c_p = \sqrt{D_{11}/I}$ is the speed of flexural waves in the plate in the x-direction, and k is the radius of gyration of the plate, then,

$$\bar{\epsilon}_x = \frac{s_1(n)}{\sqrt{M}} \quad (22)$$

where

$$s_1(n) = f_2(n) / \sqrt{f_1(n)} \quad (23)$$

This function is plotted in Fig. 4. Similarly, we have

$$\bar{\epsilon}_y = \frac{s_1(n^{-1})}{\sqrt{M}} \quad (24)$$

Equations (22) and (24) may be plotted as impact design curves, as shown in Fig. 6.

Note that in this case, the generalized strains $\bar{\epsilon}_x$ and $\bar{\epsilon}_y$ are functions not only of the structure-to-impactor mass ratio M but also of the aspect-orthotropy ratio n .

3. Clamped Plate

We may develop the design curve for clamped-edge, rectangular, orthotropic plates in a similar manner. The spring constant of such a plate with respect to a central point load may be expressed approximately (see

Appendix B) as

$$K_1 = \frac{b D_{11}}{a^3 f_3(\eta)} \quad (25)$$

The strain-deflection constant d_{12} relating the strain in the x-direction with the maximum deflection is

$$d_{12} = \frac{a^2 f_3(\eta)}{h f_4(\eta)} \quad (26)$$

where $f_3(\eta)$ and $f_4(\eta)$ are given in Appendix B.

By combining Eqs. (25) and (26) with Eq. (8), and assuming that $e = 0$

(conservation of energy), and defining the generalized strain according to Eq. (21) we obtain

$$\bar{\epsilon}_x = \frac{g_2(\eta)}{\sqrt{M}} \quad (27)$$

where

$$g_2(\eta) = f_\eta(\eta) / \sqrt{f_3(\eta)} \quad (28)$$

This function is also plotted in Fig. 4. Similarly, we have

$$\bar{\epsilon}_y = \frac{g_2(\eta^{-1})}{\sqrt{M}} \quad (29)$$

Equations (27) and (29) represent the impact design curves for a clamped rectangular plate. Again, the generalized strains $\bar{\epsilon}_x$ and $\bar{\epsilon}_y$ are functions of both the mass ratio M and the aspect-orthotropy ratio η .

4. Comprehensive Impact Strain Curve

Examination of the design-curve equations developed above, Eqs. (22), (24), (27), and (29), shows that a different $\bar{\epsilon}_x$ vs. M curve must be prepared not only for each boundary condition but also for each value of the aspect-orthotropy parameter η . These curves can be combined into a single, comprehensive design curve if we introduce a new dimensionless generalized

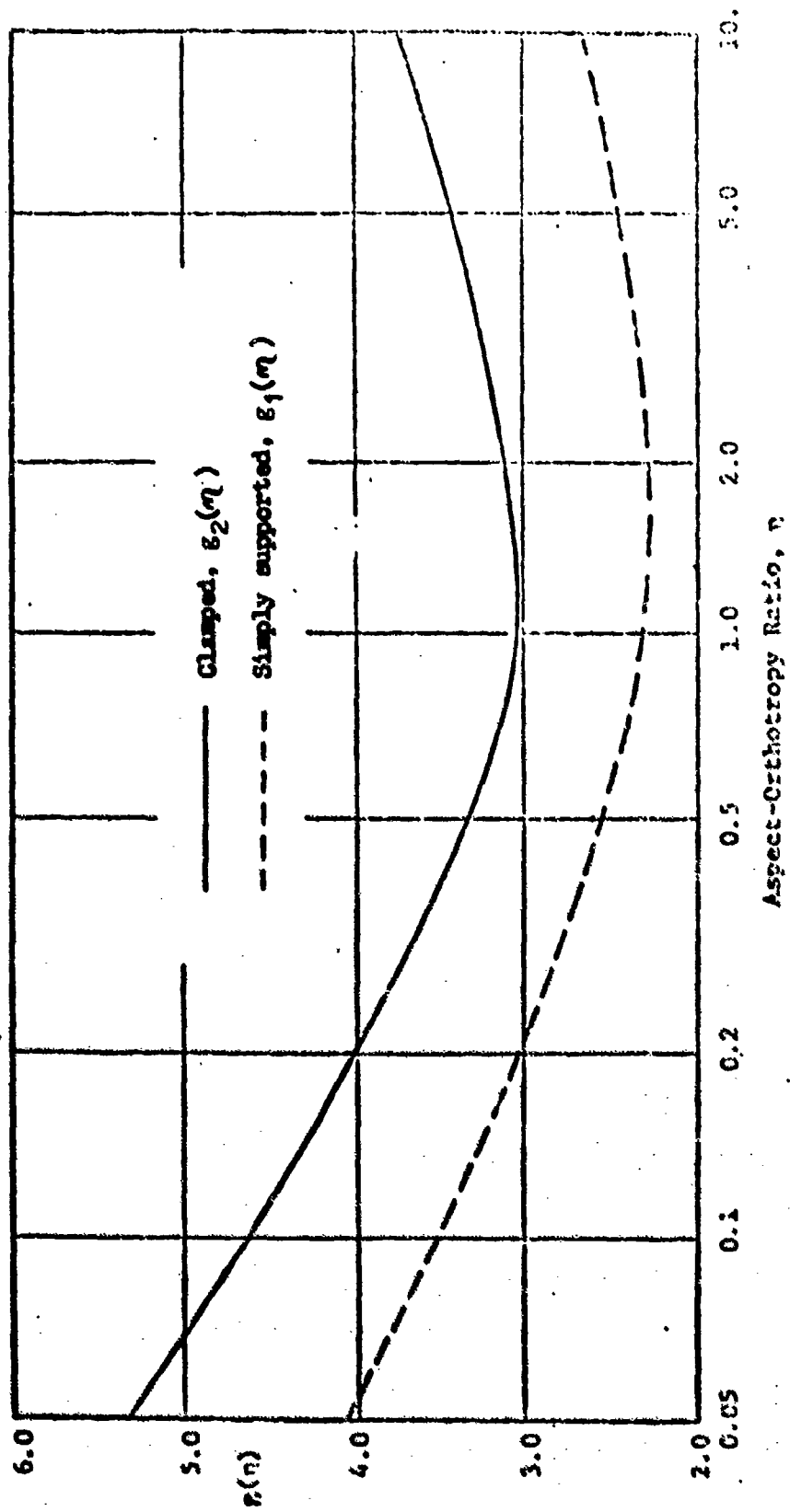


Figure 4. Functions of aspect-orthotropy parameter η for constructing impact design curves for clamped and simply supported rectangular orthotropic plates.

strain, $\bar{\epsilon}$, defined as

$$\bar{\epsilon} \equiv \frac{\bar{\epsilon}_x}{g_1(\eta)}, \quad i = 1, 2 \quad (30)$$

where $g_1(\eta)$ applies to simply supported plates and is given by Eq. (23) and $g_2(\eta)$ applies to clamped plates and is given by Eq. (28). Thus, the equation for the design curve in $\bar{\epsilon}$ vs. M coordinates becomes

$$\bar{\epsilon} = M^{-1/2} \quad (31)$$

All impact data, regardless of the boundary condition (simply supported or clamped) or the value of the parameter η may be presented on a single curve. This curve is shown in Fig. 5, in which are included data from numerous impact experiments which are discussed in detail in a later section.

5. Critical Impact Velocity Curve

The design curves in terms of $\bar{\epsilon}_x$ or $\bar{\epsilon}$ vs M give the maximum strain in the plate for a given impact situation. This strain may be compared to the ultimate failure strain of the plate (assuming a maximum-strain failure criterion) to determine whether the plate fails as a result of a given impact. However, by introducing a new parameter, the dimensionless impact velocity, we can construct an alternate form of the design curve which can be directly used to determine whether a given impact causes failure of the plate. Again, the curve may be developed either by analysis or by experiment. To do this, a dimensionless impact velocity, \bar{v} , is defined as

$$\bar{v} = \frac{vh}{c_p k} \quad (32)$$

where v is the impact velocity, h is the plate thickness, c_p is the speed of flexural waves in the plate, and k is the radius of gyration of the plate.

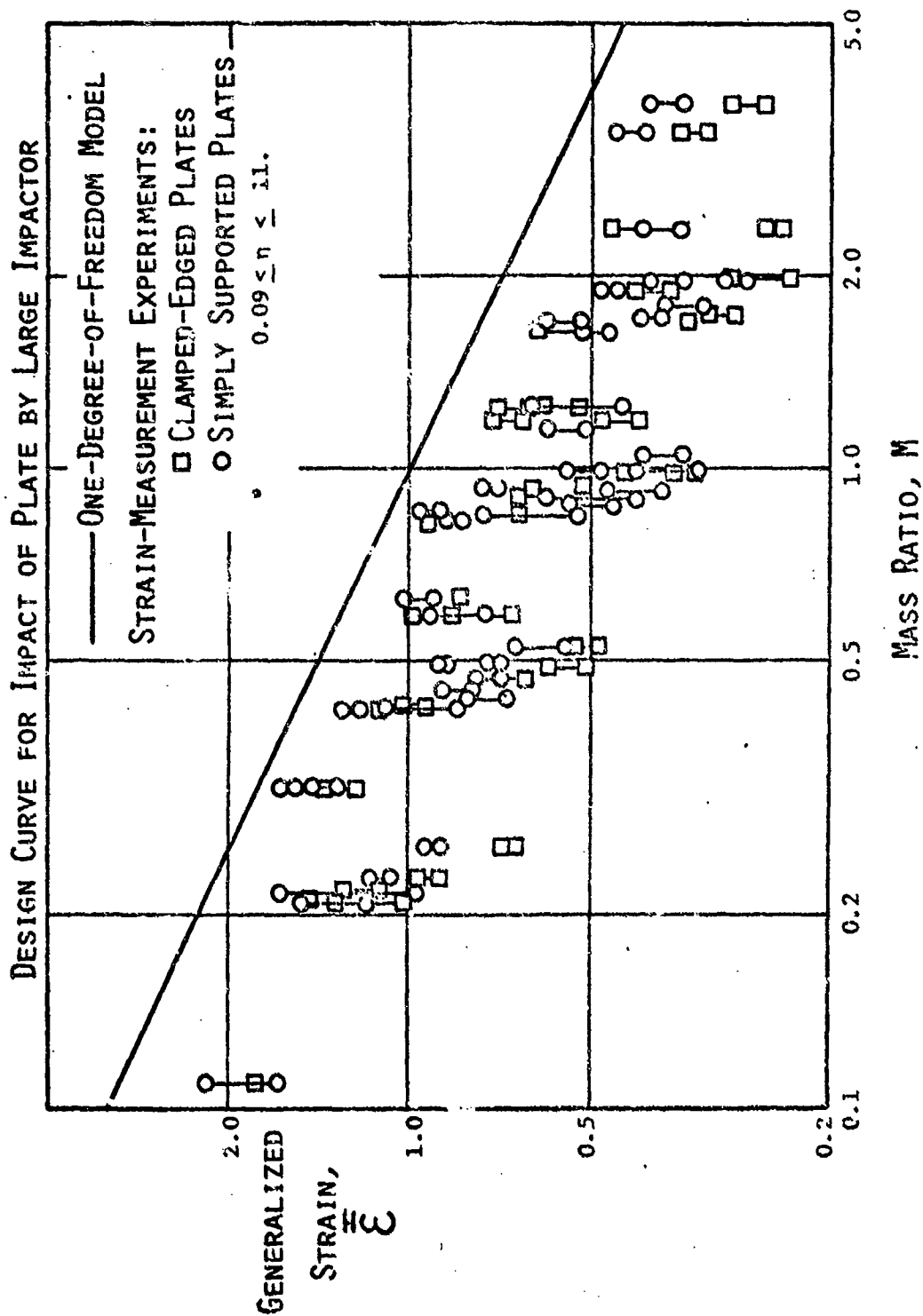


Figure 5. Comprehensive impact strain curve for simply supported and clamped rectangular plates.

Then, by Eq's (21), (22) and (32) the critical dimensionless velocity \bar{v}_c (i.e., the lowest value of \bar{v} at which failure occurs) is related to the failure strain ϵ_f by

$$\bar{v}_c = \epsilon_f \frac{\sqrt{M}}{g_1(\eta)} \quad (33)$$

In \bar{v} vs. M coordinates, the curve $\bar{v} = \bar{v}_c(M)$ divides the plane into a safe region (below the curve) in which failures due to impact do not occur (according to the assumed maximum-strain failure criterion) and an unsafe region (above the curve) in which failures do occur. That is, if the point (\bar{v}, M) corresponding to a given impact situation falls above the curve, then failure occurs; if the point falls below, no failure occurs. Thus, Eq. (33) is useful as a design curve equation. A typical \bar{v}_c vs. M curve is shown in Fig. 12.

Further, if we define a new dimensionless impact velocity $\bar{\bar{v}}$ such that

$$\bar{\bar{v}} = g_1(\eta) \bar{v}$$

then the equation of the alternate design curve, in terms of $\bar{\bar{v}}$ vs. M , is

$$\bar{\bar{v}}_c = \epsilon_f \sqrt{M} \quad (34)$$

This single curve, $\bar{\bar{v}} = \bar{\bar{v}}_c(M)$, may be used to predict impact-induced failure for all plate structures, regardless of the boundary conditions or the value of the aspect-orthotropy ratio η (provided these structures have the same value of failure strain ϵ_f). Note that the value of ϵ_f can be taken as the nominal value (say, the static ultimate strain) of the given material or can be determined by performing a single impact-to-failure test. A typical $\bar{\bar{v}}_c$ vs. M curve is shown in Fig. 13.

B. Timoshenko Solution of Transverse Plate Impact

Timoshenko's approach for solving transverse impact problems on simple beams by coupling Hertz's law of contact with the Euler beam equation has been

extended to the case of a simply supported rectangular plate by Eringen [5] and more recently to the case of a simply supported anisotropic laminated plate by Sun and Chattopadhyay [6]. In this section we review the salient points of the latter solution and show how it may be used to develop an impact design curve for anisotropic plates. In addition, a normalized form of the equations corresponding to a special case of this solution is derived, so that the dimensionless parameters governing the peak strain response may be identified. Finally, a series of numerical computations is performed, in which each of the derived parameters is systematically varied in order to demonstrate the significance of each parameter in describing the response to a given impact.

1. Description of Solution Method

The anisotropic plate equations of Whitney and Pagano [7] are used to predict the plate motion. Neglecting effects of rotatory inertia, the deflection of a symmetric cross-ply laminated plate due to a centrally applied force $F(t)$ is

$$w(x,y,t) = \frac{4}{m_1} \sum_m \sum_n \left\{ \frac{(-1)^{\frac{m+n-2}{2}}}{\omega_{mn}} \int_0^t F(\tau) \sin \omega_{mn} (t-\tau) d\tau \right. \\ \left. \cdot \sin \frac{m\pi x}{a} \sin \frac{n\pi y}{b} \right\} \quad m,n = 1,3,5,\dots,\infty \quad (35)$$

where m_1 , a , and b are the mass and planar dimensions of the plate, and ω_{mn} are natural frequencies dependant on m and n and the properties of the plate.

Hertz's law of contact is assumed to hold

$$F = k_2 a^{3/2} \quad (36)$$

where k_2 is a constant and α is the indentation of the impactor relative to the plate surface, or

$$\alpha = w_2 - w \left(\frac{a}{2}, \frac{b}{2}, t \right) \quad (37)$$

for central impact, where w_2 is the impactor displacement.

Newton's law applied to the impactor m_2 is

$$w_2 = vt - \frac{1}{m_2} \int_0^t \int_0^t F \, dt \, dt \quad (38)$$

These four equations (35-38) may be combined into a single nonlinear integral equation in terms of the contact force F between the plate and the impactor,

$$\begin{aligned} \left[\frac{F}{k_2} \right]^{2/3} &= vt - \frac{1}{m_2} \int_0^t \int_0^t F \, dt \, dt \\ &- \frac{4}{m_1} \sum_{m=1,3,5}^{\infty} \sum_{n=1,3,5}^{\infty} \frac{1}{\omega_{mn}} \int_0^t F(\tau) \sin \omega_{mn}(t-\tau) d\tau \end{aligned} \quad (39)$$

which is solved numerically by applying the small-increment method suggested by Timoshenko, in which the contact force F is assumed to be constant or linearly varying during any time increment $\Delta\tau$. Expanding the above integrals to calculate the force F_i during the i^{th} time interval, we obtain

$$\left[\frac{F_i}{k_2} \right]^{2/3} = v_i \Delta\tau - \frac{\Delta\tau^2}{m_2} \sum_{j=1}^i D_{i-j+1} F_j - \frac{4}{m_1} \sum_{j=1}^i E_{i-j+1} F_j \quad (40)$$

where

$$\begin{aligned} E_{i-j+1} &= \sum_m \sum_n \frac{1}{\omega_{mn}^2} \{ \cos[\omega_{mn}(i-j)\Delta\tau] \\ &- \cos[\omega_{mn}(i-j+1)\Delta\tau] \}, \quad m, n = 1, 3, 5, \dots, \infty \end{aligned}$$

If the contact force is approximated as a piecewise linear continuous function of time, with an average value of F_i during the i^{th} time step, then

$$\sum_{j=1}^i D_{i-j+1} F_j = 2[(i-1)F_1 + (i-2)(F_2 - F_1) + (i-3)(F_3 - F_2 + F_1) + \dots + (i-j)(F_j - F_{j-1} + F_{j-2} - \dots \pm F_1) + \dots + (F_{i-1} - F_{i-2} + F_{i-3} - \dots \pm F_1)] + \frac{1}{3}(F_i - F_{i-1} + F_{i-2} - \dots \pm F_1)$$

For computing the solution of Eq. (40), Sun and Chattopadhyay have suggested a recursion method, but we have found that such a time-saving approximation is unnecessary. A listing of the computer program for solving this equation is presented in Appendix C.

2. Dimensionless Form of Timoshenko Solutions

a. Plate Impact

By expressing the Timoshenko solution in a particular normalized (dimensionless) form, the parameters governing the impact response of plates may be identified. Specifically, it is shown that the generalized strain $\bar{\epsilon}_x$ depends on three dimensionless parameters: the mass ratio M , the aspect-orthotropy ratio η , and also another parameter which involves the geometric and material properties governing the contact effects between the plate and the impactor.

For a simply supported rectangular plate impacted at the center, let us consider the governing equation (39) and the strain equation,

$$\epsilon_x = \frac{2h\pi^2}{m_1 a^2} \sum_m \sum_n \frac{m^2}{\omega_{mn}} \int_0^t F(\tau) \sin \omega_{mn}(t-\tau) d\tau \quad (41)$$

If we assume that the plate is specially orthotropic in bending (i.e., $D_{16} = D_{26} = 0$) and further that the flexural rigidities are related by

$$D_{12} + 2D_{66} = \sqrt{D_{11} D_{22}} \quad (42)$$

(see Appendix F) then the natural frequencies are

$$\omega_{mn} = \omega_{11} A_{mn}(\eta) \quad (43)$$

where

$$\omega_{11} = \frac{\pi^2}{a^2} \left(\frac{D_{11}}{\rho h} \right)^{1/2} (1+\eta)$$

$$A_{mn}(\eta) = \frac{m^2 + \eta n^2}{1+\eta}$$

$$\eta = \left(\frac{a}{b} \right)^2 \sqrt{\frac{D_{22}}{D_{11}}} \quad (44)$$

Note that this expression for the natural frequencies is a special case of that employed in the Sun and Chattopadhyay solution, in which the approximation of Eq. (42) is not used.

In order to normalize Eqs. (39) and (41), the following dimensionless variables are defined,

$$\begin{aligned} \bar{t} &= \omega_{11} t \\ \bar{F} &= F a^3 \omega_{11} / D_{11} v b \end{aligned} \quad (45)$$

Recalling the definition of generalized strain,

$$\bar{\epsilon}_x = \frac{\epsilon_{x, \max}}{h v} c_p k \quad (21)$$

then Eqs. (39) and (41) may be written as

$$\begin{aligned} \lambda_p^{1/3} \bar{F}^{2/3} &= \bar{\tau} - \frac{M}{\pi^4 (1+\eta)^2} \int_0^{\bar{t}} \int_0^{\bar{t}} \bar{F} d\bar{\tau} d\bar{t} \\ &- \frac{4}{\pi^4} \sum_m \sum_n \frac{1}{A_{mn}(\eta)} \int_0^{\bar{t}} \bar{F}(\bar{\tau}) \sin A_{mn}(\bar{t}-\bar{\tau}) d\bar{\tau} \end{aligned} \quad (46)$$

$$\bar{\epsilon}_x = \frac{2}{\pi^4 (1+\eta)^3} \sum_m \sum_n \frac{m^2}{A_{mn}(\eta)} \int_0^{\bar{t}} \bar{F}(\bar{\tau}) \sin A_{mn}(\bar{t}-\bar{\tau}) d\bar{\tau} \quad (47)$$

where

$$M = m_1/m_2 \quad (3)$$

and

$$\lambda_p = \left(\frac{D_{11} b^3}{a^3} \right)^2 \frac{\omega_{11}}{v k_2^2} \quad (48)$$

and \bar{t} is a dummy variable for dimensionless time \bar{t} . It can be seen from these normalized equations that the generalized strain $\bar{\epsilon}_x$ depends only on the mass ratio M , aspect-orthotropy ratio η , and the parameter λ_p ; that is

$$\bar{\epsilon}_x = \bar{\epsilon}_x(M, \eta, \lambda_p) \quad (49)$$

The parameter λ_p defined in Eq. (48) may also be expressed as

$$\lambda_p = \frac{8}{\pi^6 \sqrt{3}} \left(\frac{K_1 a}{k_2 a^{3/2}} \right)^2 \left(\frac{c_p}{v} \right) \left(\frac{h}{a} \right) [f_1(\eta)^2 (1+\eta)] \quad (50)$$

Thus, the parameter λ_p can be described as the product of several dimensionless quantities.

$$\lambda_p = (\text{constant}) \times \left(\frac{\text{elastic force}}{\text{contact force}} \right)^2 \times \left(\frac{\text{wave speed}}{\text{impact velocity}} \right) \times \left(\frac{\text{plate thickness}}{\text{plate length}} \right) \times [\text{function of aspect-orthotropy ratio}]$$

b. Beam Impact

In Ref.[1], the equations for the Timoshenko solution of beam impact were presented and discussed. These equations may also be normalized by the above procedure. If we define

$$\bar{t} = \omega_1 t$$

$$\bar{F} = FL^3 \omega_1 / EI v$$

then the equations governing the response of a beam, corresponding to Eqs. (39) and (41) for the plate, may be written as

$$\lambda_b^{1/3} \bar{F}^{2/3} = \bar{t} - \frac{M}{\pi} \int_0^{\bar{t}} \int_0^{\bar{t}} \bar{F} d\bar{t} d\bar{t} - \frac{2}{\pi} \sum_1 \frac{1}{i^2} \int_0^{\bar{t}} \bar{F}(\bar{\tau}) \sin i^2(\bar{t}-\bar{\tau}) d\bar{\tau} \quad (51)$$

and

$$\bar{\epsilon} = \frac{1}{\pi} \sum_1 \int_0^{\bar{t}} \bar{F}(\bar{\tau}) \sin i^2(\bar{t}-\bar{\tau}) d\bar{\tau} \quad (52)$$

where

$$\lambda_b = \left(\frac{EI}{L^3} \right)^2 \frac{\omega_1}{v k_2} = \left(\frac{\pi}{48} \right)^2 \left(\frac{K_1 h}{k_2 h^{3/2}} \right)^2 \left(\frac{c_b}{v} \right) \left(\frac{k}{h} \right) \quad (53)$$

which may be expressed as

$$\lambda_b = (\text{constant} \times \left(\frac{\text{deflection force}}{\text{contact force}} \right)^2 \times \left(\frac{\text{wave speed}}{\text{impact velocity}} \right) \times \left(\frac{\text{radius of gyration}}{\text{depth of beam}} \right)$$

It can be seen from Eqs. (51) and (52) that in this case the generalized strain $\bar{\epsilon}$ depends only on the mass ratio M and the contact parameter λ_b , or

$$\bar{\epsilon} = \bar{\epsilon}(M, \lambda_b)$$

In Ref. [1] it was shown that for large impact masses ($M \sim 2$) the dependence of the generalized strain $\bar{\epsilon}$ on the contact parameter λ_b was only slight; that is

$$\bar{\epsilon} = \bar{\epsilon}(M) \quad \text{for small } M.$$

For the case of plate impact, the influence of the contact parameter λ_b is also relatively insignificant in determining the peak strain response to impacts by large masses. This will be demonstrated in the following section.

3. Parametric Study for Large Impactors

As can be seen from Eq. (49), the response of a specially orthotropic plate satisfying the condition of Eq. (42) is described by several parameters: M , η , and λ_p . In this section, we examine the significance of each of these parameters for cases where the mass of the impactor is large compared to the mass of the plate. It will be demonstrated that, for plates of given aspect-orthotropy ratio η , the dependence of the impact response on parameters other than M is weak for low values of M , so that

$$\bar{\epsilon}_x \approx \bar{\epsilon}_x(M, \eta) \quad \text{for small } M.$$

To determine the significance of the various parameters to the impact response, several plate impact problems have been calculated using the Timoshenko solution method. Each problem of this series is based on an impact situation with the impact constants listed in Appendix C. A parametric study was carried out by systematically varying the values of the impact velocity v , the Hertzian contact stiffness k_2 , the plate flexural stiffness matrix D_{ij} , and the impactor mass m_2 . A summary of this study, along with the computed values of the generalized strains $\bar{\epsilon}_x$ and $\bar{\epsilon}_y$ and the contact parameter λ_p , is presented in Table I.

NADC-78259-60

TABLE I

PARAMETRIC STUDY

PLATE IMPACT CASES CALCULATED BY THE TIMOSHENKO SOLUTION ($\eta=0.459$)

Mass Ratio, $M=m_1/m_2$	Impact Velocity, v/v_0	Hertz Contact Stiffness, $k_2/k_{2,0}$	Flexural Stiffness Matrix, $D_{ij}/D_{ij,0}$	Dimensionless Contact Parameter, $\lambda_p \times 10^7$	Generalized Strain	
					$\bar{\epsilon}_x$	$\bar{\epsilon}_y$
1.036	1	1	1	6.99	2.512	1.538
	$\sqrt{2}$	1	1	4.94	2.536	1.538
	1	2	1	1.748	2.592	1.556
	1	1	2	39.54	2.339	1.440
0.784	1	1	1	6.99	2.770	1.702
	$\sqrt{2}$	1	1	4.94	2.798	1.713
	1	2	1	1.748	2.848	1.731
	1	1	2	39.54	2.609	1.635
0.475	1	1	1	6.99	3.298	1.983
	$\sqrt{2}$	1	1	4.94	3.340	1.988
	1	2	1	1.748	3.425	1.999
	1	1	2	39.54	3.021	2.025
0.242	1	1	1	6.99	4.585	2.910
	$\sqrt{2}$	1	1	4.94	4.611	2.922
	1	2	1	1.748	4.678	2.946
	1	1	2	39.54	4.418	2.794

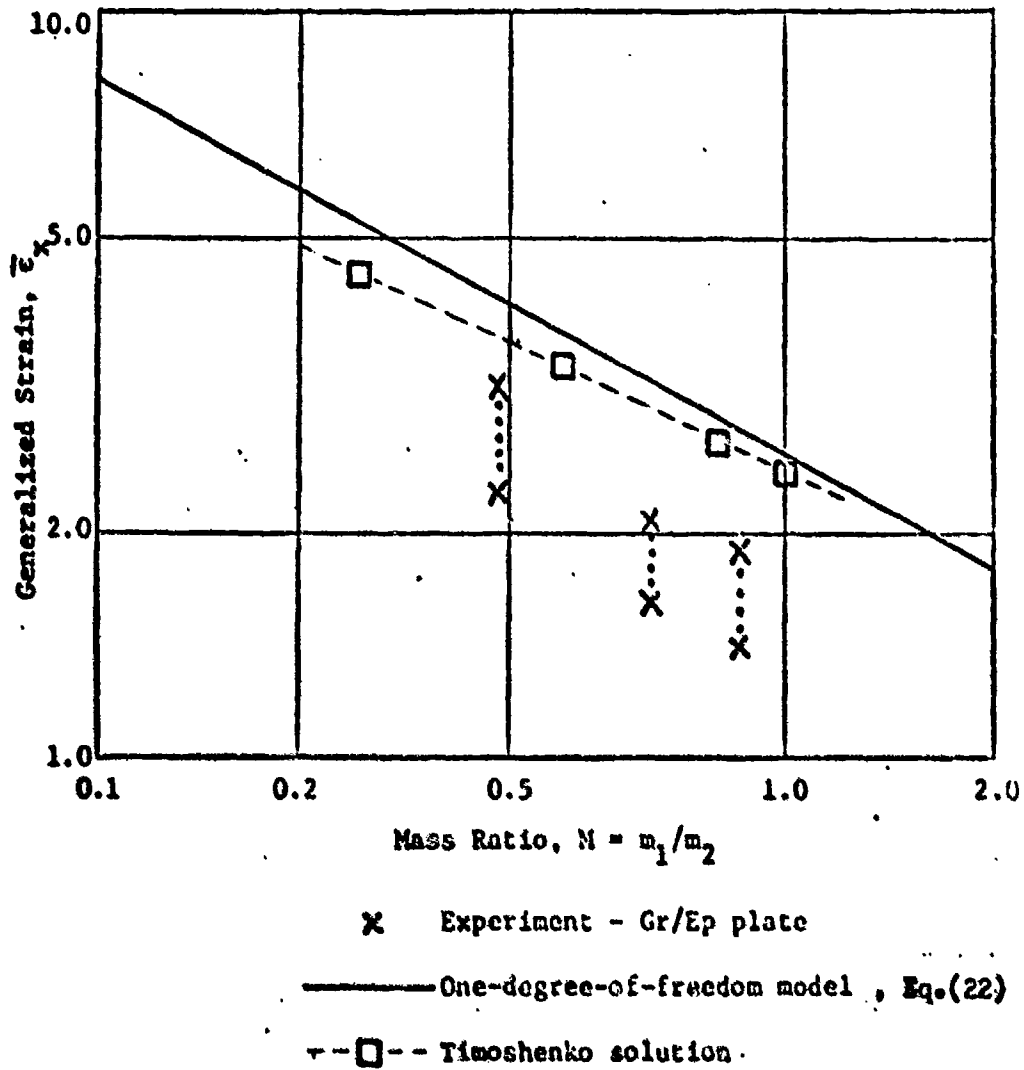


Figure 6. Generalized strain curves for simply supported rectangular orthotropic plates ($\eta=0.459$) subjected to central transverse impact.

Note that for all of these calculations the value of the aspect-orthotropy ratio η is the same ($\eta = 0.459$). An inspection of this table indicates that, for any given value of the mass ratio M , the maximum difference between any two values of $\bar{\epsilon}_x$ or of $\bar{\epsilon}_y$ is only 12%, whereas the largest value of λ_p is 22.6 times the smallest. It may be concluded, therefore, that the dependence of the generalized strain $\bar{\epsilon}_x$ or $\bar{\epsilon}_y$ on the contact parameter λ_p (or on any other parameters) is weak, and that for constant η a single $\bar{\epsilon}_x$ vs. M curve gives an acceptable representation of all impact cases. Furthermore, since the powerful Timoshenko solution, which includes the effects of contact behavior, indicates that such behavior does not significantly contribute to the impact response, then the validity of the one-degree-of-freedom model, which neglects contact effects, is thereby substantiated for the range of low M .

The Timoshenko solution may be used to construct an impact design curve by plotting calculated points on an $\bar{\epsilon}_x$ vs. M graph (Fig. 6). These calculated points alone can be approximated by a single curve which may be used as a design curve. Note that such a curve would not be very different from the curve corresponding to the one-degree-of-freedom model discussed in a previous section. Also included in Fig. 6 are results of a series of impact experiments performed on the graphite-epoxy laminated plate described in Appendix C [8].

C. Impact Experiments

Several series of impact experiments were performed on simply supported and clamped-edged plates, including strain-measurement experiments and impact-to-failure tests. The plate specimens, made of aluminum or graphite/epoxy, were impacted by blunt steel projectiles using a drop-test apparatus. In the

strain-measurement experiments, the strain in the plate was recorded using strain gages and an oscilloscope. In the impact-to-failure tests, each plate was impacted at gradually increasing impact velocities until it failed. In this section, these experiments are described in detail, and the results are compared with the theoretically derived design curves.

1. Specimens

The impact specimens included both aluminum and laminated graphite/epoxy plates. Three 6061-T6 aluminum plates were used with both simply supported and clamped boundary conditions. The dimensions and mass of these plates are: (1) 125x125x6.35 mm, 0.282 kg; (2) 250x125x6.35 mm, 0.561 kg; and (3) 375x125x6.35 mm, 0.843 kg. These dimensions and masses include only the area between the supports of the plates; an additional 10-mm margin was left along each edge to support the plates.

Graphite-epoxy specimens, fabricated from Hercules, Inc., type AS/3501-6 pre-impregnated tape at various lay-ups, were used as simply supported and clamped plates. The dimensions, mass, and lay-up of each plate are listed in Table II. These dimensions and masses again include only the area between the supports of the plates; a 10-mm margin protruded beyond the supports around each plate.

Elastic properties for the composite plates were calculated from lamination theory, using the following properties for each layer:

$$E_{11} = 17.7 \times 10^6 \text{ psi} = 1.220 \times 10^{11} \text{ N/m}^2$$

$$E_{22} = 1.3 \times 10^6 \text{ psi} = 8.96 \times 10^9 \text{ N/m}^2$$

$$\nu_{12} = \nu_{13} = 0.3$$

$$\nu_{23} = 0.2$$

$$G_{12} = G_{13} = 0.55 \times 10^6 \text{ psi} = 3.79 \times 10^9 \text{ N/m}^2$$

$$G_{23} = 0.54 \times 10^6 \text{ psi} = 3.72 \times 10^9 \text{ N/m}^2$$

TABLE II. GRAPHITE/EPOXY PLATE SPECIMENS

Series Designation and Lamination Lay-up	Plate Designation	Dimensions, $a \times b \times h$ (mm)	Mass (kg)
Basic lay-up (B-series) [($\pm 45/0_2$) ₂ / $\pm 45/0/90$] _g	B1	133 × 133 × 3.6	0.099
	B2	133 × 260 × 3.6	0.193
	B3	260 × 133 × 3.6	0.193
	B4	260 × 260 × 3.6	0.379
	B5	133 × 387 × 3.6	0.287
	B6	387 × 133 × 3.6	0.287
	B7	387 × 260 × 3.6	0.547
	B8	260 × 387 × 3.6	0.547
	B9	387 × 387 × 3.6	0.815
F-series [($\pm 45/0_2$) ₂ / $\pm 45/0/90$] _{2g}	F1	133 × 133 × 7.6	0.237
	F2	133 × 260 × 7.6	0.452
	F3	260 × 133 × 7.6	0.452
	F4	260 × 260 × 7.6	0.860
H-series [$+45/90/-45/+22.5/-67.5/-22.5/$ $+67.5/\pm 45/+67.5/+22.5/-67.5/$ $-22.5/\pm 67.5/\pm 22.5/0_2/\pm 22.5$] _g	H1	133 × 133 × 6.8	0.213
	H2	133 × 260 × 6.8	0.410
	H3	260 × 133 × 6.8	0.410
	H4	260 × 260 × 6.8	0.772

TABLE III. SHEAR AND FLEXURAL STIFFNESSES OF
GRAPHITE/EPOXY PLATE SPECIMENS

		B-series	F-series	H-series
Flexural Stiffnesses (N/m)	D_{11}	2470.	19750.	9970.
	D_{12}	710.	5080.	4710.
	D_{22}	963.	8100.	13300.
	D_{16}	-73.3	-26.7	-529.
	D_{26}	-73.3	-26.7	-267.
	D_{66}	748.	5380.	4960.
Shear Stiffnesses (N/m)	A_{44}	77700.	154000.	147000.
	A_{45}	0.	0.	0.
	A_{55}	78200.	155000.	147000.

TABLE IV: DESIGN CURVE PARAMETERS FOR GRAPHITE/EPOXY PLATE SPECIMENS

Plate Designation	$n^2 \left(\frac{a}{b}\right)^2 \frac{D_{22}}{D_{11}}$	Simply Supported		Clamped	
		$g_1(n)$	$g_1(n^{-1})$	$g_2(n)$	$g_2(n^{-1})$
B1	0.625	2.4	2.22	3.2	3.0
B2	0.164	3.1	2.4	4.2	3.4
B3	2.39	2.25	2.6	3.1	3.5
B4	0.625	2.4	2.22	3.2	3.0
B5	0.074	3.7	3.0	4.9	4.0
B6	5.29	2.4	3.1	3.4	4.1
B7	1.38	2.25	2.4	3.0	3.1
B8	0.282	2.8	2.3	3.8	3.2
B9	0.625	2.4	2.22	3.2	3.0
F1	0.641	2.4	2.2	3.2	3.0
F2	0.168	3.15	2.4	4.2	3.4
F3	2.45	2.25	2.6	3.1	3.5
F4	0.641	2.4	2.2	3.2	3.0
H1	1.15	2.25	2.35	3.0	3.05
H2	0.302	2.8	2.3	3.7	3.2
H3	4.41	2.35	2.95	3.3	3.95
H4	1.15	2.25	2.35	3.0	3.05

The computed values of the flexural and shear stiffnesses of each plate are summarized in Table III. In all further calculations, the D_{16} and D_{26} terms are neglected; that is, the entire laminate is treated as specially orthotropic.

Calculated values of the parameter η and the functions $g_1(\eta)$ and $g_2(\eta)$ necessary to construct the design curves are listed in Table IV for each graphite epoxy plate.

2. Strain-Measurement Impact Experiments

The plates were centrally impacted by blunt (6.35 , 12.7, or 25.4 mm contact radius) steel cylinders of various masses at several velocities using a drop test apparatus. The strains, ϵ_x and ϵ_y were measured, in directions parallel to the plate edges, directly opposite the impact point, using a Micro-Measurements, Inc., type EA-13-062TT-120 metal-foil 0°-90° rosette strain gage, and recorded on a Tektronix model 565 oscilloscope. Impact velocities were calculated from the drop height.

For impacts on clamped plates, the plates were clamped along all edges by a frame of rectangular steel bars (Fig. 7). The entire assembly was fastened to a large lead plate and rested on a concrete floor.

In the experiments performed on simply supported aluminum plates, each plate was rested on top of a frame of rectangular-cross-section steel bars. For the composite plates, however, the clamping device mentioned above was modified to simulate a simply supported boundary. Grooves to accommodate 3.175 mm (1/8") rods were machined in each member of the clamping device such that, when the clamping device was assembled, the specimen plate would be resting on the rods.

Experimental results of the strain-measurement tests on both clamped and simply supported plates are presented in Appendix E in both tabular and

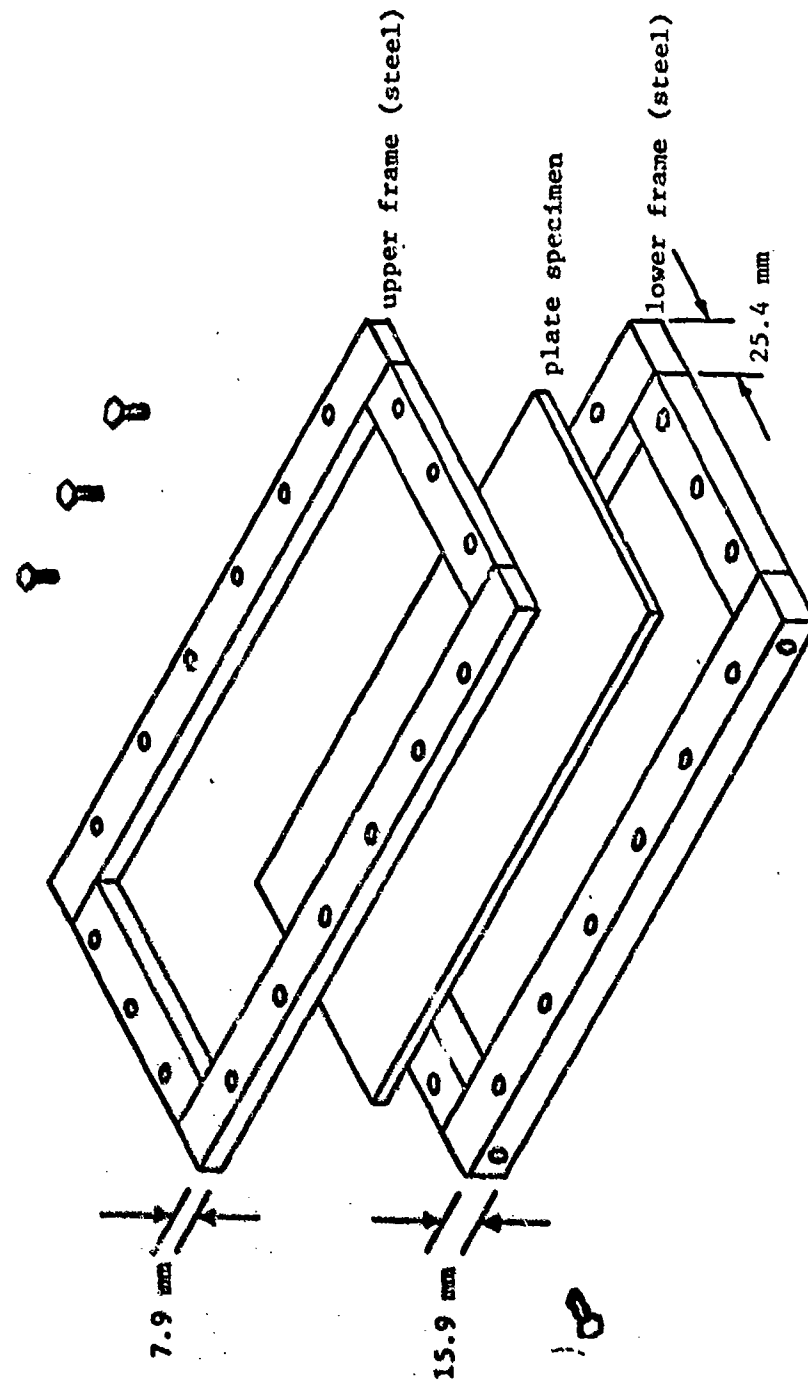


Figure 7. Exploded view of plate clamping device.

graphical ($\bar{\epsilon}$ vs. M) form. Also included in Appendix E are some typical strain vs. time oscilloscope traces. Figures 8 and 9 are typical examples of the $\bar{\epsilon}$ vs. M curves for the clamped plates and the simply supported plates, respectively. In each of these figures a dashed line has been fitted by eye through the experimental points. The maximum percentage difference (variation) between this line and the experimental data is also shown on each figure. For both the clamped and the simply supported cases, the largest value of this variation is 36%.

Experimental data from specimens having approximately the same value of the parameter η have been presented on the same design curve except the three smallest sized plates (B1, F1, and H1). Values of $\bar{\epsilon}$ for these three plates are considerably smaller than those for larger plates with the same parameter η . It is believed that, due to the small size of these plates, the boundary constraint has more influence, and the deflection mode is different from the other plates. Perhaps thick-plate, damping, and shear effects are more pronounced. Data from these plates, although presented on the $\bar{\epsilon}$ vs. M plot of Figs. 10 and 11, were not used in constructing the experimental design curve line nor in calculating the variation.

Also shown in Figs. 8 and 9, and in each design curve in Appendix E, is the theoretical (one-degree-of-freedom) design curve. Comparison of this curve and the one from experimental data shows an average discrepancy of about 40%. Note that the theoretical curve is always conservative (i.e., predicts a higher plate strain) over the range of experimental results. However, the slope of the line drawn through the experimental data is in all cases roughly the same as the slope of the theoretical curve.

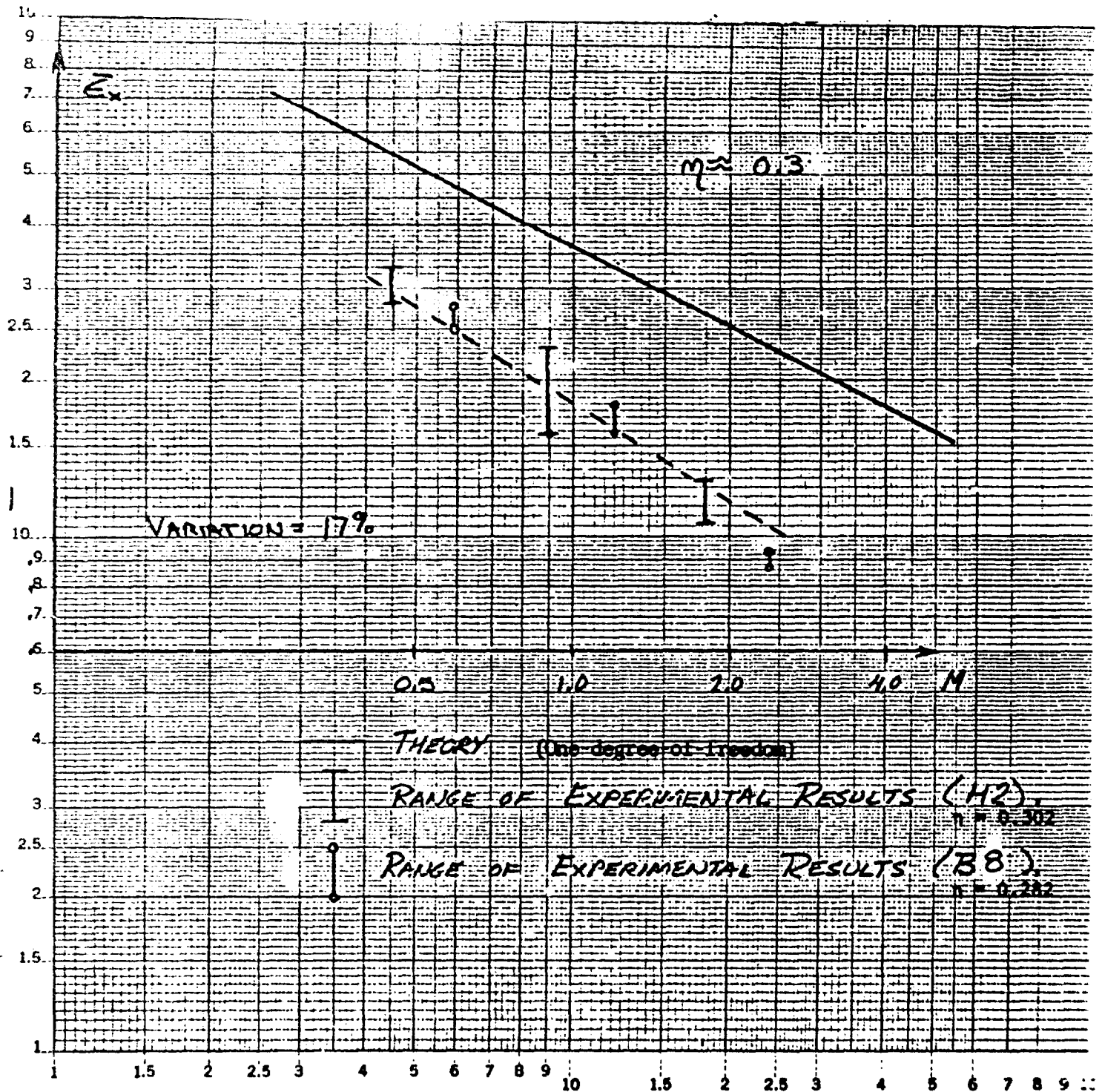


Figure 8. Typical $\bar{\epsilon}_x$ vs. M Curve for Clamped Orthotropic Plates

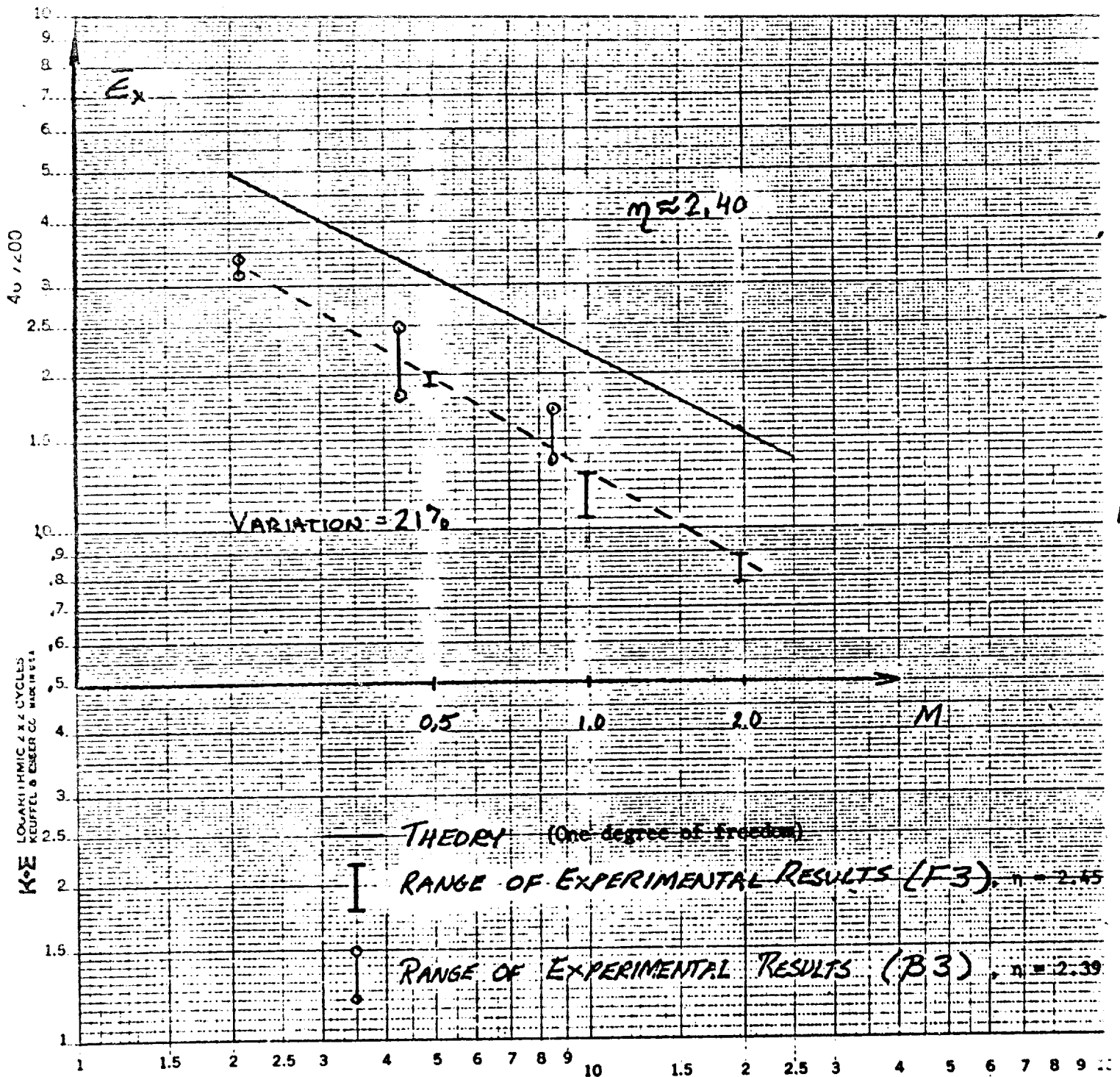


Figure 9. Typical \bar{E}_x vs. M Curve for Simply Supported Orthotropic Plates

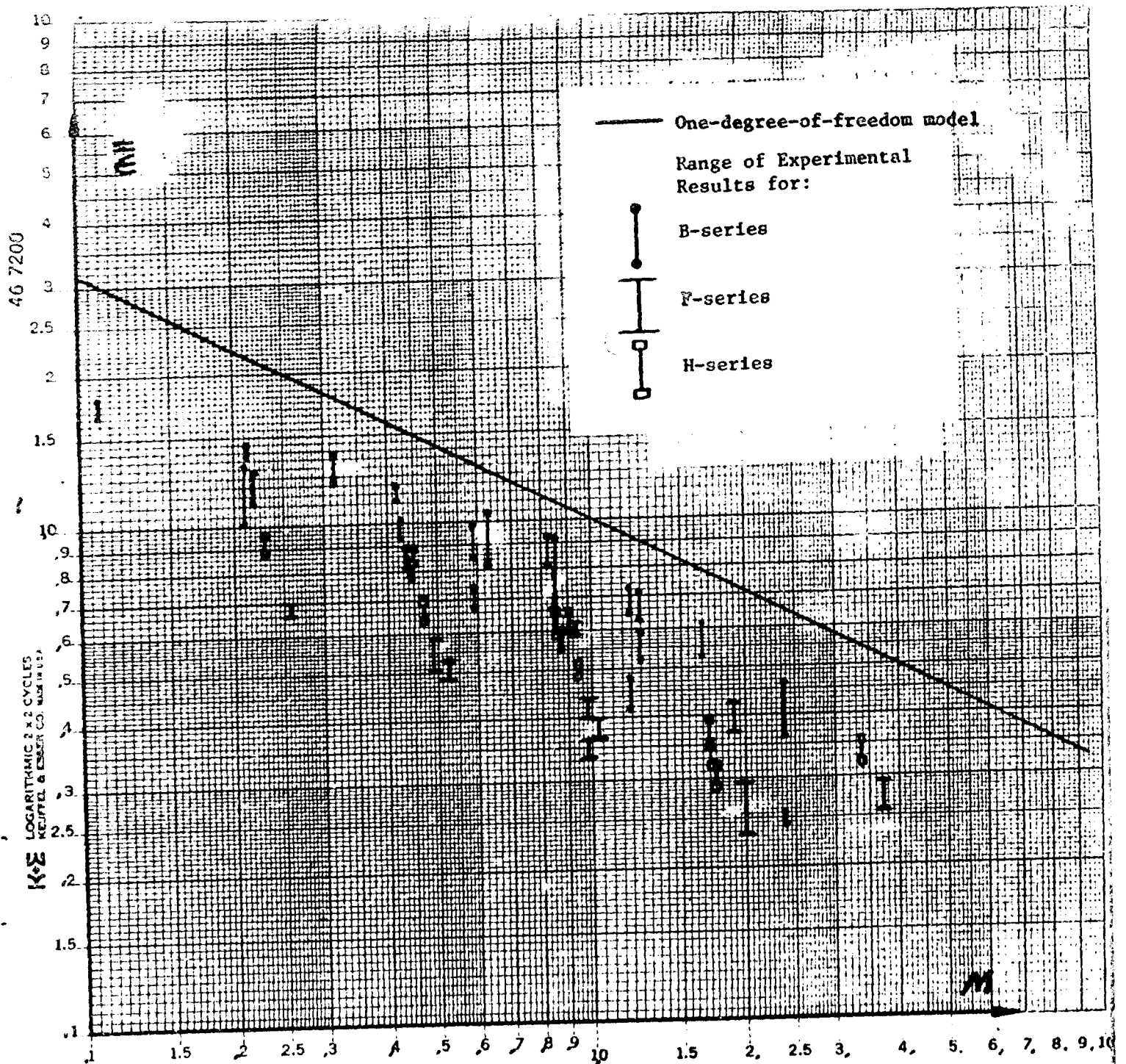


Figure 10. Strain Curve for Clamped Plate Impacted by Large Masses.

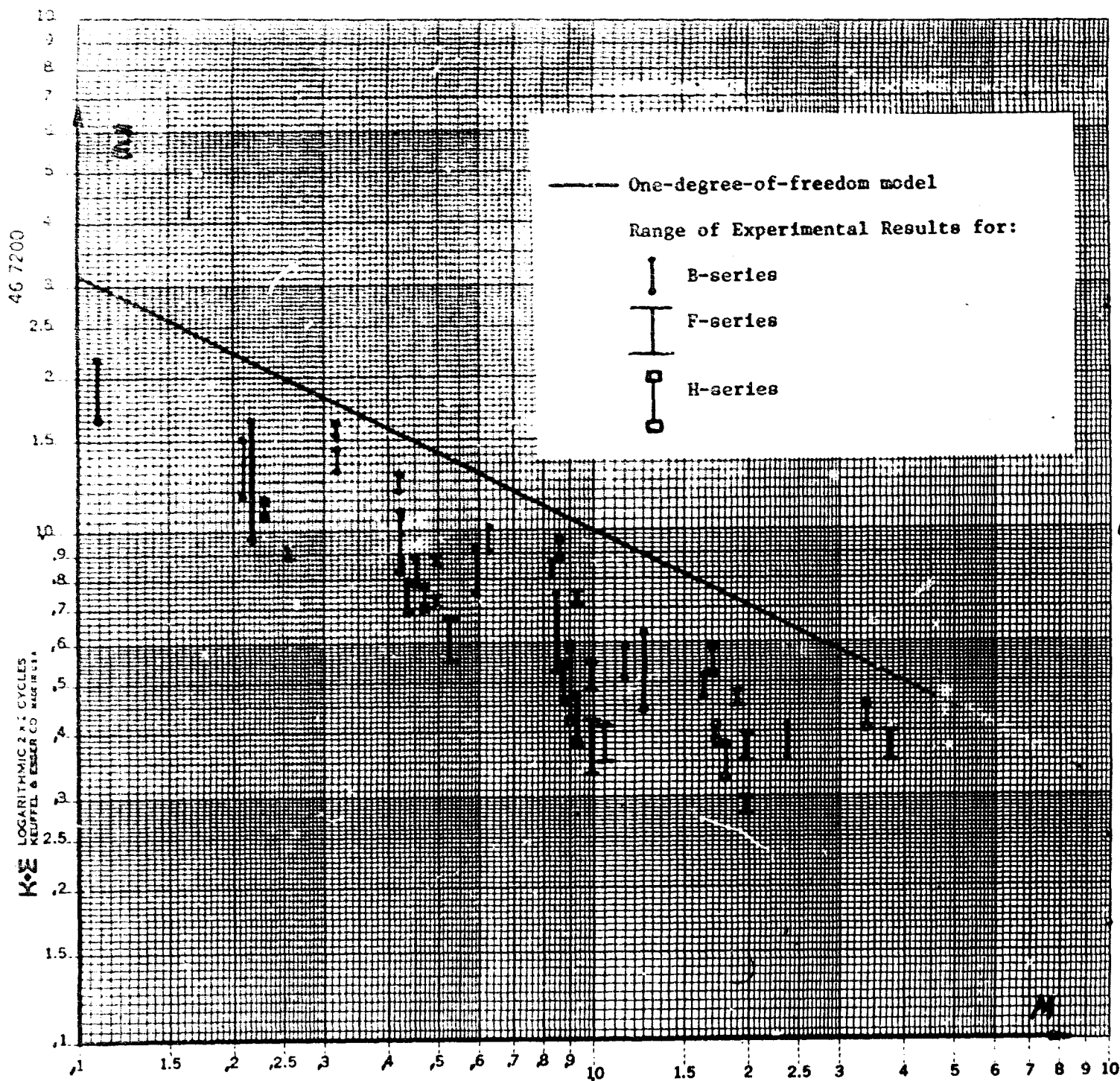


Figure 11. Strain Curve for Simply Supported Plates Impacted by Large Masses

As previously discussed, all impact data can be plotted on a single curve, $\bar{\epsilon}$ vs. M . This is done for impact data on clamped plates in Fig. 10 and on simply supported plates in Fig. 11. Note that, since $\bar{\epsilon}$ is independent of both the parameter η and the boundary conditions, both cases could have been plotted on a single figure. Because of the overlapping of experimental data, the clamped and simply supported cases, were presented separately for clarity.

3. Impact-to-Failure Experiments

In addition to the strain measurement impact experiments, a series of tests were conducted in which laminated composite plates were impacted to failure. In each of these tests, a plate was repeatedly impacted by the same projectile using a drop-weight apparatus at gradually increasing velocities (drop heights) until failure of the specimen was detected. The specimen was examined for failure after each impact both visually and ultrasonically, using a hand held pulse-echo transducer and reflectoscope.

The average between the highest impact velocity, v_d , for which a particular specimen did not fail, and the lowest velocity, v_f , for which any failure was detected, is regarded as the critical or failure velocity, v_c , or

$$v_c = \frac{v_d + v_f}{2}$$

This velocity is used in characterizing the impact resistance of each specimen.

The results of these experiments are presented in both graphical and tabular form in Appendix E. Figure 12 is a typical example of the $\bar{\epsilon}$ vs. M curves for the clamped plate. Again, a dashed line has been drawn to indicate the design curve based only on experimental results. As can be seen, there is good agreement between the experimental data and the theoretical one-degrees-of-freedom curve.

Again, a design curve independent of the parameter η and the boundary

conditions (\bar{v} vs. M) may be used to present impact data. However, from Eq. (34), it is apparent that only those plates with the same value of ϵ_f should be presented on this curve. For the composite plates, therefore, a \bar{v} vs. M curve should be prepared for each different lay-up. Figure 13 is such a plot for the experiments performed on B-series plates.

After damage was detected, several plates were ultrasonically C-scanned. Transducer output was passed through an analog to digital converter. Data was then processed by Fourier transform techniques using the first five waveforms. Typical transducer response is shown in Fig. 14 for an undamaged area of a plate. The top-surface and bottom-surface echoes are clearly visible with little evidence of internal reflection. Figures 15 and 16 show transducer response over damaged areas of two different specimens. Figure 15 shows a damaged region extending from about one-quarter of the plate thickness below the surface to the midplane of the plate. This type of damage has been observed by use of the hand-held transducer in approximately 75% of the failure tests. It is believed that this mode of failure is delamination. Figure 16 is representative of the remaining 25% of the failure tests. As can be seen, there is little indication of damage through the thickness of the plate. This, along with the absence of a bottom-surface echo indicates that the plate has probably been damaged near the top surface. It is believed that this mode of failure results from fiber breakage, due to bending and/or contact effects.

D. Design Curves for Shear Failure Due to Impact

A structure subjected to impact may also fail due to the high level of shear stress produced. In this section, a theory based on the one-degree-of-freedom impact model is developed for predicting the maximum impact-induced transverse shear stress in simply supported beams and plates.

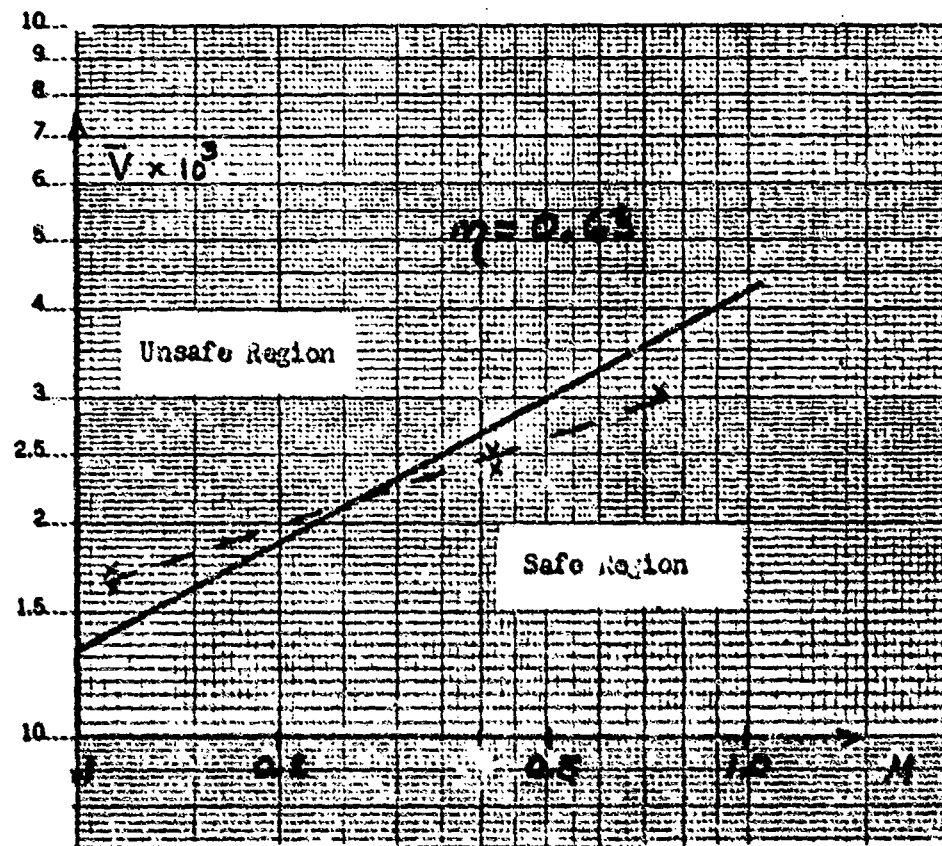


Figure 12. Typical Critical Velocity Curve, \bar{V} vs. M , for Clamped Orthotropic Plates: Experimental Data from Specimens B1 and B4

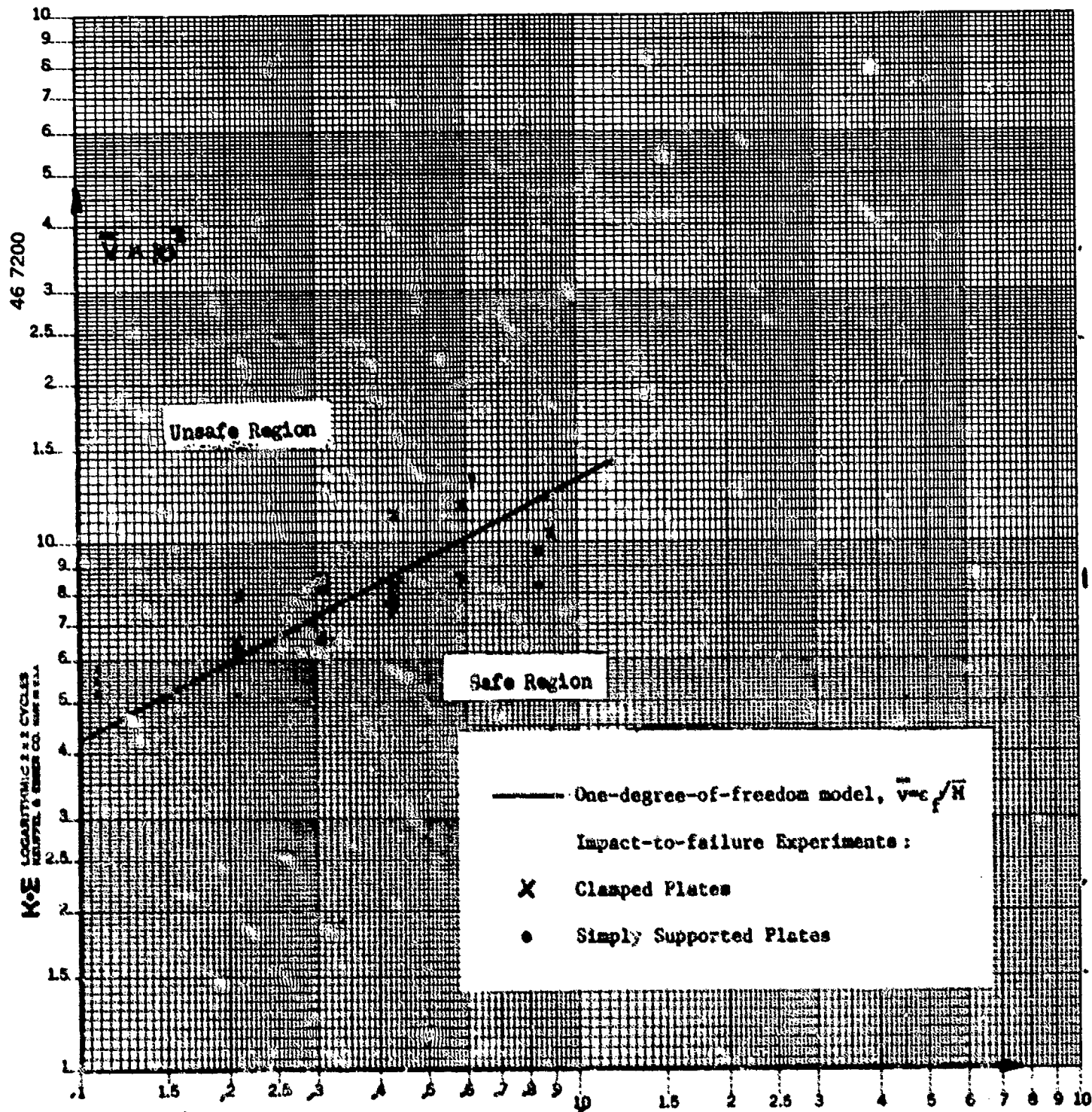


Figure 13. Critical Impact Velocity Curve for Clamped and Simply Supported Plates Impacted by Large Masses.

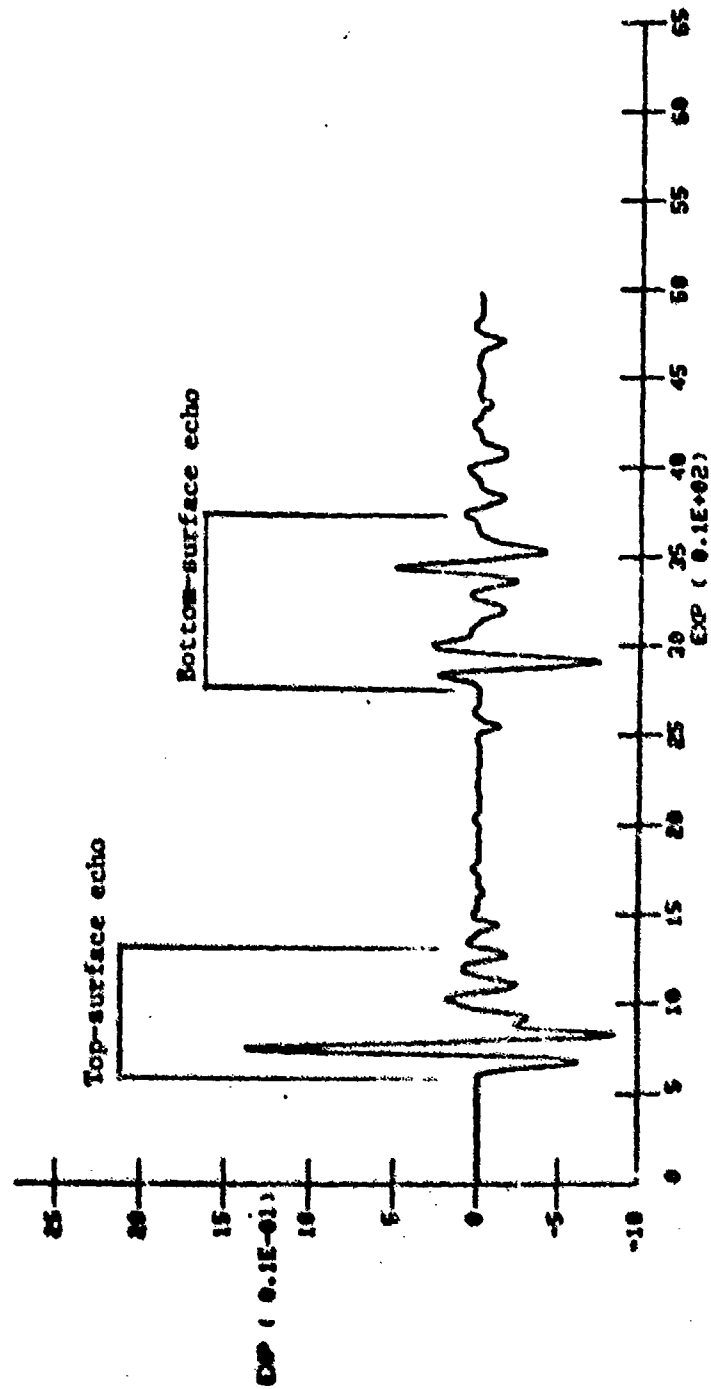


Figure 14. Typical Reflectoscope trace for undamaged plate specimen.

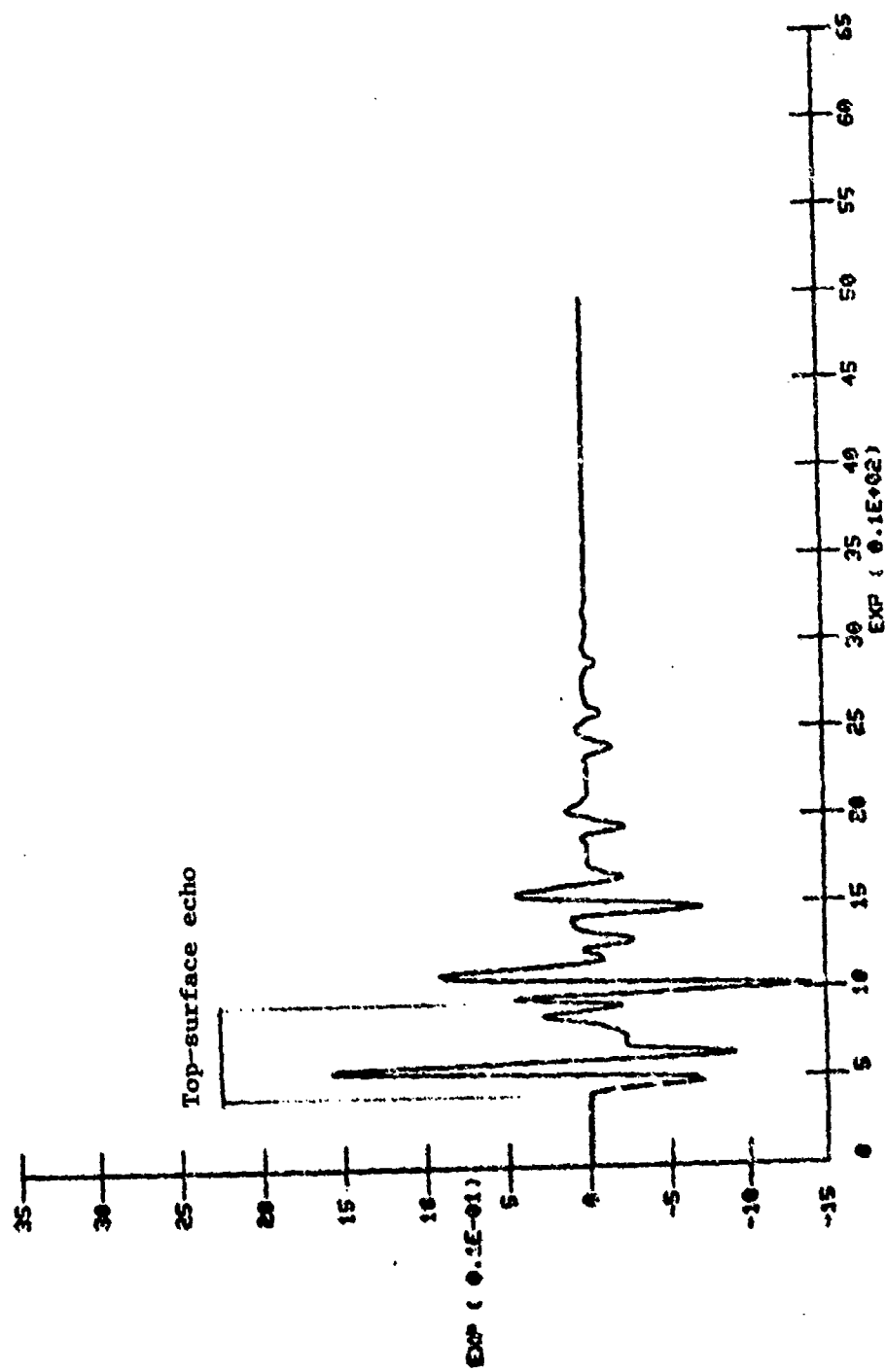


Figure 15. Typical Reflectoscope trace for plate specimen with internal damage.

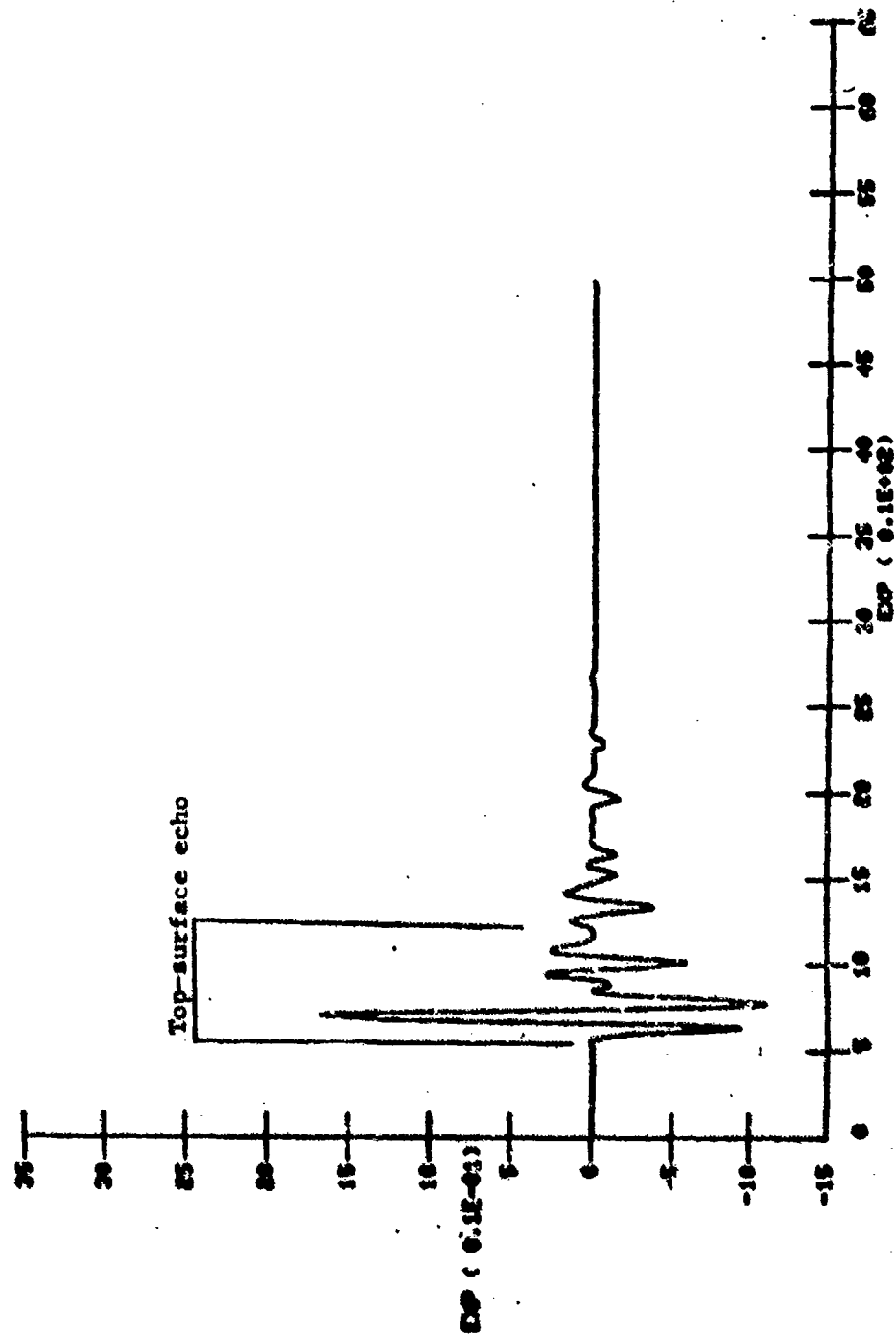


Figure 16. Typical Reflectoscope trace for plate specimen with top-surface damage.

1. Simply Supported Beam

By extending the one-degree-of-freedom, energy-conserved model previously discussed, a design curve for predicting the peak shear stress in a simply supported beam subjected to transverse impact may be generated.

First, the maximum shear stress in the beam is related to the maximum deflection by the static beam equation. The deflection of a simply supported beam subjected to a static load at midspan is

$$w(x) = w_1 \frac{x}{L} \left(3 - \frac{4x^2}{L^2} \right) \quad 0 \leq x \leq L/2 \quad (54)$$

where w_1 is the deflection at midspan. The shear force generated is

$$\begin{aligned} V &= EI \left| \frac{d^3 w}{dx^3} \right| \\ &= 24 \frac{EI}{L^3} w_1 \end{aligned} \quad (55)$$

For a beam of rectangular cross-section, the maximum shear stress occurs at the neutral axis and is given by

$$\begin{aligned} \tau_{\max} &= \frac{3V}{2A} \\ &= \frac{36EI}{AL^3} w_{1\max} \end{aligned} \quad (56)$$

The maximum deflection $w_{1\max}$ may be related to the impact velocity by the conservation-of-energy condition, which implies that the initial kinetic energy of the impactor is entirely converted into bending-strain energy in the beam.

$$w_{1\max} = \sqrt{\frac{m_2}{K_1}} v \quad (57)$$

By defining the dimensionless (generalized) shear stress as

$$\bar{\tau} = \frac{\tau_{\max} L a^2 A}{vEI} \quad (58)$$

and combining Eqs. (56) and (57), we obtain the equation for the shear-stress design curve.

$$\bar{\tau} = 3\sqrt{\frac{3}{M}} \quad (59)$$

This equation is plotted in $\bar{\tau}$ vs. M coordinates in Fig. 17.

a. Relative Importance of Shear and Bending

Depending on geometry, strength, and elastic properties, a particular beam subjected to low-velocity impact may experience failure initiated by bending or shear effects. The theories presented here for predicting bending strain and shear stress due to impact are both based on the static beam deflection curve. Therefore, the relative importance of bending and shear effects may be estimated by considering the static relations between shear and bending.

If a maximum-stress failure criterion is adopted for both shear and bending, then failure due to shear will be more likely if, for any impact velocity v , we have

$$\frac{\tau}{\tau_f} > \frac{\sigma}{\sigma_f} \quad (60)$$

where the subscript f denotes values at failure. By combining this relation with Eqs. (12), (13), (59), and (50), we obtain

$$\frac{h}{L} \frac{\sigma_f}{\tau_f} > 2 \quad (61)$$

Based on the approximate theory presented here, this inequality must be satisfied for impact failure to initiate by shear effects; if it is not satisfied, failure will initiate by bending.

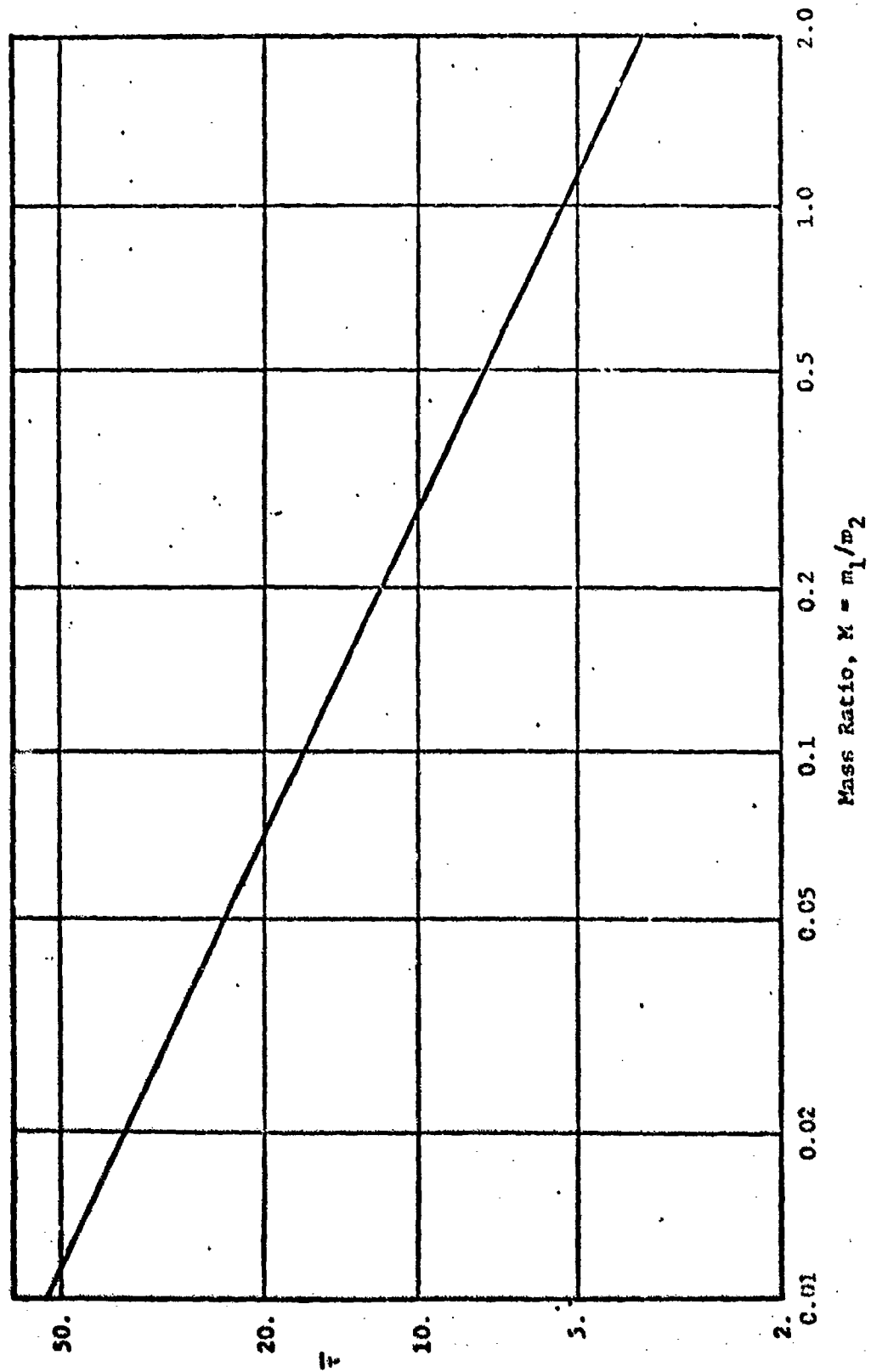


Figure 17. Shear stress curve for simply supported beam.

b. Critical Impact Velocity Curve

The relative importance of shear and bending effects in initiating failure of a particular beam may be illustrated by presenting the design curve in a form similar to that presented in Section II for plate impacts. In this alternate form, theoretical design curves and experimental data are plotted in coordinates of a dimensionless impact velocity \bar{v} or $\bar{\bar{v}}$ and the mass ratio M . Then, each critical velocity curve divides the plane into two regions: above the critical bending curve is the region bending failure occurs, and below is the no-bending-failure region. The same is true for the critical shear curve.

Specifically, if the dimensionless impact velocity for the beam is defined as

$$\bar{v} = \frac{vh}{a^2} \quad (62)$$

then the one-degree-of-freedom energy-conserved impact model, predicts that failure will initiate in the beam due to bending for

$$\bar{v}_c = \frac{2\epsilon_f}{\sqrt{3}} \sqrt{M} \quad (63)$$

where ϵ_f is the tensile failure strain, assuming a maximum-strain failure criterion.

Similarly, according to the theory discussed above for estimating the shear stress due to impact, Eq. (39), failure due to shear occurs for

$$\bar{v}_c = \frac{\tau_f}{\sqrt{3}} \frac{4L}{bh} \sqrt{M} \quad (64)$$

where τ_f is the shear stress at failure, assuming a maximum-stress failure criterion in shear.

Equations (63) and (64), plotted in \bar{v} vs. M coordinates, represent the two critical velocity design curves. The relative importance of shear and bending regarding failure of a particular structure is immediately apparent from such a plot -- the lower curve predicts failure at a smaller impact velocity, indicating that the failure mode (shear or bending) associated with the lower curve is the critical one.

Consider, for example, the impact failure tests on 22 graphite-epoxy beams. These beams were fabricated from Hercules AS3501 at a lay-up of $[\pm 45/0_2/\mp 45]_2$. All beams have a span to thickness ratio (L/h) of 48.53. Data from all the impact tests (with or without failure) performed on these beam specimens are tabulated in Appendix E and plotted in \bar{v} vs. M coordinates in Fig. 18. Also included in this figure are curves representing Eqs. (63) and (64). The value of the bending failure strain ϵ_f used is 0.0168; the value of the shear failure stress τ_f used is the value of the interlaminar shear strength given by the material manufacturer (Hercules Product Data Sheet No. 832) as 18,900 psi (130. MN/m²).

Note that the lower curve in Fig. 18, which represents Eq. (63), approximately divides the experimental points according to whether the points correspond to failure or no-failure tests. Also, the curve corresponding to shear failure falls much higher on this plot than the curve for bending failure; this indicates that for these beams the bending is the mode in which failure initiates.

2. Simply Supported Plate

A design curve for estimating the peak transverse shear stress at the edge of a simply supported, rectangular, orthotropic plate subjected to central lateral impact may also be developed.

It must be recognized that the edge shear is only a rough estimate of the maximum shear stress occurring in the plate; much higher stresses may be generated in the immediate vicinity of the impact point. However, analysis

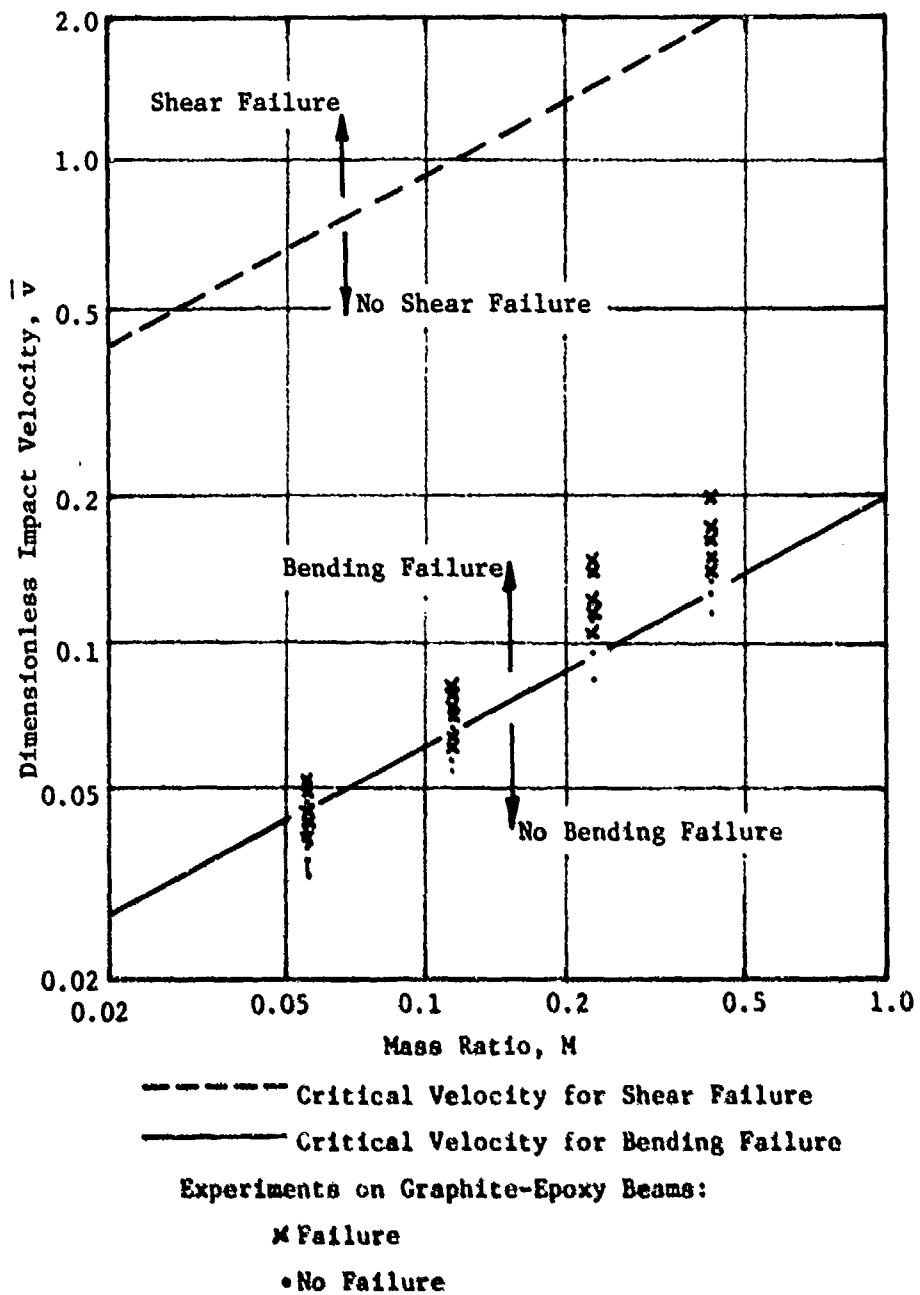


Figure 18. Critical impact velocities for shear and bending failure and experimental data--a bending-dominated case.

of the problem by plate theory alone (as is done here) leads to a singularity in the shear at this point, due to treatment of the impact load as a concentrated force. A more sophisticated analysis would focus on the three-dimensional stress field near the impact location. Still, for design purposes, knowledge of the edge shear can sometimes be useful. If, for a particular impact situation, it exceeds the allowable shear stress, failure will certainly occur; on the other hand, a low edge shear stress does not, of course, guarantee survival of the structure.

As in the previous case of the beam, the maximum edge shear stress in the plate is first related to the maximum central deflection by assuming that the static relations hold. In terms of generalized plate forces, the maximum values of the transverse shear stress components are

$$\begin{aligned}\tau_{xz} &= \frac{3Q_x}{2h} \\ \tau_{yz} &= \frac{3Q_y}{2h}\end{aligned}\tag{65}$$

for a homogeneous plate. For a specially orthotropic plate, the generalized forces are related to the deflection distribution by

$$\begin{aligned}Q_x &= -\frac{\partial}{\partial x} \left(D_{11} \frac{\partial^2 w}{\partial x^2} + H \frac{\partial^2 w}{\partial y^2} \right) \\ Q_y &= -\frac{\partial}{\partial y} \left(H \frac{\partial^2 w}{\partial x^2} + D_{22} \frac{\partial^2 w}{\partial y^2} \right)\end{aligned}\tag{66}$$

where

$$H = D_{12} + 2D_{66}$$

It is again assumed that the dynamic deflection due to impact is the same as the static deflection due to a central point load. In this case, the maximum edge shear force occurs at the middle of the edge. If it is also assumed that $H = \sqrt{D_{11} D_{22}}$, then

$$\tau_{xz_{\max}} = \frac{3\pi^3 D_{11}}{2h a^3} \frac{f_5(\eta)}{f_1(\eta)} w_{1_{\max}} \quad (67)$$

$$\tau_{yz_{\max}} = \frac{3\pi^3 D_{12}}{2h b^3} \frac{f_5(\eta^{-1})}{f_1(\eta^{-1})} w_{1_{\max}} \quad (68)$$

where

$$f_5(\eta) = \sum_{n=1,3,5}^{\infty} \sum_{n=1,3,5}^{\infty} \frac{n(-1)^{\frac{n-1}{2}}}{n^2 + n^2 \eta} \quad (69)$$

and where $f_1(\eta)$ and η are defined in Eqs. (15) and (16), respectively.

If we define the dimensionless shear stress parameters

$$\begin{aligned} \bar{\tau}_{xz} &= \tau_{xz_{\max}} \frac{a^2}{D_{11} v} \\ \bar{\tau}_{yz} &= \tau_{yz_{\max}} \frac{b^2}{D_{22} v} \end{aligned} \quad (70)$$

then Eqs. (67) and (68) may be combined with the conservation-of-energy condition, Eq. (4), to yield the design curve equations,

$$\bar{\tau}_{xz} = \frac{g_3(\eta)}{\sqrt{H}} \quad (71)$$

$$\bar{\tau}_{yz} = \frac{g_3(\eta^{-1})}{\sqrt{H}} \quad (72)$$

where

$$g_3(\eta) = \frac{\pi^3 f_5(\eta)}{\sqrt{f_1(\eta)}} \quad (73)$$

Equation (71) is plotted in Fig. 19 for a few values of η , and the function $g_3(\eta)$ is presented in Fig. 20.

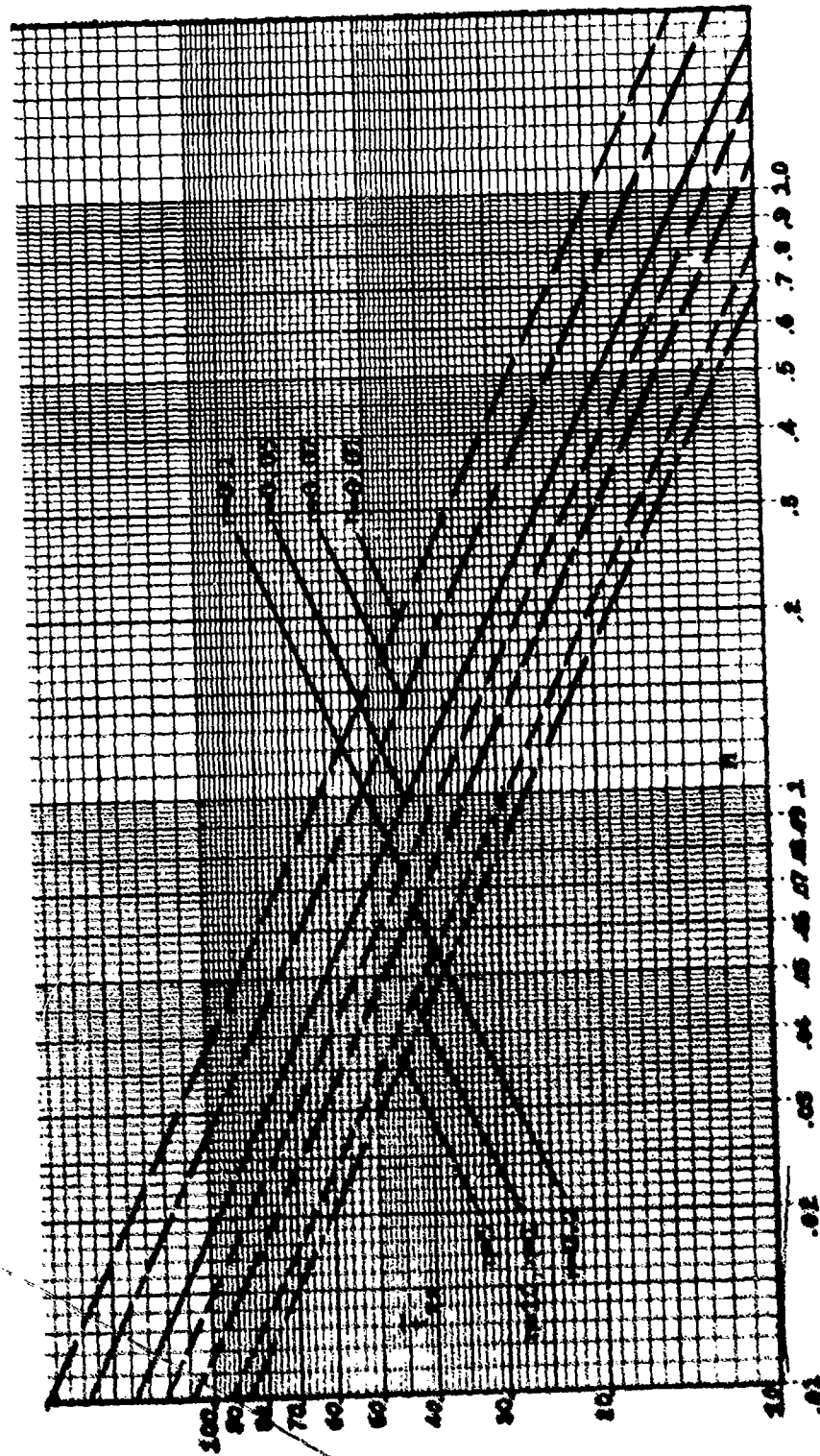


Figure 19. Edge shear stress curves for simply supported rectangular orthotropic plates.

3

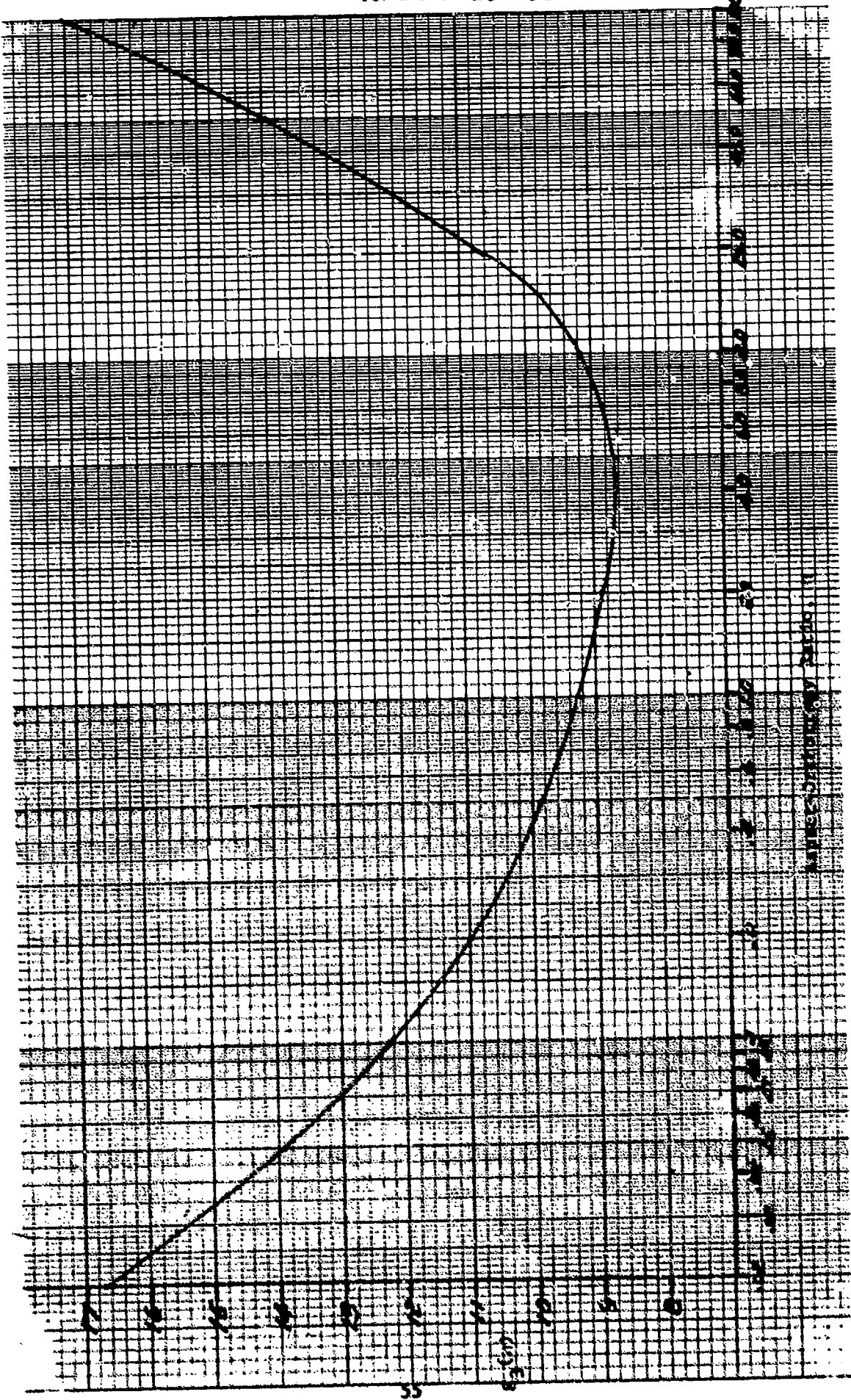


Figure 20. Function of aspect-orthotropy ratio η for shear stress curve of simply supported plate.

III. IMPACTS BY SMALL IMPACTORS

In this section, approximate equations for predicting the peak strain response of simply supported beams and plates to impacts by small impactors are derived. The accuracy of these equations is demonstrated by comparison with experimental results and with the Timoshenko solution.

A. Simply Supported Beam

1. Approximate Analysis

It has been observed in experiments and in calculations of the Timoshenko solution that for the case of small impactors (mass ratio M greater than about 2), the interaction between beam and impactor is a single, sudden blow of short duration compared to, say, the fundamental period of vibration of the beam. This is quite different from the large impactor case where multiple impacts occur. By assuming that the beam does not appreciably deflect during the short period of contact and by making a few other approximations, we may derive a relation which is useful in generating design curves.

The assumption that the beam does not deflect during contact is equivalent to assuming that the impactor is much less massive than the beam, which may thus be treated as a semi-infinite body. An approximate solution for the contact force during the elastic impact of a spherical impactor against a flat semi-infinite body has been calculated by Hunter [9] as

$$P = \begin{cases} P \sin \xi t & 0 < t < \pi/\xi \\ 0 & t > \pi/\xi \end{cases} \quad (74)$$

where

$$P = 1.068 v m_2 \xi \quad (75)$$

$$\xi = 0.9768 \left(\frac{v k_2^2}{m_2} \right)^{1/5} \quad (76)$$

The response of a simply supported beam to a centrally applied transverse dynamic load of the general form of Eq. (74) is derived in Appendix N. The maximum deflection and bending strain occur at midspan at a time about one-quarter of the fundamental period after impact. The peak strain may be expressed as

$$\epsilon_{\max} = \frac{PLh}{EI} f(\beta) \quad (77)$$

where

$$f(\beta) = \frac{1}{\pi^2} \sum_{i=1,3,5}^{\infty} \frac{2\beta}{\beta^2 - i^4} \cos \frac{i^2 \pi}{2\beta} \quad (78)$$

and

$$\beta = \frac{\xi}{\omega_1} \quad (79)$$

$$= \frac{1}{2} \left(\frac{\text{fundamental period of beam}}{\text{contact force duration}} \right)$$

Substitution of the approximate value of ξ given in Eq. (76) into Eq. (79) yields an approximate value for β .

$$\beta = (0.09897) \left(\frac{L^2}{a} \right) \left(\frac{vk_3^2}{m_2} \right)^{1/5} \quad (80)$$

This quantity may be expressed in terms of the dimensionless parameters previously derived as

$$\beta = (0.1564) \left(\frac{M^2}{\lambda_b} \right)^{1/5} \quad (81)$$

where M and λ_b are defined in Eqs. (3) and (53), respectively.

By substituting for P and β into Eq. (77) according to Eqs. (75) and (76), and recalling the definition of generalized strain, Eq. (12) we obtain

$$\bar{\epsilon} = 1.068 \pi^2 f(\beta) \frac{\beta}{M} \quad (82)$$

This result may itself be used to generate a series of design curves by plotting $\bar{\epsilon}$ vs. M for different values of β , however, this equation may be further simplified as demonstrated below.

Note that Eq. (82) shows a strong dependence of the generalized strain $\bar{\epsilon}$ on both the mass ratio M and the parameter β . Also, observe that for a constant value of β , $\bar{\epsilon}$ is inversely proportional to M , rather than \sqrt{M} as for the case of large impactors. This suggests that for small impactors the peak strain is related to the momentum of the impactor, rather than to its kinetic energy as for large impactors. That is, large- M cases are governed by the impulse exerted by the impactor, whereas small- M cases are characterized by the work done on the beam.

The influence of the value of the parameter β on the generalized strain $\bar{\epsilon}$ can be estimated by taking the limit of Eq. (82) as β becomes large.

In Table V, calculated values of $f(\beta)$ are presented (see Appendix D). Examination of this table reveals that, as β increases, the quantity $\sqrt{\beta} f(\beta)$ approaches the value 0.12412. Observe also that, for $\beta > 7$, $\sqrt{\beta} f(\beta)$ never differs from this value by more than 2%. Since most practical problems satisfy the condition $\beta > 7$, we can assume with little inaccuracy that

$$\sqrt{\beta} f(\beta) \approx 0.1241.$$

TABLE V

COMPUTER-CALCULATED VALUES OF $f(B)$

B	$f(B)$	$\sqrt{B} f(B)$
3.0	0.06466	0.11200
7.0	0.04590	0.12145
10.0	0.03903	0.12342
15.0	0.03190	0.12356
20.0	0.02780	0.12432
30.0	0.02264	0.12402
50.0	0.01755	0.12408
80.0	0.01388	0.12414
100.0	0.012413	0.12413
150.0	0.010132	0.12412
200.0	0.008777	0.12413
300.0	0.007166	0.12412
500.0	0.005551	0.12412

Substitution into Eq. (82) yields

$$\frac{\bar{\epsilon}}{\sqrt{\beta}} = \frac{1.308}{M} \quad (83)$$

or, defining a new generalized strain for the small impactor case as

$$\epsilon^* \equiv \frac{\bar{\epsilon}}{\sqrt{\beta}} \quad (84)$$

we then have

$$\epsilon^* = \frac{1.308}{M} \quad (85)$$

This simplified equation may be used as a design curve for the case of small impactors by plotting ϵ^* vs. M . In Fig. 21, such a curve is compared with the experimental data recorded in Appendix E. In general the experimentally determined values of ϵ^* are roughly 60% lower than those predicted by Eq. (85). Note, however, that the band of experimental points on this graph form a relatively narrow band; for any value of M , the variation in ϵ^* is at most $\pm 25\%$ (at about $M = 6$) and much less for the higher range of M (greater than about 10). This variation in ϵ^* is much smaller than the variation in $\bar{\epsilon}$ alone, for the same data. Also, the slope of this band is very close to that of the curve corresponding to Eq. (85). This suggests that the locus of the experimental data plotted in these particular coordinates may itself be useful as a design curve. We may conclude that Eq. (85), while not accurate, is significant in that it serves to identify the form of the relationship among the several parameters governing beam response to impacts by small masses.

2. Timoshenko Solution

Also included in Fig. 21 are several points corresponding to calculations using the Timoshenko solution; data from these calculations are summarized in Table VI. Note that these points form a very narrow band, the

TABLE VI

CALCULATIONS USING TIMOSHENKO

SOLUTION FOR LARGE MASS RATIO M

Beam Mass, Dimensions, and Material	Mass Ratio, $M=m_1/m_2$	Impact Velocity, v (m/sec)	Contact Stiffness, k_2 (N/m ^{3/2})	Generalized Strain, $\bar{\epsilon} = \epsilon a^2/hv$	$\frac{\bar{\epsilon}}{\sqrt{8}}$
0.389 kg 197 x 16 x 16 mm steel	27.7	8.72	2.466×10^{10}	0.1807	0.0405
	27.0	6.37	2.415×10^{10}	0.1782	0.0416
	"	13.17	"	0.1894	0.0412
	13.84	8.72	"	0.2835	0.0734
	"	12.19	"	0.2909	0.0728
	"	8.72	1.233×10^{10}	0.2557	0.0757
	"	17.43	2.466×10^{10}	0.2999	0.0720
	"	8.72	1.744×10^{10}	0.2696	0.0744
	6.86	5.49	2.416×10^{10}	0.4124	0.1287
	"	8.53	"	0.4240	0.1266
	3.54	6.38	"	0.5727	0.2013
	"	9.20	"	0.5865	0.1984
0.389 kg, steel 394 x 8 x 16 mm	13.84	8.72	2.466×10^{10}	0.2502	0.0322
0.389 kg, steel 394 x 16 x 16 mm	27.7	8.72	"	0.2703	0.0361
	6.92	8.72	"	0.3172	0.0559
0.389 kg, steel 197 x 8 x 32 mm	13.84	8.72	"	0.2163	0.0789
0.1943 kg, steel 197 x 8 x 16 mm	6.92	8.72	"	0.4324	0.1192

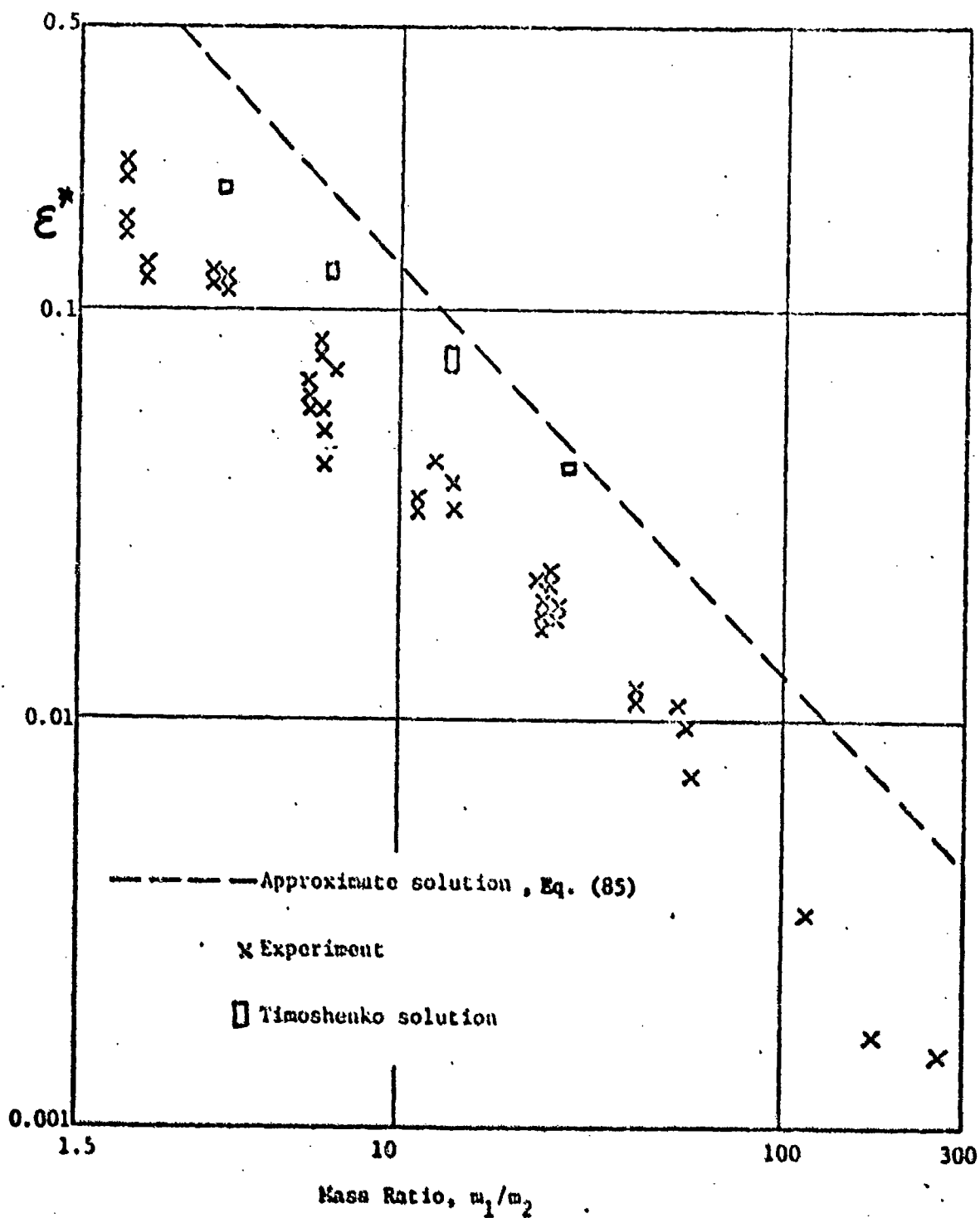


Figure 21. Generalized strain ϵ^* vs. mass ratio M for impacts of simply supported beams by small impactor.

variation being less than $\pm 5\%$; again, the variation in c^* for the same data is much larger. In addition, the band of points is much closer to the curve corresponding to Eq. (85) than are the experimental points; these points lie only 15 to 45% below the curve and appear to approach the curve as M increases. The closeness of these results implies that the lack of agreement between Eq. (85) and the experimental data is not only due to the approximations used in deriving the equation. Apparently, there are additional effects which significantly influence beam response to impacts by small masses which are not accounted for even in the powerful Timoshenko solution. Several researchers have modified the basic solution to include some of these effects, but these more involved models are too cumbersome for the development of an impact design curve, since for each effect considered, another parameter (or possibly several) must be introduced. Such complications are surely justified when one is analyzing a specific impact problem, but are of little assistance when one is designing a structure to resist potential impacts due to a range of masses, velocities, materials, etc.

B. Simply Supported Plate

In this section is developed a design curve for predicting the response of a simply supported plate to impact by a small mass using the same approach as applied above to a beam.

1. Approximate Analysis

As in the case of the beam, we assume that the plate does not appreciably deflect during the short period when the impactor is actually in contact with the plate. Again, this assumption is equivalent to supposing that the impactor is much less massive than the plate. Thus, the contact force is roughly given by the approximate solution for a sphere elastically striking a flat semi-infinite body, Eqs. (74), (75), and (76).

The dynamic response of a simply supported plate to a central transverse load $F(t)$ is given by [6]

$$W = \frac{4}{\pi^2} \sum_{m=1}^{\infty} \sum_{n=1}^{\infty} \frac{(-1)^{(m+n-2)/2}}{\omega_{mn}} \sin \frac{m\pi x}{a} \sin \frac{n\pi y}{b} \int_0^t F(\tau) \sin \omega_{mn}(t-\tau) d\tau \quad (86)$$

For a thin specially orthotropic plate, the natural frequencies are given by [10]

$$\omega_{mn}^2 = \frac{\pi^4}{\rho h} \left[D_{11} \frac{m^4}{a^4} + 2(D_{12} + 2D_{66}) \frac{m^2 n^2}{a^2 b^2} + D_{22} \frac{n^4}{b^4} \right] \quad (87)$$

If we again assume that

$$D_{12} + 2D_{66} = \sqrt{D_{11} D_{22}} \quad (43)$$

then we have

$$\omega_{mn} = \omega_{11} \frac{m^2 + \eta n^2}{1 + \eta}$$

in which

$$\omega_{11} = \frac{\pi^2}{a^2} \left(\frac{D_{11}}{\rho h} \right)^{1/2} (1 + \eta) \quad (88)$$

Substitution of the assumed form of the contact force, Eq. (74), into Eq. (86) and integration yields

$$w = \frac{4}{\pi^2 \omega_{11}} \sum_{m=1}^{\infty} \sum_{n=1}^{\infty} \frac{1 + \eta}{m^2 + \eta n^2} (-1)^{\frac{m+n-2}{2}} \sin \frac{m\pi x}{a} \sin \frac{n\pi y}{b} \frac{2P}{\xi(1 - \omega_{mn}^2/\xi^2)} \sin \omega_{mn}(t + \pi/\xi) \cos \frac{\omega_{mn} \pi}{2\xi} \quad (89)$$

In the corresponding formula for the beam, all terms in the series reach their maximum values at exactly the same time, due to a simple relationship which exists among the natural frequencies (see Appendix D, Eq. (D1)).

In the present case of the plate, the terms in Eq. (89) do not, in general, reach their peak values simultaneously; however, we can estimate an upper bound for the deflection (and also the bending strain) by letting

$$\sin \omega_{mn}(t + \pi/\xi) = 1 \quad (90)$$

for all m and n .

The maximum strain in the x -direction due to bending occurs at the center of the plate,

$$\epsilon_x = -\frac{h}{2} \frac{\partial^2 w}{\partial x^2} \bigg|_{x=\frac{a}{2}, y=\frac{b}{2}} \quad (91)$$

so that the upper bound on the strain is given by

$$\epsilon_{x,\max} = \frac{4Pha}{\pi^2 D_{11} b} \frac{1}{(1+\eta)^2} \sum_m \sum_n \frac{m^2}{A_{mn}} \frac{\beta_p}{\beta_p^2 - A_{mn}^2} \cos \frac{\pi A_{mn}}{2\beta_p} \quad (92)$$

where

$$\beta_p = \xi/\omega_{11} \quad (93)$$

and

$$A_{mn} = \frac{m^2 + \eta n^2}{1+\eta} \quad (94)$$

Substitution of the approximate value of ξ given in Eq. (76) into Eq. (93) yields an approximate value for β_p , given by

$$\beta_p = 0.09897 \left(\frac{a^2}{1+\eta} \right)^{1/5} \sqrt{\frac{\rho h}{D_{11}}} \left(\frac{vk_2^2}{m_2^2} \right) \quad (95)$$

This quantity may be expressed in terms of dimensionless parameters previously derived as

$$\beta_p = 0.1564 \left(\frac{H^2}{\lambda_p (1+\eta)^4} \right)^{1/5} \quad (96)$$

Now, if we substitute for P in Eq. (92) according to Eq. (75), we obtain

$$\epsilon_{x, \max} = 4(1.068)hv \sqrt{\frac{\rho h}{D_{11}}} \left(\frac{1}{1+\eta} \right) \left(\frac{\beta_p}{M} \right)$$

$$\sum_m \sum_n \frac{m^2}{A_{mn}} \frac{\beta_p}{\beta_p^2 - A_{mn}^2} \cos \frac{\pi A_{mn}}{2\beta_p} \quad (97)$$

Finally, if we define the generalized strain for impact of a simply supported plate by a small mass as

$$\epsilon_x^* = \frac{\epsilon_{x, \max} \sqrt{D_{11}/\rho h}}{4(1.068)hv \beta_p g(\beta_p, \eta)} \quad (98)$$

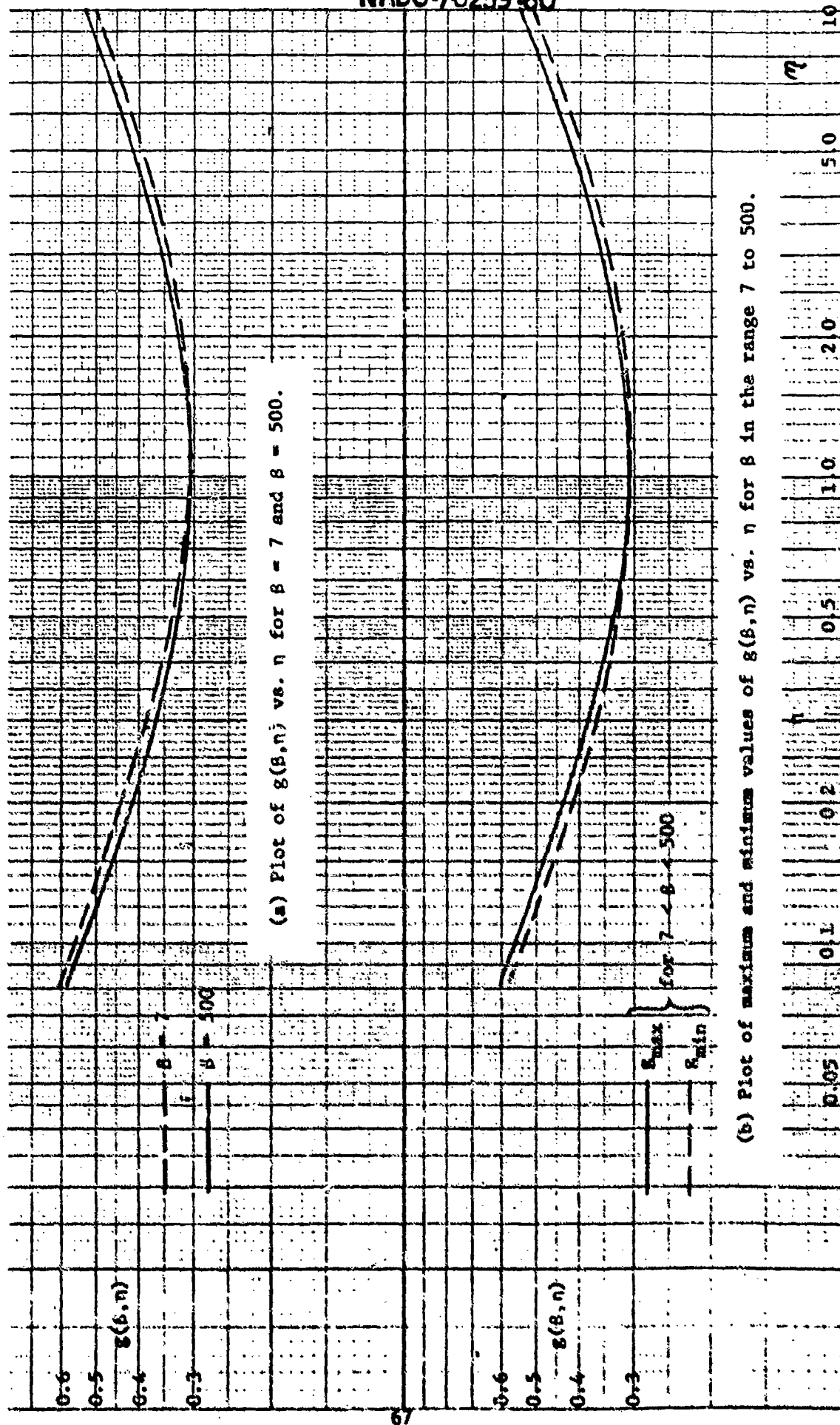
where

$$g(\beta_p, \eta) = \frac{1}{1+\eta} \sum_m \sum_n \frac{m^2}{A_{mn}} \frac{\beta_p}{\beta_p^2 - A_{mn}^2} \cos \frac{\pi A_{mn}}{2\beta_p} \quad (99)$$

then the equation for the design curve according to this approximate solution is

$$\epsilon_x^* = 1/M \quad (100)$$

Note that the function $g(\beta_p, \eta)$, plotted in Fig. 22, is practically independent of the value of β_p , at least for realistic values of β_p ($\beta_p > 7$). In Fig. 22a, $g(\beta_p, \eta)$ is plotted over η for two widely different values of β_p , 7 and 500; the two curves are almost the same. In Fig. 22b, the maximum and minimum values of $g(\beta_p, \eta)$ for β_p in the range $7 \leq \beta_p \leq 500$ are plotted for each value of η ; again, the two curves are quite close, indicating that $g(\beta_p, \eta)$ does not vary much with β_p .



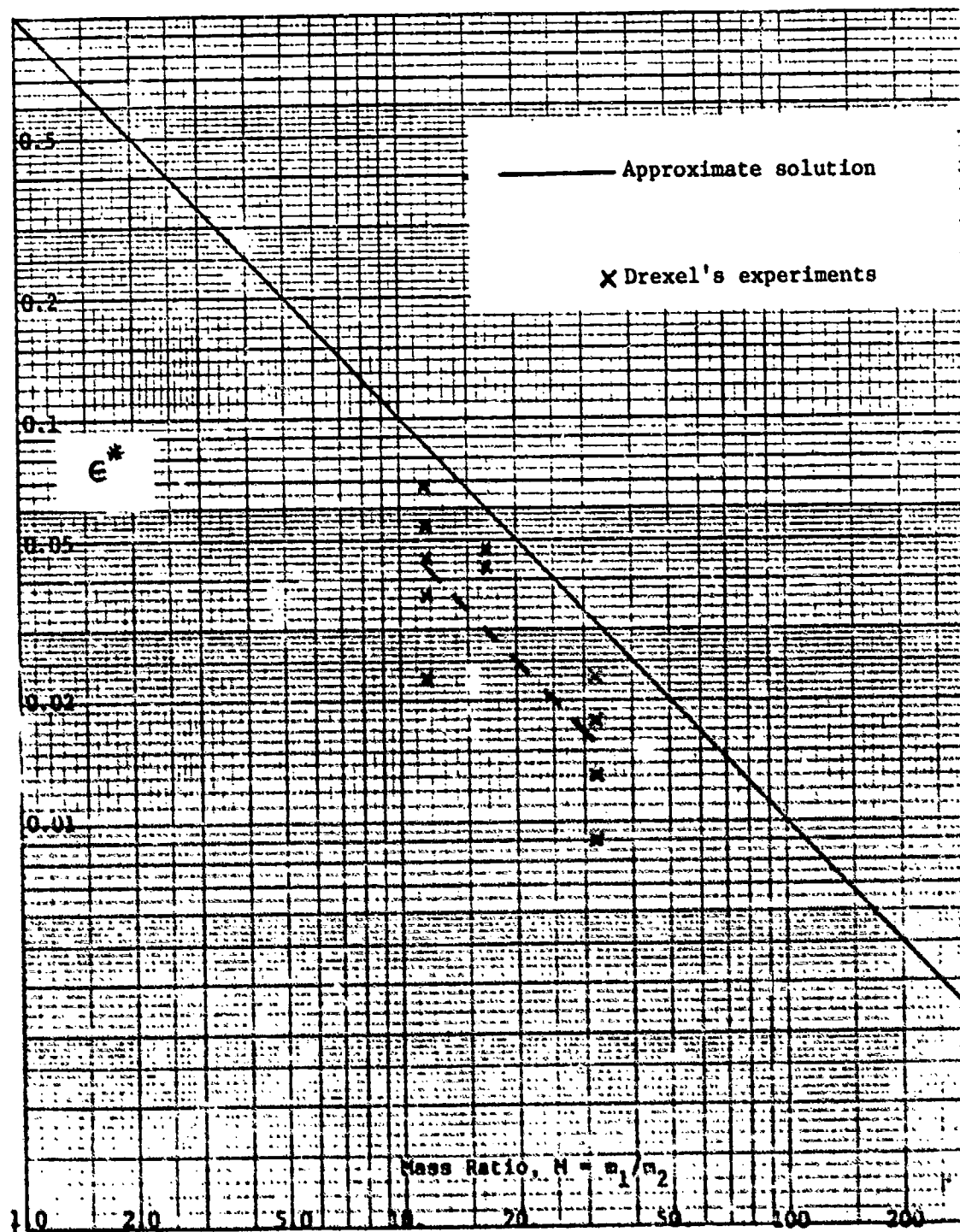


Figure 23. Strain Curve for Impact of Simply Supported Rectangular Plate by a Small Mass.

2. Comparison with Experimental Results

In Fig. 23, the design curve for impact of plates by small masses is presented along with the results from experiments performed at Drexel. Two graphite-epoxy plates which were also used in the large impactor experiments, F1 and F2, were impacted by aluminum projectiles. These experiments were performed using an air gun with the projectile velocity recorded by a photo-diode system. Data from these experiments are tabulated in Appendix E. As can be seen in Fig. 23, the agreement between the theoretical design curve and the design curve based on experimental results is of the same order as in the large impactor case; that is, the experimental curve is about 40% below the theoretical curve and has approximately the same slope.

Also tabulated in Appendix E are experimental data found in Schwieger [11]. These experiments were performed on a square Duraluminum (AlCuMg1) plate, 550 x 550 x 4.97 mm, centrally impacted by steel spheres of 20- and 30- mm radius. These data, when plotted in c^* vs. N coordinates, do not compare well with either the Drexel experiments or the theory. One explanation of this discrepancy lies in the size of the plate tested by Schwieger. In the Drexel experiments, the ratio of the plate span to thickness (L/h) has a value of 18 whereas in the experiments performed by Schwieger, this ratio has a value of 110. Thus, according to Zener [12], the response of the plate used by Schwieger is governed by membrane and wave propagation effects. Since these effects are not treated by the current theory, the data from Schwieger are not included on the design curve.

IV. DESIGN PROCEDURE

In this section, procedures are recommended for using the design curves presented in this report and for constructing new design curves for structures not treated here based either on analytical calculations or on experimental data. It is emphasized that these design curves are limited to predicting only the maximum structural response to low-velocity impact.

A. Use of Design Curves in This Report

The design curves in this report predict the peak bending strain in simply supported and clamped plates impacted by large impactors, and in simply supported beams and plates impacted by small impactors. Also, in [1], simply supported beams impacted by large masses were treated in detail. Methods for the use of each of these design curves will be discussed separately here.

1. Simply Supported Beam

Design curves for simply supported beams impacted by large impactors and by small impactors are repeated here for convenience (Figs. 24 and 25, respectively). In each case, we have selected a design curve fit by eye to the experimental results as the one we will use.

The first step in using these curves is to compute the mass ratio

$$M = \frac{m_1}{m_2} = \frac{\text{structural mass}}{\text{impactor mass}} \quad (101)$$

If M is less than 2, the impact case falls into the domain of large impactors; if $M > 2$, small impactors.

a. Large Impactors

From Fig. 24, read the value of the generalized strain $\bar{\epsilon}$ corresponding to the value of M . Then, using this value $\bar{\epsilon}$, compute the maximum impact strain,

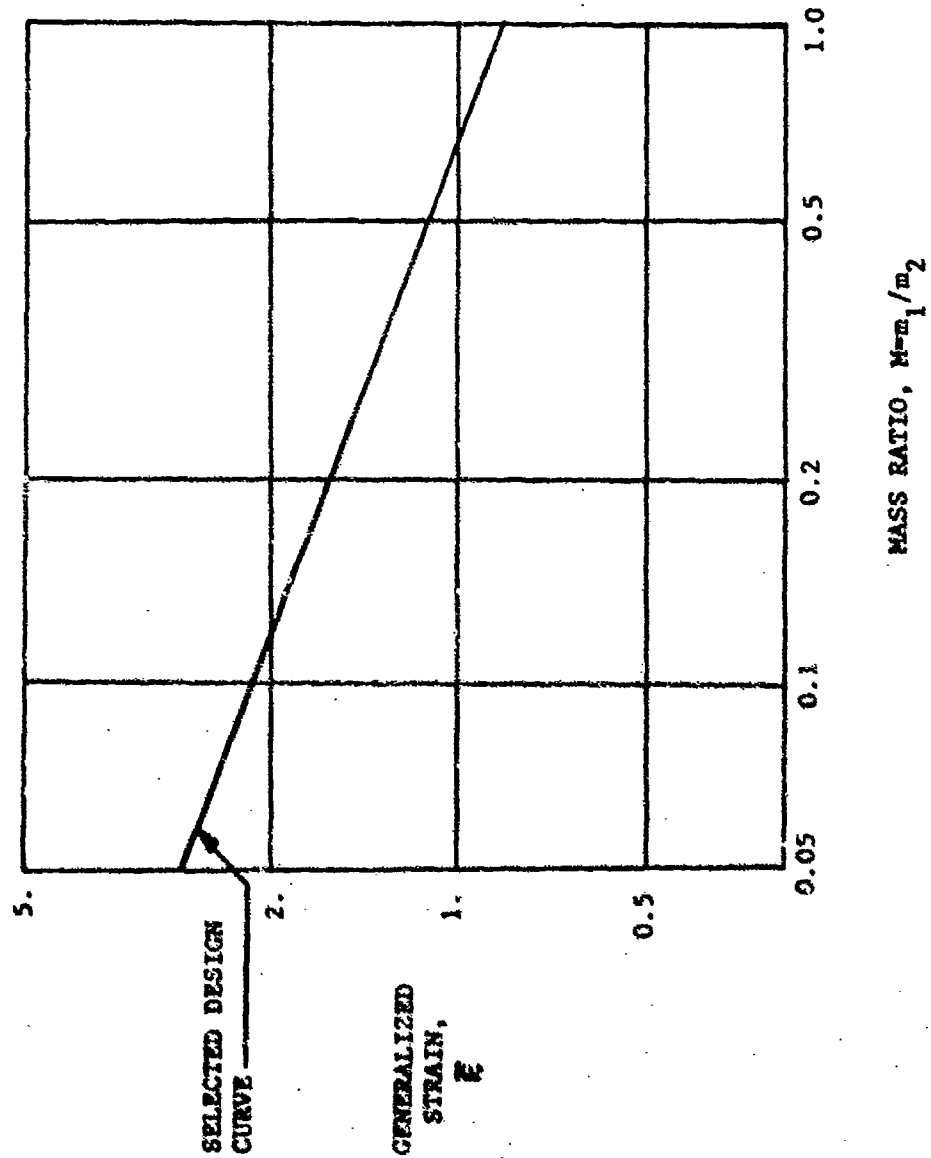


Figure 24. Selected design curve for impacts of simply supported beams by large impactors.

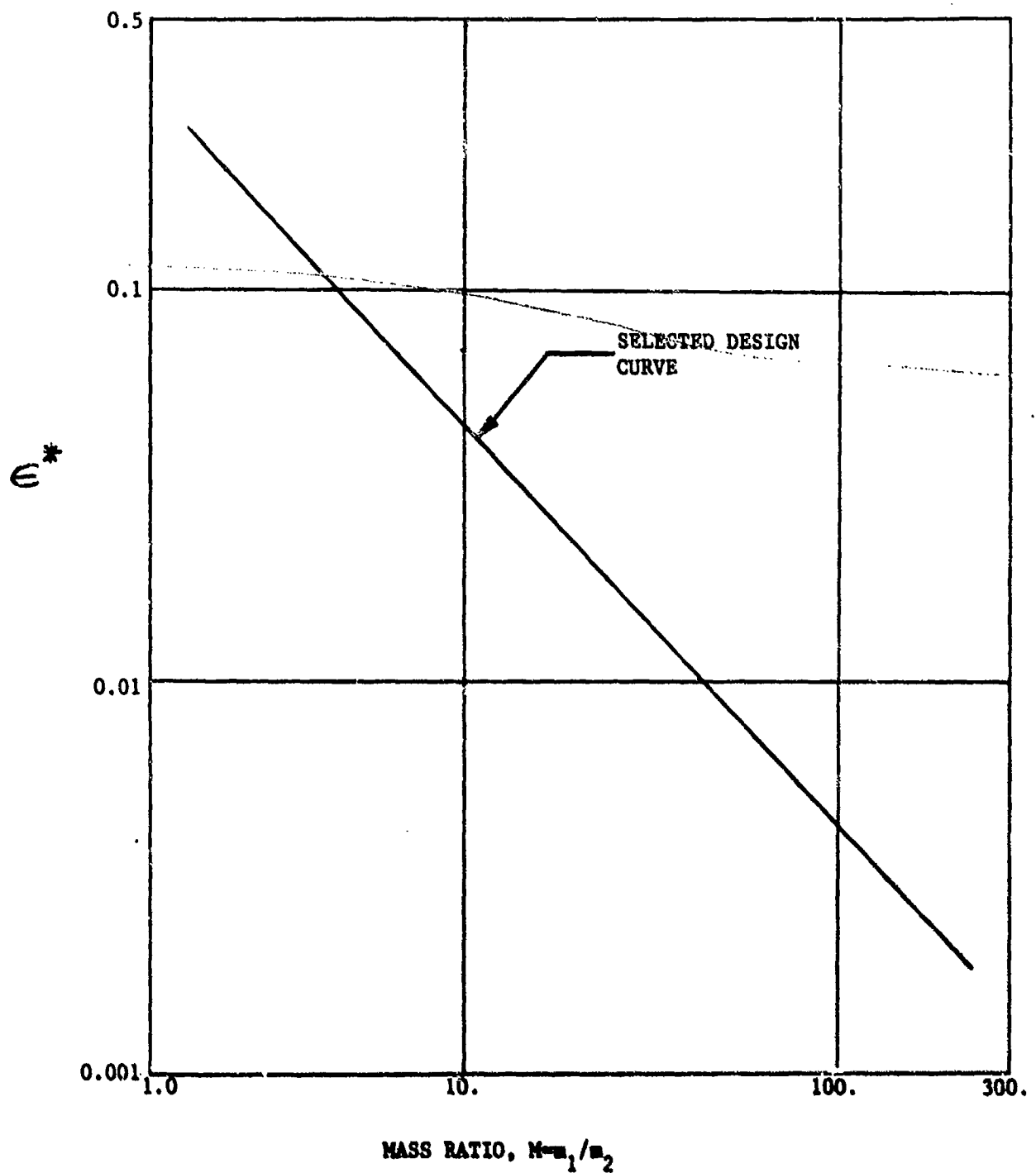


Figure 25. Selected design curve for impacts of simply supported beams by small impactors.

$$\epsilon_{\max} = \bar{\epsilon} \frac{hv}{kc} \quad (102)$$

where

h = beam depth

k = radius of gyration of beam cross-section

v = impact velocity

$c = \sqrt{E/\rho}$ = speed of flexural waves in the beam

The use of this curve will be illustrated by an example.

Example #1

For a simply supported steel (density, 7.9 g/cm^3) beam of rectangular cross-section with dimensions $L \times h \times b = 500 \times 25 \times 20 \text{ mm}$ impacted at 10 m/s by a mass of 4.0 kg , we have

$$M = \frac{m_1}{m_2} = \rho \frac{Lbh}{m_2} = \frac{(7900)(.50)(0.025)(0.020)}{4.0} \\ = 0.494$$

From Fig. 24, the value of $\bar{\epsilon}$ corresponding to $M = 0.494$ is $\bar{\epsilon} = 1.20$. Then, by Eq. (102), we have

$$\epsilon_{\max} = (1.20) \frac{(0.025)(10)}{\left(\frac{0.025}{\sqrt{12}} \frac{210 \times 10^9}{7900}\right)^{1/2}} \\ = 0.0081$$

b. Small Impactors

From Fig. 25, read the value of the generalized strain ϵ^* corresponding to the value of M . Then compute the maximum of impact strain,

$$\epsilon_{\max} = \epsilon^* \sqrt{\beta} \frac{hv}{ck} \quad (103)$$

$$\text{where } \beta = (0.09897) \frac{L^2}{ck} \left(\frac{vk_2^2}{m_2} \right)^{1/5}$$

and k_2 = Hertzian contact stiffness.

Example #2

Consider the beam of Example #1 impacted by a steel sphere of radius 20 mm at 20 m/s. Then, by Eq. (101), we have

$$M = \frac{m_1}{m_2} = \frac{(7900)(0.50)(0.025)(0.020)}{\frac{4}{3}\pi(0.020)^3(7900)}$$

$$= 7.46$$

From Fig. 25, the value of ϵ^* corresponding to $M = 7.46$ is $\epsilon^* = 0.060$. The Hertzian contact stiffness is

$$k_2 = \frac{4}{3\pi} \sqrt{R} \left[\left(\frac{1-\nu^2}{E\pi} \right)_{\text{beam}} + \left(\frac{1-\nu^2}{E\pi} \right)_{\text{impactor}} \right]^{-1}$$

$$= \frac{4}{3\pi} \sqrt{0.020} \left[\frac{1-0.3^2}{\pi 210 \times 10^9} \times 2 \right]^{-1}$$

$$= 2.176 \times 10^{10} \text{ N/m}^{3/2}$$

so that

$$\beta = (0.09897) \sqrt{\frac{(0.50)^2}{\frac{210 \times 10^9}{7900} \frac{0.025}{\sqrt{12}}}} \left[\frac{20(2.176 \times 10^{10})^2}{0.265^2} \right]^{1/5}$$

$$= 28.1$$

Therefore, the maximum bending strain is

$$\epsilon_{\text{max}} = (0.060) \sqrt{28.1} \sqrt{\frac{(0.025)(20)}{\frac{210 \times 10^9}{7900} \frac{(0.025)}{\sqrt{12}}}}$$

$$= .00427$$

2. Simply Supported and Clamped Plates

The procedures for using the design curves for rectangular plates is similar to those outlined above for the beam. For convenience, we have repeated here the design curves for simply supported and clamped plates impacted by large impactors (Figs. 26 and 27), and for simply supported plates impacted by small impactors (Fig. 28). The first step in using any of these curves is to compute the mass ratio M according to Eq. (101) and the aspect-orthotropy ratio,

$$\eta = \left(\frac{a}{b}\right)^2 \sqrt{D_{22}/D_{11}} \quad (104)$$

where a and b are the plate dimensions in the x and y directions. For the plates treated here, impact cases in which $M < 4$ fall into the domain of large impactors, while cases where $M > 4$ are in the domain of small impactors. The use of the design curves in each of these domains will be discussed separately here.

a. Large Impactors

The procedures for the clamped and simply supported plates are the same but different curves are employed. For simply supported plates, read $g_1(\eta)$ from the lower curve of Fig. 4 and $\bar{\epsilon}$ corresponding to the value of M from Fig. 26; for clamped plates, read $g_2(\eta)$ from the upper curve of Fig. 4 and $\bar{\epsilon}$ from Fig. 27. Then, the maximum strain may be computed from the formula

$$\epsilon_{x,\max} = g_1(\eta) \bar{\epsilon} \frac{vh}{\sqrt{D_{11}}} \quad (105)$$

where

v = impact velocity

h = plate thickness

ρ = plate density

D_{11} = plate flexural rigidity

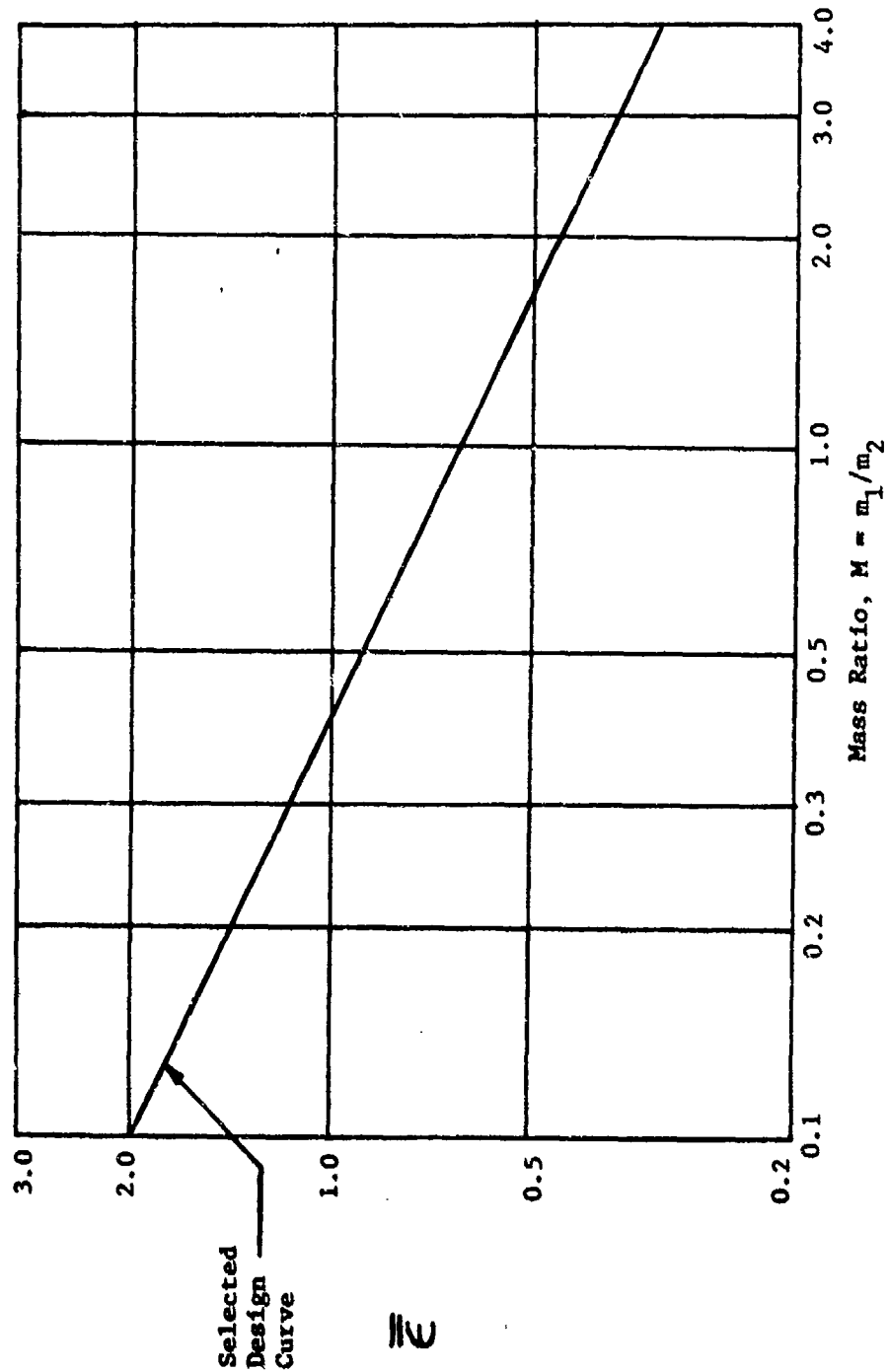


Figure 26. Selected Design Curve for Simply Supported Plates Impacted by Large Impactors.

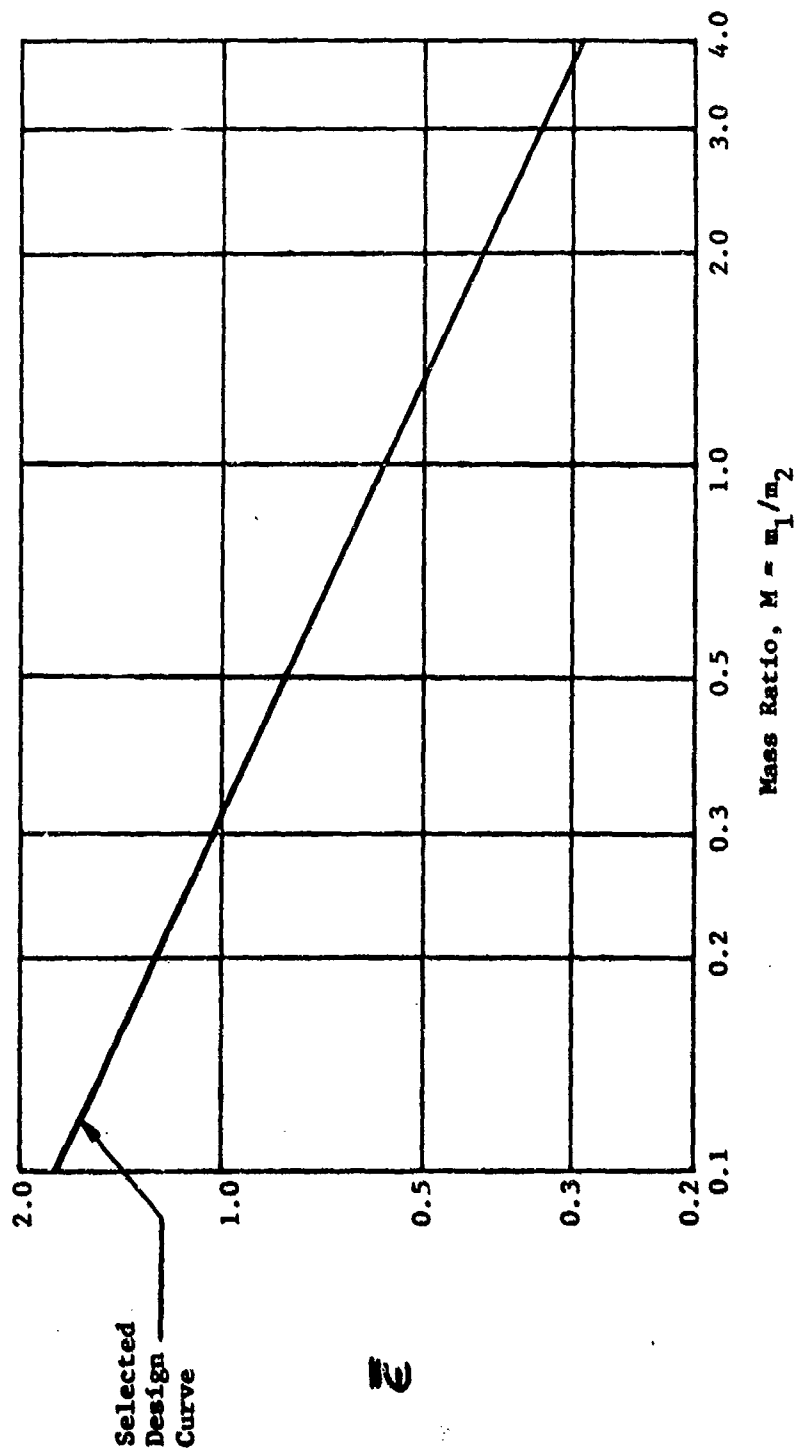


Figure 27. Selected Design Curve for Clamped Plate Impacted by Large Impactors.

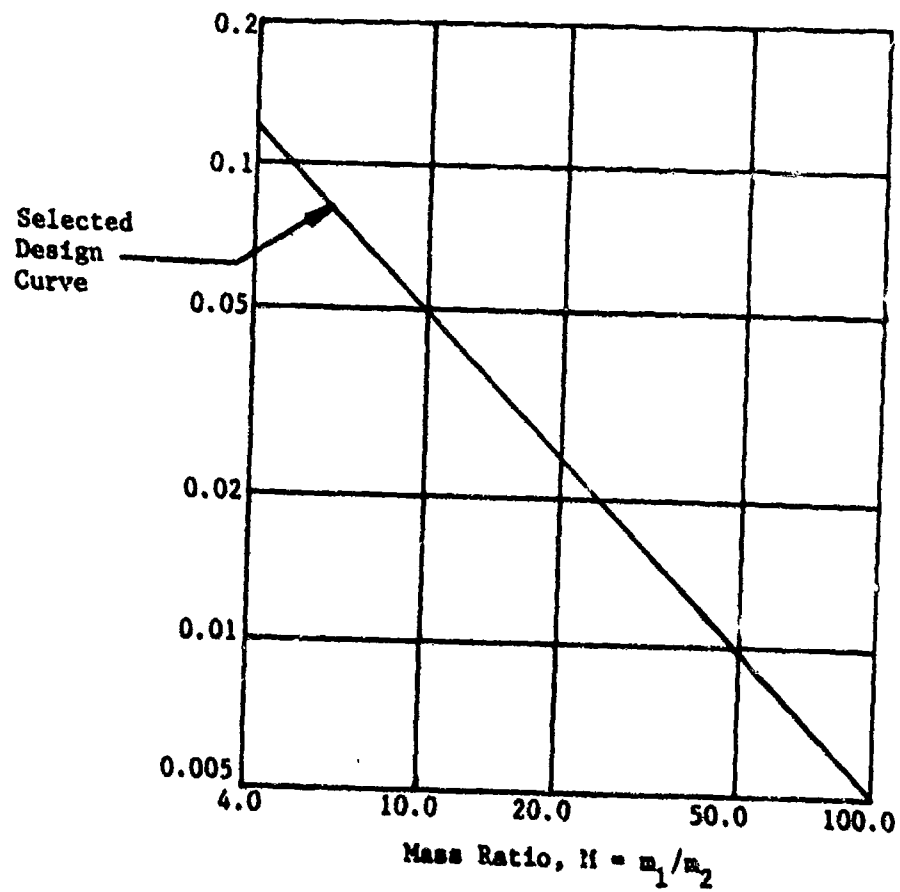


Figure 28. Selected Design Curve for Impact of Simply Supported Rectangular Plate by a Small Impactor.

This procedure will be illustrated by an example.

Example #3

For a rectangular simply supported plate with the following properties

$$\begin{aligned} D_{11} &= 680. \text{ N-m} & h &= 7 \text{ mm} \\ D_{22} &= 2490. \text{ N-m} & \rho &= 1.7 \text{ g/cm}^3 \\ a &= 170 \text{ mm} & E &= 8.96 \text{ Gpa} \\ b &= 350 \text{ mm} & \nu &= 0.3 \end{aligned}$$

impacted by a projectile with the following properties

$$\begin{aligned} R &= 25 \text{ mm} & \nu &= 0.33 \\ m_2 &= 1.42 \text{ kg} & v &= 3.0 \text{ m/s} \\ E &= 2.1 \times 10^2 \text{ Gpa} \end{aligned}$$

we first compute the values of the mass ratio and aspect-orthotropy ratio

$$M = 0.5 \qquad \eta = 0.451$$

From Fig. 4, we find $g_1(0.451) = 0.26$, and from Fig. 26, $\bar{\epsilon} = 0.91$ corresponds to $M = 0.5$. The maximum strain in the x-direction is

$$\begin{aligned} \epsilon_{x,\max} &= (0.26)(0.91) \left[\frac{(3.0)(0.007)}{680} \right]^{1/2} \\ &= 6.57 \times 10^{-4} \end{aligned}$$

b. Small Impactors

The design curve for impact of plates by small impactors can handle only simply supported boundary conditions. To use the design curve, read the value of generalized strain ϵ_x^* from Fig. 28, and the value of $g(\beta_p, \eta)$ from Fig. 22. (Note that $g(\beta_p, \eta)$ does not depend significantly on β_p for $\beta_p > 7$). Then, the maximum strain may be computed from the formula

$$\epsilon_{x,\max} = \epsilon_x^* 4(1.068) g(\beta_p, \eta) \beta_p \sqrt{\frac{h\nu}{D_{11}/\rho h}} \quad (106)$$

where

$$\beta_p = 0.09897 \frac{a^2}{1+\eta} \sqrt{\frac{\rho h}{D_{11}}} \left(\frac{v k_2^2}{m_2^2} \right)^{1/5}$$

This procedure is illustrated by an example.

Example #4

Consider the same impact situation as in Example #3 but change the impactor mass to $m_2 = 0.035$ kg. Now we have $M=20$, a small impactor case. From Fig. 28, we read $\epsilon_x^* = 0.025$; and from Fig. 22, $g(\beta_p, 0.451) = 0.35$. Computing β_p , we get

$$\begin{aligned} \beta_p &= (0.09897) \frac{(0.170)}{1+0.451} \sqrt{\frac{(1700)(0.007)}{680}} \\ &\quad \cdot \left[\frac{(3.0)(2.008 \times 10^9)^2}{(0.035)^2} \right]^{1/5} \\ &= 6.54 \end{aligned}$$

Therefore, the maximum strain is

$$\begin{aligned} \epsilon_{x,max} &= 4(0.025)(1.068)(0.35)(6.54) \frac{(0.007)(3.0)}{\sqrt{\frac{680}{(1700)(0.007)}}} \\ &= 6.79 \times 10^{-4} \end{aligned}$$

B. Construction of New Design Curves by Experiments

For beams and plates with boundary conditions different from those considered in this report, design curves may also be constructed based on impact experiments. For these structures, the parameters governing the impact response have the same form, but the relationships (and thus the design curves)

are different. For still other structures (e.g., shells, rods), new parameters may have to be defined.

1. Impact Strain Curves

To construct new design curves for large impactors, one may perform a series of impact experiments and measure the maximum bending strain which occurs in the structure during each impact. Then, compute the value of the generalized strain according to the appropriate formula:

$$\bar{\epsilon} = \epsilon_{\max} \frac{c_b k}{h v} \quad \text{for beams}$$

$$\bar{\epsilon}_x = \epsilon_{y,\max} \frac{c_p k}{h v} \quad \text{for plates}$$

Plot one point for each impact in $\bar{\epsilon}$ vs. M coordinates, Logarithmic scales are most convenient. Finally, estimate a curve to fit these points. This design curve may then be used to predict the response of similar structures having different dimensions subject to various impact conditions, as described in Section A above.

2. Critical Impact Velocity Curves

In simple impact-to-failure experiments when the strain is not simultaneously measured, all that is determined is the lowest impact velocity (or critical velocity) at which the structure fails. However, this is sufficient to construct a design curve useful in predicting failures due to other impact situations.

For each experiment, the dimensionless critical velocity \bar{v} , defined for plates in Eq. (33) and for beams in Eq. (62), is plotted vs. the mass ratio M . Then these points may be connected to form the design curve.

Note that for different impact conditions, different mechanisms (bending, shear, torsion, etc.) may be responsible for failure; consequently, several design curves may be required, especially to completely describe a series of widely varying impact experiments.

Finally, note that since the contact effects depend on the impact velocity, through a non-linear relation, this approach is not useful in the small impactor domain.

C. Construction of New Design Curves by Analytical Tools

Using analytical methods, design curves for some structures which are not treated in this report may be constructed. We can offer a few suggestions on approaches to follow in order to construct such curves.

1. Design Curves Based on Generalized One-Degree-of-Freedom Model

For impacts of other structures in the large-impactor regime, the generalized one-degree-of-freedom model presented in Section II may be applied. To follow this approach, the equivalent structural stiffness K_1 and the strain-displacement factor d_{12} must be found; these may be either derived from the exact solution of the corresponding static problem or computed numerically using some approximate solution (such as the finite-difference or finite-element methods). Then the equation of the design curve may be derived directly from Eq. (8). For beams, the form of the generalized strain will be the same as in Eq. (12); for plates, the generalized strain defined in Eq. (21) can be employed. For other structures, a new form may have to be defined.

2. Design Curves Based on Impact Calculations

Several dynamic solution methods are available for determining impact response of structures on a problem-by-problem basis. These include the finite-element method (in particular, NASTRAN; see Ref. [1]), Timoshenko-type solution methods (application of this approach to several beam and plate structures is outlined in [5]), and possibly some approximate solutions based on the Timoshenko method (similar to those presented in this report for small impactors). Design curves may be constructed by plotting the results of a few calculations using one of these methods in coordinates of the appropriate generalized strain ($\bar{\epsilon}$ for large impactors, ϵ^* for small impactors) vs. the mass ratio M over the range of M of interest. These plotted points may then be connected to form the design curve.

V. SUMMARY

In this report, a method for generating a design curve which predicts the peak response of a structure subjected to low-velocity impact has been presented. Only a few experiments or analytical calculations are required to construct such a curve for a given type of structure. The importance of such a curve is that all impact cases, involving various impact velocities, structural dimensions, and material properties, fall on the same curve within a variation tolerable to the designer.

To facilitate our study, we have divided all impacts into two regimes, large and small impactors, each of which exhibits different kinematic behavior. Specifically, massive impactors have been observed to produce multiple impacts, the peak response of the structure depending on the initial kinetic energy of the impactor; in contrast, small impactors strike the structure only once, the maximum response being governed chiefly by the impactor's initial momentum and by contact effects at the impact point. These differences in impact response are accounted for in the distinct forms of the design curves for each domain.

Design curves have been developed here for predicting the impact response of simply supported beams and simply supported and clamped-edge anisotropic plates. These curves have been constructed using both results of analytical solutions and data from impact experiments. In addition, detailed procedures have been described for using the design curves presented in this report, as well as for generating new curves for structures not treated here.

VII. REFERENCES

1. Chou, P.C., and Flis, W.J., "Design Curves for Structural Response due to Impact Loading," Report No. NADC-76380-30, Naval Air Development Center, Warminster, Pa. October 1976.
2. Clebsch, A., Theorie de l'elasticite des corps solides, trans. B. de St.-Venant and M. Flamant, Dunod, Paris, 1883.
3. McQuillen, E. J., Llorens, R. E., and Gause, L. W., "Low Velocity Transverse Normal Impact of Graphite-Epoxy Composite Laminates." Report No. NADC-75119-30, Naval Air Development Center, Warminster, Pa., June 1975.
4. Timoshenko, S.P., "Zur Frage nach der Wirkung eines Stosses auf einer Balken," Z. Math. Phys., Vol. 62, 1913, No. 2, p. 198.
5. Eringen, A.C., "Transverse Impact on Beams and Plates," J. Appl. Mech., Vol. 20, 1953, p. 461.
6. Sun, C.T., and Chattopadhyay, S., "Dynamic Response of Anisotropic Plates Under Initial Stress due to Impact of a Mass," Trans. A.S.M.E., J. Appl. Mech., Vol. 42, 1975, p. 693.
7. Whitney, J.M., and Pagano, N.J., "Shear Deformation in Heterogeneous Anisotropic Plates," Trans. A.S.M.E., J. Appl. Mech., Vol. 37, p. 1031.
8. Chou, P.C., and Mortimer, N.W., "Impact Behavior of Polymeric Matrix Composite Materials," Report No. AFML-TT-76-242, Air Force Materials Laboratory, Wright-Patterson AFB, Ohio, December, 1976.
9. Hunter, S.C., "Energy Absorbed by Elastic Waves during Impact," J. Mech. Phys. Solids, Vol. 5, 1957, p. 162.
10. Lekhnitskii, S.G., Anisotropic Plates, trans. S.W. Tsai and T. Cheron, Gordon and Breach, N.Y., 1968.
11. Schwieger, H., "Vereinfachte Theorie des elastischen Biegestosses auf eine dünne Platte und ihre experimentelle Überprüfung," Forsch. Ing.-Wes., Vol. 41, No. 4, p. 122, (1975).
12. Zener, C., "The Intrinsic Inelasticity of Large Plates," Physical Review, Vol. 59, 1941, p. 669.
13. Timoshenko, S. and Woinowsky-Krieger, S., Theory of Plates and Shells, 2nd ed., McGraw-Hill, N.Y., 1959.
14. Ashton, J.E., and Whitney, J.M., Theory of Laminated Plates, Technomic, Stanford, Conn., 1970.

15. Ambartsumyan, S.A., Theory of Anisotropic Plates, trans T. Cheron, Technomic, Stamford, Conn., 1970.
16. Anonymous, Advanced Composites Design Guide, 3rd ed., Air Force Materials Laboratory, Wright-Patterson AFB, Ohio, January 1973.
17. Young, D., "Clamped Rectangular Plates with a Central Concentrated Load," Trans. A.S.M.E., J. Appl. Mech., Vol. 6 1939, p. A-114.
18. Goldsmith, W., Impact, the Theory and Physical Behaviour of Colliding Solids, Edward Arnold, Ltd., London, 1960.

APPENDIX A

STATIC SOLUTION OF A
SIMPLY SUPPORTED ORTHOTROPIC PLATE

In this appendix, we will present the details of the derivation of the constants K_1 and d_{12} for the central transverse impact of a simply supported orthotropic plate. As explained in the main text, these constants are needed for developing the design curve.

The static deflection of such a plate due to an arbitrary load distribution $p(x,y)$ is, according to Timoshenko and Woinowsky-Krieger [13],

$$w(x,y) = \sum_{m=1}^{\infty} \sum_{n=1}^{\infty} \frac{p_{mn} \sin \frac{m\pi x}{a} \sin \frac{n\pi y}{b}}{\frac{m^4 \pi^4}{a^4} D_x + 2H \frac{m^2 n^2 \pi^4}{a^2 b^2} + \frac{n^4 \pi^4}{b^4} D_y} \quad (A1)$$

where

$$H = \nu_y D_x + 2 D_{xy}$$

and

$$p_{mn} = \frac{4}{ab} \int_0^b \int_0^a p(x,y) \sin \frac{m\pi x}{a} \sin \frac{n\pi y}{b} dx dy$$

For a centrally applied point load P ,

$$p_{mn} = \frac{4P}{ab} \sin \frac{m\pi}{2} \sin \frac{n\pi}{2}$$

The maximum deflection occurring at the center of the plate is,

$$W_1 = W\left(\frac{a}{2}, \frac{b}{2}\right) = \sum_{m=1,3,5}^{\infty} \sum_{n=1,3,5}^{\infty} \frac{4Pab}{\pi^4 D_x} \left(\frac{a}{b}\right)^2 \frac{1}{C_{mn}}$$

where

$$C_{mn} = m^4 + 2m^2n^2\left(\frac{a}{b}\right)^2 \frac{H}{D_x} + n^4\left(\frac{a}{b}\right)^4 \frac{D_y}{D_x}$$

We will assume that

$$H = \sqrt{D_x D_y} \quad (A2)$$

so that

$$C_{mn} = m^4 + 2m^2n^2\eta + n^4\eta^2 \quad (A3)$$

where

$$\eta = \left(\frac{a}{b}\right)^2 \sqrt{\frac{D_y}{D_x}} \quad (A4)$$

Therefore, recalling that

$$K_1 = P/w_1$$

we have

$$K_1 = \frac{\pi^4 D_x}{4ab \left(\frac{a}{b}\right)^2 f_1(\eta)} \quad (A5)$$

where

$$f_1(\eta) = \sum_{m=1,3,5}^{\infty} \sum_{n=1,3,5}^{\infty} \frac{1}{C_{mn}} \quad (A6)$$

The tensile strain in the x-direction due to bending is

$$\epsilon_x = -z \frac{\partial^2 w}{\partial x^2}$$

which will have its maximum value at

$$(x, y, z) = (a/2, b/2, h/2)$$

We will derive the relationship between the strain at this point ϵ_2 and the maximum deflection.

$$\epsilon_2 = -\frac{h}{2} \frac{\partial^2 w}{\partial x^2} \bigg|_{x=a/2, y=b/2}$$

$$= \frac{2Ph}{\pi^2 D_x} \left(\frac{a}{b}\right) f_2(\eta)$$

(A7)

where

$$f_2(\eta) = \sum_{m=1,3,5}^{\infty} \sum_{n=1,3,5}^{\infty} \frac{m^2}{c_{mn}}$$

Substituting for P, we obtain

$$\epsilon_2 = \frac{2K_1 h}{\pi^2 D_x} \left(\frac{a}{b}\right) f_2(\eta) w_1$$

(A8)

so that

$$d_{12} = \frac{\pi^2 D_x}{2K_1 h (a/b) f_2(\eta)}$$

The approximation assumption used above, eq. (A2), has been suggested by Timoshenko and Woinowsky-Krieger [13] for simplifying the mathematics of several plate-bending problems and is exact for the

case of an isotropic plate. The advantage of this assumption is to reduce the parameters for describing the geometry and anisotropy of the plate to a single quantity, η . For the composite plate on which the impact experiments were performed, the computed values are

$$H = D_{12} + 2 D_{66} = 1484.6 \text{ N-m}$$

$$\sqrt{D_x D_y} = \sqrt{D_{11} D_{22}} = 1301.2 \text{ N-m}$$

a difference of 14%.

APPENDIX B

STATIC DEFLECTION OF A CLAMPED RECTANGULAR
ORTHOTROPIC PLATE DUE TO A CENTRAL POINT LOAD

In constructing an impact design curve for a particular structure according to the generalized one-degree-of-freedom model presented in the main text, it is necessary to know the relationships between load, deflection, and strain in the parallel static problem for the structure of interest. However, in the case of a clamped rectangular orthotropic plate, a review of recent literature indicates that an exact solution for the static deflection due to a centrally applied concentrated load does not exist. In fact, the most advanced related solutions found in the literature include a single-term Ritz solution of the case with uniform load (see Lekhnitskii [10] or Ashton and Whitney [14]) and an exact solution of the simply supported case with point load (see Ambartsoumian [15] or Advanced Composites Design Guide [16]).

Therefore, in this appendix, the deflection and bending strain of a centrally loaded clamped-edge rectangular orthotropic plate are derived from the solution for a similarly loaded and supported isotropic plate due to Young [17] . This is accomplished by reducing the governing equations for both problems to the same

dimensionless form by making a simplifying assumption suggested by Timoshenko and Woinowsky-Krieger [13], and then transforming the isotropic solution into terms of the dimensionless variables corresponding to the orthotropic case.

Young's Solution

In Young's solution for the static deflection of a clamped isotropic plate, the solution for a simply supported plate with a central concentrated load is combined with that for a simply supported plate with distributed bending moments along the edges. The edge moments are then chosen so that the deflection slope vanishes at the boundaries. The superimposed solution consists of three parts,

$$w = w_1 + w_2 + w_3 \quad (B1)$$

where the first term is the solution for a simply supported rectangular plate.

$$w_1 = \frac{Pa^2}{2\pi^3 D} \sum_{m=1,3,5}^{\infty} \frac{1}{m^3} \left[\left(\tanh \alpha_m - \frac{\alpha_m}{\cosh^2 \alpha_m} \right) \cosh \frac{m\pi y}{a} - \sinh \frac{m\pi y}{a} - \tanh \alpha_m \frac{1}{a} \sinh \frac{m\pi y}{a} + \frac{m\pi y}{a} \cosh \frac{m\pi y}{a} \right] \quad (B2)$$

where

$$\alpha_m = \frac{m\pi b}{2a}$$

$$\beta_m = \frac{m\pi a}{2b}$$

The other two terms are the deflections of a simply supported plate with moments applied along the pairs of edges $y = \pm b/2$ and $x = \pm a/2$, respectively.

$$w_2 = -\frac{Pa^2}{2\pi^2 D} \sum_m A_m \frac{(-1)^{\frac{m-1}{2}}}{m^2 \cosh \alpha_m} \cos \frac{m\pi x}{a} \left[\frac{m\pi y}{a} \sinh \frac{m\pi y}{a} - \alpha_m \tanh \alpha_m \cosh \frac{m\pi y}{a} \right] \quad (B3)$$

and

$$w_3 = -\frac{Pb^2}{2\pi^2 D} \sum_m B_m \frac{(-1)^{\frac{m-1}{2}}}{m^2 \cosh \beta_m} \cos \frac{m\pi y}{b} \left[\frac{m\pi x}{b} \sinh \frac{m\pi x}{b} - \beta_m \tanh \beta_m \cosh \frac{m\pi x}{b} \right] \quad (B4)$$

The edge moments corresponding to w_2 and w_3 are

$$(M_y)_{y=\pm b/2} = P \sum_m (-1)^{\frac{m-1}{2}} A_m \cos \frac{m\pi x}{a} \quad (B5)$$

$$(M_x)_{x=\pm a/2} = P \sum_m (-1)^{\frac{m-1}{2}} B_m \cos \frac{m\pi y}{b} \quad (B6)$$

in which the coefficients A_m and B_m are determined from the condition that the slope at the boundaries is zero. Young has computed approximate values of the first few of these coefficients for several values of the aspect ratio (b/a).

Modified Young's Solution

In using the solution for static deflection to construct a design curve for impact response, we are interested in the relationship between strain and deflection. In Young's solution as described above, differentiation of the term w_1 (twice) to obtain an expression for bending strain leads to an infinite series which is divergent. To avoid this difficulty, an alternate solution, Navier's solution, which yields a bounded value of bending strain, is substituted for w_1 . Thus, we instead let

$$w_1 = \frac{4Pab}{\pi^4 D} \left(\frac{a}{b}\right)^2 \sum_m \sum_n \frac{\cos \frac{m\pi x}{a} \cos \frac{n\pi y}{b}}{\left[m^2 + n^2 \left(\frac{a}{b}\right)^2\right]^2} \quad (B7)$$

Transformation to Orthotropic Plate

The governing differential equation for the deflection w of an isotropic plate subjected to a lateral distributed load $q(x,y)$ is

$$\frac{\partial^4 w}{\partial x^4} + 2 \frac{\partial^4 w}{\partial x^2 \partial y^2} + \frac{\partial^4 w}{\partial y^4} = \frac{q(x,y)}{D} \quad (B8)$$

Letting $\bar{x} = x/a$, $\bar{y} = y/b$, and $\bar{w} = w/a$, this equation may be expressed

as

$$\frac{\partial^4 \bar{w}}{\partial \bar{x}^4} + 2 \left(\frac{a}{b}\right)^2 \frac{\partial^4 \bar{w}}{\partial \bar{x}^2 \partial \bar{y}^2} + \left(\frac{a}{b}\right)^4 \frac{\partial^4 \bar{w}}{\partial \bar{y}^4} = \frac{q a^3}{D} \quad (B9)$$

Likewise, the governing equation for an orthotropic plate

$$D_x \frac{\partial^4 W}{\partial x^4} + 2H \frac{\partial^4 W}{\partial x^2 \partial y^2} + D_y \frac{\partial^4 W}{\partial y^4} = q(x, y) \quad (B10)$$

may be expressed in terms of the same dimensionless variables as

$$\frac{\partial^4 \bar{W}}{\partial \bar{x}^4} + 2\eta \frac{\partial^4 \bar{W}}{\partial \bar{x}^2 \partial \bar{y}^2} + \eta^2 \frac{\partial^4 \bar{W}}{\partial \bar{y}^4} = \frac{qa^3}{D_x} \quad (B11)$$

where

$$\eta = \left(\frac{a}{b}\right)^2 \sqrt{\frac{D_y}{D_x}} \quad (B12)$$

and where it is assumed that $H = \sqrt{D_x D_y}$.

Note the similarity between eqs. (B9) and (B11). The solution of Eq. (B9) is of the form

$$\bar{v} = f\left(\left[\frac{a}{b}\right]^2, qa^3/D_x, \bar{x}, \bar{y}\right) \quad (B13)$$

and the solution of eq. (B11) is the same function but involving different dimensionless parameters,

$$\bar{w} = f\left(\eta, qa^3/D_x, \bar{x}, \bar{y}\right) \quad (B14)$$

Now eq. (B13) may be obtained by simply writing the known solution, eqs. (B1), (B3), (B4), and (B7), of the isotropic case in terms of the dimensionless variables \bar{x} , \bar{y} and \bar{v} . Then, substitution of η for

$(a/b)^2$ and of qa^3/D_x for qa^3/D yields eq. (B14), which is the solution of eq. (B11). Finally, by returning eq. (B14) so obtained to dimensional variables x , y , and w , we obtain the solution of the orthotropic equation (B10).

The terms to the right of the equals signs in eqs. (B9) and (B11) represent dimensionless forcing functions for an arbitrary distributed load $q(x,y)$, and have the form $\bar{q} = qa^3/D$. In the case of a uniformly distributed load, $q(x,y) = q_0$, we would have $\bar{q} = q_0 a^3/D$, or, in terms of total load $P = q_0 ab$, $\bar{q} = Pa^2/bD$. This suggests that in the case of a concentrated load P the dimensionless forcing function is also $\bar{q} = Pa^2/bD$ for the isotropic case, or $\bar{q} = Pa^2/bD_x$ for the orthotropic case. Therefore, in obtaining eq. (B14) from eq. (B13), Pa^2/bD_x is substituted for Pa^2/bD .

For example, equation (B7) may be written in terms of dimensionless variables as

$$\bar{w}_1 = \frac{w_1}{a} = \frac{4Pa^2}{\pi^4 bD} \sum_m \sum_n \frac{\cos m\pi\bar{x} \cos n\pi\bar{y}}{[m^2 + n^2 (\frac{a}{b})^2]^2} \quad (B15)$$

This represents a portion of the solution to eq. (B13).

Substitute η for $(a/b)^2$ and (Pa^2/bD_x) for (Pa^2/bD) to obtain

$$\bar{w}_1 = \frac{4Pa^2}{\pi^4 bD_x} \sum_m \sum_n \frac{\cos m\pi\bar{x} \cos n\pi\bar{y}}{[m^2 + n^2 \eta]^2} \quad (B16)$$

which represents a portion of eq. (B14). Rewriting this equation in

terms of dimensional variables yields the final solution for the orthotropic case.

$$W_1 = \frac{4Pa^3}{\pi^4 b D_x} \sum_m \sum_n \frac{\cos \frac{m\pi x}{a} \cos \frac{n\pi y}{b}}{[m^2 + n^2 \eta]^2} \quad (B17)$$

Similarly, from eqs. (B3) and (B4), we obtain

$$W_2 = \frac{-Pa^3}{2\pi^2 b D_x} \frac{1}{\sqrt{\eta}} \sum_m A_m \frac{(-1)^{\frac{m-1}{2}}}{m^2 \cosh \alpha_m} \cos \frac{m\pi x}{a} \left[\frac{m\pi y}{b\sqrt{\eta}} \sinh \frac{m\pi y}{b\sqrt{\eta}} - \alpha_m \tanh \alpha_m \cosh \frac{m\pi y}{b\sqrt{\eta}} \right] \quad (B18)$$

$$W_3 = \frac{-Pa^3}{2\pi^2 b D_x} \frac{1}{\eta \sqrt{\eta}} \sum_m B_m \frac{(-1)^{\frac{m-1}{2}}}{m^2 \cosh \beta_m} \cos \frac{m\pi y}{b} \left[\frac{m\pi \sqrt{\eta} x}{a} \sinh \frac{m\pi \sqrt{\eta} x}{a} - \beta_m \tanh \beta_m \cosh \frac{m\pi \sqrt{\eta} x}{a} \right] \quad (B19)$$

By assembling eqs. (B17), (B18) and (B19) according to eq. (B1), we obtain the solution for the deflection of a rectangular clamped-edge orthotropic plate subjected to a centrally applied concentrated load. The coefficients A_m and B_m , which are functions of (a/b) in the isotropic case, are now functions of η .

Evaluating the deflection solution at the center of the plate ($x = 0, y = 0$), we obtain the maximum deflection of the plate which may be expressed as

$$W_{max} = \frac{a^3}{b D_x} f_3(\eta) P \quad (B20)$$

so that

$$K_1 = \frac{b D_x}{a^3 f_3(\eta)} \quad (\text{B21})$$

where

$$f_3(\eta) = \frac{4}{\pi^4} \sum_m \sum_n [m^2 + n^2 \eta]^{-2} - \frac{1}{2\pi^2 \sqrt{\eta}} \sum_m \frac{(-1)^{\frac{m-1}{2}}}{m^2} \alpha_m \left[A_m \frac{\tanh \alpha_m}{\cosh \alpha_m} + B_m \frac{\tanh \beta_m}{\cosh \beta_m} \right] \quad (\text{B22})$$

and where we now have

$$\alpha_m = \frac{m\pi}{2\sqrt{\eta}} \quad \beta_m = \frac{m\pi}{2} \sqrt{\eta} \quad (\text{B23})$$

The maximum bending strain occurs at the point directly opposite the load and may be expressed as

$$\epsilon_{x_{\max}} = \frac{h a}{b D_x} f_4(\eta) P \quad (\text{B24})$$

where

$$f_4(\eta) = \frac{2}{\pi^2} \sum_m \sum_n m^2 [m^2 + n^2 \eta]^{-2} + \frac{1}{4\sqrt{\eta}} \sum_m (-1)^{\frac{m-1}{2}} \left[A_m \alpha_m \frac{\tanh \alpha_m}{\cosh \alpha_m} + \frac{B_m}{\eta^2} \frac{2 - \beta_m \tanh \beta_m}{\cosh \beta_m} \right] \quad (\text{B25})$$

Combining eqs. (B20) and (B24) we obtain

$$d_{12} = \frac{W_{\max}}{E_{x\max}} = \frac{a^2}{h} \frac{f_3(\eta)}{f_4(\eta)}$$

(B26)

APPENDIX C

COMPUTER PROGRAM FOR CALCULATING
TIMOSHENKO SOLUTION OF PLATE IMPACT

This appendix presents a listing of the FORTRAN computer program, named SMINC3, for calculating the Timoshenko small-increment solution of the central transverse impact of a rectangular orthotropic plate, Eq. (40).

The program as listed is set up to solve an impact problem having the following parameters:

$$\begin{aligned}v &= 2.45 \text{ m/sec} \\a \times b \times h &= 171 \times 349 \times 7.1 \text{ mm} \\m_1 &= 0.660 \text{ kg} \\m_2 &= 0.816 \text{ kg}\end{aligned}$$

The plate bending stiffnesses, computed according to the Whitney-Pagano (1970) anisotropic plate theory, are:

$$\begin{aligned}D_{11} &= 680.4 \text{ N-m} \\D_{12} &= 473.2 \text{ N-m} \\D_{22} &= 2488.8 \text{ N-m} \\D_{66} &= 505.7 \text{ N-m} \\D_{16} = D_{26} &= -49.1 \text{ N-m} \\A_{44} = A_{55} &= 2.687 \times 10^7 \text{ N/m}\end{aligned}$$

The plate is treated as specially orthotropic in bending and the D_{16} and D_{26} terms are neglected.

The program itself calculates the value of the Hertzian contact stiffness constant k_2 based on supplied values of isotropic elastic

NADC-78259-60

properties of the plate and impactor. The values used are:

$$\text{plate (Gr/Ep)} \quad \begin{cases} E = 9.8 \times 10^9 \text{ N/m}^2 \\ \nu = 0.3 \end{cases}$$

$$\text{impactor (steel)} \quad \begin{cases} E = 2.1 \times 10^{11} \text{ N/m}^2 \\ \nu = 0.33 \end{cases}$$

The contact radius of the impactor is 25.4 mm.

NADC-78259-60

```

C      SMINC3  == PLATE IMPACT
COMPUTATION OF TIMOSHENKO-TYPE SMALL-INCREMENT SOLUTION OF HERTZIAN
C      IMPACT OF A SIMPLY SUPPORTED ORTHOTROPIC RECTANGULAR PLATE
C      MODIFIED SUN & CHATTOPADHYAY METHOD
C      DT = TIME INCREMENT
C      NDT = NO. OF TIME INCREMENTS CALCULATED
C      TOL = TOLERANCE OF ERROR IN NONLINEAR SOLUTION
C      V = IMPACT VELOCITY
C      XA, YB, H = DIMENSIONS OF PLATE IN X, Y, Z DIRECTIONS
C      M1, M2 = MASS OF PLATE, IMPACTOR
C      E1, E2 = ELASTIC MODULUS OF PLATE, IMPACTOR
C      PR1, PR2 = POISSON'S RATIO OF PLATE, IMPACTOR
C      NHM, NHM = NUMBER OF VIBRATION MODES CONSIDERED
C      K2 = HERTZIAN CONTACT STIFFNESS
C      XNX, YNY = INITIAL STRESSES IN X,Y DIRECTIONS
      REAL L,M1,M2,K2,L11,L12,L13,L22,L23,L33
      DIMENSION F(5000),GW(5000),GXX(5000),GY(5000)
C*****  PROBLEM DATA  *****
      NHM=25
      NHN=25
      NDT=100
      TOL=1.0E-05
      DT=1.0E-06
      XNX=0.
      YNY=0.
      D11=680.4
      D12=473.2
      D22=2488.8
      D66=505.7
      A44=2.687E 07
      A55=A44
      XNX=0.
      YNY=0.
      XA=0.171
      YB=0.349
      H=0.0071
      M1=0.660
      M2=0.816
      R1=0.0254
      PR1=0.3
      PR2=0.33
      E1=9.8E 09
      E2=2.10E 11
      V=2.45
C*****
      Z=H/2.
      PI=3.14159265398
1001 FORMAT(4X,'N',8X,'TIME',14X,'FORCE',12X,'APPROACH',10X,'DEFLECTION
1',10X,'STRAIN X',10X,'STRAIN Y',10X,'STRAIN XY')
      DEL1=(1.-PR1**2)/E1/PI
      DEL2=(1.-PR2**2)/E2/PI
      K2=4.*SQRT(R1)/(DEL1+DEL2)/PI/3.
      CAY=PI**2/12.
      A44=A44*CAY
      A55=A55*CAY
      B=DT**2/3.0/M2
      C= 4.0/M1
      P=M1/XA/YB

```

```

PRINT1001
CALCULATE NATURAL FREQUENCIES OF PLATE
DO90K=1,NDT
GW(K)=0.
GXX(K)=0.
90 GYY(K)=0.
DO247M=1,NHM,2
TERMA=M*PI/XA
TERMA2=TERMA**2
L13=A55*TERMA
DO247N=1,NHN,2
TERMB=N*PI/YB
TERMB2=TERMB**2
L11=D11*TERMA2+ D66*TERMB2+A55
L12=(D12+D66)*TERMA*TERMB
L22=D66*TERMA2+D22*TERMB2+A44
L23=A44*TERMB
L33=(A55+XNX)*TERMA2+(A44+YNY)*TERMB2
Q=L11*L22-L12**2
DETERM=Q*L33+2.*L12*L23*L13-L22*L13**2-L11*L23**2
AC=(L12*L23-L22*L13)/Q*TERMA
BC=(L12*L13-L11*L23)/Q*TERMB
OMEGA2=DETERM/Q/P
OMEGA=SQRT(OMEGA2)
IF((M.EQ.1).AND.(N.EQ.1))PRINT1002,OMEGA
1002 FORMAT('  OMEGA,1,1 = ',E15.8)
TERM1=DT*OMEGA
C2=1.0
DO247K=1,NDT
C1=C2
C2=COS(K*TERM1)
AAA=(C1-C2)/OMEGA2
CONSTRUCT TABLES OF SUMMATION FUNCTIONS
GW(K)=GW(K)+AAA
GXX(K)=GXX(K)+AAA*AC
247 GYY(K)=GYY(K)+AAA*BC
P=B+C*GW(1)
Q=1./3.
S=2./3.
DO100N=1,NDT
CREATE HEADINGS FOR DATA AT TOP OF EVERY PAGE
IF(MOD(N,61).NE.0)GOTO70
1003 FORMAT(1H1)
PRINT1003
PRINT1001
70 T=N*DT
A=V*T
IF(N.EQ.1)GOTO14
SUM=0.
NM1=N-1
SUMI=0.
SUM=0.
DO5J=1,NM1
K=N-J
R=K
SUMI=F(J)-SUMI
SUM=SUM+R*SUMI
5 BUM=BUM+F(J)*GW(K+1)

```

NADC-78259-60.

```
A=A-C*BUM
A=A-DT**2*(2.*SUM-SUMI/3.)/M2
COMPUTE SOLUTION FOR F(N) USING NEWTON'S ITERATIVE METHOD
GOTO13
14 FNEW=SQRT(A**3)/K2
13 FN=FNEW
B=SIGN(1.0,FN)/K2**2-3.0*A*P**2
FFN=P**3*FN**3+B*FN**2
1 +3.0*A**2*P*FN-A**3
FPFN=3.0*P**3*FN**2+2.0*B*FN+3.0*A**2*P
82 FNEW=FN-FFN/FPFN
ERROR=ABS((FNEW-FN)/FN)
IF(ERROR.GT.TOL)GOTO13
IF(N.GT.1)GOTO10
CHECK THAT F(1) IS POSITIVE
IF(FNEW.GT.0.)GOTO10
FNEW=-FNEW
GOTO13
10 F(N)=FNEW
IF(FNEW.LT.0.)F(N)=0.
CALCULATE STRAIN AND DEFLECTION
W=0.
PSIXX=0.
PSIYY=0.
DO21J=1,N
K=N-J+1
W=W+F(J)*GW(K)
PSIXX=PSIXX+F(J)*GXX(K)
21 PSIYY=PSIYY+F(J)*GYK(K)
W=W*C
EPSX=-PSIXX*C*Z
EPSY=-PSIYY*C*Z
GAMMA=0.
ALPHA=SIGN(1.0,FNEW)*(ABS(FNEW)/K2)**S
PRINT100,N,T,F(N),ALPHA,W,EPSX,EPSY,GAMMA
100 CONTINUE
STOP
1000 FORMAT(1X,I4,7(3X,E15.8))
END
```

APPENDIX D

SIMPLY SUPPORTED BEAM

CENTRALLY LOADED BY HALF-SINE PULSE

In this appendix are derived expressions for the deflection and bending strain in a simply supported beam subjected to a half-sine pulse laterally applied at midspan.

The deflection of a simply supported beam due to an arbitrary force $F(t)$ applied at midspan is

$$W(x,t) = \frac{2}{\rho A L} \sum_{i=1,3,5}^{\infty} \frac{(-1)^{\frac{i-1}{2}}}{\omega_i} \sin \frac{i\pi x}{L} \int_0^t F(\tau) \sin \omega_i (t-\tau) d\tau \quad (D1)$$

where

$$\omega_i = i^2 \pi^2 a^2 / L^2$$

We will consider the case where the applied force is represented by a half-sine pulse with respect to time.

$$F(t) = \begin{cases} P \sin \frac{\pi}{2} t & \text{for } 0 < t < \pi/\frac{\pi}{2} \\ 0 & \text{for } t \geq \pi/\frac{\pi}{2} \end{cases} \quad (D2)$$

Then the solution for each time domain (during and after the pulse) may be written in terms of the convolution integral

$$W(x,t) = \frac{2P}{\rho AL} \sum_{i=1,3,5}^{\infty} \frac{(-1)^{\frac{i-1}{2}}}{\omega_i} \sin \frac{i\pi x}{L} \int_0^t \sin \xi \tau \sin \omega_i (t-\tau) d\tau, \text{ for } 0 < t < \pi/\xi \quad (D3)$$

and

$$W(x,t) = \frac{2P}{\rho AL} \sum_{i=1,3,5}^{\infty} \frac{(-1)^{\frac{i-1}{2}}}{\omega_i} \sin \frac{i\pi x}{L} \int_0^{\pi/\xi} \sin \xi \tau \sin \omega_i (t-\tau) d\tau, \text{ for } t \geq \pi/\xi \quad (D4)$$

Evaluating the integral, the deflection during the pulse is given by

$$W(x,t) = \frac{2PL^3}{\pi^4 EI} \sum_{i=1,3,5}^{\infty} \frac{(-1)^{\frac{i-1}{2}}}{i^4 - \beta^2} \sin \frac{i\pi x}{L} \cdot \left(\sin \xi t - \frac{\beta}{i^2} \sin \omega_i t \right), \text{ for } 0 < t < \pi/\xi$$

$$\beta = \xi/\omega_1 \quad (D5)$$

If $\beta = 1^2$, however, the denominator of this expression is zero, and the result is undefined. In this case, $\omega_1 = 1^2 \omega_1 = \beta \omega_1 = \xi$; for a steady-state vibration problem, this would correspond to a resonant forcing function. For this special case, the following term must be substituted.

$$W_i = \frac{2PL^3}{\pi^4 EI} \sin \frac{i\pi x}{L} \frac{(-1)^{\frac{i-1}{2}}}{2i^2} \left(\sin^3 \xi t - i^2 \omega_1 t \cos \xi t + \frac{1}{2} \cos \xi t \sin 2\xi t \right) \quad (D6)$$

After the pulse, the deflection is

$$W(x,t) = \frac{2PL^3}{\pi^4 EI} \sum_{i=1,3,5}^{\infty} \frac{\beta(-1)^{\frac{i-1}{2}}}{(\beta^2 - i^2)i^2} \sin \frac{i\pi x}{L} \cdot \left\{ \sin \omega_i t + \sin \omega_i (t - \pi/\xi) \right\} \text{ for } t > \pi/\xi \quad (D7)$$

unless $\beta = i^2$, in which case the i th term must be replaced by

$$W_i = \frac{2PL^3}{\pi^4 EI} \sin \frac{i\pi x}{L} \frac{(-1)^{\frac{i+1}{2}}}{2\beta} \pi \cos \xi t \quad (D8)$$

The strain due to bending is

$$\epsilon = -Z \frac{\partial^2 W}{\partial x^2} \quad (D9)$$

The maximum value of this strain is reached at midspan. If we define a dimensionless strain as

$$\hat{\epsilon} = \frac{\pi^2 EI}{h PL} \epsilon_{x=L/2} \quad (D10)$$

then the solution in terms of this quantity is

$$\hat{\epsilon} = \begin{cases} \sum_{i=1,3,5}^{\infty} \frac{i^2}{i^4 - \beta^2} \left(\sin \xi t - \frac{\beta}{i^2} \sin \omega_i t \right), & 0 < t < \pi/\xi \\ \sum_{i=1,3,5}^{\infty} \frac{\beta}{\beta^2 - i^4} \left(\sin \omega_i t + \sin \omega_i [t - \pi/\xi] \right), & t > \pi/\xi \end{cases} \quad (D11)$$

$$\hat{\epsilon} = \begin{cases} \sum_{i=1,3,5}^{\infty} \frac{i^2}{i^4 - \beta^2} \left(\sin \xi t - \frac{\beta}{i^2} \sin \omega_i t \right), & 0 < t < \pi/\xi \\ \sum_{i=1,3,5}^{\infty} \frac{\beta}{\beta^2 - i^4} \left(\sin \omega_i t + \sin \omega_i [t - \pi/\xi] \right), & t > \pi/\xi \end{cases} \quad (D12)$$

unless $\beta = i^2$, in which case the i th term must be replaced by

$$\hat{E} = \begin{cases} \frac{1}{2i^2} (\sin^3 \xi t - \omega_1 t \cos \xi t + \frac{1}{2} \cos \xi t \sin 2\xi t), & 0 < t < \pi/\xi \\ -\frac{\pi}{2\beta} \cos \xi t, & t > \pi/\xi \end{cases} \quad (D13)$$

$$(D14)$$

For most problems involving small impactors (large M), the contact duration is short compared with the fundamental period of beam vibration. Therefore, it is of interest to determine the peak bending strain when the pulse duration is short. It is observed in this case that the peak strain occurs after the pulse, that is, in the domain of eq. (D12), which may be written as

$$\hat{E} = \sum_{i=1,3,5}^{\infty} \frac{2\beta}{\beta^2 - i^4} \sin \left[i^2 \omega_1 \left(t - \frac{\pi}{\xi} \right) / 2 \right] \cos \frac{i^2 \pi}{2\beta}$$

This quantity reaches its maximum at

$$t = \frac{\pi}{\omega_1} + \frac{\pi}{\xi}$$

when it has the value

$$\hat{E}_{max} = \sum_{i=1,3,5}^{\infty} \frac{2\beta}{\beta^2 - i^4} \cos \frac{i^2 \pi}{2\beta}$$

which is a function of β only. This function is plotted in Fig. D1.

Then

$$f(\beta) = \frac{1}{\pi^2} \hat{E}_{max}$$

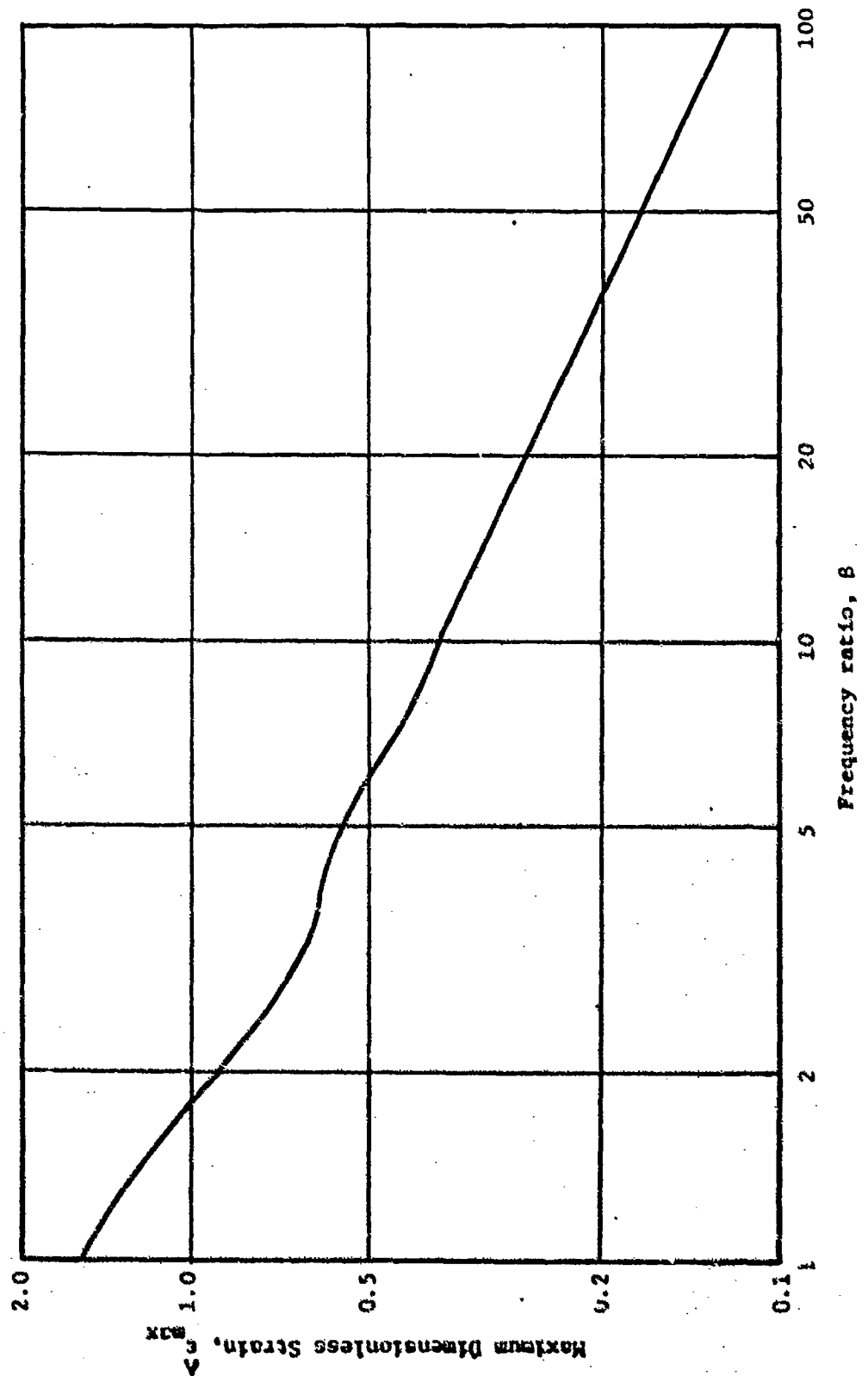


Fig. 4. Maximum dimensionless strain ϵ_{max}^A vs. frequency ratio β for a simply supported beam subjected to a half-sine pulse.

NADC-78259-60

APPENDIX E

DETAILED RESULTS OF IMPACT EXPERIMENTS

In this appendix, data from all impact experiments conducted at Drexel and also some reported in the literature are presented in both tabular and graphical form. For completeness, several figures which appear in the text have been included in this appendix.

1. Results of Large-Impactor Strain Measurement Experiments

Strain measuring impact tests have been performed on both aluminum and composite (graphite-epoxy) plates. A total of 475 experiments were performed on specimens with clamped edges and 573 on specimens with simply supported edges.

Index to Large Impactor Design Curves

<u>Clamped Plates</u>		<u>Simply Supported Plates</u>	
<u>η</u>	<u>Figure</u>	<u>η</u>	<u>Figure</u>
0.074	E12	0.074	E34
0.111	E5	0.111	E27
0.166	E3	0.166	E30
0.189	E15	0.189	E37
0.227	E21	0.227	E43
0.25	E3	0.25	E25
0.30	E18	0.30	E40
0.417	E11	0.417	E33
0.64	E6	0.64	E28
0.80	E17	0.80	E39
1.0	E1	1.0	E23
1.25	E16	1.25	E38
1.56	E7	1.56	E9
2.4	E10	2.4	E32
3.3	E19	3.3	E41
4.0	E2	4.0	E24
4.41	E20	4.41	E42
5.29	E14	5.29	E36
6.02	E9	6.02	E31
9.0	E4	9.0	E26
13.51	E13	13.51	E35

TABLE E1 TRANSVERSE IMPACT EXPERIMENTS ON CLAMPED ALUMINUM PLATES

Specimen Dimensions, $a \times b \times h$ (mm)	Impact Mass, m_2 (kg)	Impact Velocity, v (m/sec)	Number of Tests Performed	Maximum Measured Strain		Generalized Strain			Mass Ratio, $M = \frac{m_1}{m_2}$
				Average $\epsilon_x \times 10$	Coeff. of Variation, per cent	Average $\epsilon_y \times 10$	Coeff. of Variation, per cent	$\epsilon_x = \frac{2}{\epsilon_x} \frac{\epsilon_y}{h v}$	$\epsilon_y = \frac{2}{\epsilon_y} \frac{\epsilon_x}{h v}$
125x125x6.35 $\eta = 1.0$	0.495	2.44	3	2567	1.1	2517	6.1	1.589	1.558
		2.99	4	3088	5.2	2988	5.5	1.560	1.509
		3.46	4	3638	3.6	3525	5.5	1.588	1.539
		4.23	-	-	-	-	-	-	-
	0.784	2.44	9	2633	9.4	2639	6.5	1.630	1.633
		2.99	5	3880	4.9	3710	4.0	1.960	1.874
		3.46	-	-	-	-	-	-	-
		4.23	-	-	-	-	-	-	-
	1.057	2.44	6	3550	4.5	3433	4.8	2.197	2.125
		2.99	7	4600	9.2	4471	11.1	2.324	2.258
		3.46	4	6238	2.1	6138	9.0	2.723	2.679
		4.23	-	-	-	-	-	-	-
150x125x6.35 $\eta = 4.0$	0.495	2.44	3	1723	1.7	2150	2.3	1.073	1.331
		2.99	4	2225	6.7	2750	3.6	1.124	1.389
		3.46	5	2450	2.8	3420	1.3	1.244	1.493
		4.23	3	1317	6.1	4283	3.6	1.184	1.529
	0.784	2.44	3	2500	5.3	2983	1.0	1.547	1.846
		2.99	4	3238	5.4	3775	1.7	1.636	1.907
	0.495								
	0.784								

TABLE E1 (continued)

Specimen Dimensions $a \times b \times h$ (mm)	Impactor Mass, m_2 (kg)	Impact Velocity v (m/sec)	Number of Tests Performed	Maximum Measured Strain				Generalized Strain		Mass Ratio, $\frac{m_1}{M} = \frac{m_2}{m_2}$
				Average $\epsilon_x \times 10^6$	Coeff. of Variation per cent	Average $\epsilon_y \times 10^6$	Coeff. of Variation per cent	$\bar{\epsilon}_x = \epsilon_{x \frac{2}{hv}}$	$\bar{\epsilon}_y = \epsilon_{y \frac{2}{hv}}$	
250 x 125 x 6.35 $\eta = 4.0$	1.057	2.44	3	2967	1.0	3583	2.9	1.837	2.218	0.531
		2.99	4	3588	9.2	4562	8.9	1.812	2.304	
		3.46	3	4083	3.5	5433	2.3	1.782	2.372	
		4.22	3	5433	2.8	7050	1.4	2.372	2.517	
375 x 125 x 6.35 $\eta = 9.0$	0.784	3.46	3	3800	1.3	4583	2.7	1.659	2.000	0.716
		4.23	4	4912	3.3	6100	3.8	1.754	2.178	
		2.44	3	1633	1.8	2067	1.4	1.011	1.279	
		2.99	3	1983	1.5	2617	1.1	1.002	1.322	
	0.495	3.46	3	2367	2.4	3150	1.6	1.033	1.375	1.685
		4.23	3	3067	2.5	4017	4.0	1.095	1.434	
		2.44	3	2150	4.0	2850	1.8	1.331	1.764	
		2.99	3	2850	0.0	3600	0.0	1.440	1.818	
	0.784	3.46	3	3250	4.6	4400	2.0	1.419	1.921	1.063
		4.23	3	3967	1.5	5283	1.4	1.416	1.886	
		2.44	3	2533	2.3	3217	3.2	1.568	1.991	
		2.99	3	3233	7.9	4233	3.8	1.633	2.138	
	1.057	3.46	3	3600	6.4	4983	3.2	1.571	2.175	0.788
		4.23	3	5235	3.9	7117	1.5	1.868	2.541	

TABLE E2
DATA FROM STRAIN-MEASUREMENT IMPACT EXPERIMENTS
ON CLAMPED GRAPHITE-EPOXY PLATES

Specimen B1 (11-0.625)

IMPACTOR MASS M_2 , Kg	IMPACTOR RADIUS r , mm	IMPACTOR VELOCITY V , m/sec	NUMBER OF TESTS	AVERAGE MEASURED STRAINS				GENERALIZED STRAINS	
				$\epsilon_x \times 10^6$	C.O.V.	$\epsilon_y \times 10^6$	C.O.V.	$\bar{\epsilon}_x$	$\bar{\epsilon}_y$
0.228 ($M=0.44$)	6.35	1.73	2	2500	0	3500	2.02	2.84	2.48
	12.7	1.73	2	2400	5.89	3400	8.32	2.72	2.41
		2.45	2	3425	3.09	5200	0	2.74	2.51
		2.99	2	4150	1.70	5500	2.57	2.72	2.25
0.453 ($M=0.22$)	6.35	1.73	2	3600	0	4800	0	4.08	3.40
	12.7	1.73	2	3250	2.18	4700	0	3.69	3.93
		2.45	2	4767	1.21	6970	2.19	3.82	3.49
		2.77	2	6000	0	8750	2.42	3.93	3.58
0.907 ($M=0.109$)	6.35	1.73	2	4900	2.88	6700	0	5.56	4.75
	12.7	1.73	2	4750	1.42	6600	0	5.39	4.68

TABLE E2, continued

Specimen B2 ($\eta=0.164$)

IMPACTOR MASS M_2 , Kg	IMPACTOR RADIUS r , mm	IMPACTOR VELOCITY V , m/sec	NUMBER OF TESTS	AVERAGE MEASURED STRAINS			GENERALIZED STRAINS	
				$\bar{\epsilon}_x \times 10^2$	C.O.V.	$\bar{\epsilon}_y \times 10^2$	C.O.V.	$\bar{\epsilon}_x$
0.228 ($M=0.85$)	6.35	1.73	2	2550	0	3700	0	2.89
	12.7	1.73	2	2450	2.88	3725	0.95	2.78
		2.45	3	3750	2.31	5217	6.38	3.00
		2.49	3	4434	3.45	6300	1.59	2.91
0.453 ($M=0.43$)	6.35	1.73	2	3400	0	5200	0	3.86
	12.7	1.73	2	3550	1.99	4850	1.46	4.03
		2.45	2	5030	1.00	6850	1.03	4.05
		2.77	2	6350	1.11	8650	1.21	4.16
0.907 ($M=0.213$)	6.35	1.73	2	5200	0	7200	1.96	5.84
	12.7	1.73	2	5100	0	6800	0	5.77

TABLE E2, continued

Specimen B3 (n=2.39)

IMPACTOR MASS M_2 , kg	IMPACTOR RADIUS r , mm	IMPACTOR VELOCITY V , m/sec	NUMBER OF TESTS	AVERAGE MEASURED STRAINS				GENERALIZED STRAINS	
				ϵ_x $\times 10^6$	C.O.V.	ϵ_y $\times 10^6$	C.O.V.	$\bar{\epsilon}_x$	$\bar{\epsilon}_y$
0.228 ($M = 0.85$)	6.35	1.73	2	2250	3.14	3600	0	2.55	2.55
	12.7	1.73	2	2175	4.63	3700	3.82	2.47	2.62
		2.45	2	2800	0	5600	0	2.25	2.81
		2.49	2	4250	4.99	7200	0	2.78	2.95
0.453 ($M = 0.43$)	6.35	1.73	2	2300	6.14	4950	1.42	2.61	3.51
	12.7	1.73	2	2300	0	4800	0	2.61	3.40
		2.45	2	3400	8.31	6750	1.04	2.73	3.98
		2.49	2	3600	0	7200	0	2.36	2.95
0.907 ($M = 0.21$)	6.35	1.73	2	3400	8.31	7200	0	3.86	5.11
	12.7	1.73	2	3400	8.31	7150	0.98	3.86	5.07
		2.45	2	4600	8.44	9800	2.89	3.69	4.91

TABLE E2, continued

Specimen B4 (r=0.625)

IMPACTOR MASS M_2 , Kg	IMPACTOR RADII r , mm	IMPACTOR VELOCITY V , m/sec	NUMBER OF TESTS	AVERAGE MEASURED STRAINS				GENERALIZED STRAINS	
				$\epsilon_x \times 10^6$	C.O.V.	$\epsilon_y \times 10^6$	C.O.V.	$\bar{\epsilon}_x$	$\bar{\epsilon}_y$
0.228 ($M=1.061$)	6.35	1.73	2	1575	2.24	2200	0	1.79	1.56
	12.7	1.73	2	1612	3.29	2388	0.74	1.83	1.69
		2.45	2	2250	3.14	3200	4.42	1.80	1.61
		2.99	2	2950	3.89	4025	0.88	1.93	1.65
0.453 ($M=0.84$)	6.35	1.73	2	2575	1.37	3375	1.04	2.92	2.99
	12.7	1.73	2	2400	0	3450	2.05	2.72	2.45
		2.45	2	3300	0	4600	0	2.65	2.31
		2.77	2	4200	0	5450	1.29	2.75	2.23
0.907 ($M=0.42$)	6.35	1.73	3	3300	3.03	4533	5.67	3.74	3.21
	12.7	1.73	3	3267	3.53	4100	0	3.71	2.91

TABLE E2, continued

Specimen B5 ($\eta=0.074$)

IMPACTOR MASS M_2 , Kg	IMPACTOR RADIUS r , mm	IMPACTOR VELOCITY V , m/sec	NUMBER OF TESTS	AVERAGE MEASURED STRAINS				GENERALIZED STRAINS	
				ϵ_x $\times 10^6$	C.O.V.	ϵ_y $\times 10^6$	C.O.V.	$\bar{\epsilon}_x$	$\bar{\epsilon}_y$
0.228 ($M=1.26$)	6.35	1.73	2	2300	0	2850	2.48	2.61	2.02
		1.73	2	2475	1.42	3000	4.71	2.81	2.13
	12.7	2.45	2	3500	0	4200	0	2.81	2.11
		2.99	2	4225	0.84	5400	0	2.76	2.21
0.453 ($M=0.63$)	6.35	1.73	2	3800	0	4550	1.55	4.31	3.23
		1.73	2	3500	4.04	4500	3.14	3.97	3.19
	12.7	2.45	2	5050	1.00	6450	1.29	4.05	3.23
		2.99	2	6600	0	8800	0	4.32	3.27
0.907 ($M=0.32$)	6.35	1.73	2	5500	2.57	7000	0	6.24	4.96
	12.7	1.73	2	5300	2.67	6850	1.03	6.01	4.86

TABLE E2, continued

Specimen B6 (n=5.29)

IMPACTOR MASS M_2 , Kg	IMPACTOR RADIUS r , mm	IMPACTOR VELOCITY V , m/sec	NUMBER OF TESTS	AVERAGE MEASURED STRAINS			GENERALIZED STRAINS	
				$\bar{\epsilon}_x \times 10^6$	C.O.V.	$\bar{\epsilon}_y \times 10^6$	C.O.V.	$\bar{\epsilon}_x$
0.228 ($M=1.26$)	6.35	1.73	2	2025	1.74	2875	3.68	2.30
	12.7	1.73	3	2000	0	3033	1.91	2.27
		2.45	2	2700	0	4530	1.53	2.16
		2.77	2	3225	1.09	5500	1.27	2.12
0.453 ($M=0.64$)	6.35	1.73	3	3050	1.64	5334	1.08	3.46
	12.7	1.73	2	3075	1.15	5050	0	3.49
		2.45	2	4000	0	7150	0.98	3.28
		2.77	4	4600	7.32	8125	3.42	3.01
0.907 ($M=0.32$)	6.35	1.73	2	3850	5.5	7000	0	4.37
	12.7	1.73	2	3850	5.5	7050	1.01	4.37
								5.00

TABLE E2, continued

Specimen B7 (n=1.38)

IMPACTOR MASS M_2 , kg	IMPACTOR RADIUS r , mm	IMPACTOR VELOCITY V , m/sec	NUMBER OF TESTS	AVERAGE MEASURED STRAINS				GENERALIZED STRAINS	
				$\bar{\epsilon}_x$ $\times 10^6$	C.O.V.	ϵ_y $\times 10^6$	C.O.V.	$\bar{\epsilon}_x$	$\bar{\epsilon}_y$
0.228 ($M=2.38$)	6.35	1.73	2	1000	0	1800	0	1.13	1.28
	12.7	1.73	2	1000	0	1800	0	1.13	1.28
		2.45	2	1400	0	2400	0	1.12	1.20
		2.99	2	1900	4.88	3000	0	1.24	1.23
0.453 ($M=1.2$)	6.35	1.73	2	1800	0	2800	0	2.04	1.99
	12.7	1.73	2	1850	3.82	2750	2.58	2.10	1.95
		2.45	2	2550	2.77	3850	1.83	2.05	1.93
		2.99	2	3050	2.82	4700	0	2.00	1.92
0.907 ($M=0.59$)	6.35	1.73	2	2550	2.77	4150	1.70	2.89	2.94
	12.7	1.73	2	2450	2.88	4150	1.70	2.78	2.94
		2.45	2	3400	8.32	6050	1.16	2.73	3.03

TABLE E2, continued

Specimen B8 ($\eta=0.282$)

IMPACTOR MASS M_2, kg	IMPACTOR RADIUS r, mm	IMPACTOR VELOCITY $V, \text{m/sec}$	NUMBER OF TESTS	AVERAGE MEASURED STRAINS				GENERALIZED STRAINS	
				$\epsilon_x \times 10^6$	C.O.V.	$\epsilon_y \times 10^6$	C.O.V.	$\bar{\epsilon}_x$	$\bar{\epsilon}_y$
0.228 ($M=2.32$)	6.35	1.73	2	800	0	1600	0	0.91	1.13
	12.7	1.73	2	800	0	1600	0	0.91	1.13
		2.45	2	1100	0	2350	3.00	0.88	1.17
		2.99	2	1400	0	3000	0	0.92	1.23
0.453 ($M=1.2$)	6.35	1.73	2	1500	0	2800	0	1.70	1.99
	12.7	1.73	2	1450	4.87	2800	0	1.64	1.99
		2.45	2	2050	3.45	3850	1.83	1.64	1.93
		2.77	2	2700	0	4700	0	1.77	1.92
0.907 ($M=0.59$)	6.35	1.73	2	2400	0	4250	1.66	2.72	3.01
	12.7	1.73	2	2300	6.14	4350	4.88	2.61	3.08
		2.45	2	3200	4.72	6000	0	2.56	3.01

TABLE E2, continued

Specimen F1 (m=0.641)

Impactor Mass M_2 , kg	Impactor Radius r , mm	Impactor Velocity V , m/sec	Number of Tests	Average Measured Strains				Generalized Strains	
				$\bar{\epsilon}_x$ $\times 10^6$	C.O.V.	$\bar{\epsilon}_y$ $\times 10^6$	C.O.V.	$\bar{\epsilon}_x$	$\bar{\epsilon}_y$
0.228 ($M=1.041$)	6.35	1.73	2	1100	0	1525	2.32	1.16	1.03
		1.73	2	1137	1.55	1625	0	1.20	1.10
	12.7	2.45	2	1675	2.11	2338	1.05	1.25	1.12
		2.99	2	2000	0	2925	3.65	1.22	1.14
0.453 ($M=0.512$)	6.35	1.73	2	1475	2.39	2250	0	1.56	1.52
		1.73	2	1525	2.32	2300	0	1.61	1.56
	12.7	2.45	2	2225	1.01	3300	0	1.66	1.58
		2.99	2	2750	0	4150	0	1.68	1.62
0.907 ($M=0.26$)	6.35	1.73	2	2025	1.75	3050	2.32	2.14	2.07
		1.73	2	2025	1.75	3100	0	2.14	2.10
	12.7	2.45	2	3000	0	4500	0	2.24	2.16

TABLE E2, continued

Specimen F2 (n=0.168)

IMPACTOR MASS, M_2 , kg	IMPACTOR RADIUS R, mm	IMPACTOR VELOCITY V , m/sec	NUMBER OF TESTS	AVERAGE MEASURED STRAINS				GENERALIZED STRAINS	
				ϵ_x $\times 10^6$	C.O.V.	ϵ_y $\times 10^6$	C.O.V.	$\bar{\epsilon}_x$	$\bar{\epsilon}_y$
0.228 ($M=1.99$)	6.35	1.73	2	988	1.79	1298	1.43	1.05	0.839
	12.7	1.73	2	963	1.84	1250	0	1.02	0.847
		2.45	2	1338	1.32	1788	0.98	1.00	0.857
		2.99	2	1588	1.11	2213	0.79	0.97	0.866
0.453 ($M=0.99$)	6.35	1.73	2	1325	0	1938	0.91	1.40	1.31
	12.7	1.73	2	1413	1.25	1925	1.83	1.50	1.30
		2.45	2	2000	0	2738	0.95	1.50	1.31
		2.99	2	2450	0	3375	1.04	1.50	1.32
0.907 ($M=0.49$)	6.35	1.73	2	2075	0	3000	0	2.19	2.03
	12.7	1.73	2	2100	0	2975	1.19	2.20	2.02
		2.45	3	2917	2.62	4183	3.45	2.18	2.00

TABLE E2, continued

Specimen F3 (n=2.45)

IMPACTOR MASS M_2 , kg	IMPACTOR RADIUS r , mm	IMPACTOR VELOCITY V , m/sec	NUMBER OF TESTS	AVERAGE MEASURED STRAINS			GENERALIZED STRAINS		
				ϵ_x $\times 10^6$	C.O.V.	ϵ_y $\times 10^6$	C.O.V.	$\bar{\epsilon}_x$	$\bar{\epsilon}_y$
0.228 ($M=1.93$)	6.35	1.73	2	838	2.11	1275	2.77	0.89	0.864
	12.7	1.73	2	750	0	1238	1.43	0.79	0.859
		2.45	2	1150	2.17	1825	1.94	0.86	0.875
		2.77	2	1313	1.35	2165	2.04	0.80	0.846
0.453 ($M=0.99$)	6.35	1.73	2	1775	3.0	2163	0.82	1.24	1.47
	12.7	1.73	2	1250	0	2200	0	1.32	1.49
		2.45	2	1700	0	3050	0	1.27	1.46
		2.77	2	2200	0	3650	1.94	1.34	1.43
0.907 ($M=0.49$)	6.35	1.73	2	1700	0	2975	1.19	1.79	2.02
	12.7	1.73	2	1600	0	2900	0	1.69	1.97
		2.45	2	2200	0	4100	1.62	1.65	1.96

TABLE E2, continued

Specimen F4 (p0.641)

Impactor Mass M_2 , kg	Impactor Radius r , mm	Impactor Velocity V , m/sec	Number of Tests	Average Measured Strains				Generalized Strains	
				ϵ_x $\times 10^6$	C.O.V.	ϵ_y $\times 10^6$	C.O.V.	$\bar{\epsilon}_x$	$\bar{\epsilon}_y$
0.220 ($M = 3.77$)	6.35	1.73	2	838	2.11	1225	2.08	0.89	0.830
		1.73	2	800	0	1238	1.43	0.85	0.839
	12.7	2.44	2	1162	1.52	1786	0.99	0.87	0.857
		2.49	2	1463	1.21	2213	0.79	0.89	0.866
0.453 ($M = 1.34$)	6.35	1.73	2	1188	1.49	1725	0	1.26	1.17
		1.73	2	1238	1.43	1738	3.05	1.31	1.18
	12.7	2.45	2	1688	1.04	2350	0	1.26	1.13
		2.47	2	2000	0	2750	0	1.22	1.08
0.907 ($M = 0.45$)	6.35	1.73	2	1850	0	2675	1.32	1.96	1.81
		1.73	2	1850	0	2700	0	1.96	1.83
	12.7	2.45	2	2500	0	3675	0.96	1.87	1.76
		2.45	2						

TABLE E2, continued

Specimen H1 (n=1,15)

IMPACTOR MASS M_2 , kg	IMPACTOR RADIUS r , mm	IMPACTOR VELOCITY V , m/sec	NUMBER OF TESTS	AVERAGE MEASURED STRAINS				GENERALIZED STRAINS	
				ϵ_x $\times 10^6$	C.O.V.	ϵ_y $\times 10^6$	C.O.V.	$\bar{\epsilon}_x$	$\bar{\epsilon}_y$
0.228 ($M=0.234$)	6.35	1.73	2	1650	0	1387	3.82	1.47	1.43
		1.73	2	1687	3.14	1425	4.96	1.51	1.47
	12.7	2.45	2	2325	1.52	2000	0	1.47	1.46
		2.49	2	3000	0	2425	1.46	1.55	1.44
0.453 ($M=0.457$)	6.35	1.73	2	2200	3.21	2000	0	1.97	2.06
		1.73	2	2275	1.55	2000	0	2.03	2.06
	12.7	2.45	2	3275	1.08	2700	0	2.07	1.97
		2.49	2	4025	0.88	3300	0	2.08	1.97
0.907 ($M=0.923$)	6.35	1.73	3	3184	0.91	2684	2.85	2.85	2.77
	12.7	1.73	2	3025	1.17	2575	1.37	2.70	2.66
		2.45	2	4400	0	4000	0	2.78	2.92

TABLE E2, continued

Specimen H2 ($\eta=0.302$)

IMPACTOR MASS M_2 , kg	IMPACTOR RADIUS r , mm	IMPACTOR VELOCITY V , m/SEC	NUMBER OF TESTS	AVERAGE MEASURED STRAINS				GENERALIZED STRAINS	
				ϵ_x $\times 10^6$	C.O.V.	ϵ_y $\times 10^6$	C.O.V.	$\bar{\epsilon}_x$	$\bar{\epsilon}_y$
0.228 ($M=1.8$)	6.35	1.73	2	1350	0	1038	1.71	1.21	1.07
	12.7	1.73	2	1313	1.35	1063	4.99	1.17	1.10
		2.45	2	1975	1.79	1525	2.32	1.25	1.10
	6.35	2.99	2	2450	2.88	1850	2.82	1.26	1.10
0.453 ($M=0.90$)		1.73	2	2400	0	1825	1.93	2.14	1.83
	12.7	1.73	2	2400	0	1850	0	2.14	1.91
		2.45	2	3475	1.02	2700	0	2.20	1.97
	6.35	2.99	2	4375	0.81	3400	0	2.26	2.02
0.907 ($M=0.44$)		1.73	2	3500	0	2625	1.34	3.13	2.71
	12.7	1.73	2	3375	1.04	2600	0	3.02	2.68
		2.45	2	5000	0	3725	0.95	3.16	2.72

TABLE E2, continued

Specimen H3 (n=4.41)

IMPACTOR MASS M_2 , kg	IMPACTOR RADIUS r , mm	IMPACTOR VELOCITY V , m/sec	NUMBER OF TESTS	AVERAGE MEASURED STRAINS			GENERALIZED STRAINS	
				ϵ_x $\times 10^6$	C.O.V.	ϵ_y $\times 10^6$	$\bar{\epsilon}_x$	$\bar{\epsilon}_y$
0.228 ($M=1.75$)	6.35	1.73	2	1063	1.66	1100	0.95	1.13
	12.7	1.73	2	1063	1.66	1113	0.95	1.15
		2.45	2	1525	2.32	1675	0.96	1.22
		2.99	2	2038	0.87	2200	1.05	1.31
0.453 ($M=0.88$)	6.35	1.73	2	2000	0	2200	1.79	2.27
	12.7	1.73	2	2050	0	2213	1.83	2.28
		2.45	2	3000	0	3150	1.90	2.30
		2.99	2	3750	1.88	3950	1.94	2.35
0.907 ($M=0.44$)	6.35	1.73	2	2875	1.23	3200	2.57	3.3
	12.7	1.73	2	3000	0	3125	2.68	3.22
		2.45	2	4300	0	4625	2.72	3.30

TABLE E2, continued

Specimen B4 (n=1.15)

IMPACTOR MASS M_2 , kg	IMPACTOR RADIUS r , mm	IMPACTOR VELOCITY V , m/sec	NUMBER OF TESTS	AVERAGE MEASURED STRAINS			GENERALIZED STRAINS		
				ϵ_x $\times 10^6$	C.O.V.	ϵ_y $\times 10^6$	C.O.V.	$\bar{\epsilon}_x$	$\bar{\epsilon}_y$
0.228 ($M=3.39$)	6.35	1.73	2	1200	0	975	3.63	1.07	1.01
	12.7	1.73	2	1200	0	1000	0	1.07	1.03
		2.45	2	1600	4.42	1375	2.57	1.01	1.00
		2.99	2	1963	0.90	1725	2.04	1.01	1.03
0.453 ($M=1.7$)	6.35	1.73	2	1275	2.77	1100	0	1.14	1.13
	12.7	1.73	2	1225	2.63	1100	0	1.10	1.13
		2.45	2	1700	0	1350	5.24	1.07	0.99
		2.99	2	2150	0	1650	4.28	1.11	0.98
0.907 ($M=0.84$)	6.35	1.73	2	2025	1.74	1450	4.87	1.81	1.50
	12.7	1.73	2	2025	1.74	1375	2.57	1.81	1.42
		2.45	2	3150	2.24	2800	0	1.99	2.04

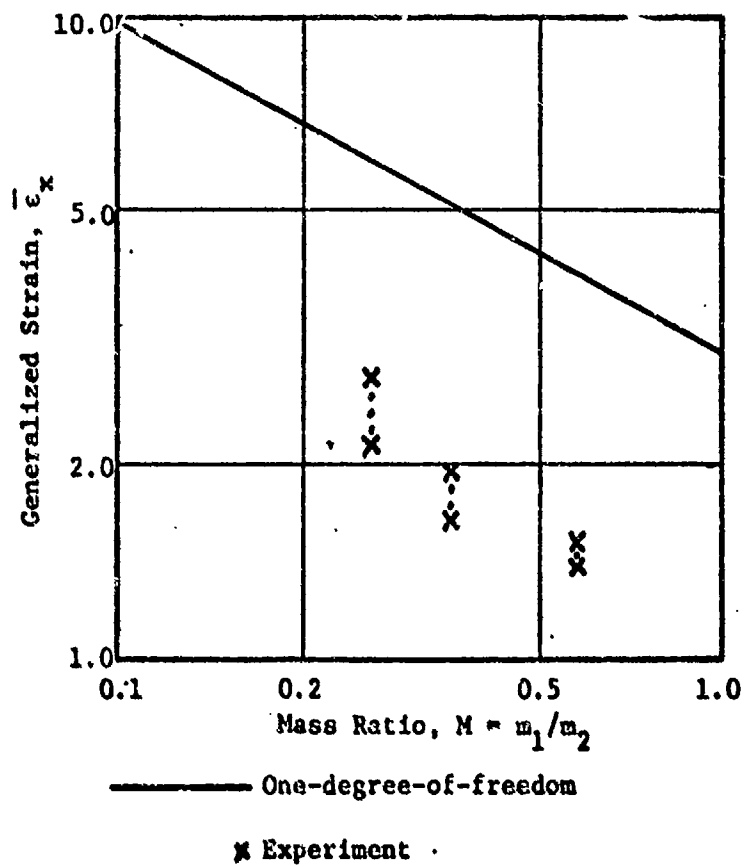


Figure E1. Design curve and experimental data for impact of a clamped aluminum plate ($\eta = 1.0$).

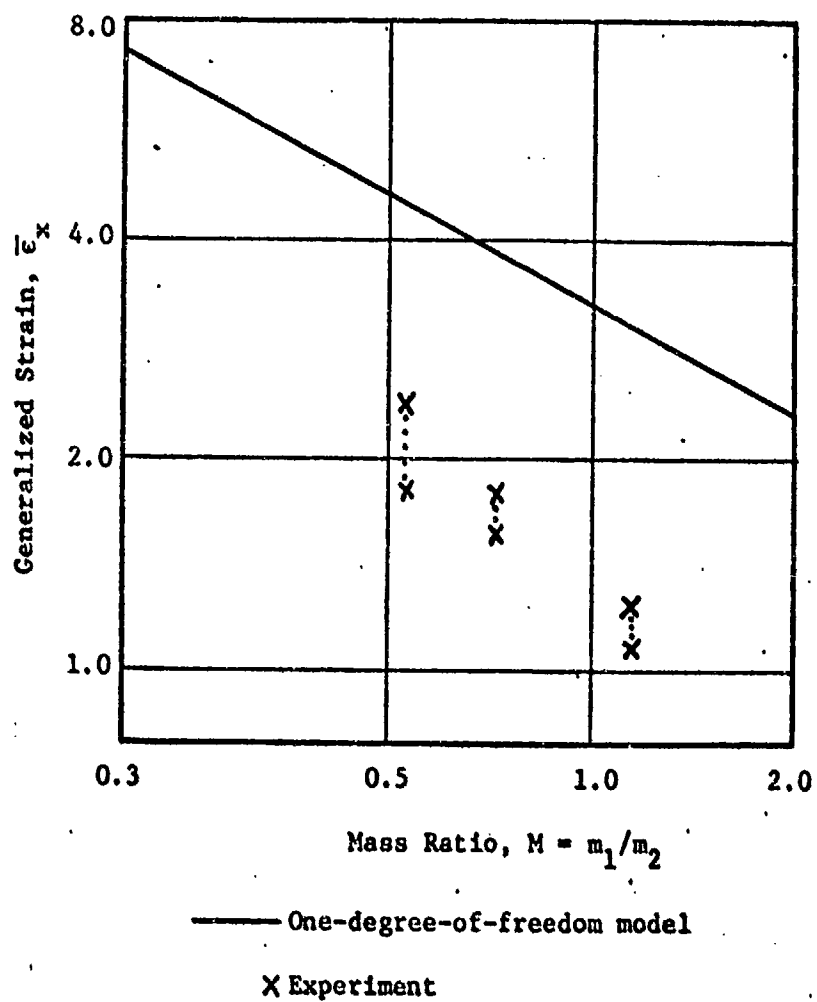
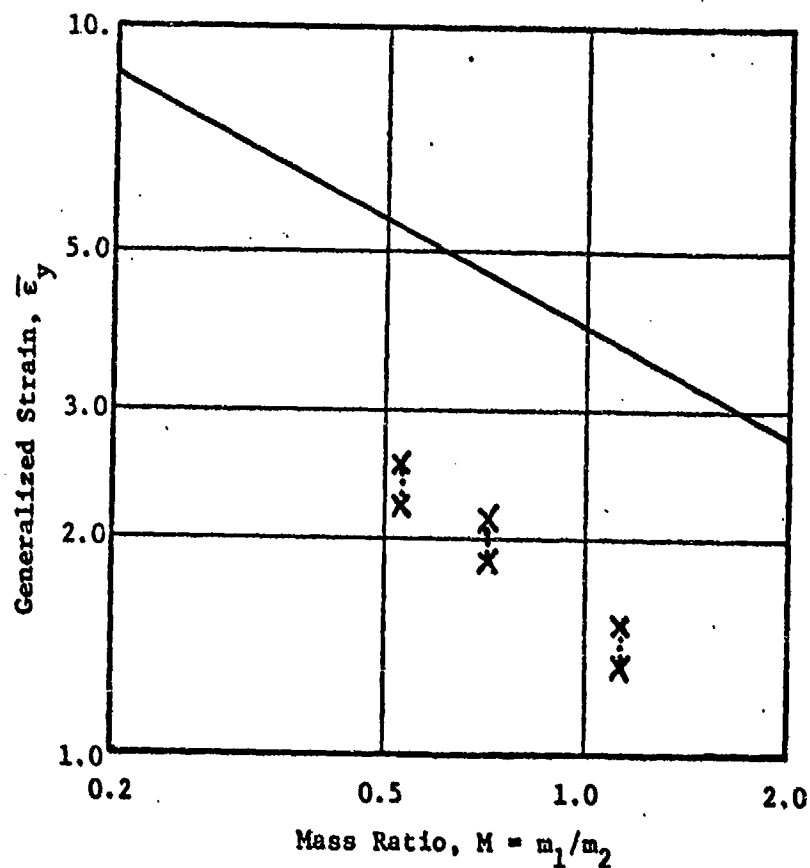


Figure E2. Design curve and experimental data for impact of a clamped aluminum plate ($\eta = 4.0$).



X Impact Experiments on Aluminum Plates

— One-Degree-of-Freedom Model

Figure E3. Design curve and experimental data for impact of a clamped aluminum plate ($1/\eta = 0.25$).

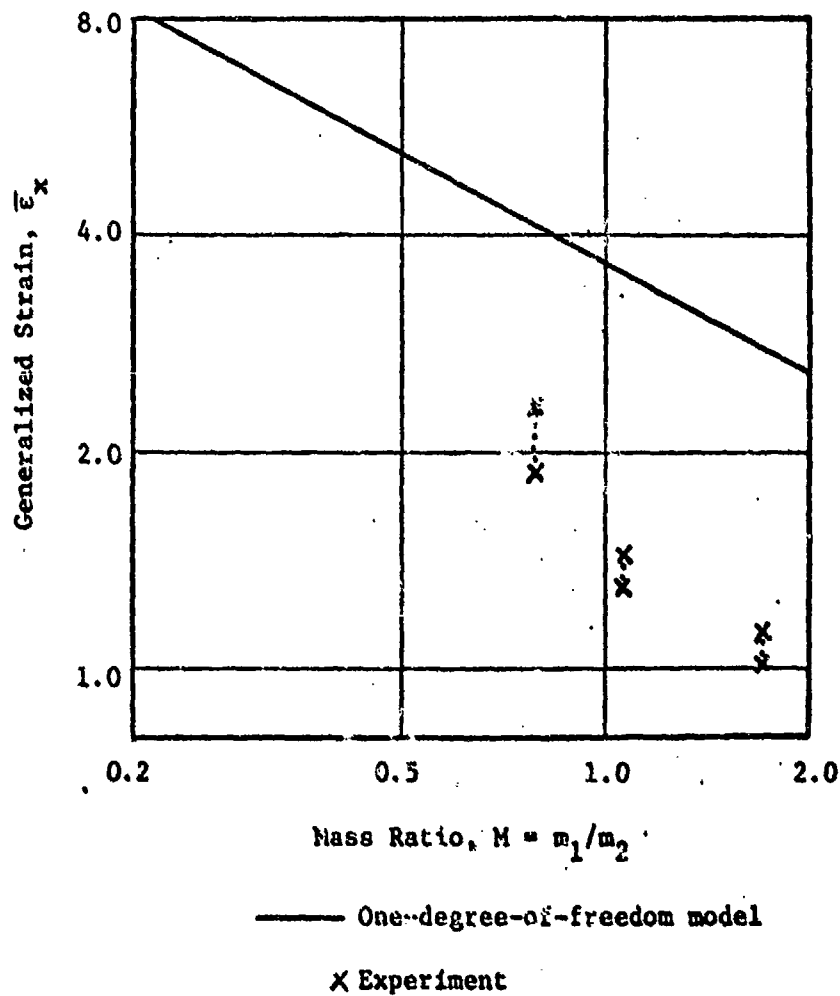


Figure E4. Design curve and experimental data for impact of a clamped aluminum plate ($\eta = 9.0$).

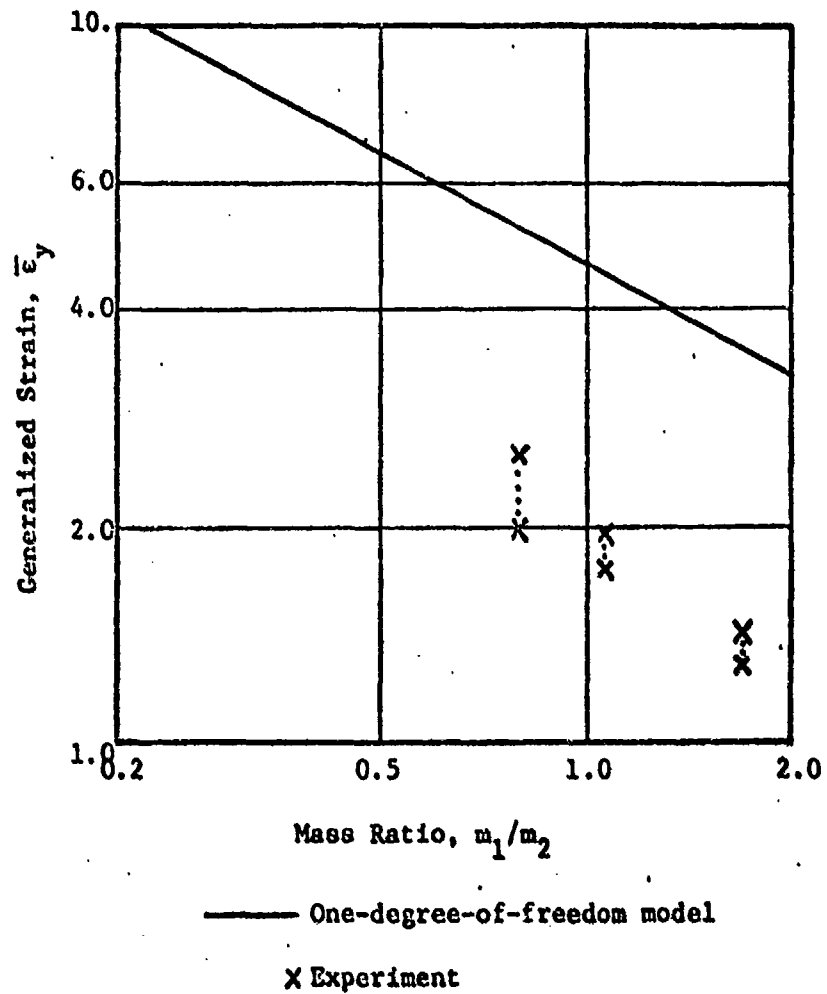


Figure E5. Design curve and experimental data for impact of a clamped aluminum plate ($1/\eta = 0.111$).

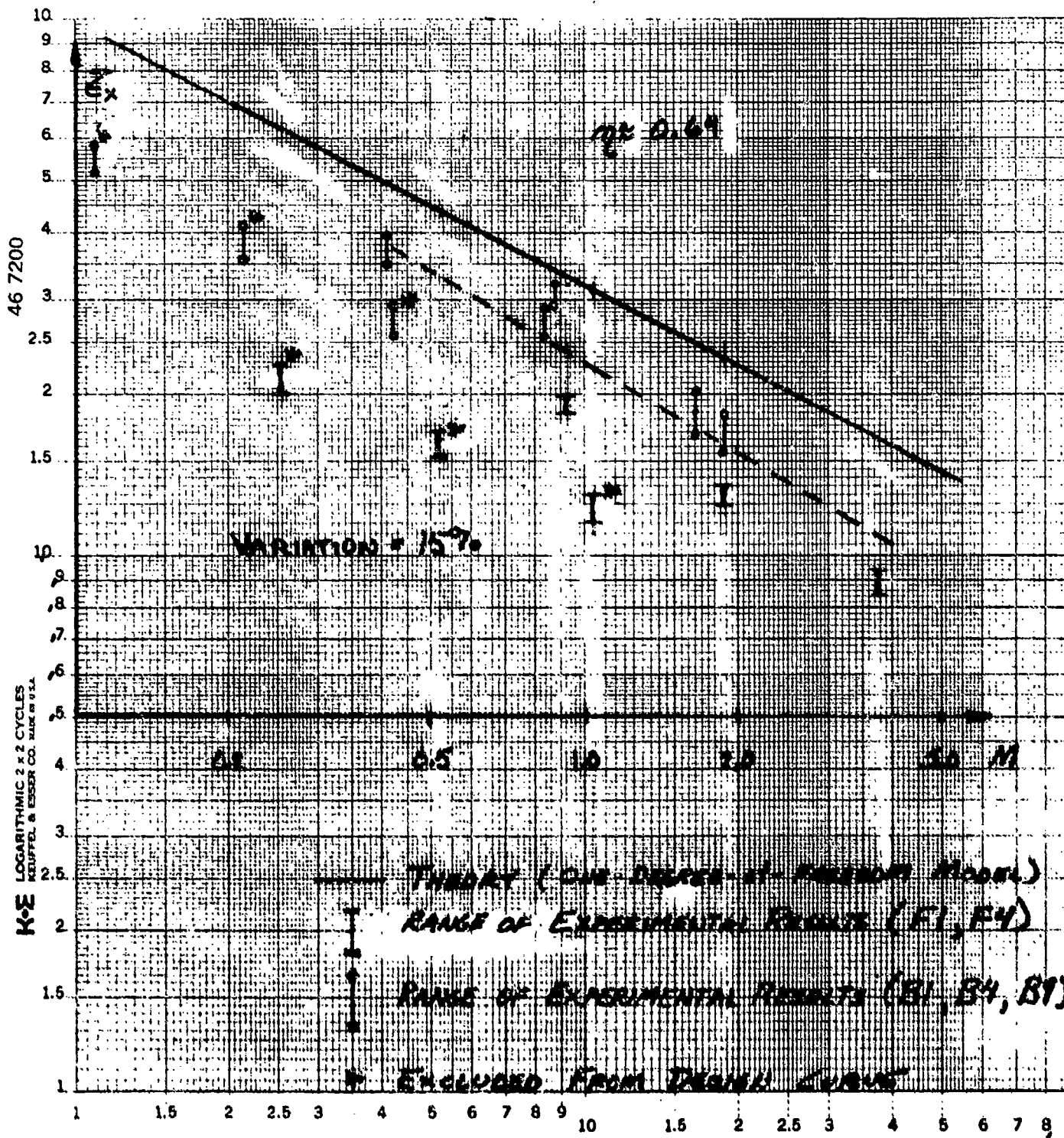


Figure B6. \bar{E}_x vs. M : Clamped Orthotropic Plate

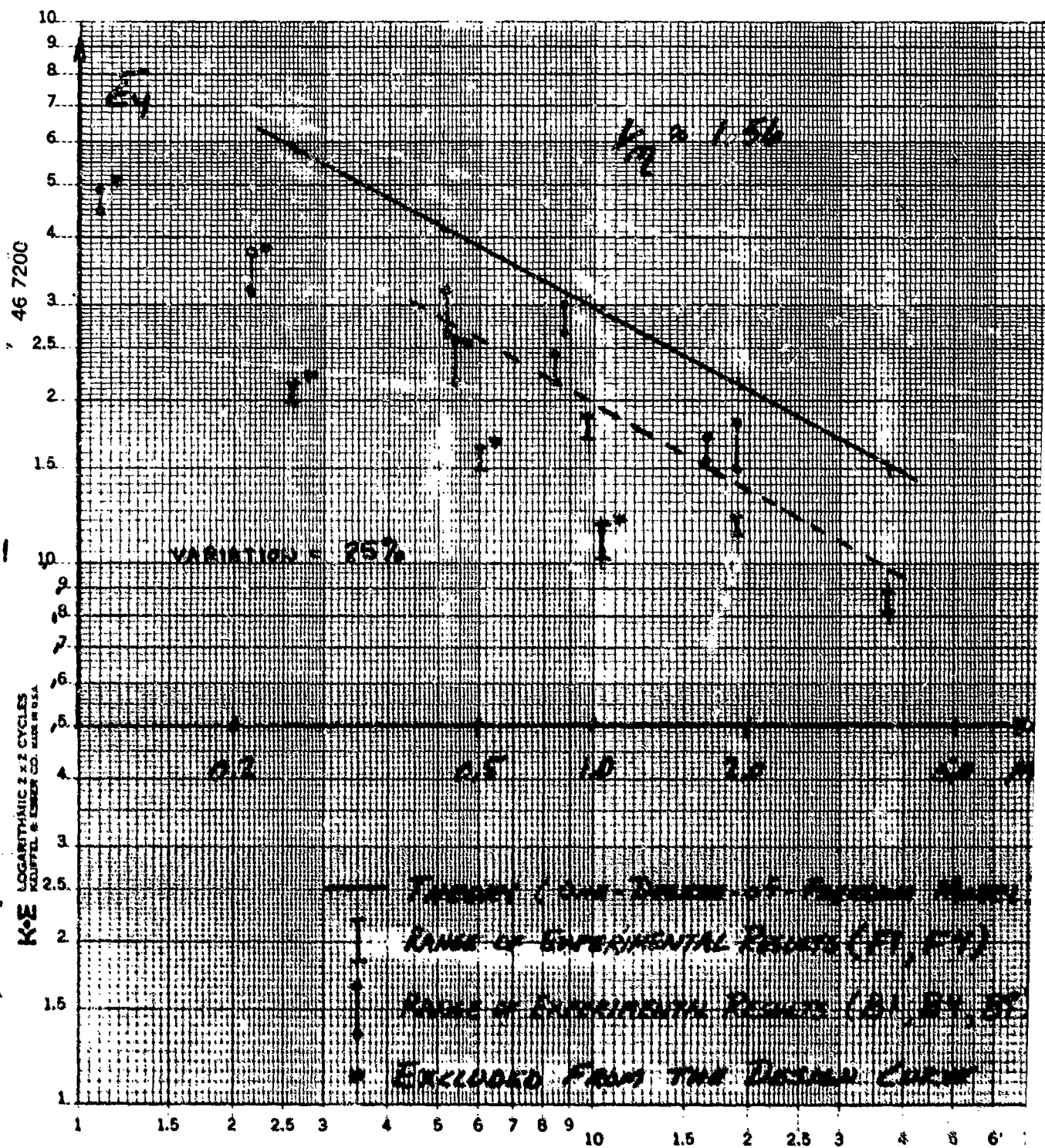


Figure E7. E_y vs. M_1 Clamped Orthotropic Plate

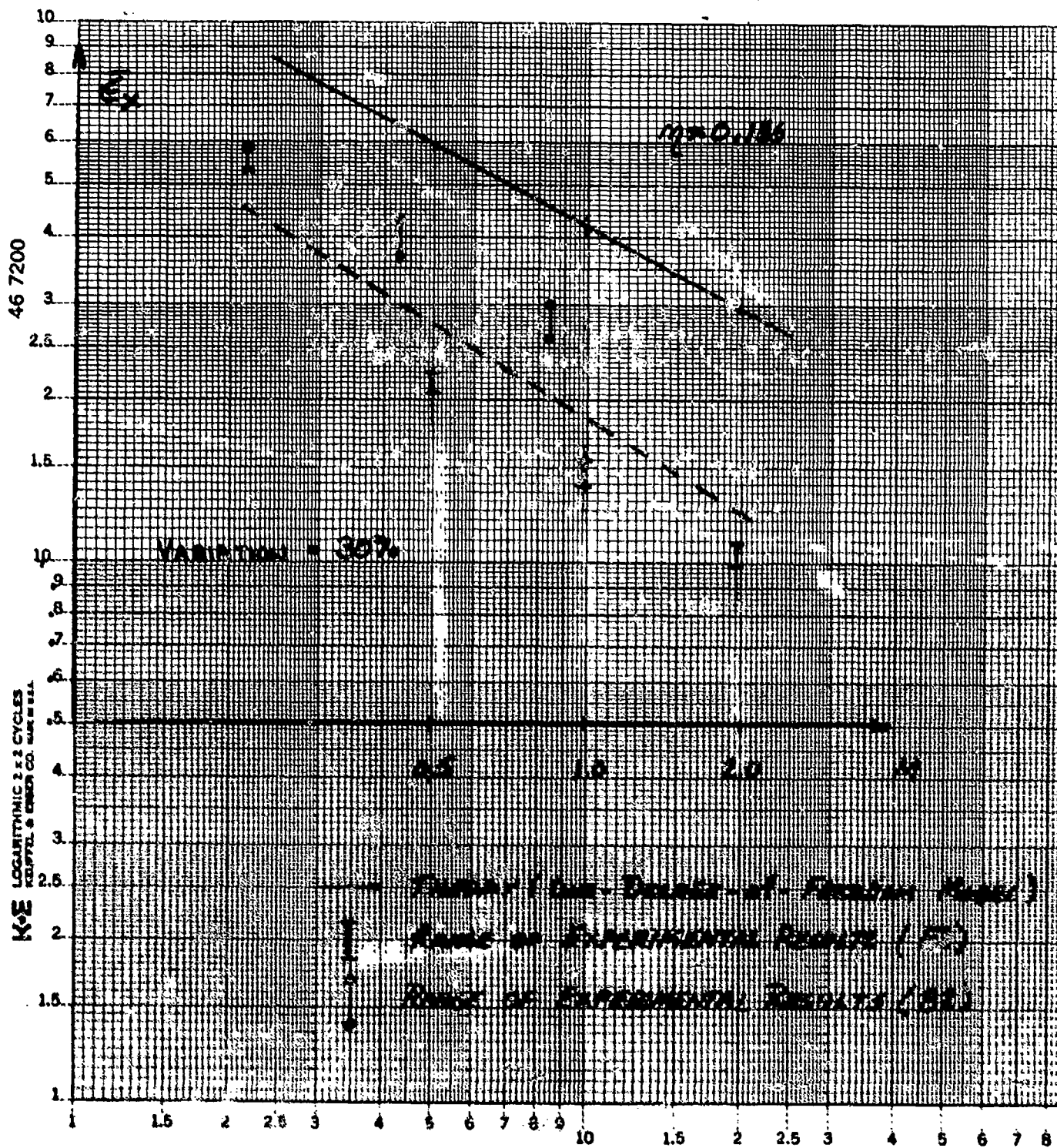


Figure B3. \bar{E}_x vs. N_1 Clamped Orthotropic Plate

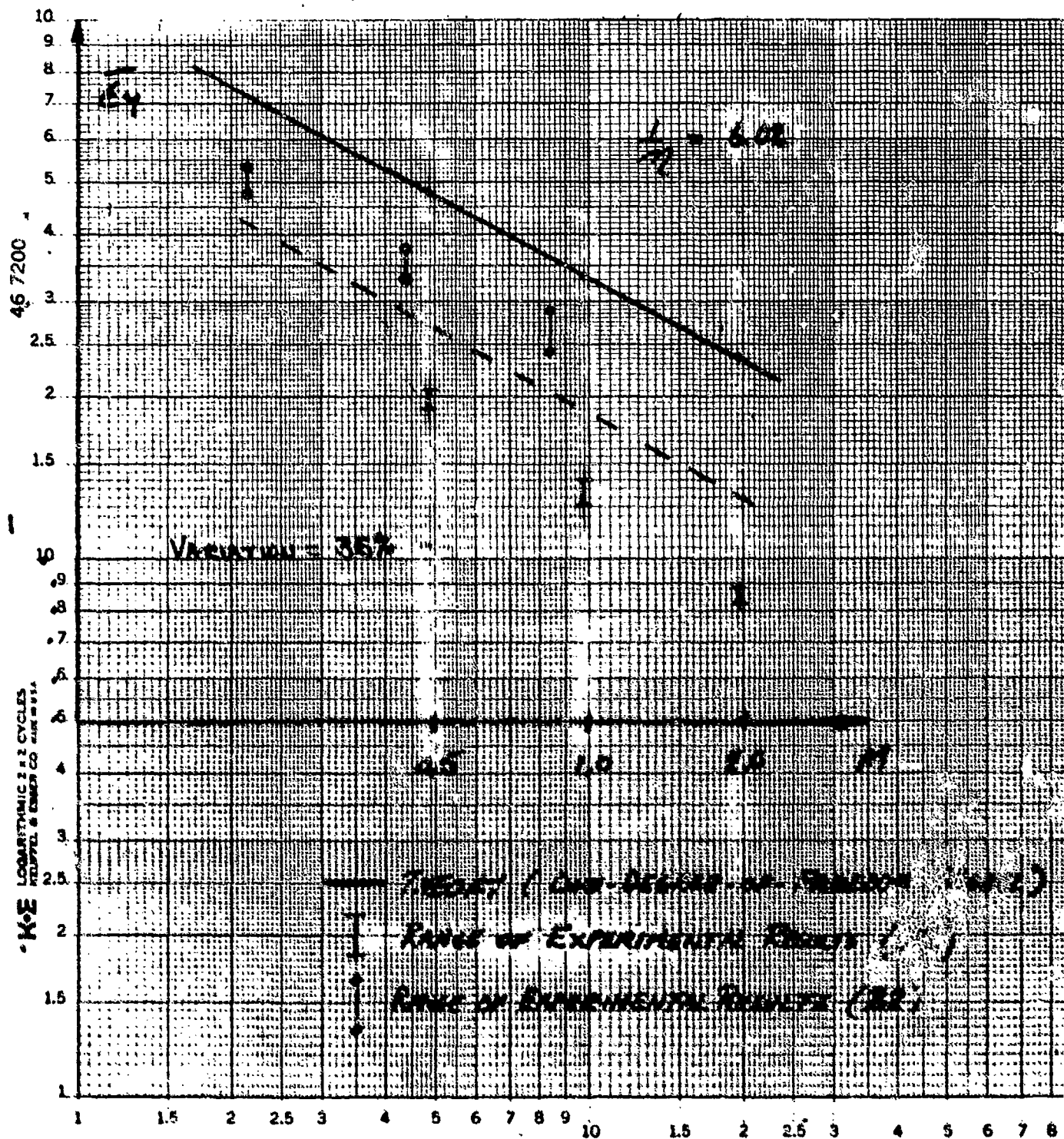


Figure E9. \bar{E}_y vs. N : Clamped Orthotropic Plate

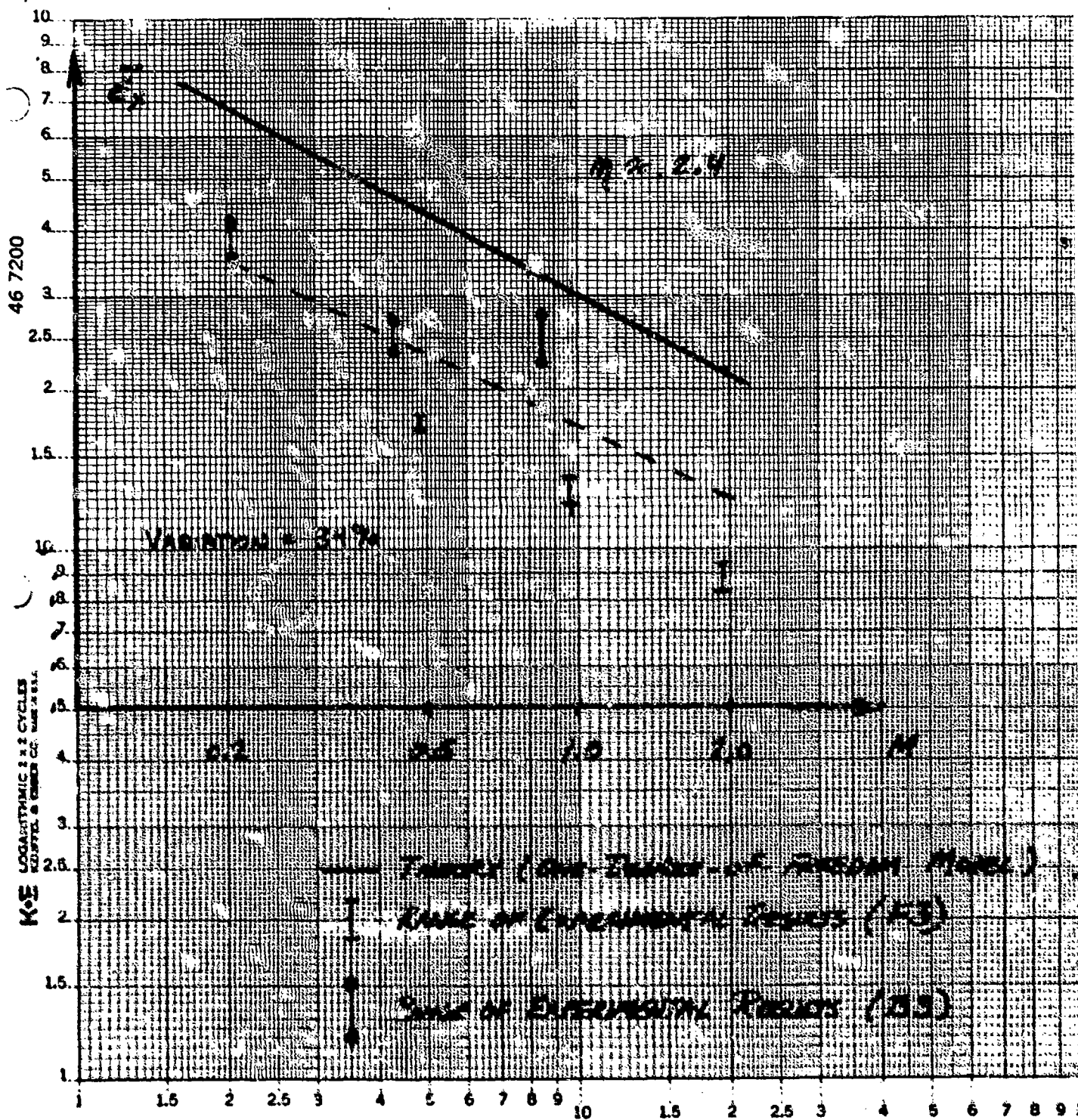


Figure E10. E_p vs. N : Glamped Orthotropic Plate

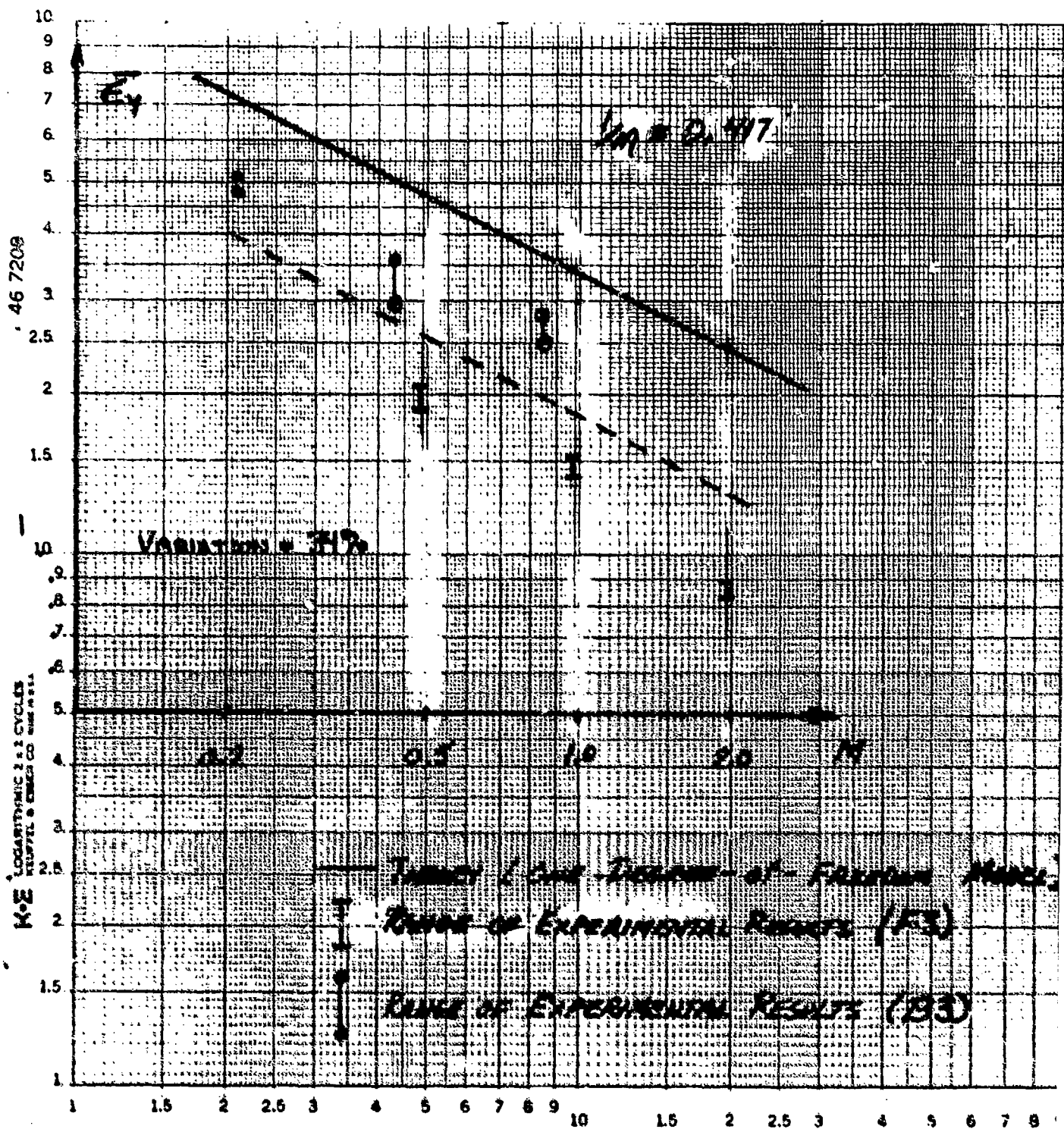


Figure E11. \bar{E}_y vs. N : Clamped Orthotropic Plate

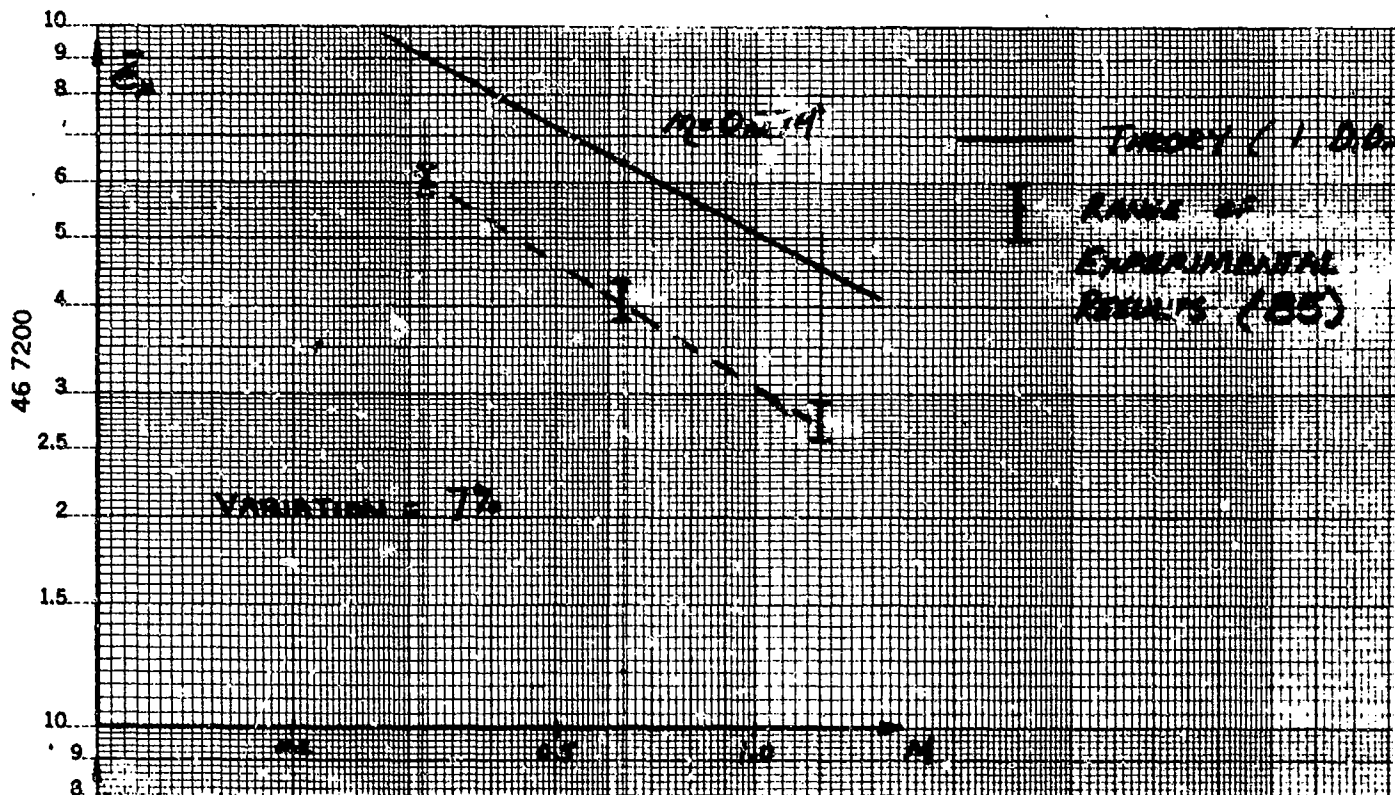


Figure E12. ϵ_x vs. M : Clamped Orthotropic plate

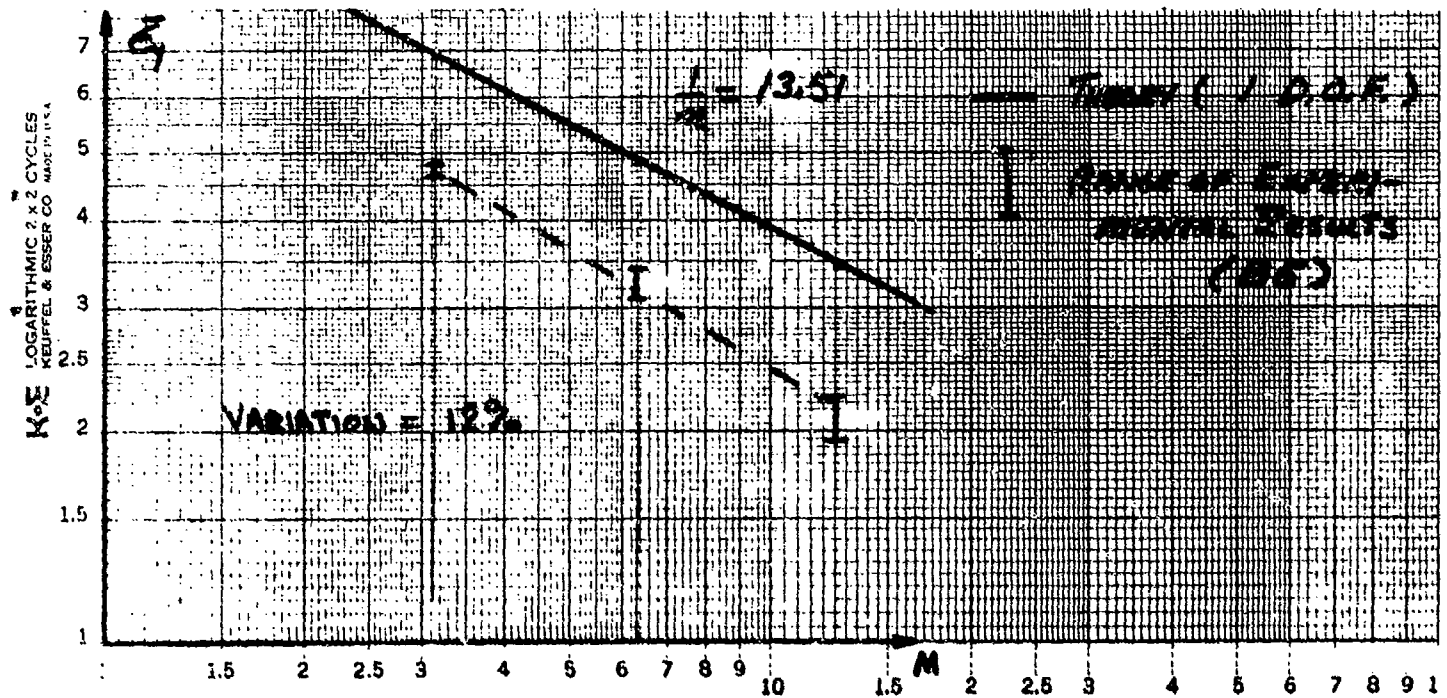


Figure E13. \bar{E}_y vs. M : Clamped Orthotropic Plate

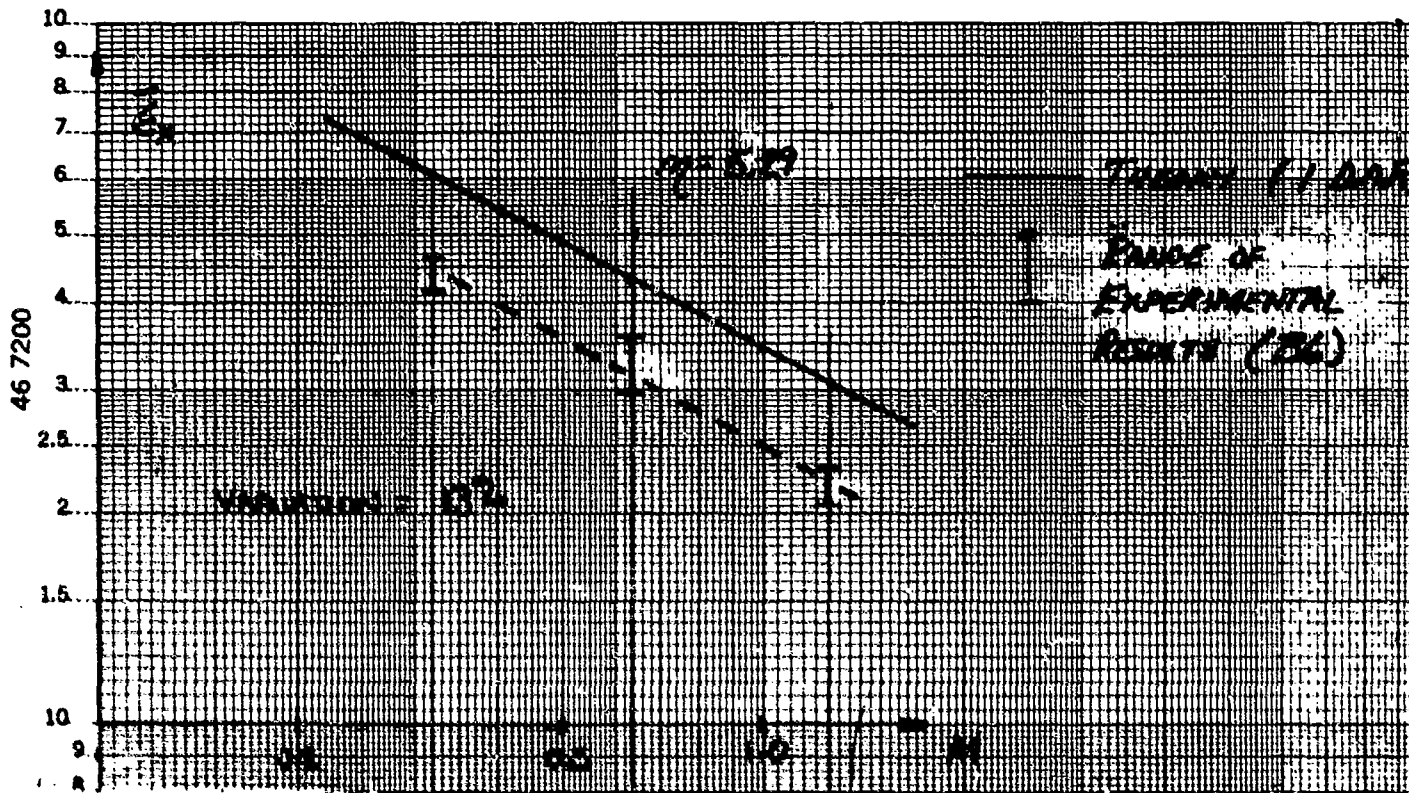


Figure E14. \bar{E}_x vs. M : Clamped Orthotropic Plate

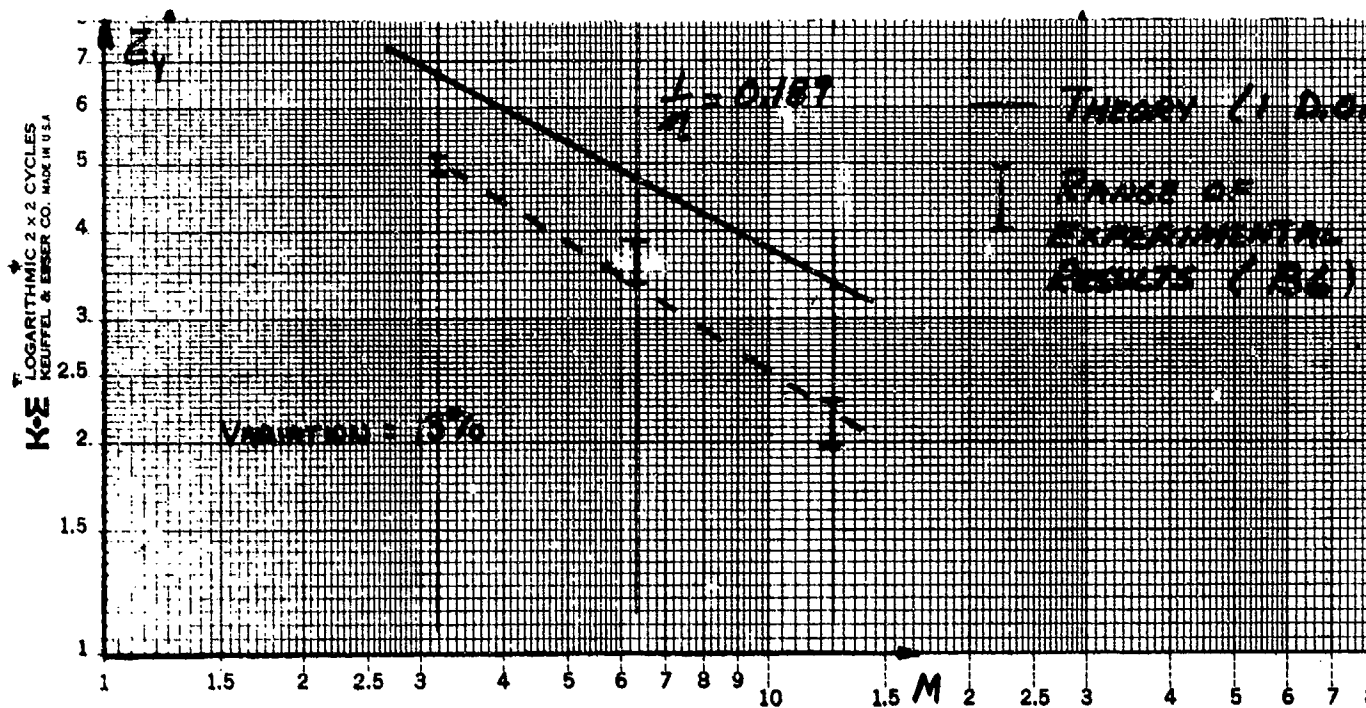


Figure E15. $\bar{\epsilon}_y$ vs. M : Clamped Orthotropic Plate

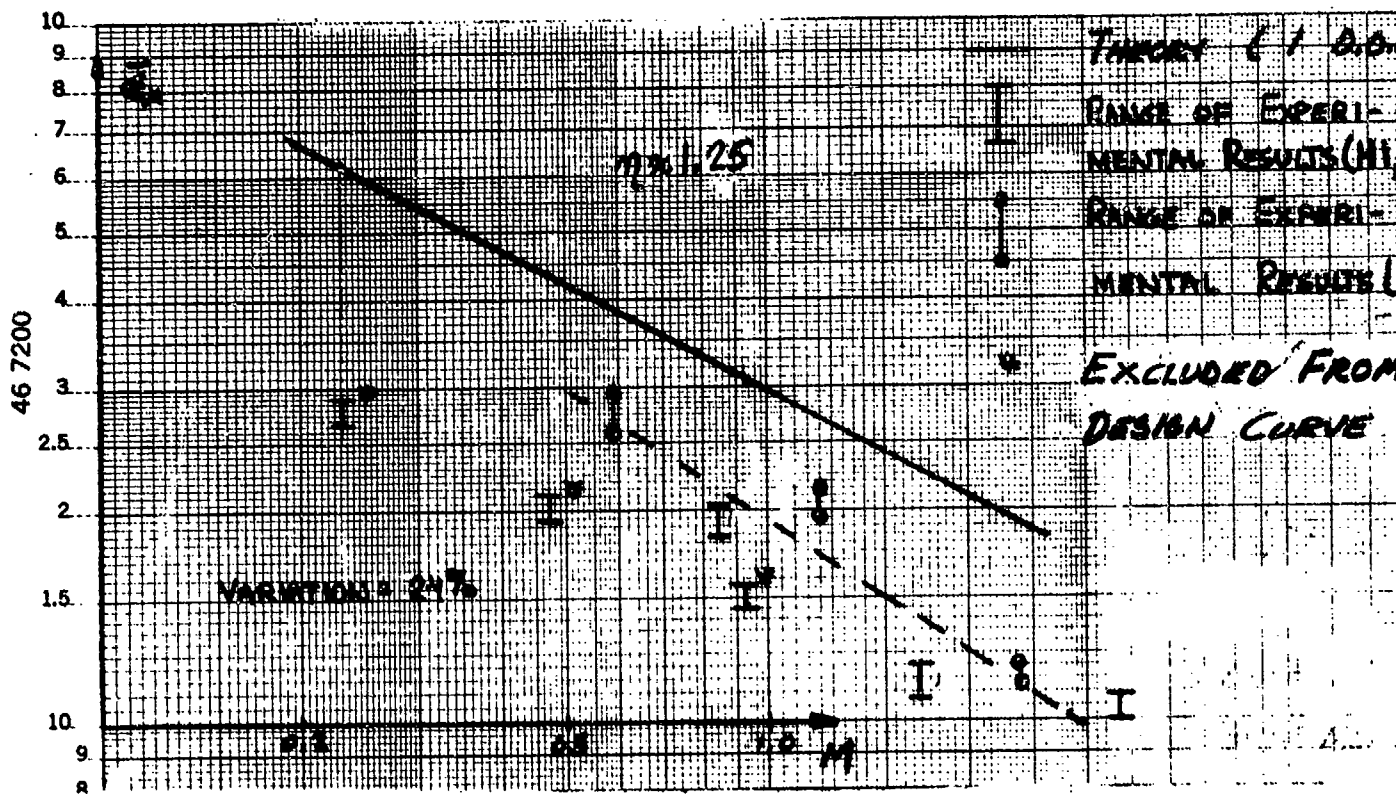


Figure E16. $\bar{\epsilon}_x$ vs. M : Clamped Orthotropic Plate

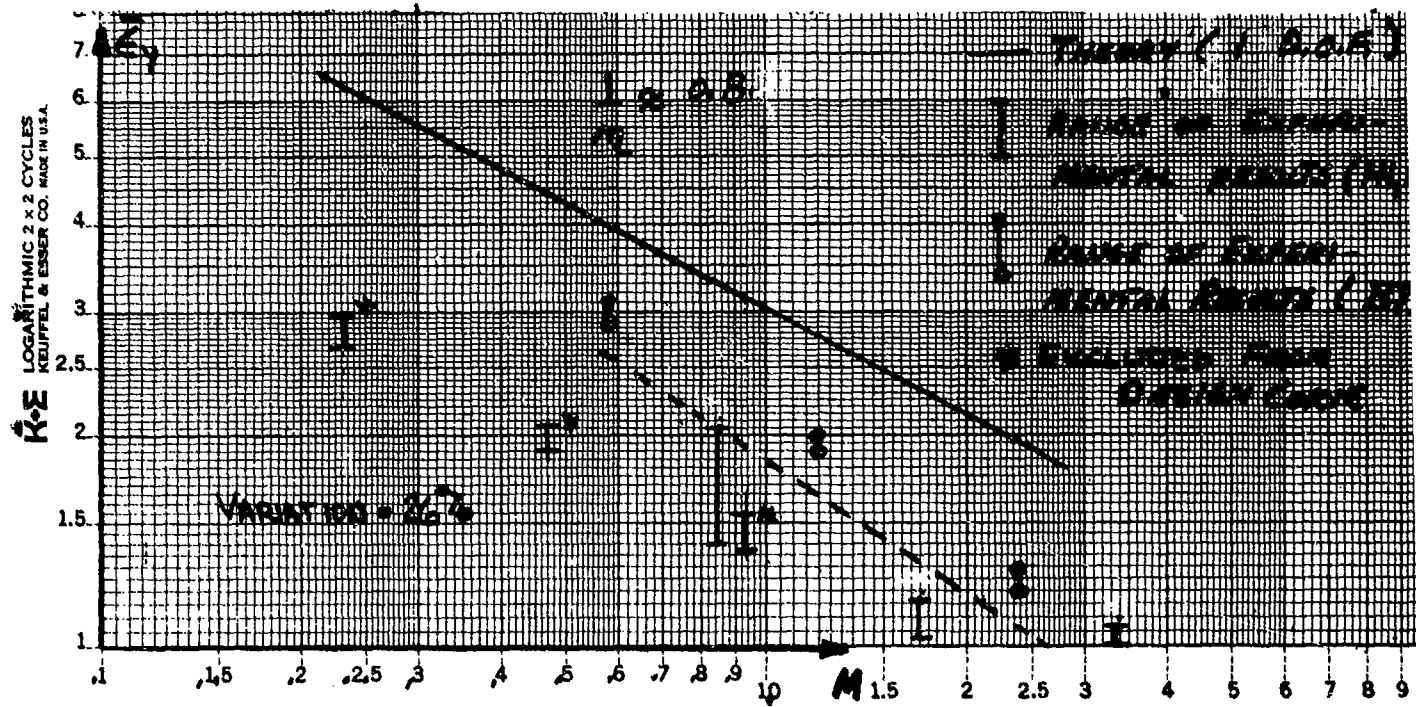


Figure E17. $\bar{\epsilon}_y$ vs. M : Clamped Orthotropic Plate

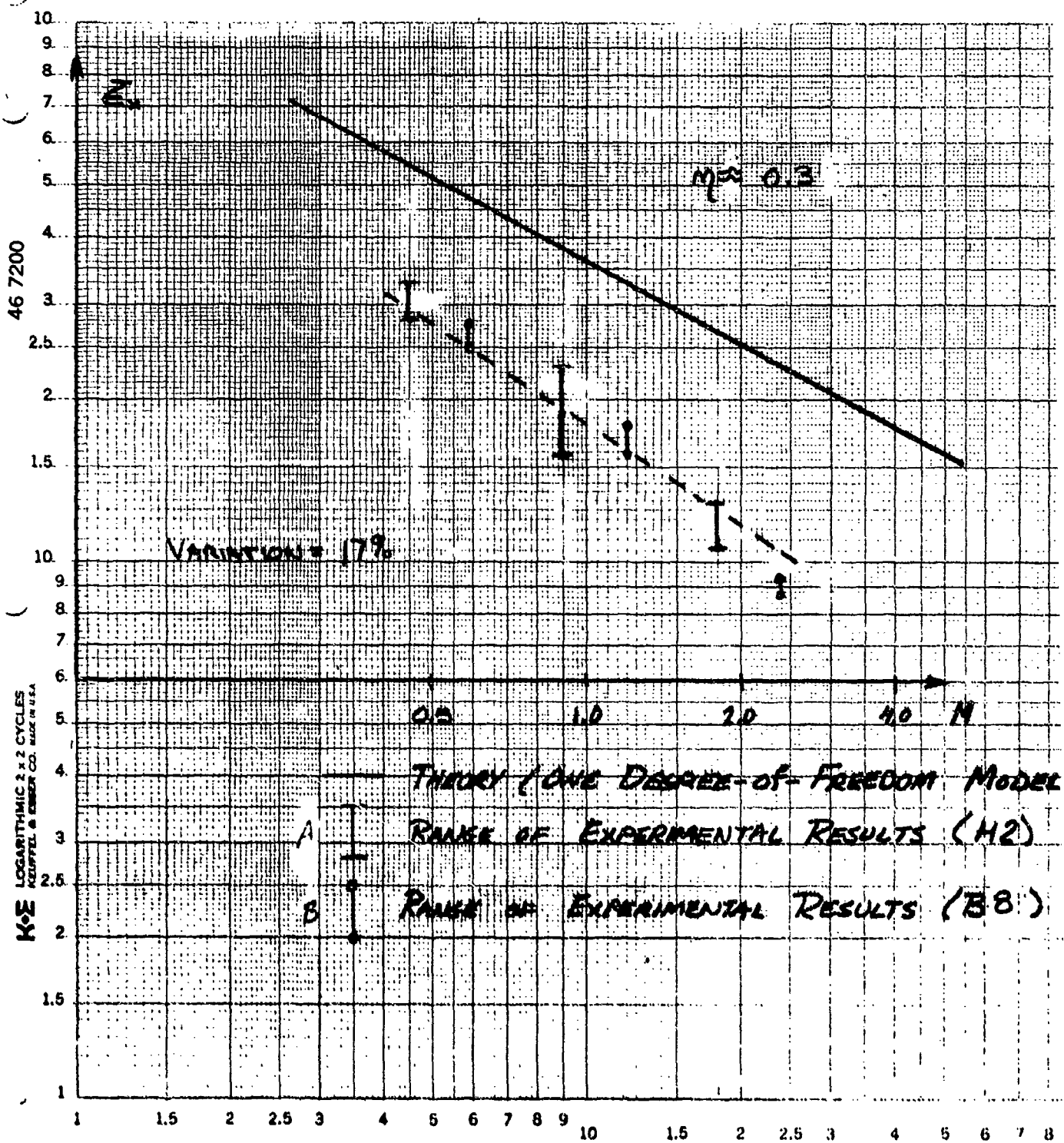


Figure E18. \bar{C}_n vs. M : Clamped Orthotropic Plate

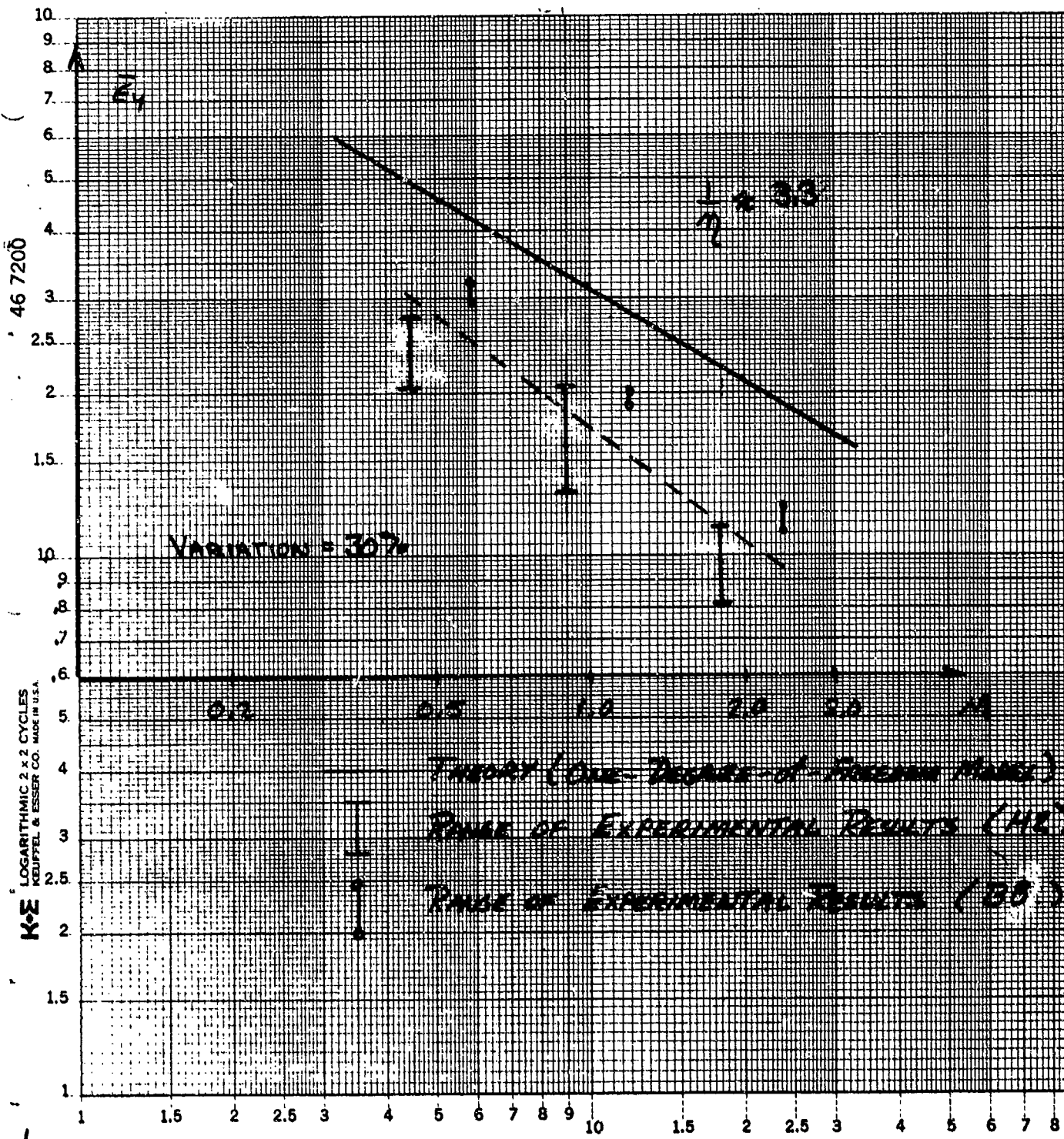


Figure E19. E_y vs. M : Clamped Orthotropic Plate

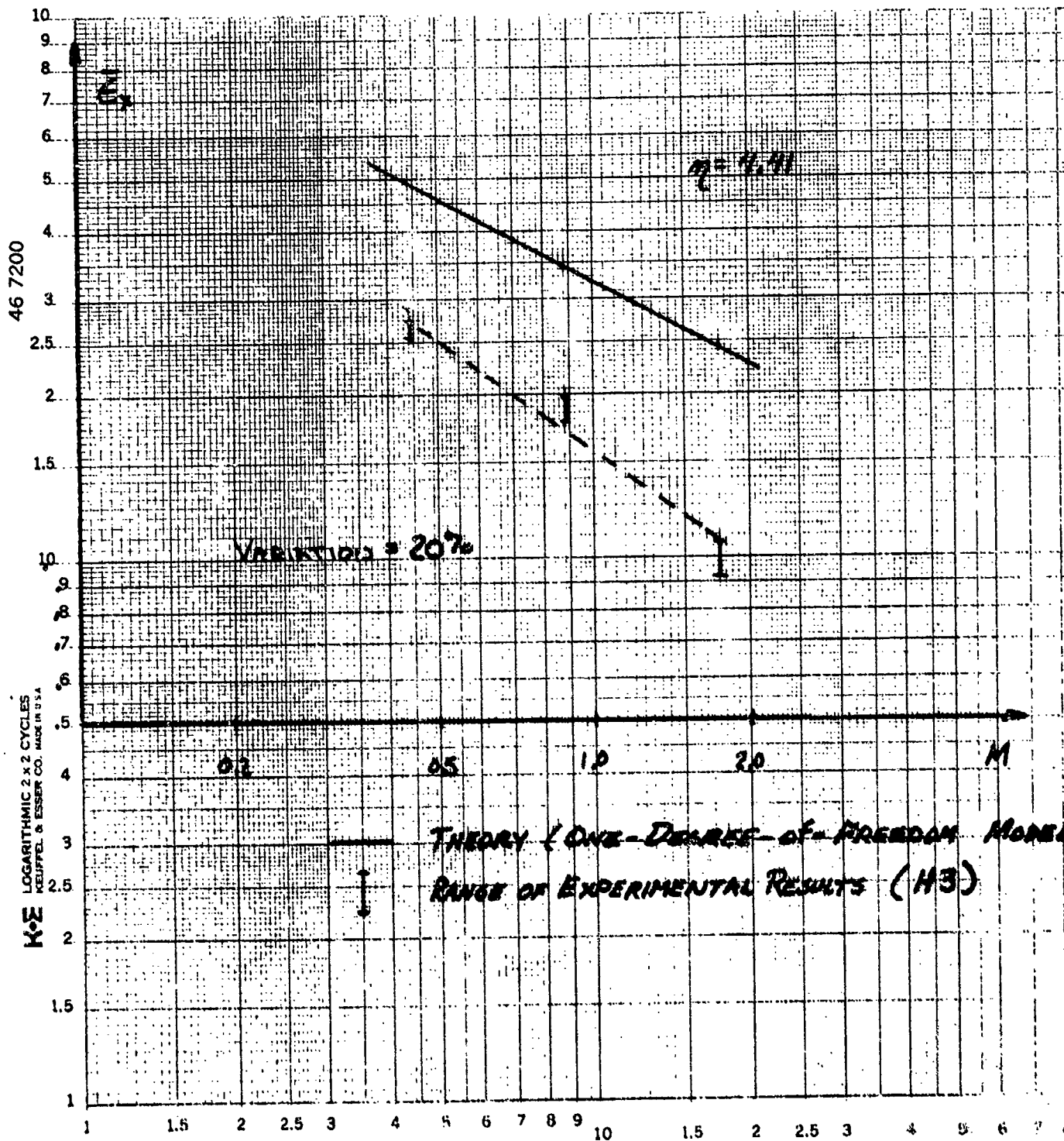


Figure E20'. \bar{Z}_x vs. M: Clamped Orthotropic Plate

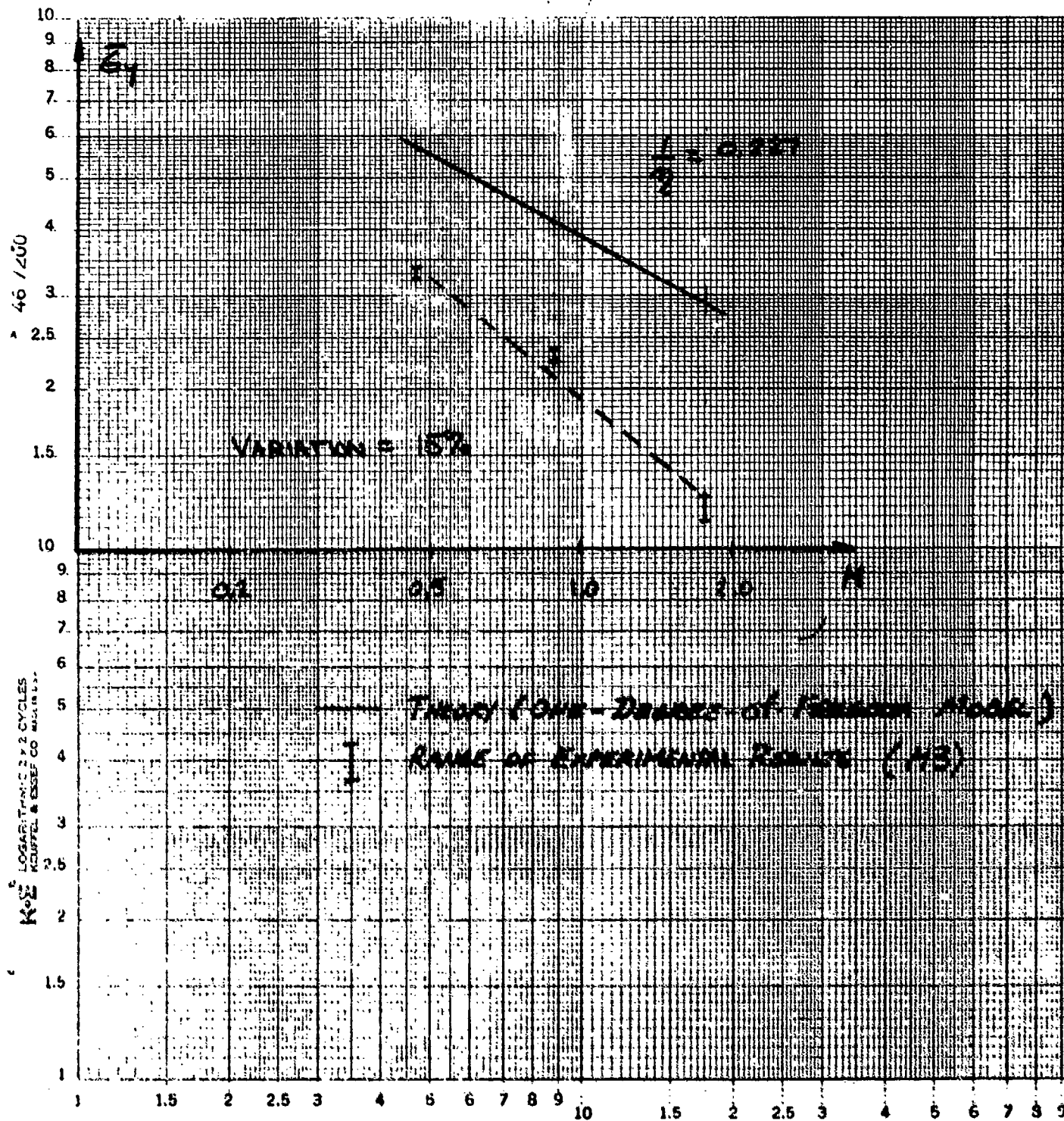


Figure E21. \bar{E}_y vs. M_1 Clamped Orthotropic Plate

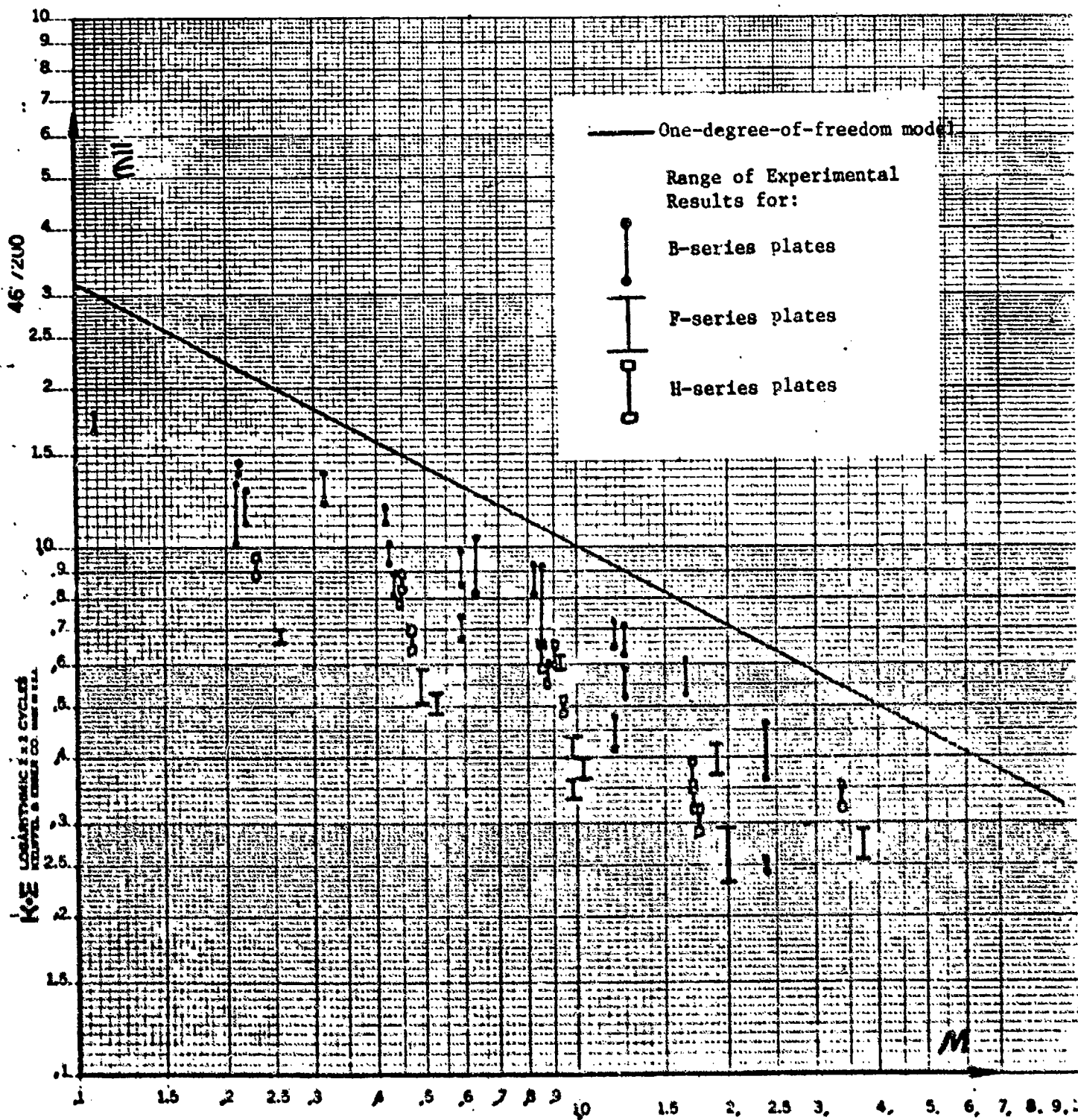


Figure B22. Strain Curve for Clamped Plate Impacted by Large Impactors.

TABLE E3. TRANSVERSE IMPACT EXPERIMENTS ON SIMPLY SUPPORTED ALUMINUM PLATES

Specimen Dimensions, $a \times b \times h$ (mm)	Impact Mass, m_2 (kg)	Impact Velocity, v (m/sec)	Number of Tests Performed	Maximum Measured Strain			Generalized Strain		Mass Ratio, $\frac{m_1}{m_2}$
				Average, $\epsilon_x \times 10^6$	Coeff. of Variation per cent	Average, $\epsilon_y \times 10^6$	Coeff. of Variation per cent	$E_x = \epsilon_x \times \frac{s^2}{h v}$	$E_y = \epsilon_y \times \frac{s^2}{h v}$
125x125x6.35 $\eta = 1.0$	0.495	2.44	4	2262	4.2	2338	2.0	1.400	1.447
		2.99	3	2983	1.0	2983	1.0	1.507	1.507
		3.46	4	3425	6.9	3488	1.8	1.495	1.522
		4.23	4	4150	4.6	4225	3.6	1.482	1.509
	0.784	2.44	4	2638	2.8	2662	2.8	1.633	1.648
		2.99	5	3080	5.3	3260	6.0	1.556	1.647
		3.46	4	3650	5.7	3925	2.4	1.593	1.713
		4.23	3	5033	1.1	5200	0.0	1.797	1.857
	1.057	2.44	4	2900	8.9	2900	8.9	1.795	1.795
		2.99	4	3800	4.8	3925	1.3	1.919	1.983
		3.46	5	4500	5.9	4500	4.4	1.964	1.964
		4.23	4	7075	8.9	7300	4.6	2.526	2.606
250x125x6.35 $\eta = 4.0$	0.495	2.44	5	2030	6.7	1960	6.6	1.257	1.213
		2.99	6	2758	3.7	2717	3.6	1.393	1.372
		3.46	4	3300	5.5	3500	2.3	1.440	1.528
		4.23	4	4150	4.2	4850	2.1	1.482	1.732
	0.784	2.44	4	2650	4.9	2625	1.9	1.640	1.625
		2.99	5	3360	3.4	3530	2.4	1.697	1.783
	1.135	2.44	4	2650	4.9	2625	1.9	1.640	1.625
		2.99	5	3360	3.4	3530	2.4	1.697	1.783
		3.46	4	3300	5.5	3500	2.3	1.440	1.528
		4.23	4	4150	4.2	4850	2.1	1.482	1.732
	0.716	2.44	4	2650	4.9	2625	1.9	1.640	1.625
		2.99	5	3360	3.4	3530	2.4	1.697	1.783
		3.46	4	3300	5.5	3500	2.3	1.440	1.528
		4.23	4	4150	4.2	4850	2.1	1.482	1.732

TABLE E3. (continued)

Specimen Dimensions a x b x h (mm)	Impactor Mass, m ₂ (kg)	Impact Velocity, v (m/sec)	Number of Tests Performed	Maximum Measured Strain				Generalized Strain		Mass Ratio, $\frac{m_1}{m_2}$ M = $\frac{m_1}{m_2}$
				Average, ε _x x 10 ⁶	Coeff. of Variation per cent	Average, ε _y x 10 ⁶	Coeff. of Variation per cent	$\frac{\epsilon_x}{\epsilon_y} = \frac{c_x}{c_y} \frac{s_x}{s_y} \frac{h_y}{h_x} \frac{2}{2}$	$\frac{\epsilon_y}{\epsilon_x} = \frac{c_y}{c_x} \frac{s_y}{s_x} \frac{h_x}{h_y} \frac{2}{2}$	
250x125x 6.35 (continued)	1.057	2.44	4	3288	4.4	3438	1.4	2.035	2.129	0.531
		2.99	4	3675	1.4	4375	1.1	1.856	2.210	
		3.46	4	4675	5.3	5200	1.6	2.041	2.270	
		4.23	2	-	-	8000	0.0	-	2.856	
375x125x 6.35 η = 4.0	0.784	3.46	5	3720	4.8	4220	3.5	1.624	1.842	0.716
		4.23	4	4575	1.1	5225	1.0	1.633	1.866	
		2.44	3	1317	2.2	1883	5.5	0.815	1.156	
		2.99	3	1767	1.6	2467	4.7	0.893	1.246	
	0.784	3.46	8	2069	5.2	2831	3.8	0.903	1.258	1.685
		4.23	5	2190	9.2	3290	0.7	0.782	1.175	
		2.44	4	2188	3.9	3125	0.9	1.354	1.934	
		2.99	4	2388	4.7	3500	0.0	1.181	1.768	
1.057	3.46	8	2975	9.1	4012	2.1	1.299	1.751	1.063	
	4.23	4	3900	3.0	4800	0.0	1.392	1.714		
	2.44	6	2567	4.0	3650	1.5	1.589	2.259		
	2.99	4	3400	4.2	4450	2.9	1.717	2.248		
	1.057	3.46	4	4325	5.1	5075	3.7	1.888	2.215	0.788
		4.23	4	5375	4.4	6250	3.8	1.919	2.232	

TABLE EA
DATA FROM STRAIN-MEASUREMENT IMPACT EXPERIMENTS
ON SIMPLY SUPPORTED GRAPHITE-EPOXY PLATES

Specimen B1 ($\eta=0.625$)

Impactor Mass M_i , Kg.	Impactor Radius r , mm	Impactor Velocity V , m/sec	Number of Tests	AVERAGE MEASURED STRAINS				GENERALIZED STRAINS	
				$\epsilon_x \times 10^6$	C.O.V.	$\epsilon_y \times 10^6$	C.O.V.	$\bar{\epsilon}_x$	$\bar{\epsilon}_y$
0.228 ($M=0.24$)	6.35	1.73	5	1710	15.8	2535	15.58	1.94	1.80
		1.73	6	1741	15.5	2591	13.8	1.98	1.84
	12.7	2.45	5	2700	16.3	3970	15.2	2.17	1.99
		2.99	3	3700	7.15	5350	2.47	2.42	2.19
0.453 ($M=0.24$)	6.35	1.73	4	2475	3.86	3437	5.98	2.81	2.44
		1.73	6	2725	15.89	4033	21.9	3.09	2.86
	12.7	2.45	5	3760	18.8	5330	17.6	3.02	2.67
		2.99	5	5220	16.1	7010	21.7	3.42	2.87
0.907 ($M=0.24$)	6.35	1.73	4	3775	6.96	4750	3.65	4.28	3.37
	12.7	1.73	5	4440	3.42	6420	1.30	5.04	4.55

TABLE E4, continued

Specimen B2 ($\eta=0.614$)

IMPACTOR MASS M_2 , Kg.	IMPACTOR RADIUS r , mm	IMPACTOR VELOCITY V , m/sec	NUMBER OF TESTS	AVERAGE MEASURED STRAINS				GENERALIZED STRAINS	
				$\bar{\epsilon}_x$ $\times 10^6$	C.O.V.	$\bar{\epsilon}_y$ $\times 10^6$	C.O.V.	$\bar{\epsilon}_x$	$\bar{\epsilon}_y$
0.228 ($M=0.455$)	6.35	1.73	2	1600	0	2250	9.42	1.82	1.60
	12.7	1.73	4	1550	5.88	1925	3.35	1.79	1.36
		2.45	9	2211	7.56	3194	8.30	1.77	1.60
		2.99	11	3018	7.85	4005	10.72	1.98	1.64
0.453 ($M=0.455$)	6.35	1.73	5	2400	3.89	3090	6.51	2.72	2.19
	12.7	1.73	5	2710	11.4	3520	14.1	3.07	2.50
		2.45	5	3710	12.14	4780	10.7	2.98	2.40
		2.99	6	4608	17.39	6608	3.12	3.02	2.71
0.907 ($M=0.213$)	6.35	1.73	5	3550	7.04	4600	6.33	4.03	3.26
	12.7	1.73	5	3860	2.32	5510	4.07	4.38	3.91

TABLE E4, continued

Specimen B3 (n=2.39)

IMPACTOR MASS M_2 , Kg	IMPACTOR RADIUS r , mm	IMPACTOR VELOCITY V , m/sec	NUMBER OF TESTS	AVERAGE MEASURED STRAINS				GENERALIZED STRAINS	
				$\bar{\epsilon}_x \times 10^6$	C.O.V.	$\epsilon_y \times 10^6$	C.O.V.	$\bar{\epsilon}_x$	$\bar{\epsilon}_y$
0.228 ($M=0.35$)	6.35	1.73	2	1250	5.66	2250	3.14	1.42	1.60
	12.7	1.73	2	1250	5.66	2300	6.15	1.42	1.63
		2.45	2	1850	3.82	3550	5.97	1.40	1.78
		2.99	2	2550	2.77	4550	1.55	1.67	1.86
0.453 ($M=0.87$)	6.35	1.73	2	1750	12.12	3700	3.82	1.99	2.62
	12.7	1.73	2	1850	3.82	3600	0	2.10	2.55
		2.45	2	2900	4.87	5250	1.34	2.33	2.63
		2.99	2	3700	3.82	6700	2.11	2.42	2.74
0.907 ($M=0.21$)	6.35	1.73	2	2800	0	5300	0	3.08	3.76
	12.7	1.73	2	2850	2.48	5300	0	3.23	3.76
		2.45	2	4200	0	8000	0	3.37	4.01

TABLE E4, continued

Specimen B4 ($\eta=0.625$)

IMPACTOR MASS M_2 , kg.	IMPACTOR RADIUS r , mm	IMPACTOR VELOCITY V , m/sec	NUMBER OF TESTS	AVERAGE MEASURED STRAINS				GENERALIZED STRAINS	
				ϵ_x $\times 10^6$	C.O.V.	ϵ_y $\times 10^6$	C.O.V.	$\bar{\epsilon}_x$	$\bar{\epsilon}_y$
0.228 ($M=1.66$)	6.35	1.73	2	1100	0	1600	0	1.25	1.13
	12.7	1.73	2	1025	3.45	1662	3.19	1.16	1.18
		2.45	2	1525	2.32	2175	4.87	1.22	1.09
		2.99	3	2000	2.50	2867	5.33	1.31	1.17
0.453 ($M=0.84$)	6.35	1.73	2	1775	1.99	2575	1.37	2.01	1.85
	12.7	1.73	2	1775	1.99	2450	0	2.01	1.74
		2.45	3	2500	0	3517	4.57	2.00	1.76
		2.99	2	3000	0	4425	0.79	1.97	1.81
0.907 ($M=0.42$)	6.35	1.73	2	2700	0	3900	3.63	3.06	2.77
	12.7	1.73	2	2575	1.37	3050	1.84	2.92	2.73

TABLE E4, continued

Specimen B5 ($n=0.074$)

IMPACTOR MASS M_2 , Kg.	IMPACTOR RADIUS r , mm	IMPACTOR VELOCITY V , m/sec	NUMBER OF TESTS	AVERAGE MEASURED STRAINS				GENERALIZED STRAINS	
				$\bar{\epsilon}_x$ $\times 10^6$	C.O.V.	$\bar{\epsilon}_y$ $\times 10^6$	C.O.V.	$\bar{\epsilon}_x$	$\bar{\epsilon}_y$
0.228 ($M=1.26$)	6.35	1.73	4	1888	5.02	2413	5.71	2.14	1.71
	12.7	1.73	7	1707	8.69	2307	6.55	1.94	1.64
		2.45	5	2640	4.90	3240	5.92	2.12	1.62
		2.99	5	3230	4.85	3960	5.16	2.12	1.62
0.453 ($M=0.63$)	6.35	1.73	4	3125	3.06	3650	3.54	3.55	2.59
	12.7	1.73	4	3050	1.89	3625	2.64	3.46	2.57
		2.45	4	4375	1.14	5250	2.69	3.51	2.63
		2.99	4	5275	4.21	5925	3.74	3.46	2.43
0.907 ($M=0.32$)	6.35	1.73	4	4350	2.29	5200	2.72	4.94	3.69
	12.7	1.73	4	4325	5.13	5400	2.62	4.91	3.83

TABLE E4, continued

Specimen B6 (n=5.29)

Impactor Mass M_2 , Kg.	Impactor Radius r , mm	Impactor Velocity V , m/sec	Number of Tests	Average Measured Strains				Generalized Strains	
				$\epsilon_x \times 10^6$	C.O.V.	$\epsilon_y \times 10^6$	C.O.V.	$\bar{\epsilon}_x$	$\bar{\epsilon}_y$
0.228 ($M=1.26$)	6.35	1.73	2	1100	0	2000	0	1.25	1.42
	12.7	1.73	2	1175	3.0	2125	1.66	1.33	1.51
		2.45	4	1600	13.25	2975	12.61	1.28	1.49
		2.99	2	2100	0	3925	0.9	1.38	1.61
0.453 ($M=0.64$)	6.35	1.73	2	2025	1.75	3600	0	2.30	2.55
	12.7	1.73	2	2000	0	3600	0	2.27	2.55
		2.45	2	2950	0	5025	0.7	2.37	2.52
		2.99	3	3600	0	5800	2.99	2.36	2.37
0.907 ($M=0.32$)	6.35	1.73	2	3300	0	5025	4.93	3.74	3.56
	12.7	1.73	2	3275	1.08	5050	1.40	3.72	3.58

TABLE E4, continued

Specimen B7 (n=1.38)

IMPACTOR MASS M_2 , Kg	IMPACTOR RADIUS r , mm	IMPACTOR VELOCITY V , m/sec	NUMBER OF TESTS	AVERAGE MEASURED STRAINS				GENERALIZED STRAINS	
				$\bar{\epsilon}_x$ $\times 10^6$	C.O.V.	ϵ_y $\times 10^6$	C.O.V.	$\bar{\epsilon}_x$	$\bar{\epsilon}_y$
0.228 ($M=2.38$)	6.35	1.73	2	800	0	1400	0	0.91	0.99
	12.7	1.73	2	750	9.42	1350	5.24	0.85	0.96
		2.45	2	1000	0	1750	4.04	0.80	0.88
		2.97	2	1250	5.66	2100	6.73	0.82	0.86
0.453 ($M=1.2$)	6.35	1.73	2	1000	0	1900	0	1.13	1.35
	12.7	1.73	2	1000	0	1900	0	1.13	1.35
		2.45	2	1600	0	2750	2.57	1.28	1.38
		2.99	2	2000	0	3450	2.05	1.31	1.41
0.907 ($M=6.59$)	6.35	1.73	2	1650	2.05	2850	7.44	1.87	2.02
	12.7	1.73	2	1700	0	2950	2.39	1.93	2.09
		2.45	2	2400	5.89	4250	1.66	1.93	2.13

TABLE E4, continued

Specimen F1 (r=0.641)

IMPACTOR MASS M_2 , Kg	IMPACTOR RADIUS r , mm	IMPACTOR VELOCITY V , m/sec	NUMBER OF TESTS	AVERAGE MEASURED STRAINS				GENERALIZED STRAINS	
				$\epsilon_x \times 10^6$	C.O.V.	$\epsilon_y \times 10^6$	C.O.V.	$\bar{\epsilon}_x$	$\bar{\epsilon}_y$
0.228 ($M=1.04$)	6.35	1.73	2	825	0	1175	3.0	0.873	0.80
	12.7	1.73	2	813	2.18	1163	1.52	0.86	0.79
		2.45	3	1175	3.68	1938	2.98	0.879	0.926
		2.99	2	1625	2.18	2600	0	0.99	1.02
0.453 ($M=0.52$)	6.35	1.73	2	1313	1.35	2013	0.87	1.39	1.36
	12.7	1.73	2	1275	2.77	2038	4.33	1.35	1.38
		2.45	2	2000	0	2925	3.63	1.50	1.40
		2.99	3	2600	0	3683	3.13	1.59	1.44
0.907 ($M=0.26$)	6.35	1.73	2	2000	0	3000	0	2.12	2.03
	12.7	1.73	2	2000	0	3000	0	2.12	2.03
		2.45	2	2950	2.4	4275	0.83	2.21	2.05

TABLE E4, continued

Specimen F2 ($n=0.168$)

IMPACTOR MASS M_2 , Kg	IMPACTOR RADIUS r , mm	IMPACTOR VELOCITY V , m/sec	NUMBER OF TESTS	AVERAGE MEASURED STRAINS				GENERALIZED STRAINS	
				$\epsilon_x \times 10^6$	C.O.V.	$\epsilon_y \times 10^6$	C.O.V.	$\bar{\epsilon}_x$	$\bar{\epsilon}_y$
0.228 ($M=1.99$)	6.35	1.73	2	825	4.29	1150	0	0.87	0.78
	12.7	1.73	2	850	0	1150	0	0.90	0.78
		2.45	2	1108	1.48	1675	0	0.89	0.81
		2.99	2	1438	3.68	2050	1.72	0.88	0.80
0.453 ($M=0.99$)	6.35	1.73	3	1059	3.61	1675	1.49	1.12	1.14
	12.7	1.73	2	1113	1.57	1750	0	1.18	1.19
		2.45	2	1675	2.11	2975	1.48	1.25	1.43
		2.99	2	2100	0	3013	0.58	1.28	1.18
0.907 ($M=C.49$)	6.35	1.73	2	2063	0.86	2925	1.21	2.18	1.98
	12.7	1.73	2	2038	0.86	2925	1.21	2.16	1.98
		2.45	2	2950	2.39	3950	1.79	2.21	1.89

TABLE E4, continued

Specimen F3 (n=2.45)

IMPACTOR MASS M_2 , Kg	IMPACTOR RADIUS r , mm	IMPACTOR VELOCITY V , m/sec	NUMBER OF TESTS	AVERAGE MEASURED STRAINS				GENERALIZED STRAINS	
				$\bar{\epsilon}_x$ $\times 10^6$	C.O.V.	$\bar{\epsilon}_y$ $\times 10^6$	C.O.V.	$\bar{\epsilon}_x$	$\bar{\epsilon}_y$
0.228 ($M=1.98$)	6.35	1.73	2	775	4.56	1200	0	0.82	0.81
	12.7	1.73	2	800	0	1213	1.46	0.85	0.82
		2.45	2	1163	1.52	1700	0	0.87	0.815
		2.99	2	1400	0	2200	0	0.86	0.86
0.453 ($M=0.99$)	6.35	1.73	2	1075	0	1900	0	1.14	1.29
	12.7	1.73	2	1000	0	1800	0	1.06	1.22
		2.45	2	1588	1.11	3000	0	1.19	1.44
		2.99	2	2050	3.44	3700	0	1.25	1.45
0.907 ($M=0.49$)	6.35	1.73	2	1800	0	3100	0	1.91	2.10
	12.7	1.73	2	1800	0	3150	2.24	1.91	2.13
		2.45	3	2583	1.11	4367	1.32	1.93	2.09

TABLE E4, continued

Specimen E4 (m=0.641)

IMPACTOR MASS M_2 , Kg	IMPACTOR RADIUS r , mm	IMPACTOR VELOCITY V , m/sec	NUMBER OF TESTS	AVERAGE MEASURED STRAINS			GENERALIZED STRAINS	
				$\epsilon_x \times 10^6$	C.O.V.	$\epsilon_y \times 10^6$	$\bar{\epsilon}_x$	$\bar{\epsilon}_y$
0.228 ($M=3.77$)	6.35	1.73	2	858	2.11	1113	0.89	0.75
	12.7	1.73	2	875	4.04	1138	0.93	0.77
		2.45	2	1213	1.46	1638	0.91	0.79
		2.97	2	1513	1.17	1988	0.92	0.78
0.453 ($M=1.89$)	6.35	1.73	2	1075	0	1325	1.14	0.90
	12.7	1.73	2	1025	0	1400	1.09	0.95
		2.45	2	1500	0	1875	1.12	0.90
		2.97	2	1713	1.03	2350	1.05	0.92
0.907 ($M=0.95$)	6.35	1.73	2	1600	0	2150	1.69	1.46
	12.7	1.73	2	1600	0	2150	1.69	1.46
		2.45	2	2400	0	3300	1.80	1.58
		2.97	2	2400	0	3300	1.80	1.58

TABLE E4, continued

Specimen H1 (m1.15)

IMPACTOR MASS M_2 , Kg	IMPACTOR RADII r , mm	IMPACTOR VELOCITY V , m/sec	NUMBER OF TESTS	AVERAGE MEASURED STRAINS				GENERALIZED STRAINS	
				$\bar{\epsilon}_x$ $\times 10^6$	C.O.V.	ϵ_y $\times 10^6$	C.O.V.	$\bar{\epsilon}_x$	$\bar{\epsilon}_y$
0.228 ($M=0.94$)	6.35	1.73	2	988	1.79	800	0	0.88	0.83
	12.7	1.73	2	988	1.79	813	2.18	0.88	0.84
		2.45	2	1475	2.39	1200	0	0.93	0.86
		2.49	2	2033	2.60	1638	1.07	1.05	0.98
0.453 ($M=0.47$)	6.35	1.73	2	1913	0.93	1600	0	1.71	1.65
	12.7	1.73	2	1813	0.97	1575	0	1.62	1.62
		2.45	2	2700	0	2350	0	1.71	1.71
		2.49	2	3338	0.53	2750	2.57	1.72	1.64
0.907 ($M=0.23$)	6.35	1.73	2	2800	0	2400	0	2.51	2.48
	12.7	1.73	2	2800	0	2400	0	2.51	2.48
		2.45	2	3950	1.79	3475	3.05	2.50	2.53
			2						

TABLE E4, continued

Specimen H2 ($\eta=0.302$)

IMPACTOR MASS M_2 , Kg.	IMPACTOR RADIUS r , mm	IMPACTOR VELOCITY V , m/sec	NUMBER OF TESTS	AVERAGE MEASURED STRAINS				GENERALIZED STRAINS	
				ϵ_x $\times 10^6$	C.O.V.	ϵ_y $\times 10^6$	C.O.V.	$\bar{\epsilon}_x$	$\bar{\epsilon}_y$
0.228 ($M=1.80$)	6.35	1.73	2	1013	1.75	913	1.94	0.91	0.94
	12.7	1.73	2	1013	1.75	950	7.44	0.91	0.98
		2.45	2	1538	1.15	1400	0	0.97	1.02
		2.99	2	1925	3.67	1775	3.98	0.99	1.06
0.453 ($M=0.90$)	6.35	1.73	2	1300	0	1025	0	1.16	1.06
	12.7	1.73	2	1300	6.44	1150	6.15	1.16	1.19
		2.45	2	2300	0	1900	0	1.45	1.39
		2.99	2	3100	0	2600	0	1.59	1.55
0.907 ($M=0.44$)	6.35	1.73	2	2400	0	2050	3.45	2.15	2.11
	12.7	1.73	2	2425	1.46	1900	7.44	2.17	1.96

TABLE E4, continued

Specimen B3 (r=4.41)

IMPACTOR MASS M_2 , Kg	IMPACTOR RADIUS r , mm	IMPACTOR VELOCITY V , m/sec	NUMBER OF TESTS	AVERAGE MEASURED STRAINS				GENERALIZED STRAINS	
				$\epsilon_x \times 10^6$	C.O.V.	$\epsilon_y \times 10^6$	C.O.V.	$\bar{\epsilon}_x$	$\bar{\epsilon}_y$
0.228 ($M=1.75$)	6.35	1.73	2	1053	1.74	950	0	0.91	0.98
	12.7	1.73	2	1000	0	975	0	0.89	1.01
		2.45	2	1438	3.68	1375	0	0.91	1.00
		2.99	2	1800	0	1633	1.06	0.93	0.99
0.453 ($M=0.88$)	6.35	1.73	2	1175	0	1250	0	1.05	1.30
	12.7	1.73	2	1213	7.28	1300	5.43	1.08	1.34
		2.45	2	1900	0	2100	0	1.20	1.53
		2.99	2	2375	1.48	2600	0	1.23	1.55
0.907 ($M=0.44$)	6.35	1.73	2	2100	0	2300	0	1.88	2.37
	12.7	1.73	2	2175	1.62	2400	0	1.94	2.48
		2.45	2	3275	3.23	3600	0	2.07	2.63

TABLE E4, continued

Specimen H4 (M1.15)

IMPACTOR MASS M_2 , Kg	IMPACTOR RADIUS r , mm	IMPACTOR VELOCITY V , m/sec	NUMBER OF TESTS	AVERAGE MEASURED STRAINS				GENERALIZED STRAINS	
				$\bar{\epsilon}_x$ $\times 10^6$	C.O.V.	$\bar{\epsilon}_y$ $\times 10^6$	C.O.V.	$\bar{\epsilon}_x$	$\bar{\epsilon}_y$
0.228 ($M=3.39$)	6.35	1.73	2	1075	3.29	875	4.04	0.96	0.93
	12.7	1.73	2	1125	3.14	925	3.82	1.01	0.95
		2.45	2	1600	0	1325	2.67	1.01	0.97
		2.99	2	1963	0.90	1600	0	1.01	0.95
0.453 ($M=1.70$)	6.35	1.73	2	1400	0	1225	2.88	1.25	1.26
	12.7	1.73	2	1375	2.57	1225	2.88	1.23	1.26
		2.45	2	2050	0	1775	1.99	1.30	1.29
		2.99	2	2600	0	2275	1.56	1.34	1.35
0.907 ($M=0.84$)	6.35	1.73	2	2275	1.56	1875	1.88	2.03	1.93
	12.7	1.73	2	2375	1.49	2050	3.45	2.12	2.11
		2.45	2	3200	0	2550	2.77	2.02	1.86

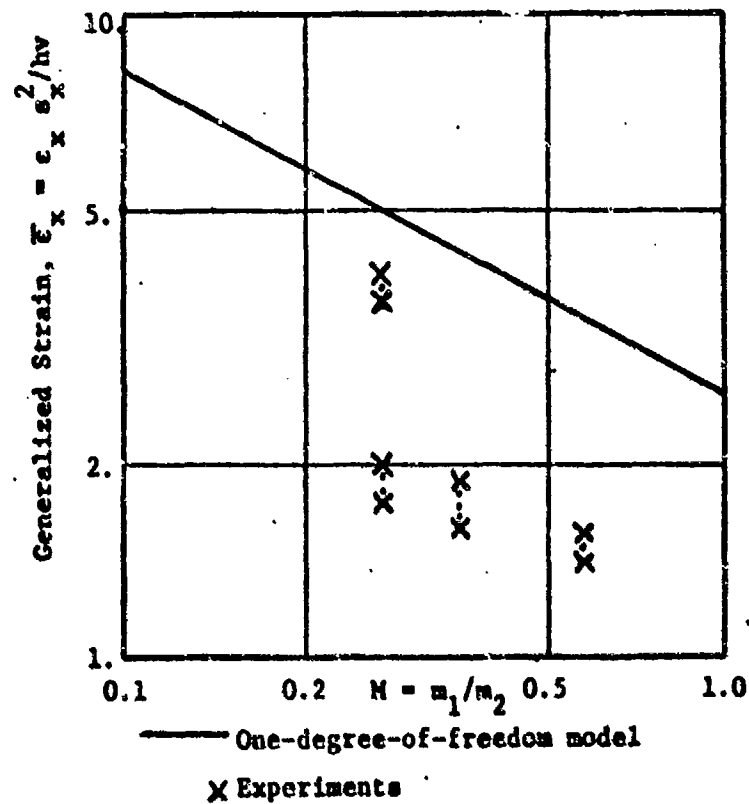


Figure E23. Design curve and experimental data for impact of a simply supported aluminum plate ($\eta = 1.0$).

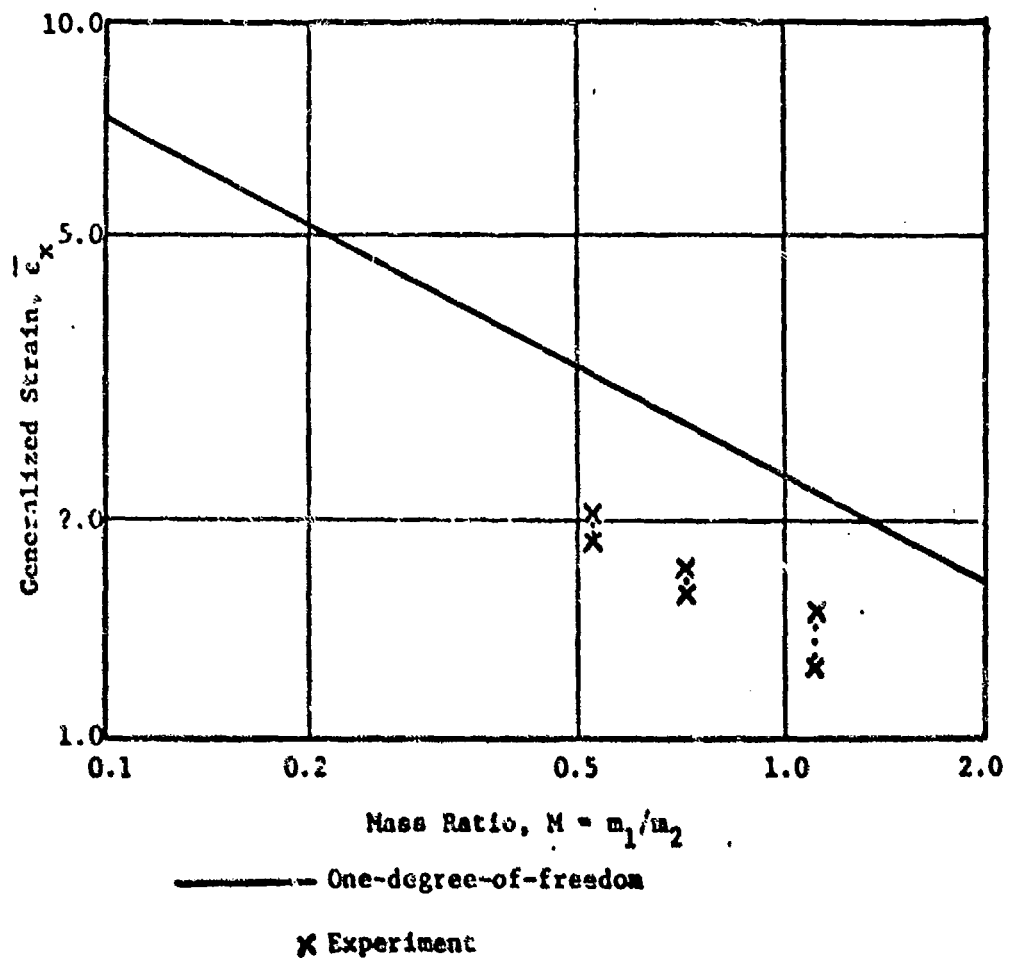


Figure E24. Design curve and experimental data for impact of a simply supported plate ($\eta = 4.0$).

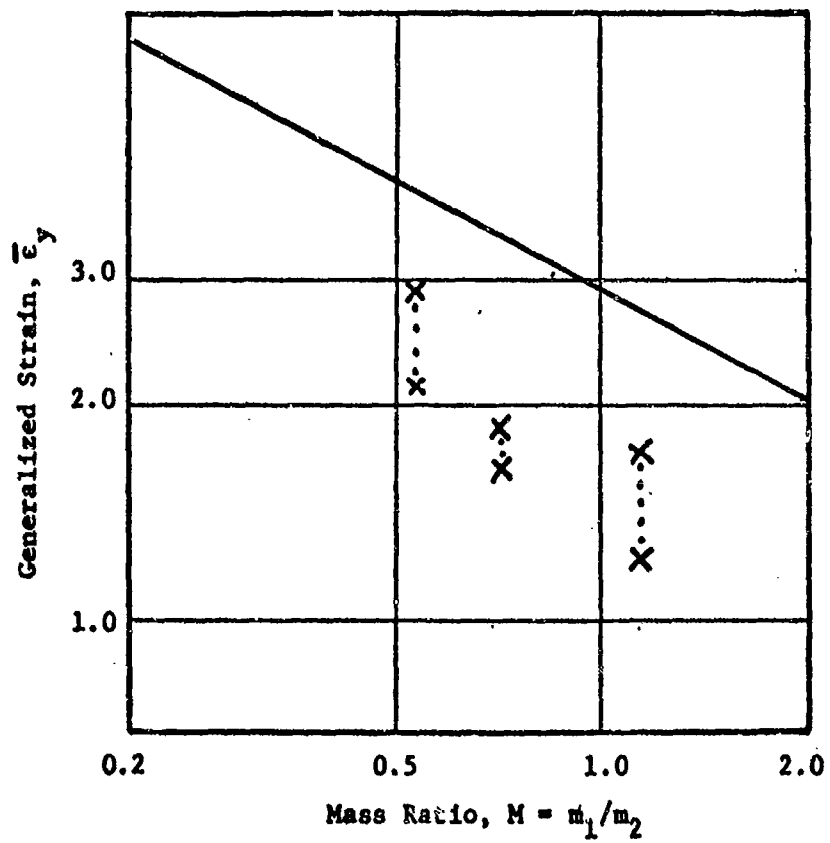


Figure E25. Design curve and experimental data for impact of a simply supported aluminum plate ($1/\eta = 0.25$).

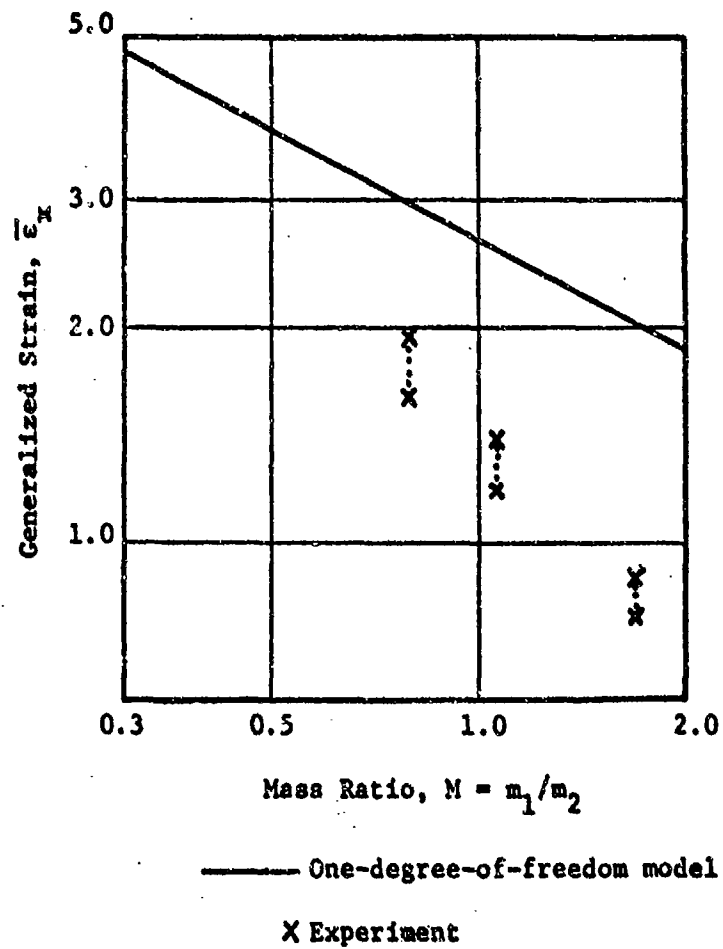


Figure E26. Design curve and experimental data for impact of a simply supported aluminum plate ($\eta = 9.0$).

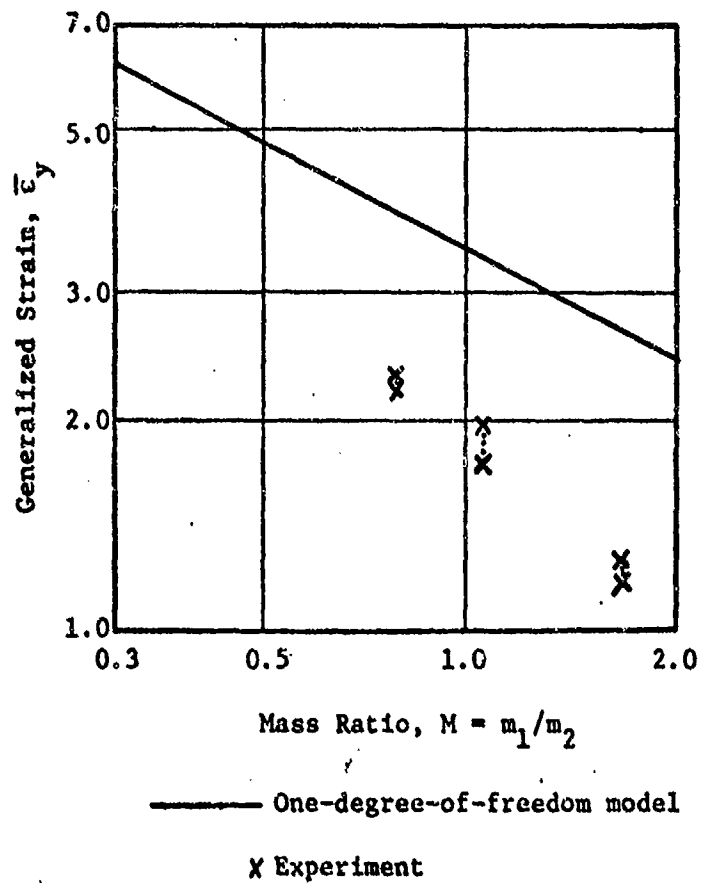


Figure E27. Design curve and experimental data for impact of a simply supported aluminum plate ($1/\eta = 0.111$).

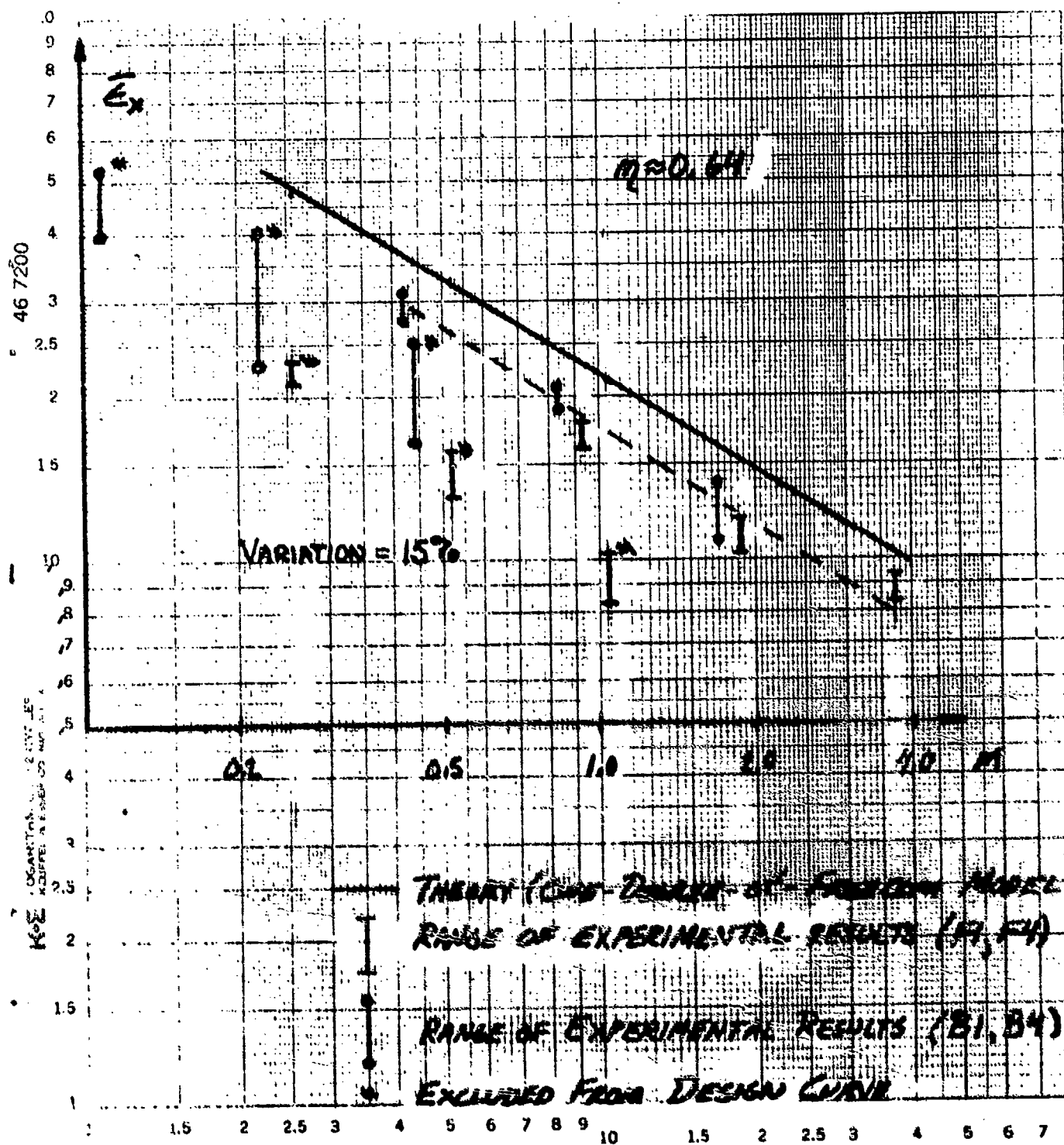


Figure E28. E_x vs. M_1 Simply Supported Orthotropic Plate

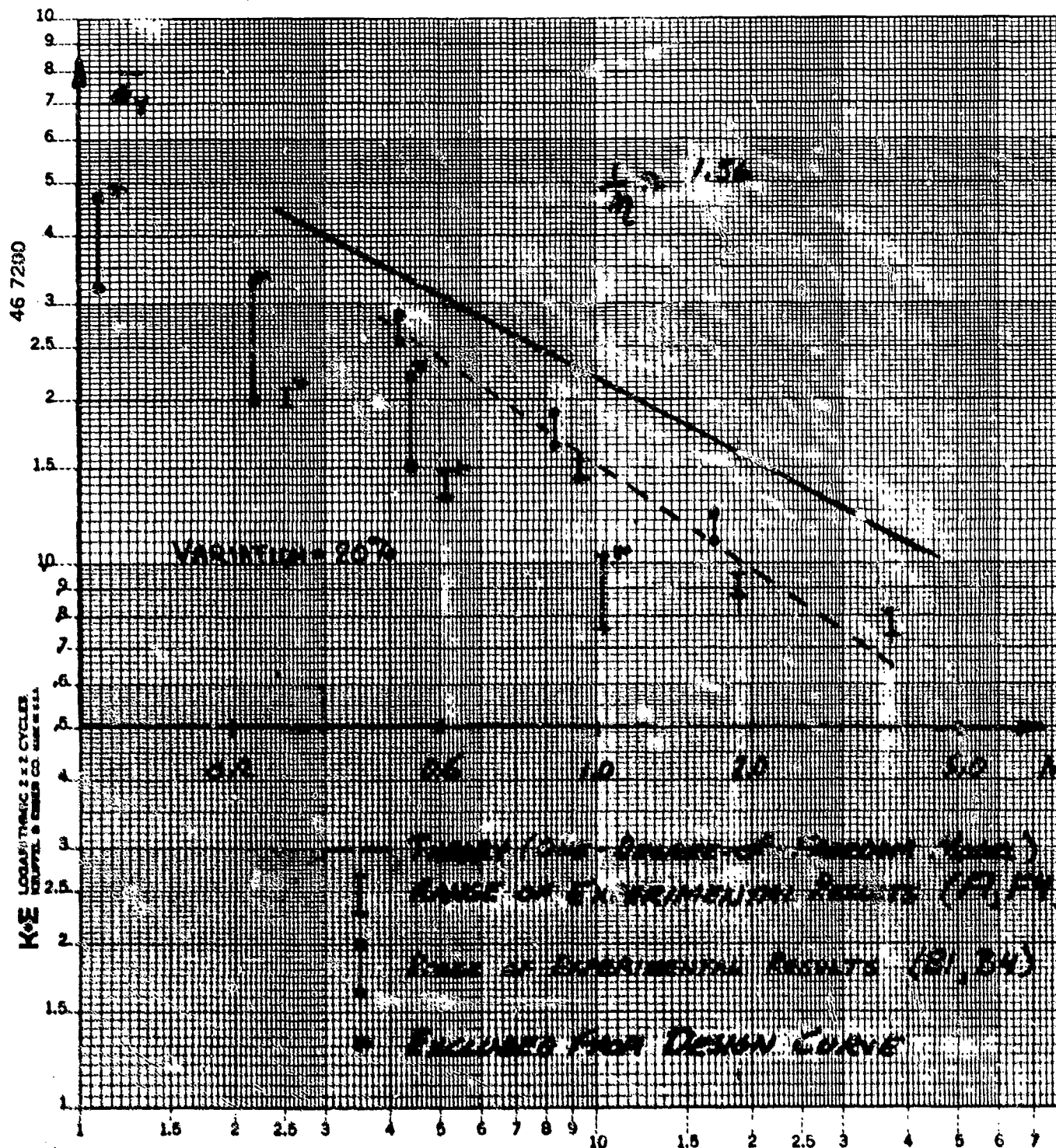


Figure E29. \bar{E}_y vs. H : Simply Supported Orthotropic Plate

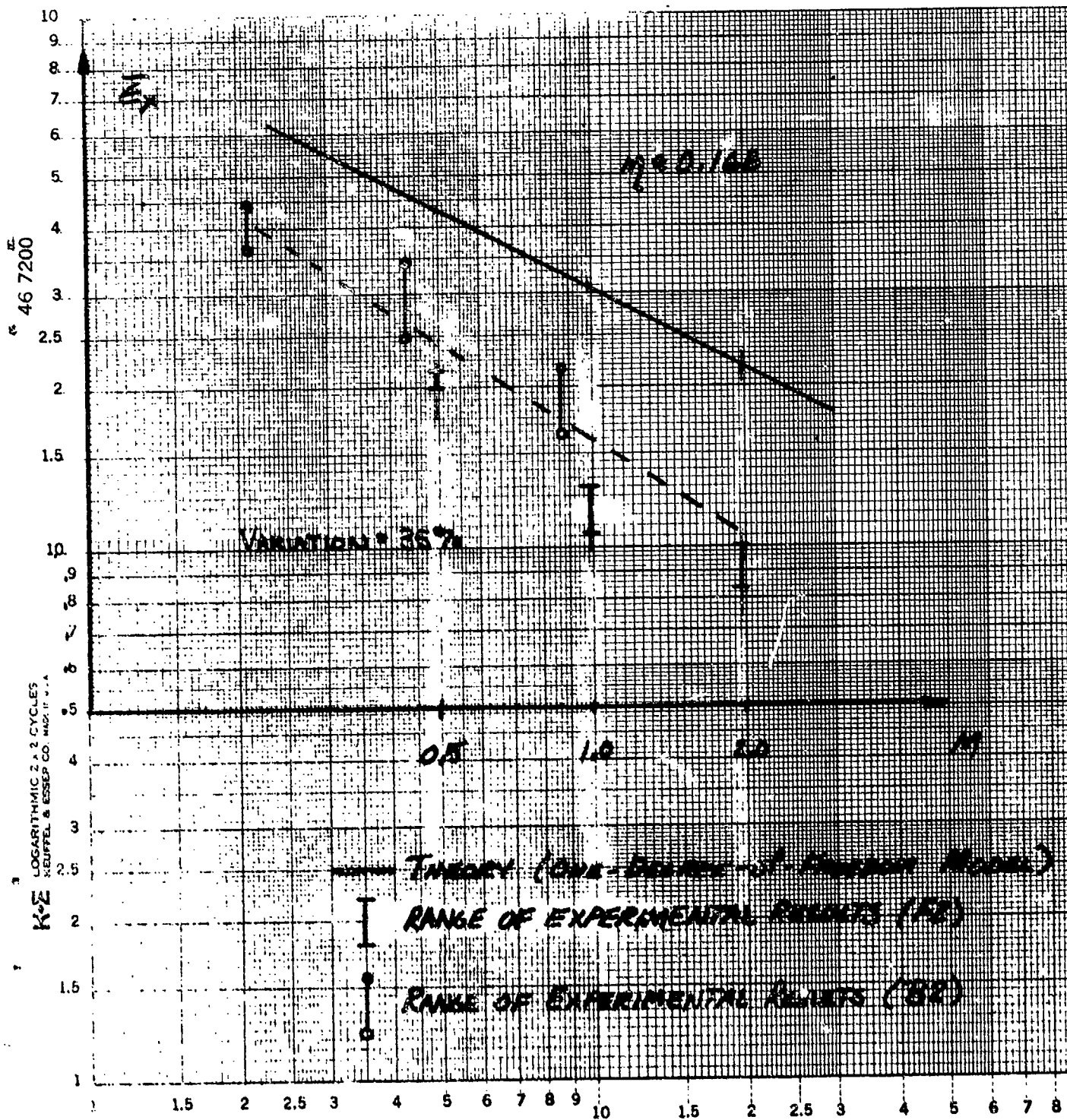


Figure E30. $\bar{\sigma}_M$ vs. M : Simply Supported Orthotropic Plate

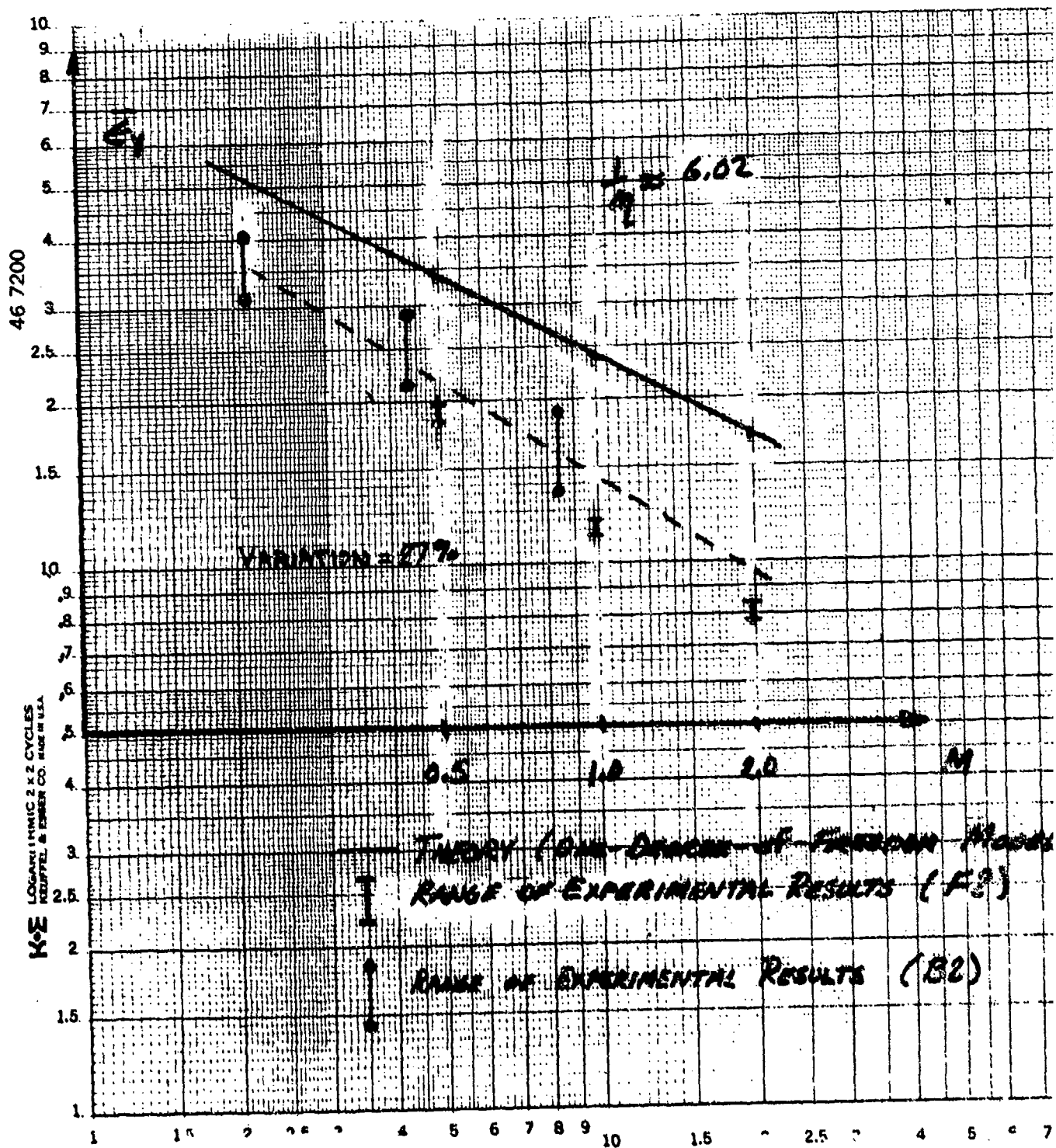


Figure E31. \bar{E}_y vs. ν . Simply Supported Orthotropic Plate

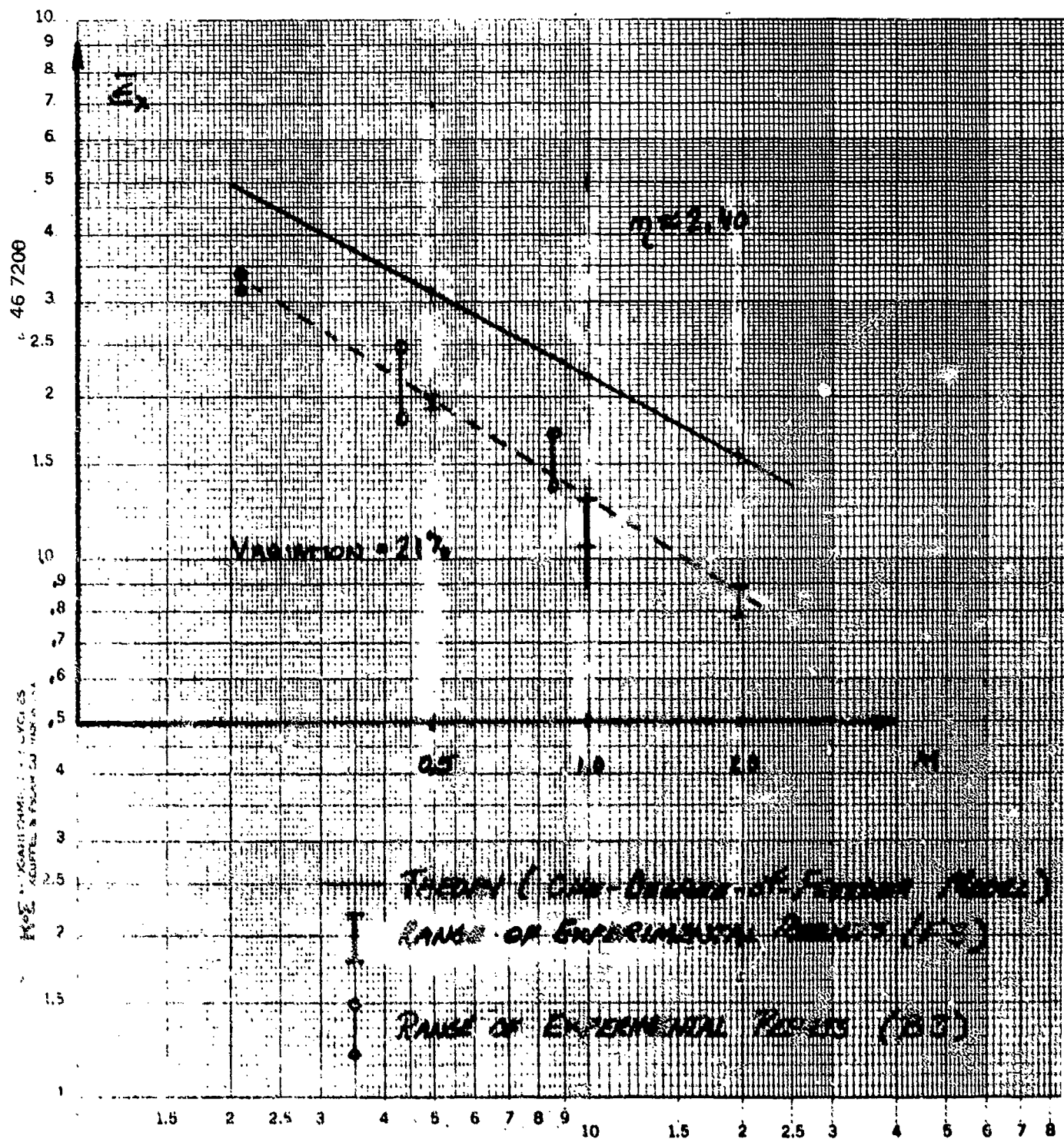
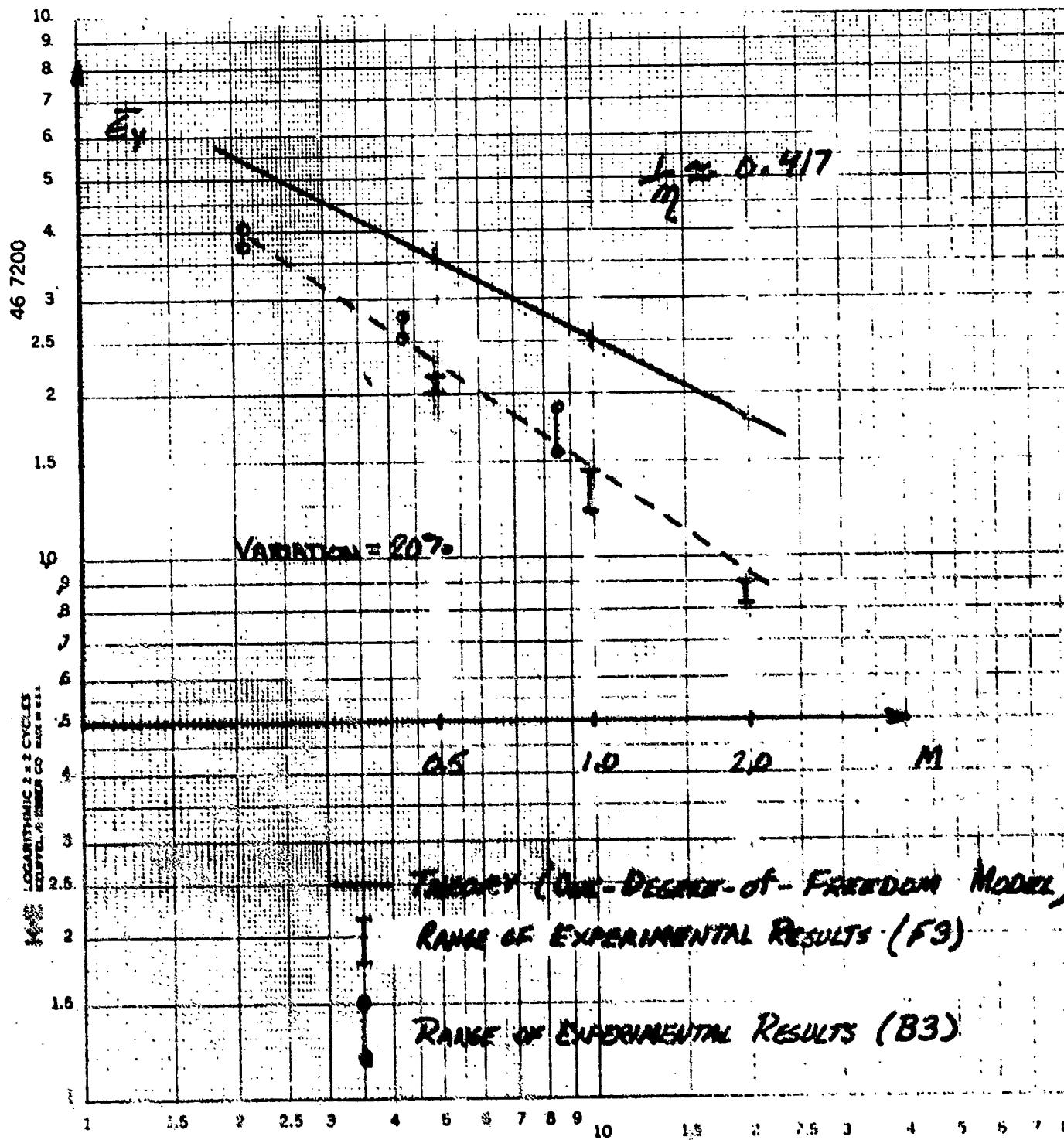


Figure B32. \bar{E}_x vs. M : Simply Supported Orthotropic Plate

Figure E33. \bar{E}_y vs. M : Simply Supported Orthotropic Plate

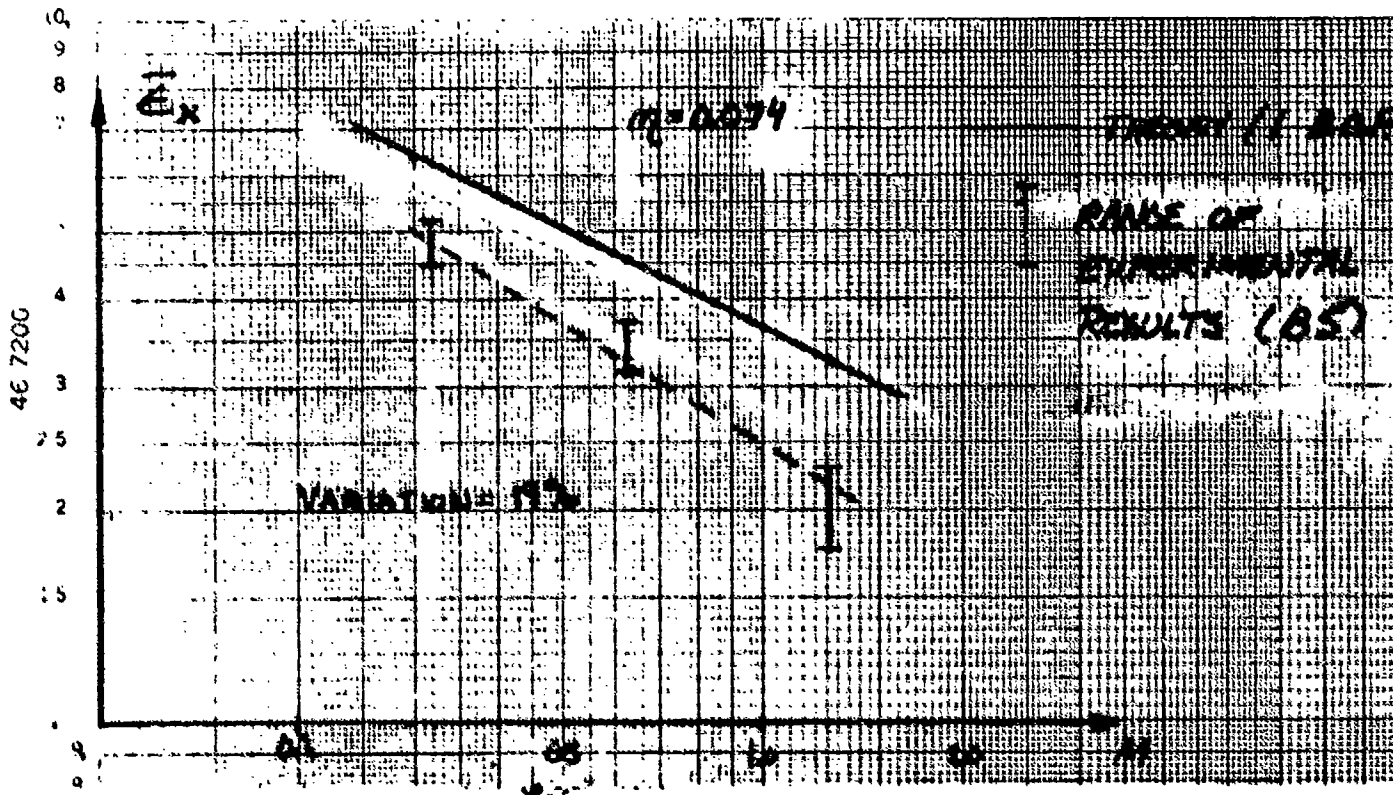


Figure E34. \bar{E}_x vs. N : Simply Supported Orthotropic Plate

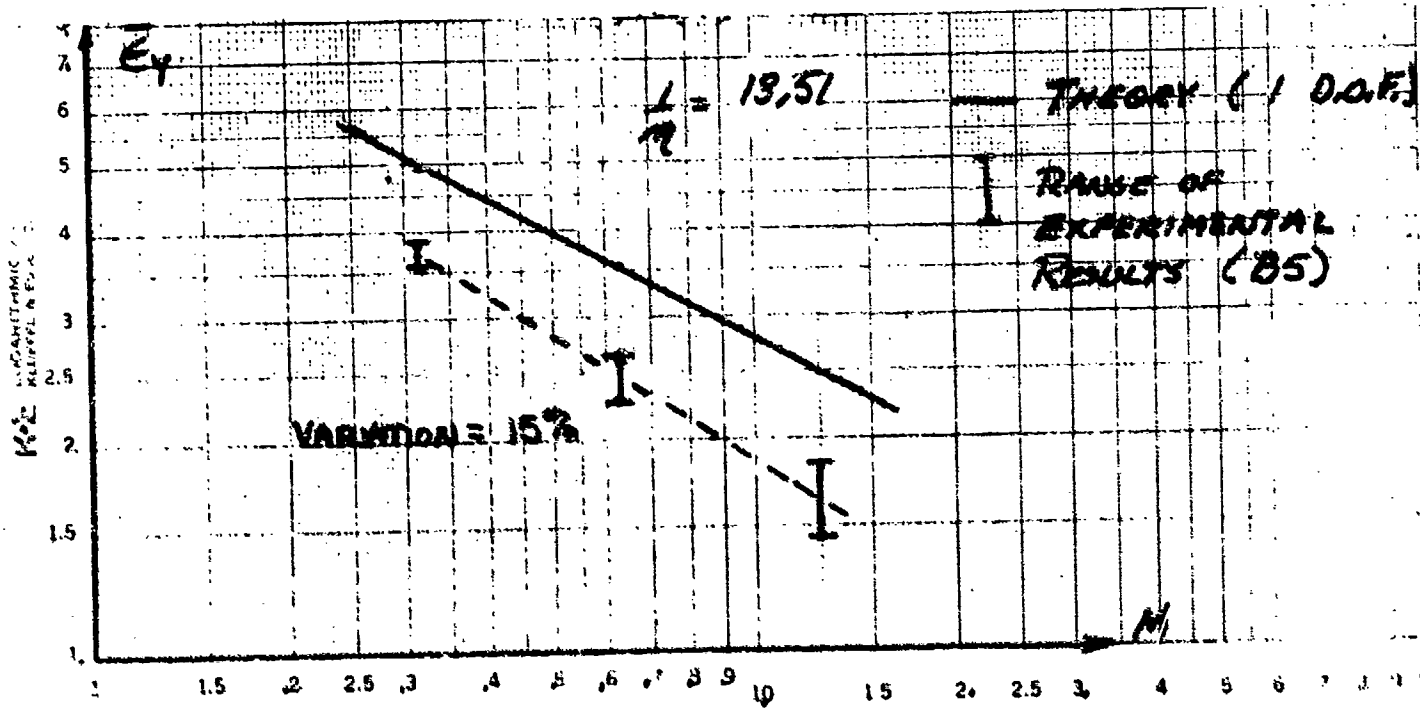


Figure E35. \bar{E}_y vs. M_1 Simply Supported Orthotropic Plate

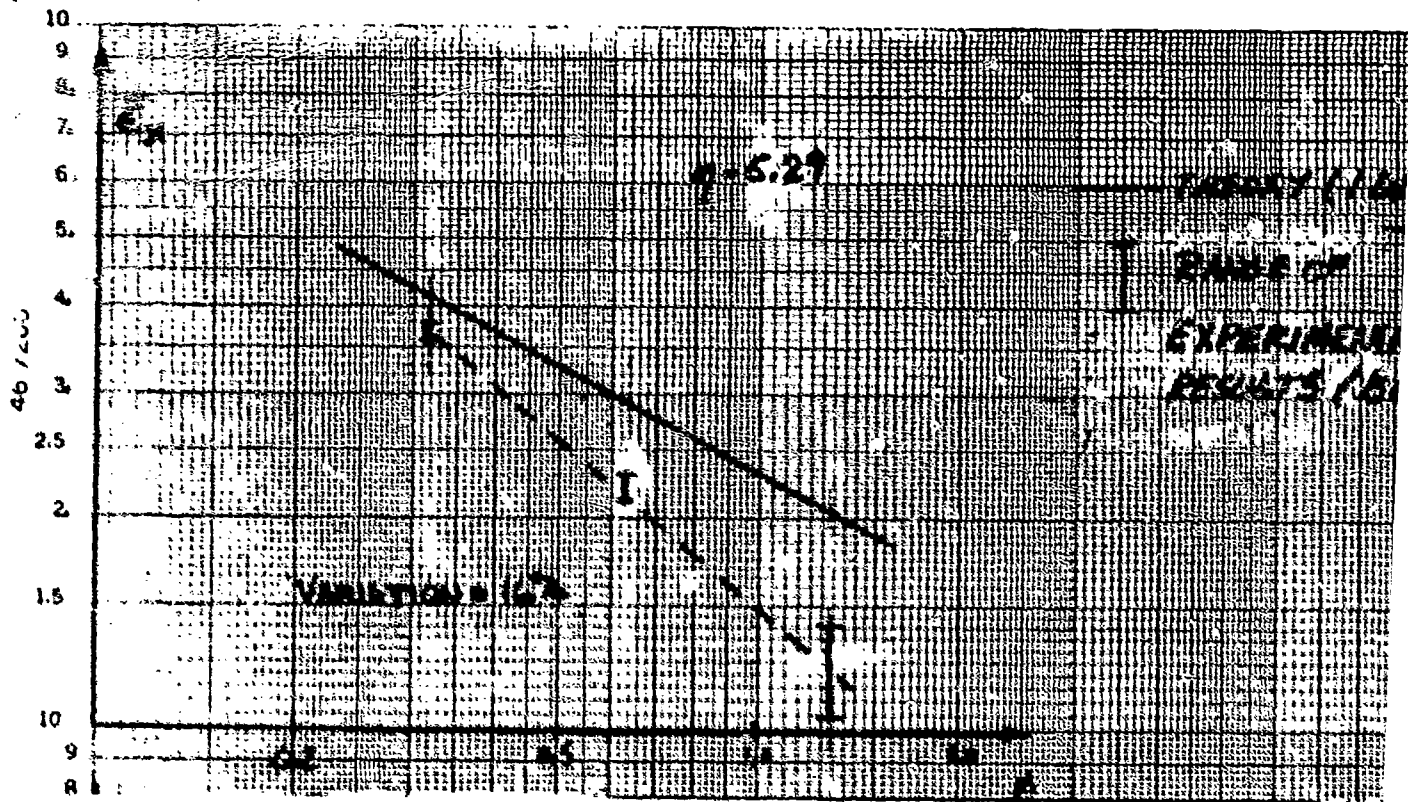


Figure E36. \bar{E}_y vs. N : Simply Supported Orthotropic Plate

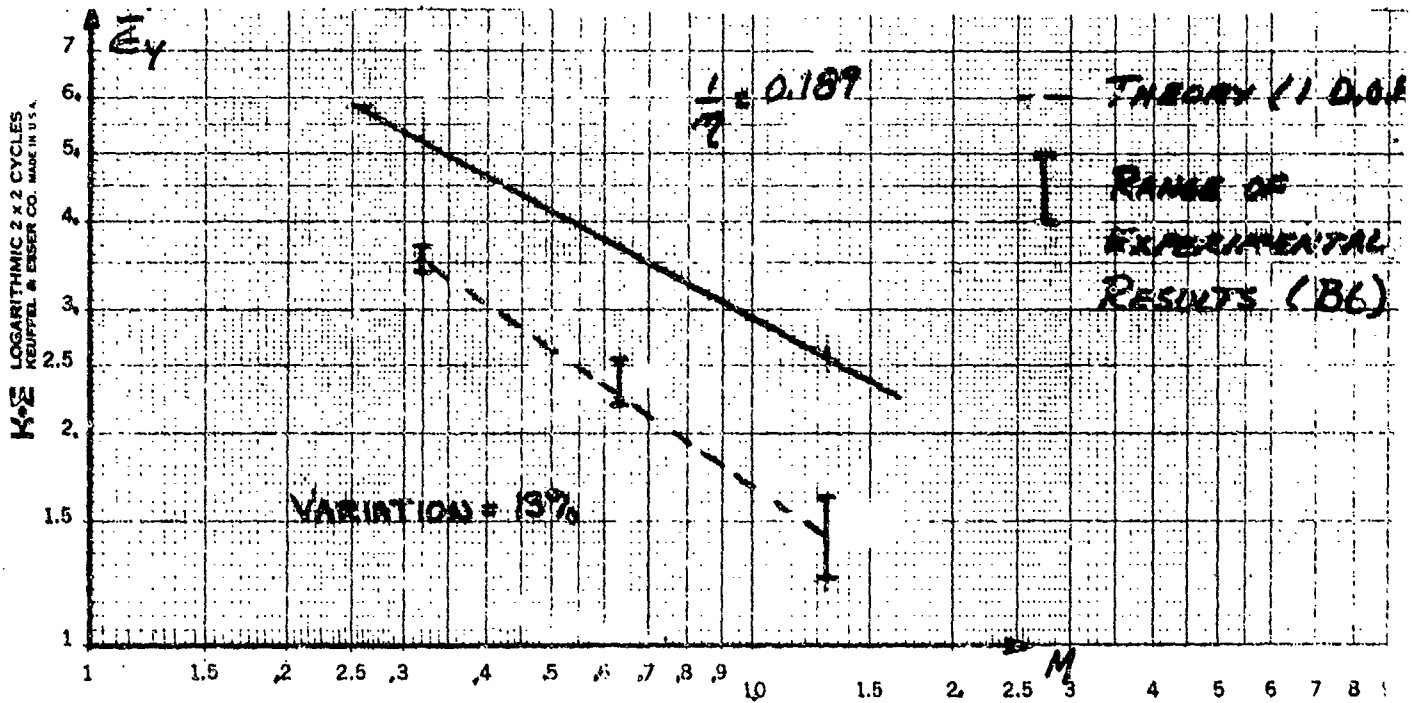


Figure E37. \bar{E} vs. M : Simply Supported Orthotropic Plate

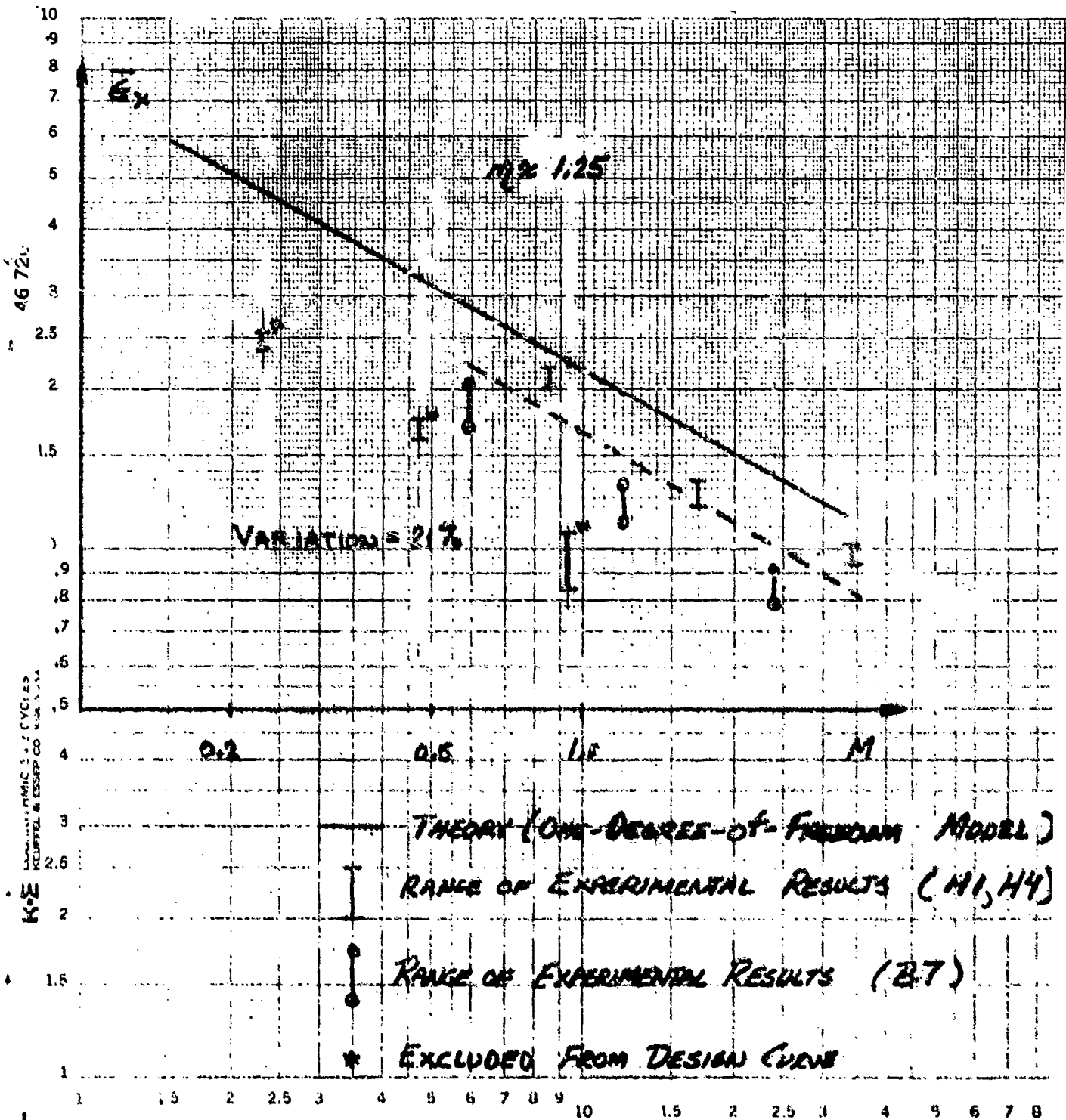


Figure E38i. \bar{E}_x vs. M : Simply Supported Orthotropic Plate

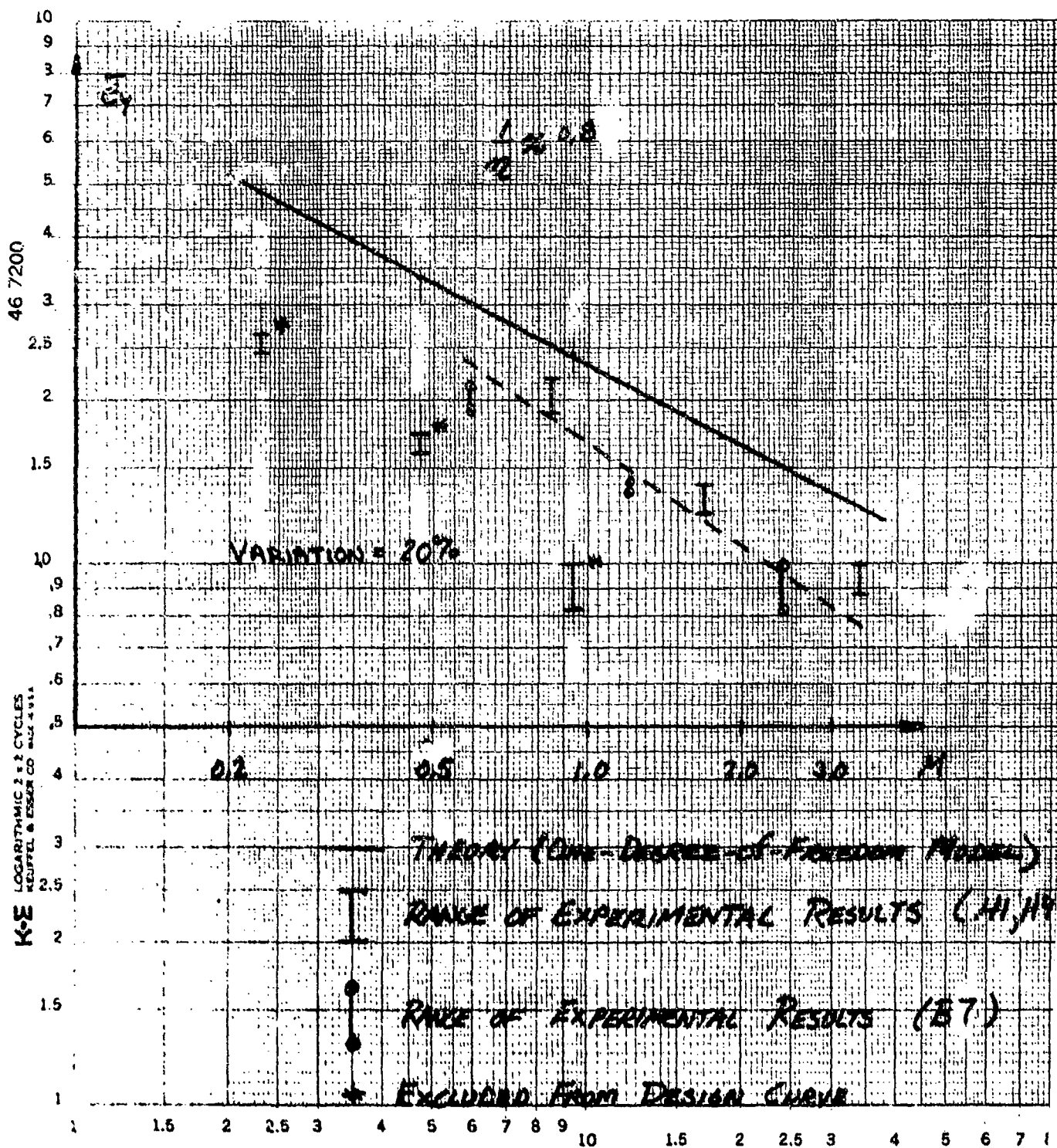


Figure E39. $\bar{\epsilon}_y$ vs. M : Simply Supported Orthotropic Plate

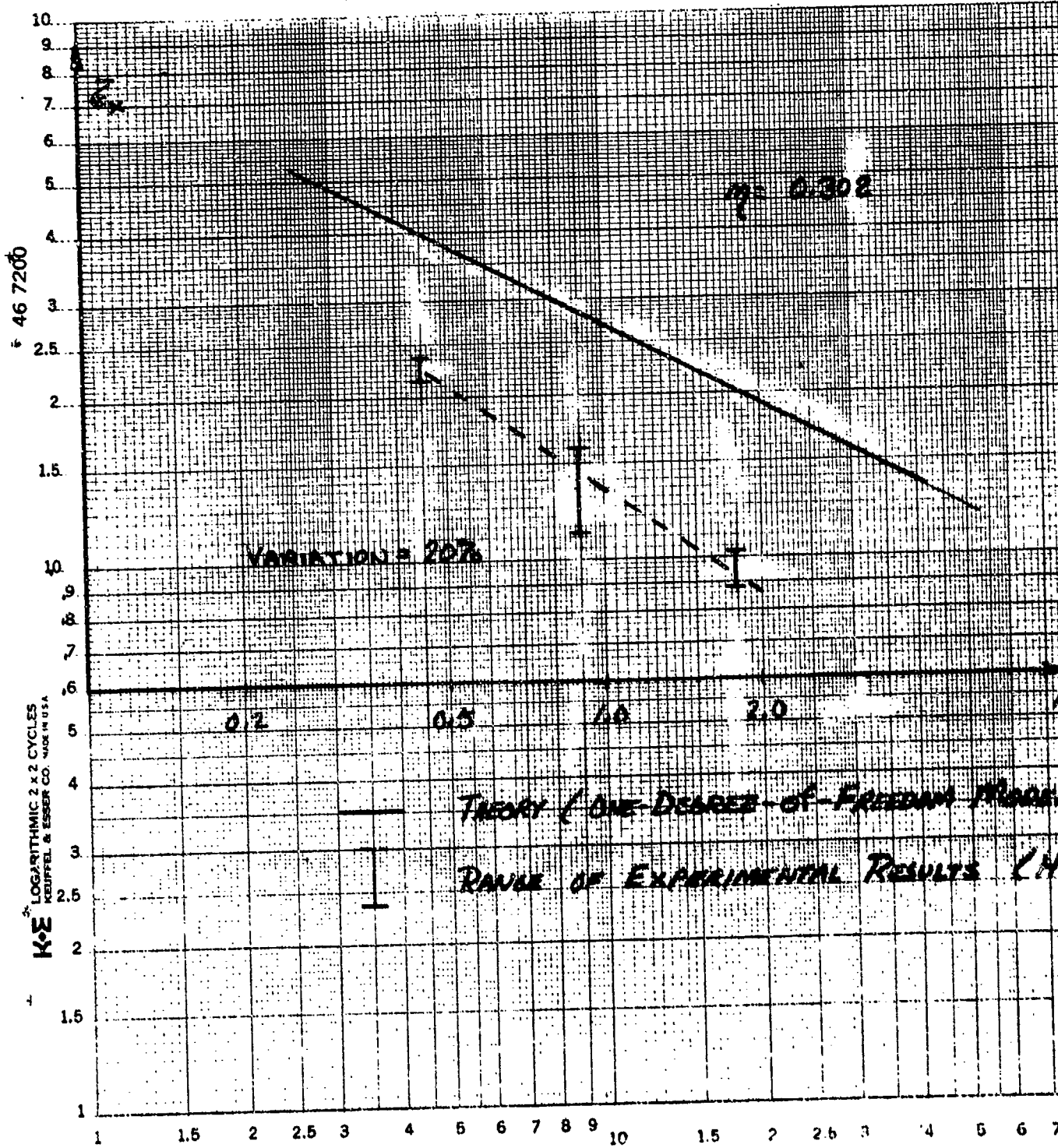


Figure E40. \bar{E}_x vs. M_1 , Simply Supported Orthotropic Plate

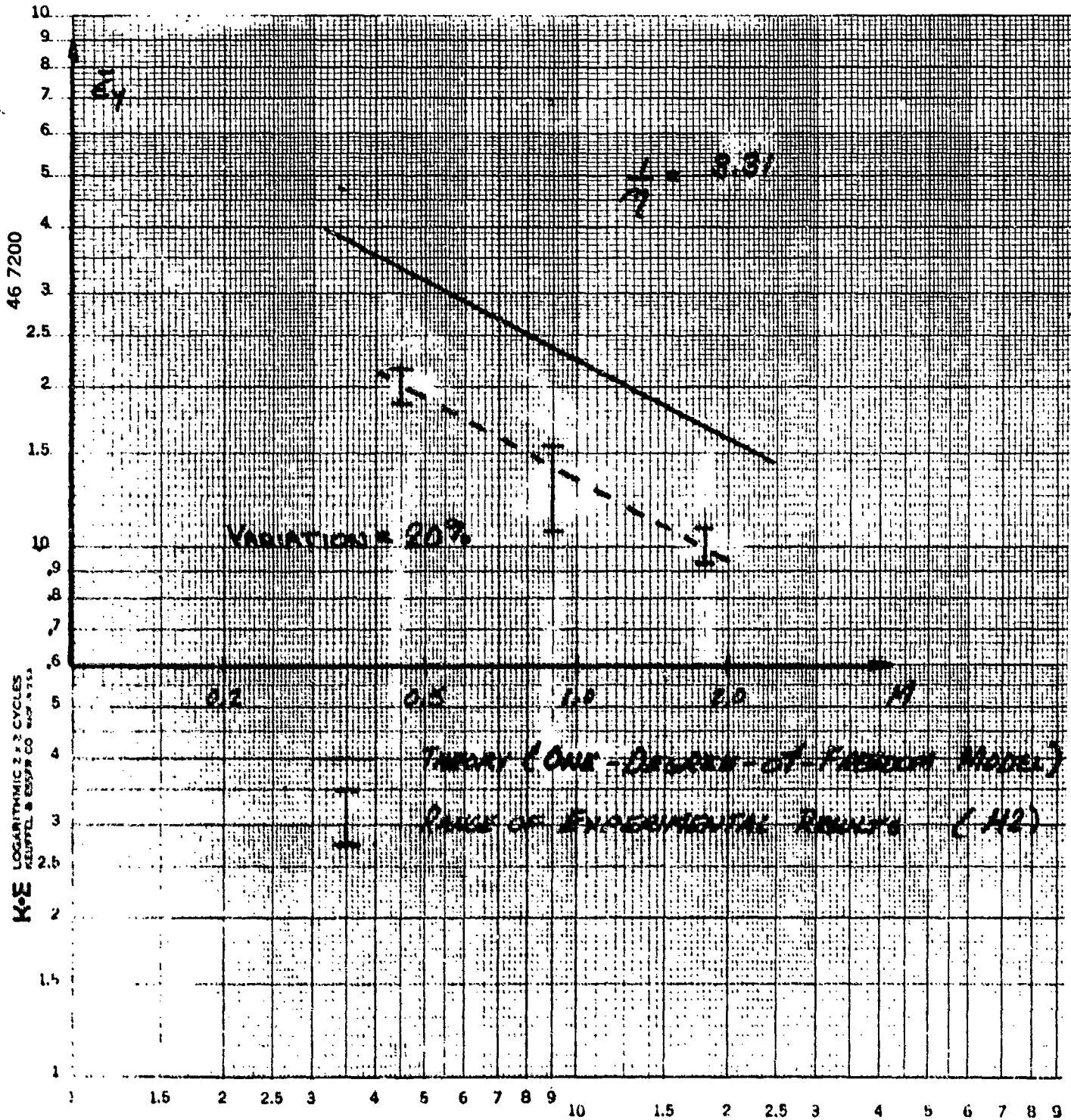


Figure E41. \bar{E}_y vs. M_1 Simply Supported Orthotropic Plate

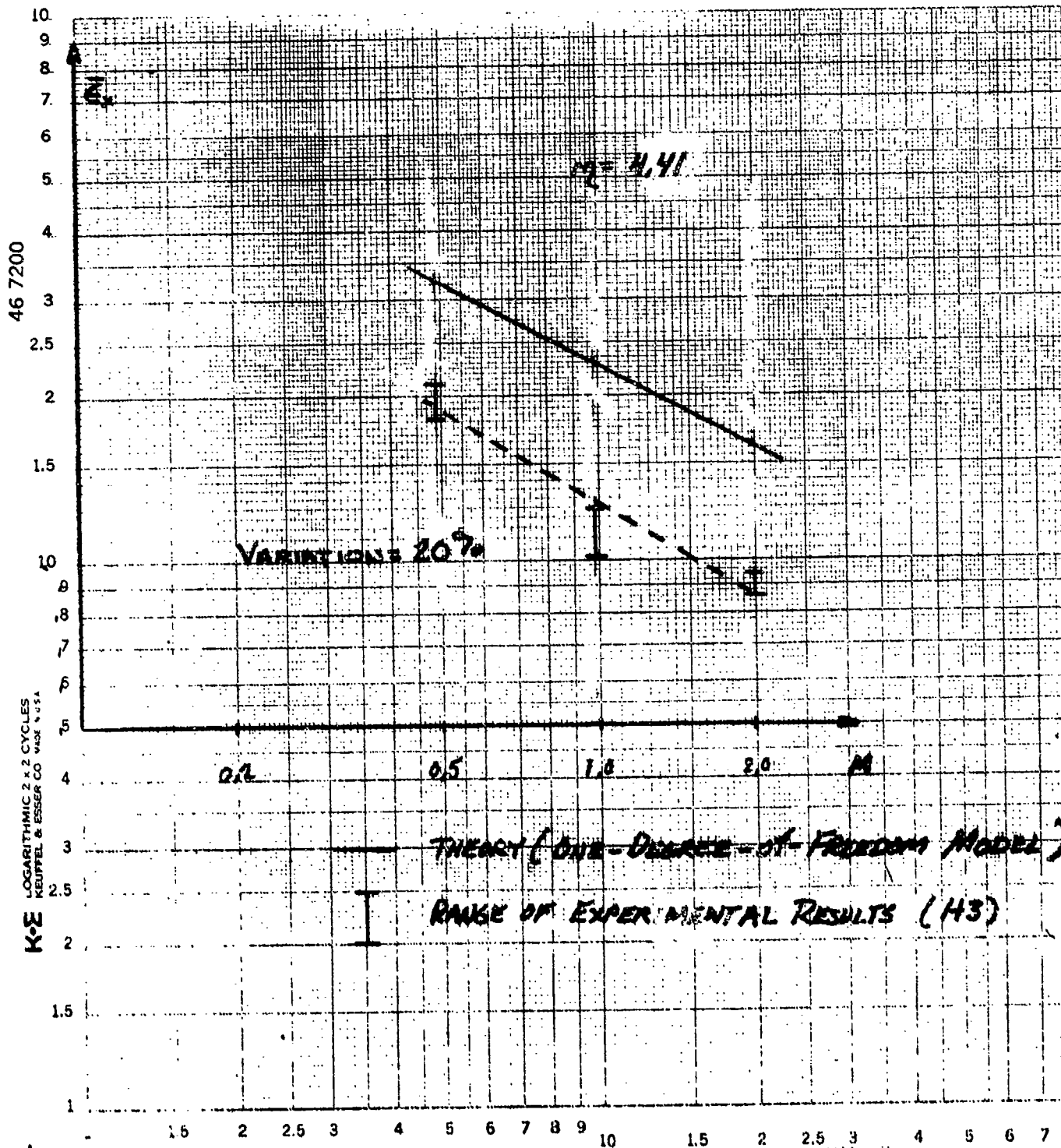


Figure E42. \bar{E}_x vs. M : Simply Supported Orthotropic Plate

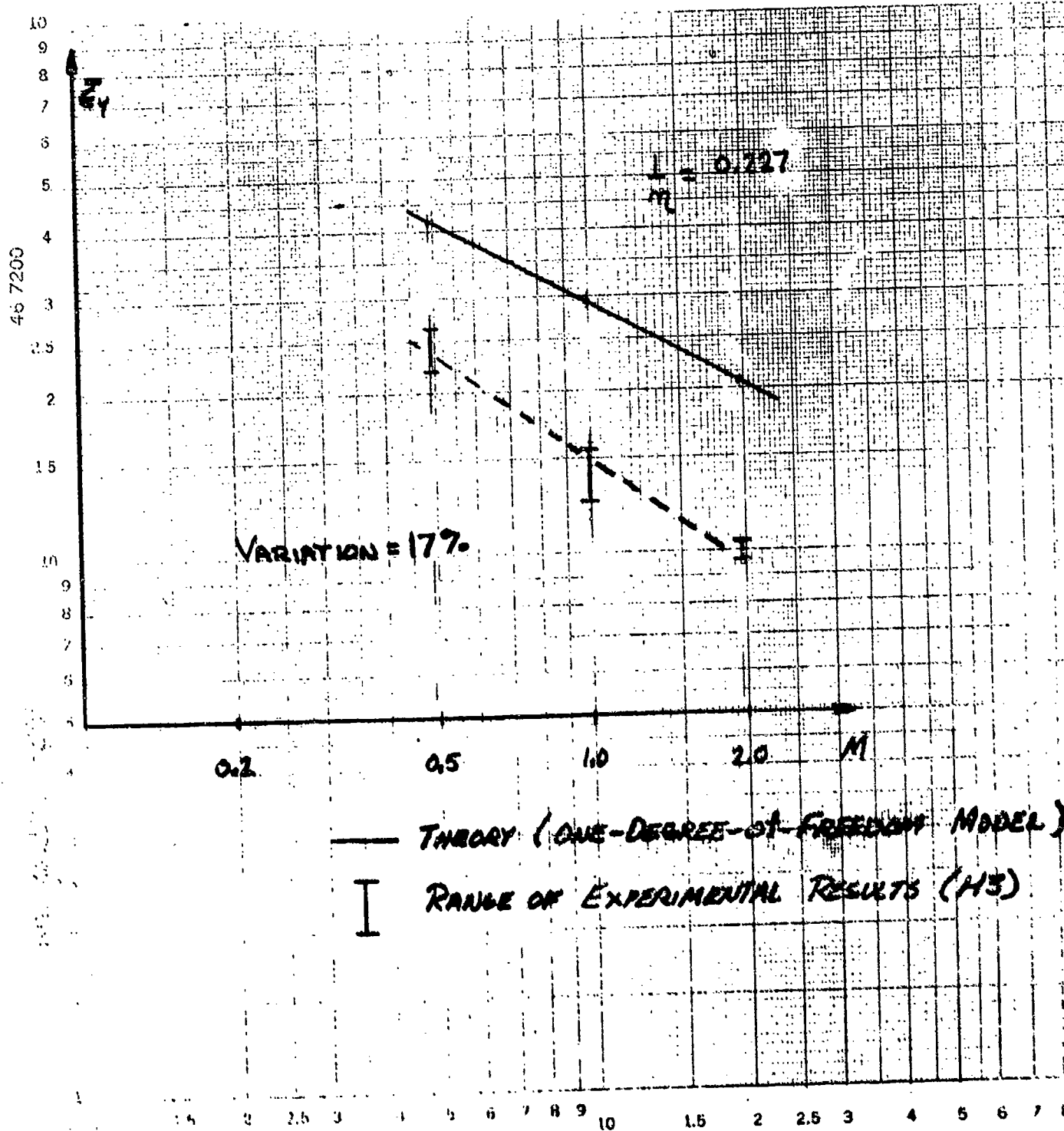


Figure E43. \bar{z}_y vs. M : Simply Supported Orthotropic Plate

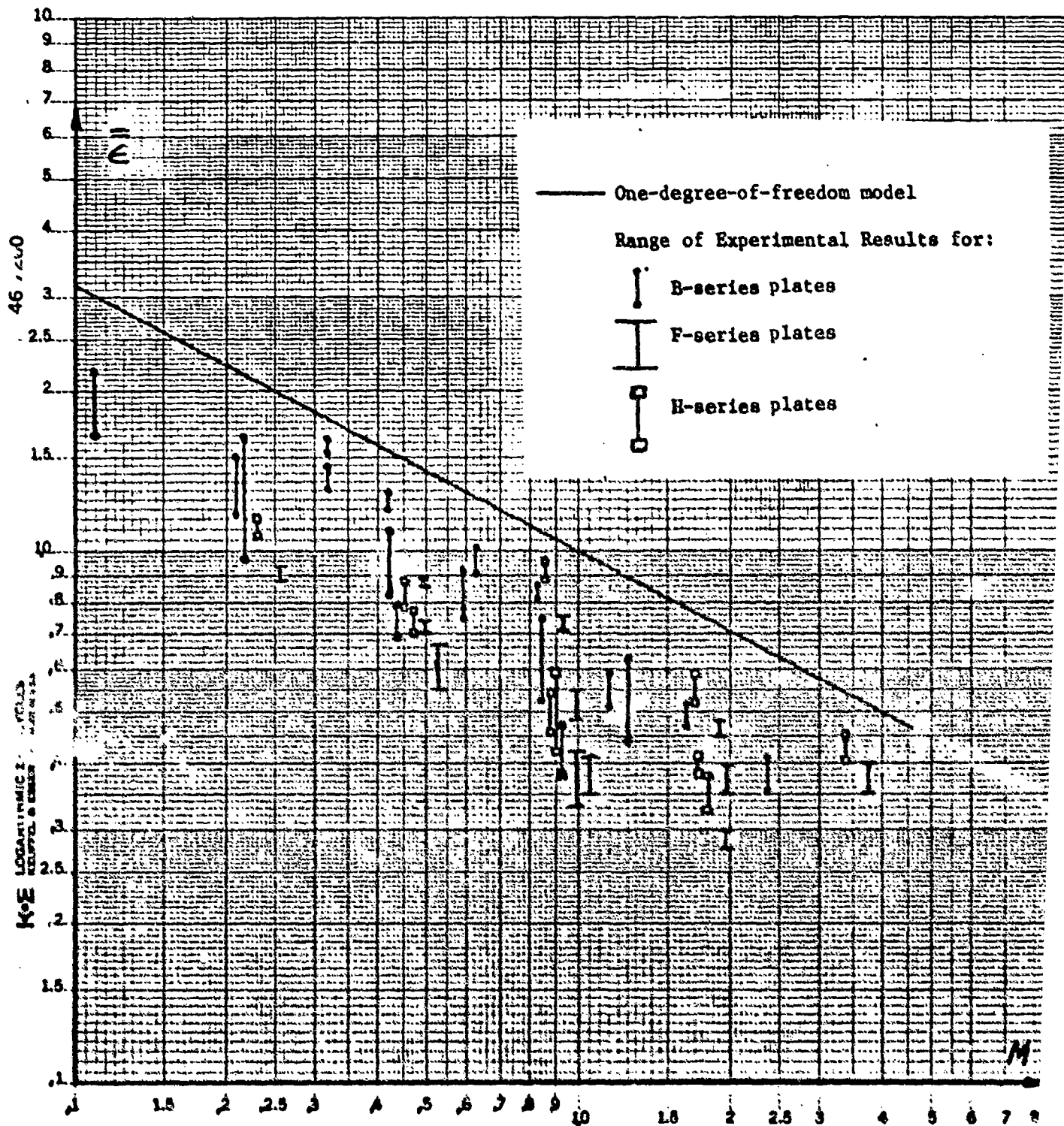


Figure E4. Strain Curve for Simply Supported Plates Impacted by Large Impactors.

2. Results of Impact-to-Failure Experiments

Each specimen was impacted at a gradually increasing velocity until damage was detected either by inspection or by use of a hand held ultrasonic transducer and oscilloscope system.

The theoretical failure strain, ϵ_f , used in constructing the one-degree-of-freedom model design curve is the surface strain obtained when the strain in the outermost 0° lamina reaches the failure strain supplied by the manufacturer (0.0112).

TABLE E5

IMPACT FAILURE EXPERIMENTS PERFORMED ON

COMPOSITE BEAM SPECIMENS

Impact Mass, m_2 (kg)	Mass Ratio, $M=m_1/m_2$	Impact Velocity, v (m/sec)	Failure Occurred	Dimensionless Impact Velocity, $\bar{v} = vh/a^2$
0.1095	0.0562	5.63	No	0.00333
		6.32	No	0.00374
		6.77	No	0.00400
		6.95	No	0.00411
		7.90	No	0.00467
		7.00	Yes	0.00414
		7.35	Yes	0.00435
		7.53	Yes	0.00445
		7.65	Yes	0.00452
		8.25	Yes	0.00488
		8.66	Yes	0.00512
0.0566	0.1089	9.31	No	0.00550
		9.42	No	0.00557
		10.30	No	0.00609
		11.20	No	0.00662
		11.13	Yes	0.00658
		11.27	Yes	0.00666
		11.47	Yes	0.00678

TABLE B5 (continued)

Impact Mass, m_2 (kg)	Mass Ratio, $M=m_1/m_2$	Impact Velocity, v (m/sec)	Failure Occurred	Dimensionless Impact Velocity, $\bar{v} = vh/a^2$
0.0566	0.1089	11.72	Yes	0.00693
		12.97	Yes	0.00767
0.0280	0.220	13.03	No	0.00770
		15.45	No	0.00913
		17.59	Yes	0.01040
		19.17	Yes	0.01133
		20.12	Yes	0.01190
		23.07	Yes	0.01364
		24.07	Yes	0.01423
		24.10	Yes	0.01425
0.01434	0.429	19.05	No	0.01126
		21.17	No	0.01252
		21.97	No	0.01299
		22.66	Yes	0.01340
		23.39	Yes	0.01383
		26.24	Yes	0.01551
		28.42	Yes	0.01680
		33.43	Yes	0.01976

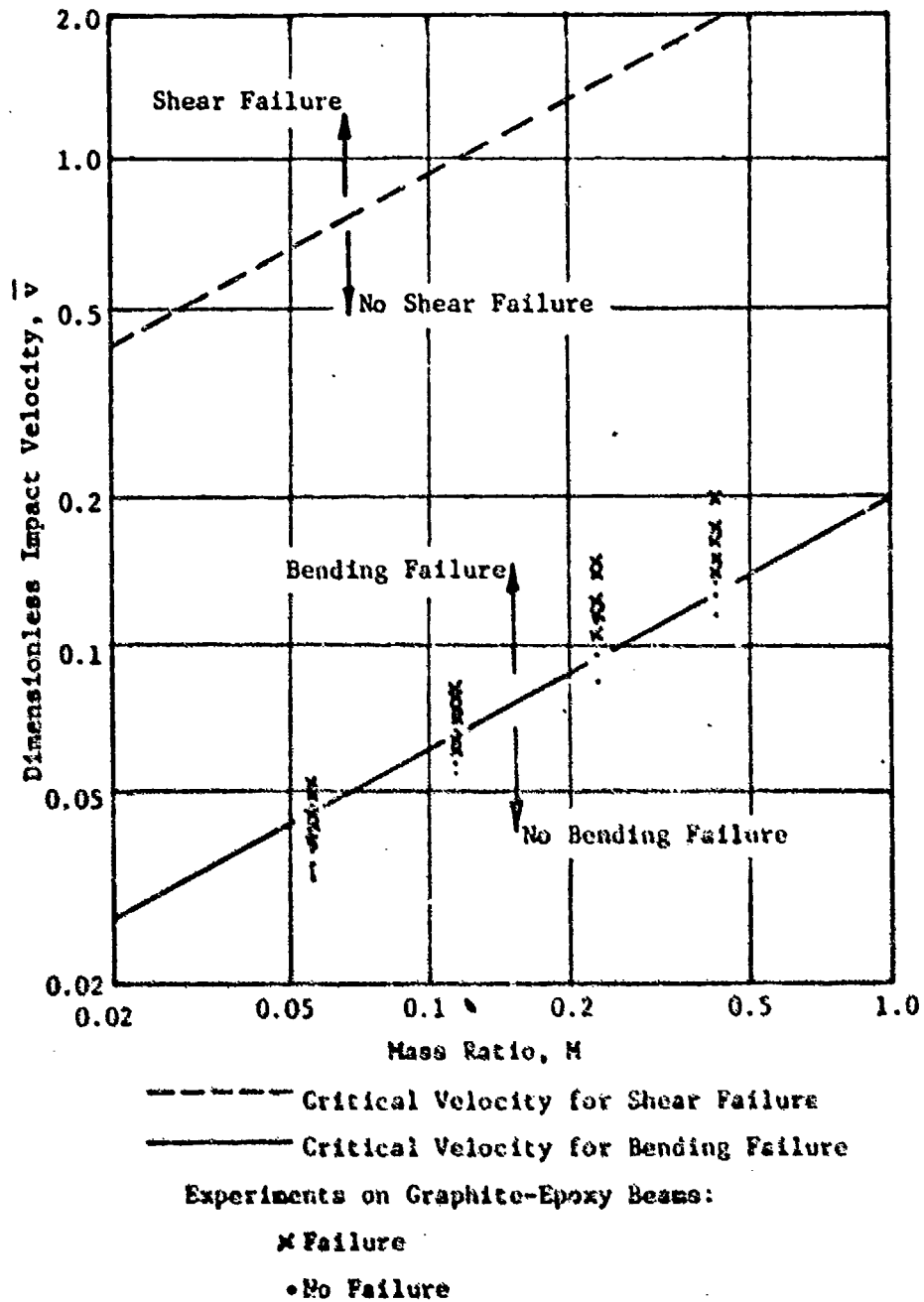


Figure E45. Critical impact velocities for shear and bending failure and experimental data--a bending-dominated case.

TABLE B6. IMPACT-TO-FAILURE EXPERIMENTS PERFORMED ON COMPOSITE PLATES

SPECIMEN	η	IMPACTOR RADIUS, mm	SUPPORT	M	HIGHEST Ab- FAIL VELOCITY m/sec	LOWEST FAIL VELOCITY m/sec	FAILURE VELOCITY V_c , m/sec	\bar{V} $\times 10^3$	\bar{V} $\times 10^3$
B1-1	0.63	6.37	CLAMPED	0.11	3.98	3.46	3.42	1.74	5.57
B1-2	0.63	6.37	CLAMPED	0.11	2.99	3.46	3.23	1.64	5.25
B1-3	0.63	6.37	SIMPLE	0.22	4.89	5.19	5.04	2.57	6.17
B1-4	0.63	6.37	SIMPLE	0.11	4.58	4.89	4.74	2.41	5.78
B2-1	0.16	6.37	CLAMPED	0.21	3.74	3.82	3.77	1.92	7.97
B2-2	0.16	6.37	CLAMPED	0.21	3.74	3.82	3.77	1.92	7.97
B2-3	0.16	12.7	CLAMPED	0.43	5.19	5.47	5.33	2.72	11.23
B3-1	2.39	6.37	CLAMPED	0.21	3.74	3.87	3.81	1.94	6.02
B3-2	2.39	6.37	CLAMPED	0.43	4.58	4.89	4.73	2.41	7.47
B3-3	2.39	6.37	SIMPLE	0.43	6.47	6.62	6.55	3.34	7.52
B3-4	2.39	12.7	CLAMPED	0.21	3.87	4.24	4.05	2.06	6.39
B3-5	2.39	6.37	SIMPLE	0.21	4.24	4.58	4.41	2.25	5.06
B3-6	2.39	6.37	CLAMPED	0.43	5.19	5.29	5.24	2.67	8.28
B4-1	0.63	6.37	CLAMPED	0.42	4.63	4.68	4.66	2.38	7.62
B4-2	0.63	6.37	CLAMPED	0.84	5.82	5.99	5.91	3.01	9.68

TABLE B6, continued

SPECIMEN	η	INSTRUMENT RADIUS, mm	SUPPORT	M	HIGHEST NO- FARE VELOCITY m/sec	LOWEST FARE VELOCITY m/sec	FAILURE VELOCITY V_c , m/sec	\bar{V} $\times 10^3$	\bar{V} $\times 10^3$
B4-3	0.63	6.37	SAMPLE	0.84	6.47	6.70	6.58	3.35	8.04
B4-4	0.63	12.7	CLAMPED	0.42	4.79	4.89	4.84	2.47	7.91
B5-1	0.07	6.37	CLAMPED	0.32	3.46	3.60	3.52	1.80	8.64
B5-2	0.07	6.37	CLAMPED	0.32	3.31	3.39	3.35	1.71	8.21
B5-3	0.07	6.37	SAMPLE	0.63	6.85	7.06	6.96	3.55	19.14
B6-1	5.29	6.37	CLAMPED	0.32	3.87	3.93	3.90	1.99	6.57
B6-2	5.29	12.7	SAMPLE	0.32	5.19	5.47	5.33	2.71	6.50
B6-3	5.29	6.37	SAMPLE	0.32	5.19	5.47	5.33	2.71	6.50
B7	1.38	6.37	CLAMPED	0.59	5.47	5.74	5.60	2.85	8.55
B8	0.28	6.37	CLAMPED	0.57	5.79	6.24	6.11	3.11	11.82
B9	0.63	6.37	CLAMPED	0.89	6.24	6.47	6.36	3.24	10.37
F1	0.64	6.37	CLAMPED	0.26	4.98	5.38	5.18	2.83	9.06
F2	0.168	6.37	CLAMPED	0.49	4.78	4.98	4.88	2.67	11.22

TABLE E6, continued

SPECIMEN	η	INSTRUMENT DINOS, mm	SUPPORT	M	HIGHEST NO. FAIL VELOCITY m/sec	LOWEST FAIL VELOCITY m/sec	FAILURE VELOCITY V_c , m/sec	$\bar{V} \times 10^3$	$\bar{V} \times 10^3$
F3	2.45	6.37	CLAMPED	0.49	5.18	5.46	5.28	2.98	9.24
F4	0.64	6.37	CLAMPED	0.95	6.70	6.92	6.81	3.72	11.91
H1	1.15	6.37	CLAMPED	0.25	3.31	3.59	3.46	1.94	5.92
H2	0.302	6.37	CLAMPED	0.45	3.73	3.99	3.86	2.17	6.93
H3	4.41	6.37	CLAMPED	0.45	4.46	4.88	4.68	2.62	10.35
H4	1.15	6.37	CLAMPED	0.84	5.99	6.24	6.11	3.42	10.43

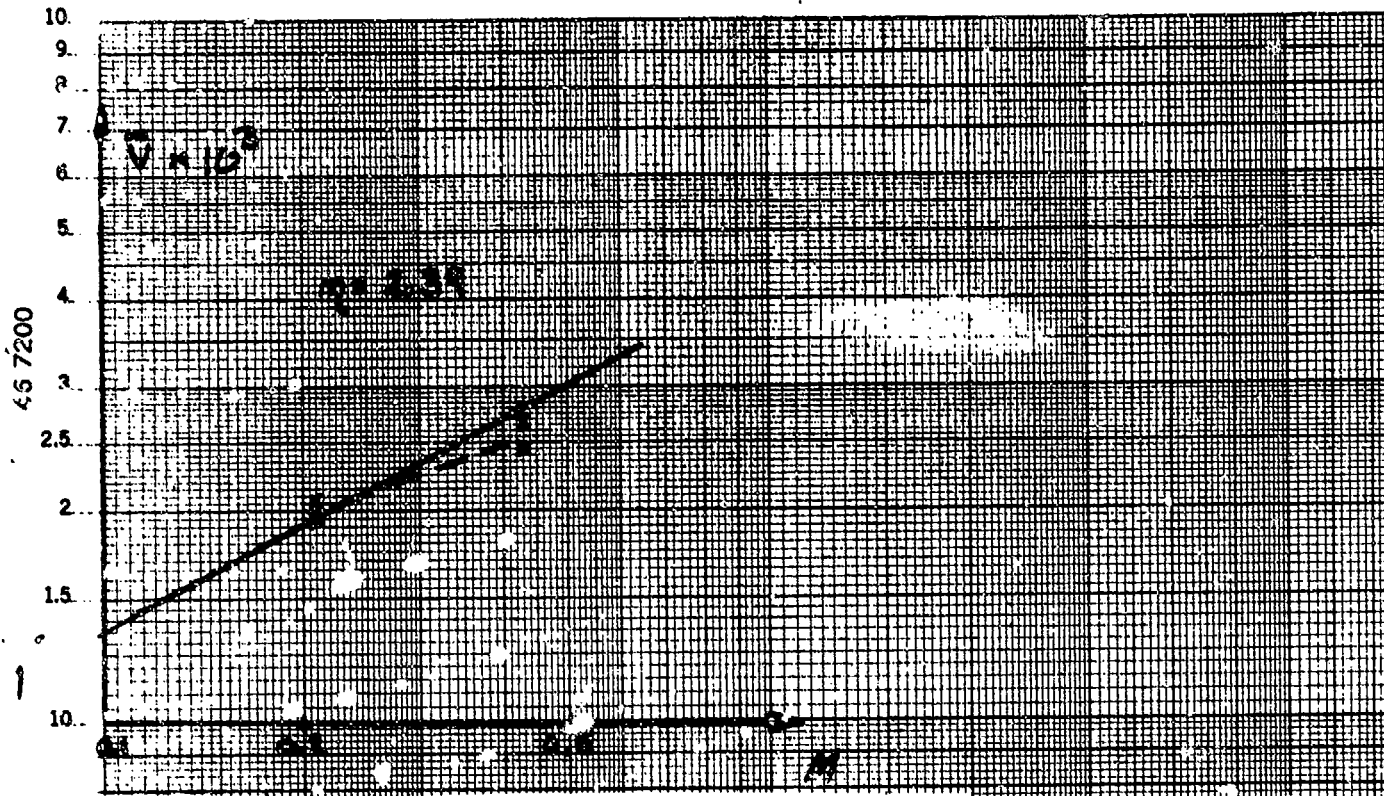
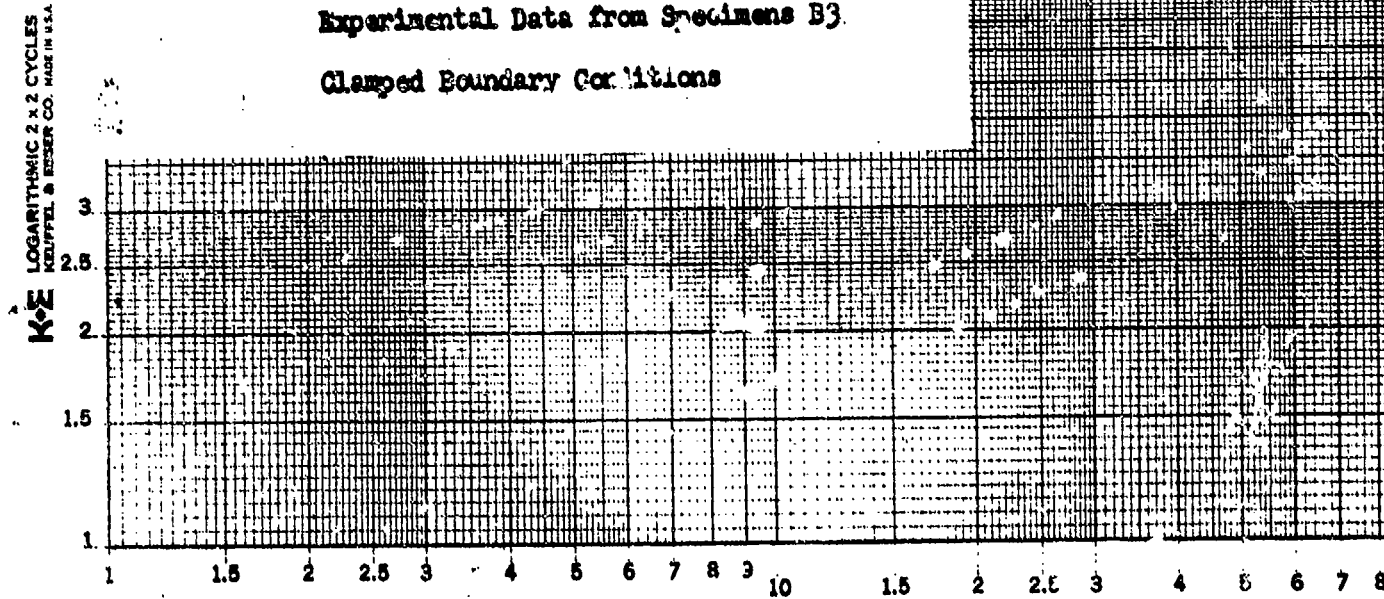


Figure B46. Critical Impact Velocity Curve, \bar{V} vs. M
Experimental Data from Specimens B3
Clamped Boundary Conditions



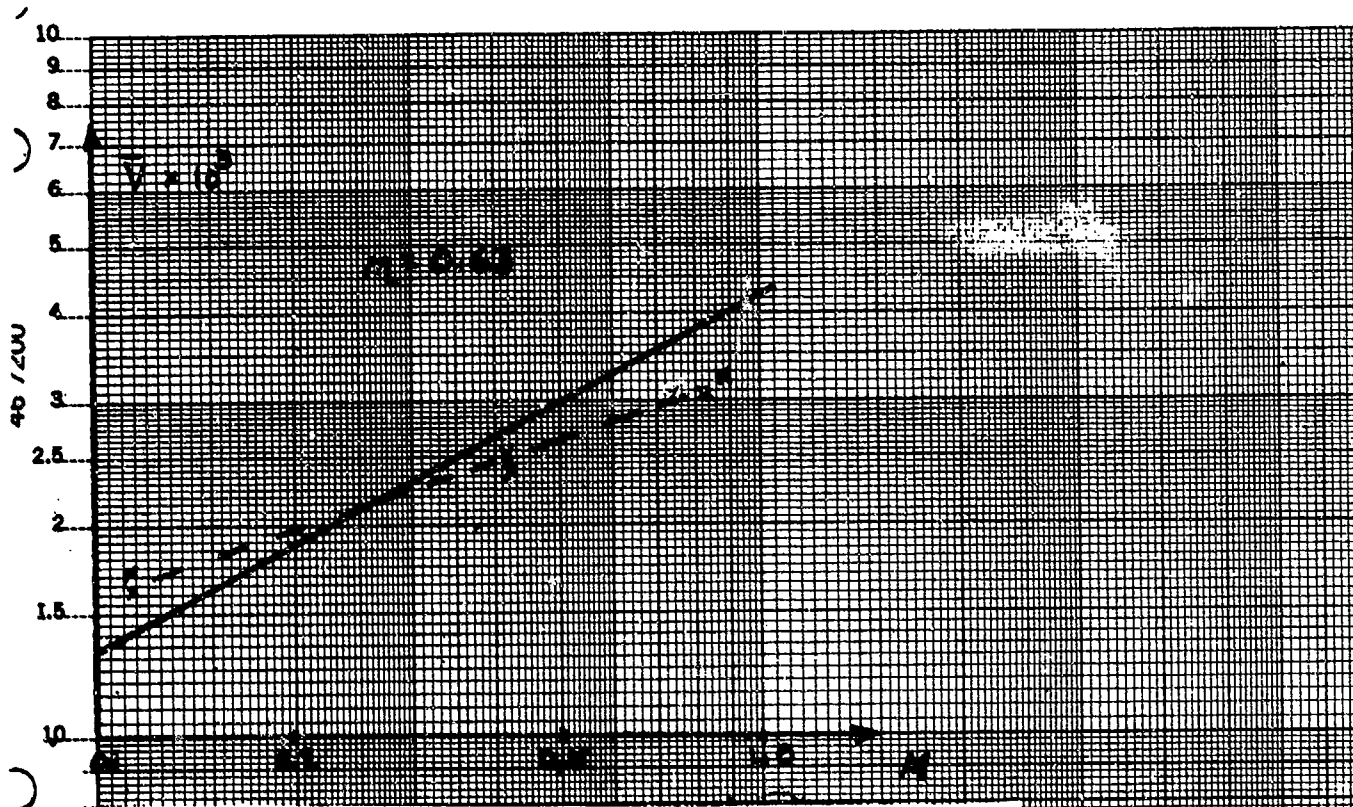
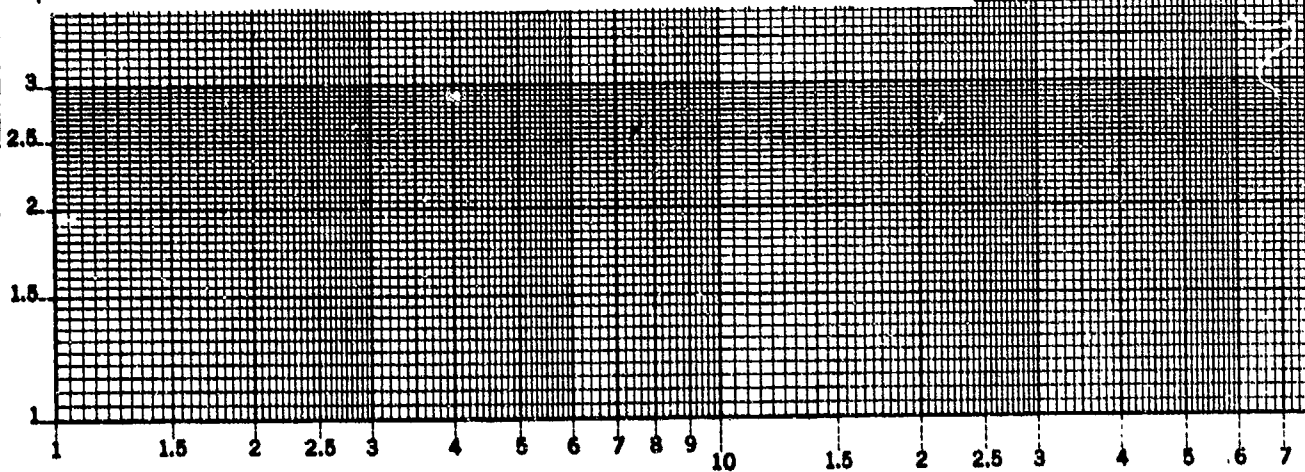


Figure E47. Critical Impact Velocity Curve, \bar{V} vs. M
 Experimental Data from Specimens B1, B4, and B9
 Clamped Boundary Conditions

K-E LOGARITHMIC 2 x 2 CYCLES
 KELFREL & BENDER CO. MADE IN U.S.A.



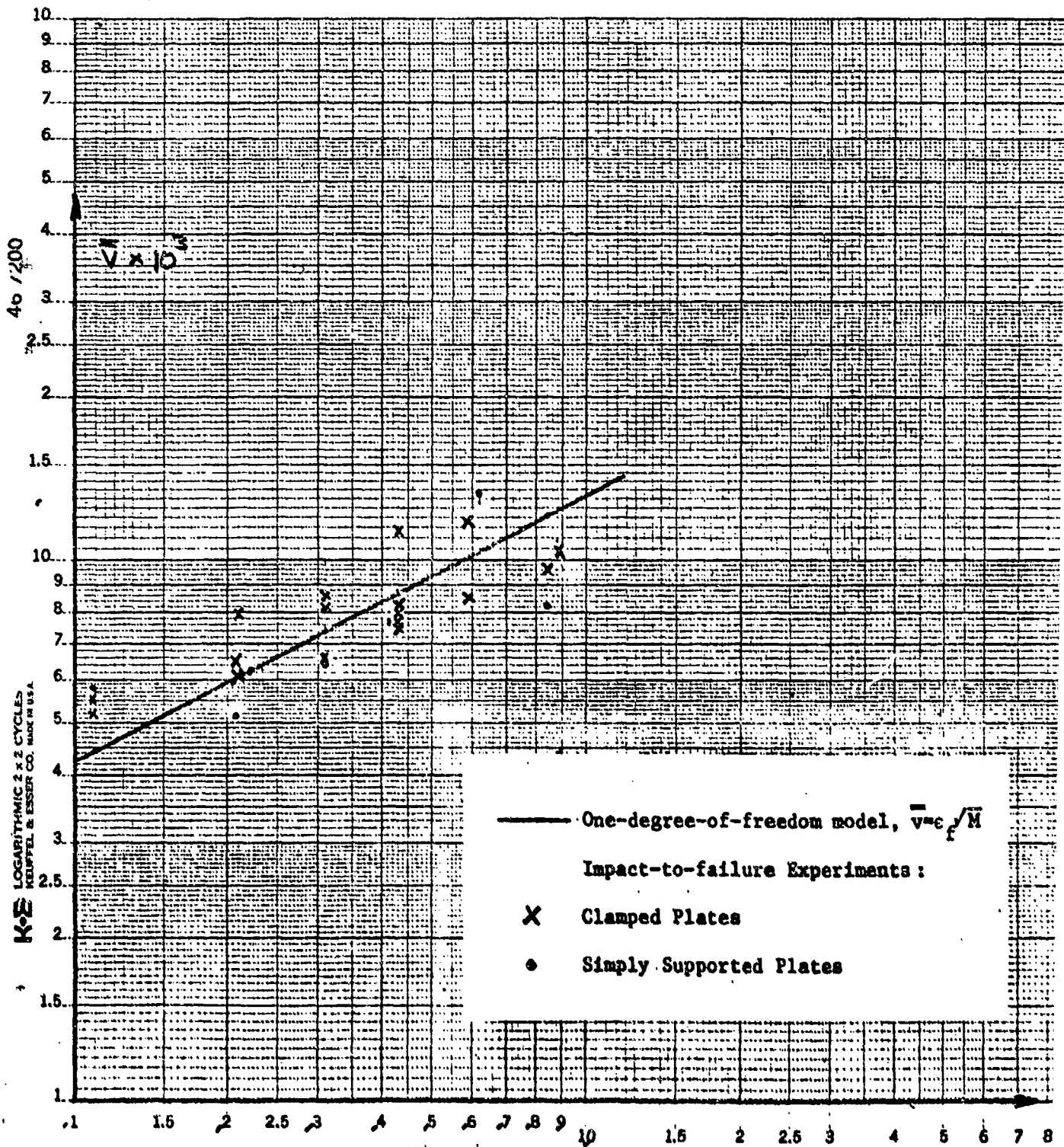
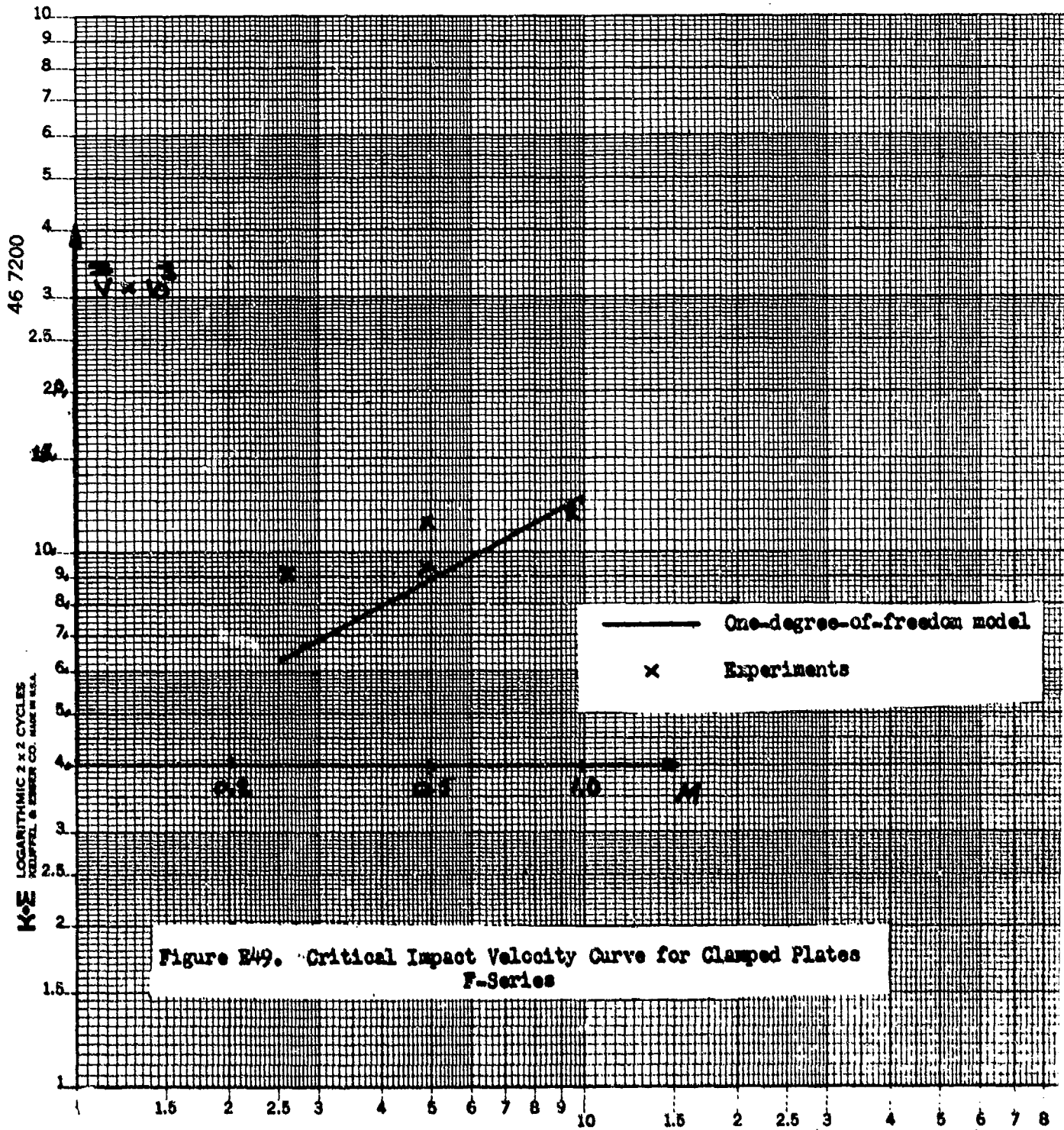


Figure E48. Critical Impact Velocity Curve for Clamped and Simply Supported Plates Impacted by Large Masses.



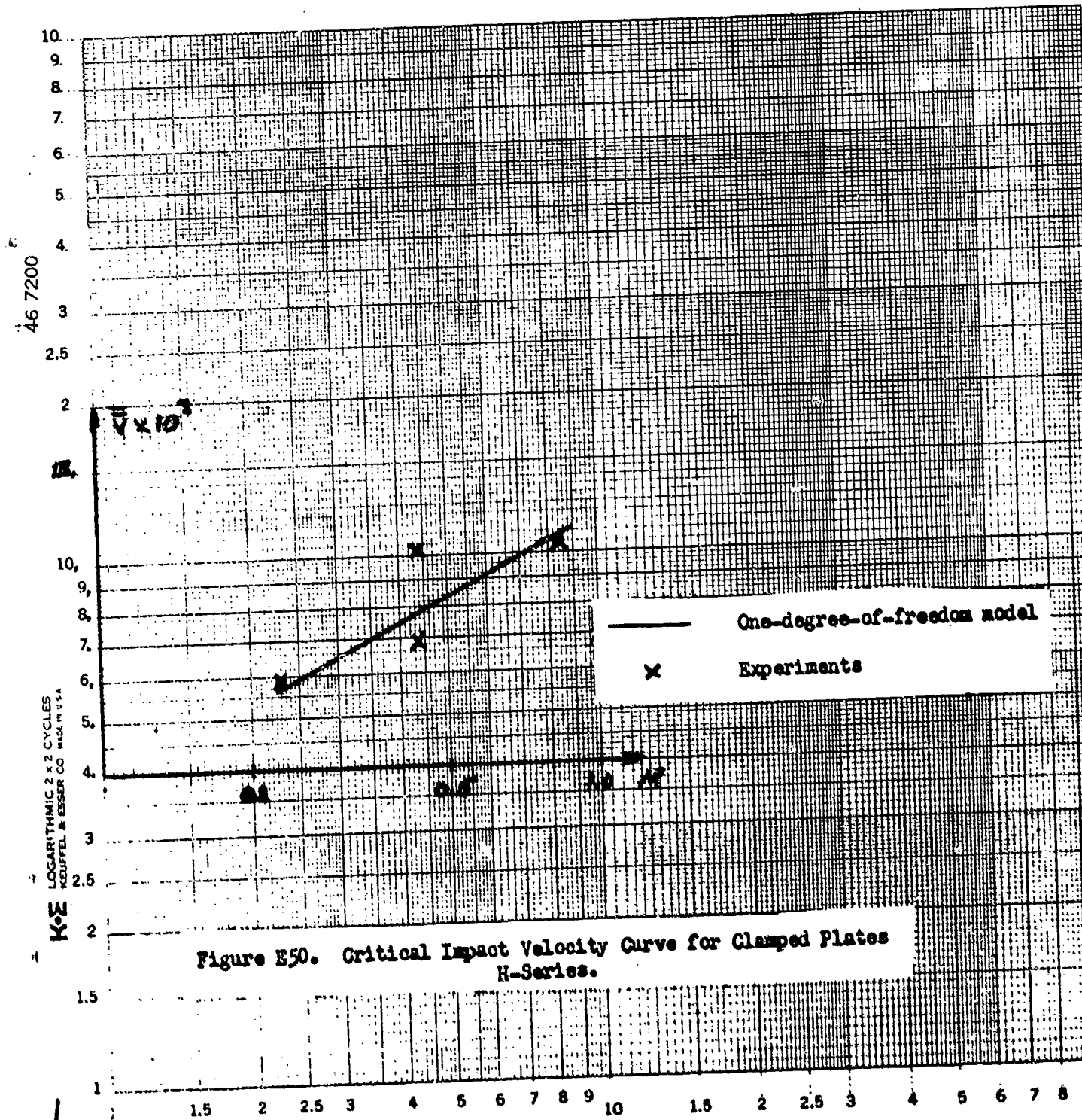


Figure E50. Critical Impact Velocity Curve for Clamped Plates H-Series.

3. Results of Small Impactor Strain Measuring Experiments

Plate specimens were impacted by 1"(25mm) radii aluminum projectiles fired from an air gun. Impactor velocities were recorded using a photo-diode system. Plate strain was recorded using type EA-13-062TT rosettes and a type 565 dual beam oscilloscope.

TABLE E7

DATA FROM EXPERIMENTS ON SIMPLY SUPPORTED

BEAMS IMPACTED BY SMALL MASSES

Beam Mass, Dimensions, and Material	Mass Ratio, $M=m_1/m_2$	Impact Velocity, v (m/sec)	Contact Stiffness, k_2 (N/m ^{3/2})	Generalized Strain, $\bar{\epsilon} = \epsilon a^2/hv$	$\frac{\bar{\epsilon}}{\sqrt{B}}$
0.389 kg 192 x 16 x 16 mm steel	27.0	6.37	2.466×10^{10}	0.0795	0.0184
	"	13.17	"	0.0814	0.0175
	13.8	8.72	"	0.1229	0.0315
	"	12.19	"	0.1489	0.0369
	6.85	5.49	"	0.2388	0.0739
	"	8.53	"	0.2512	0.0743
	3.54	6.28	"	0.3224	0.1123
	"	9.33	"	0.3493	0.1171
0.601 kg 305 x 16 x 16 mm steel	41.8	10.88	"	0.0800	0.01142
	"	14.87	"	0.0790	0.01092
	23.8	7.92	"	0.1033	0.01703
	"	11.06	"	0.1076	0.01716
	11.2	7.50	"	0.1766	0.0341
	"	12.37	"	0.1800	0.0330
	5.88	6.16	"	0.2678	0.0554
	"	8.11	"	0.2662	0.0579
0.1096 kg, aluminum	1.93	4.39	"	0.475	0.1689
152 x 20 x 12.7 mm	"	6.92	"	0.462	0.1569

TABLE E7 (continued)

Beam Mass, Dimensions, and Material	Mass Ratio, $M=m_1/m_2$	Impact Velocity, v (m/sec)	Contact Stiffness k_2 (N/m ^{3/2})	Generalized Strain, $\bar{\epsilon} = \epsilon a^2/hv$	$\frac{\bar{\epsilon}}{\sqrt{\beta^*}}$
0.601 kg 305 x 16 x 16 mm steel	41.8	10.58	1.744×10^{10}	0.0760	0.01166
	"	12.71	"	0.0761	0.01146
	23.8	9.42	"	0.1242	0.0216
	"	12.53	"	0.1235	0.0208
	11.2	5.33	"	0.1534	0.0328
	"	12.01	"	0.1611	0.0317
	5.88	5.39	"	0.2345	0.0570
	"	7.71	"	0.2799	0.0656
0.360 kg 185 x 16 x 16 mm steel	25.0	11.31	2.466×10^{10}	0.0868	0.0203
	"	14.42	"	0.0978	0.0223
	12.8	8.11	"	0.1523	0.0421
	"	10.70	"	0.1647	0.0442
	6.34	8.20	"	0.2563	0.0814
	"	10.52	"	0.2434	0.0754
	3.27	5.73	"	0.3252	0.1221
	"	8.60	"	0.3203	0.1155
0.1074 kg, steel 98 x 15 x 9 mm	1.89	3.90	"	0.458	0.2222
	"	6.40	"	0.465	0.2147

TABLE B8

DATA FROM GOLDSMITH (1960)

Beam Mass, Dimensions, and Material	Mass Ratio, $M=m_1/m_2$	Impact Velocity, v (m/sec)	Contact Stiffness, k_2 (N/m ^{3/2})	Generalized Strain, $\bar{\epsilon} = \epsilon a^2/hv$	$\frac{\bar{\epsilon}}{\sqrt{B^2}}$
3.66 kg 762 x 25.4 x 25.4 mm steel	6.44	0.405	3.487×10^{10}	0.262	0.0563
	"	1.338	"	0.286	0.0500
	"	2.54	"	0.311	0.0510
	2.12	0.408	"	0.520	0.1278
	"	1.271	"	0.564	0.1237
	"	1.777	"	0.584	0.1239
56.9 kg 2900 x 50 x 50 mm steel	57.0	2.40	4.894×10^{10}	0.148	0.00932
	23.7	2.47	"	0.247	0.01855
	"	3.00	"	0.237	0.01740
	"	3.40	"	0.260	0.01886
	"	4.75	"	0.239	0.01676
	11.41	2.40	"	0.365	0.03173
	6.34	2.40	"	0.420	0.04107
3.66 kg, steel 724x25.4x25.4 mm	55.0	1.725	1.744×10^{10}	0.0802	0.01065
2.170 kg, steel 762x19x19 mm	266.	45.7	1.233×10^{10}	0.0268	0.001486
1.447 kg, steel 762x19x12.7 mm	177.2	45.7	"	0.0359	0.001625
0.965 kg, steel 762x12.7x12.7 mm	118.2	45.7	"	0.0713	0.003228
0.482 kg, steel 762x6.3x12.7 mm	59.1	45.7	"	0.1578	0.007143

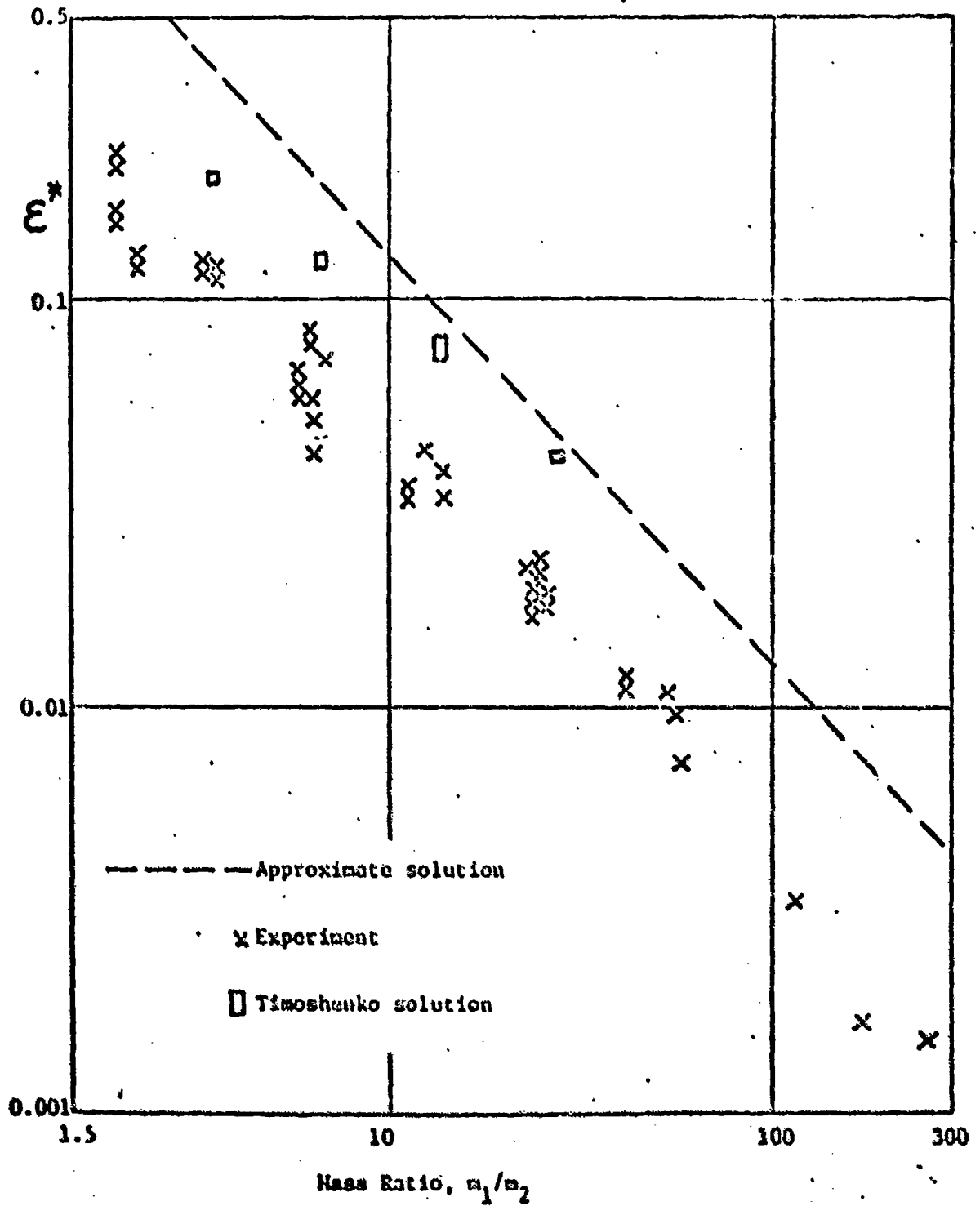


Figure E51. Design curve for impacts of simply supported beams by small masses.

TABLE E9

Impact of Composite Plates by Small Masses

SAMPLE	M	$E_{max} \times 10^6$	V, m/s	β	E^*
F1	16.9	4000	26.8	4.38	0.0471
		3600	26.8	4.38	0.0423
	11.9	3000	24.8	3.75	0.045
		1600	17.7	3.50	0.0359
		1100	17.7	3.50	0.0247
		5000	26.8	3.80	0.068
		3600	24.7	3.75	0.054
F2	32.3	3000	26.8	6.03	0.0181
		4000	26.8	6.03	0.0241
		1100	18.3	5.59	0.0103
		950	18.3	5.59	0.0090

TABLE E10

Data From Schwieger

M	$\epsilon_{\max} \times 10^6$	$N, m/s$	β	ϵ^*
4.67	170	0.25	18.7	0.0428
	354	0.50	21.5	0.0388
	531	0.75	23.3	0.0358
	730	1.00	25.0	0.0344
	901	1.25	25.8	0.0331
	1150	1.50	26.7	0.0327
	1283	1.75	27.6	0.0313
	1482	2.00	28.3	0.0308
15.5	332	0.50	31.8	0.0239
	486	0.75	34.5	0.0221
	663	1.00	36.6	0.0213
	774	1.25	38.2	0.0190
	973	1.50	39.7	0.0192
	1017	1.75	40.9	0.0167
	1194	2.00	42.0	0.0167

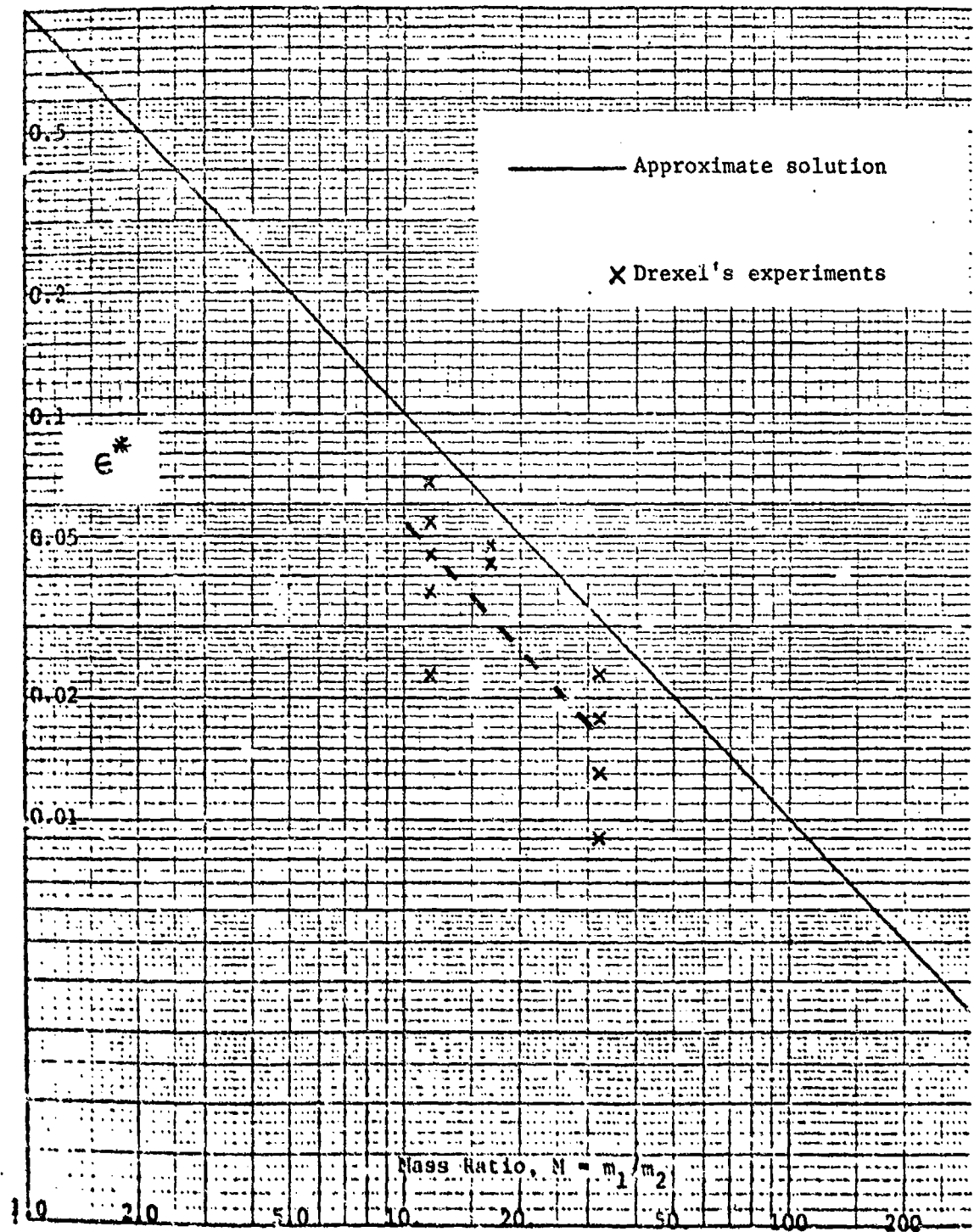
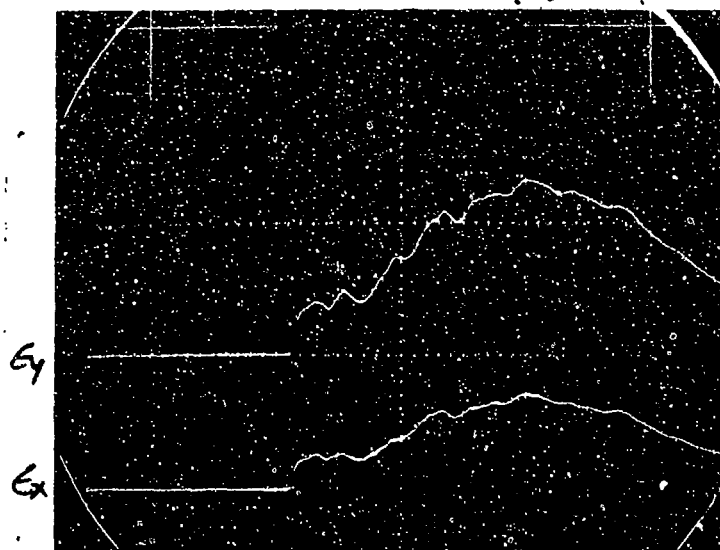


Figure E52. Strain Curve for Impact of Simply Supported Rectangular Plate by a Small Impactor.

4. Typical Strain vs. Time Oscilloscope Traces for Impact of Clamped and Simply Supported Orthotropic Plates by Large Impactors.

8-16-77 #19



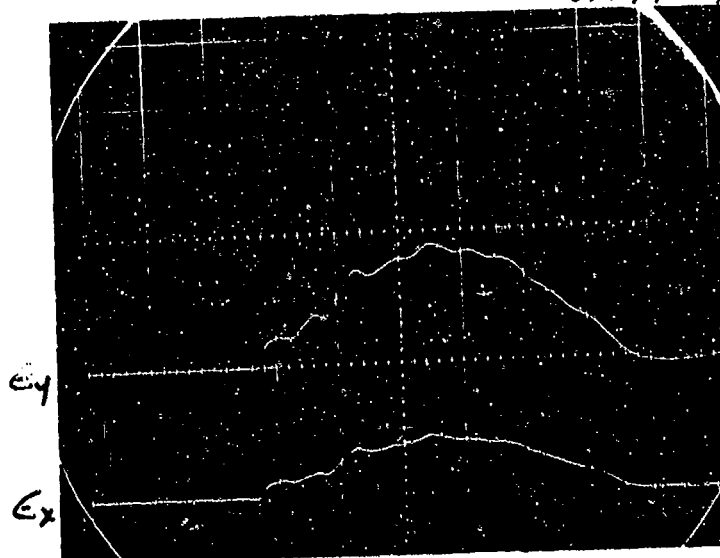
Scale:

2000 $\mu \frac{\text{mm}}{\text{mm}}/\text{div}$
vertical

0.5 msec/div
horizontal

a) Simply Supported

8/10/77 #14



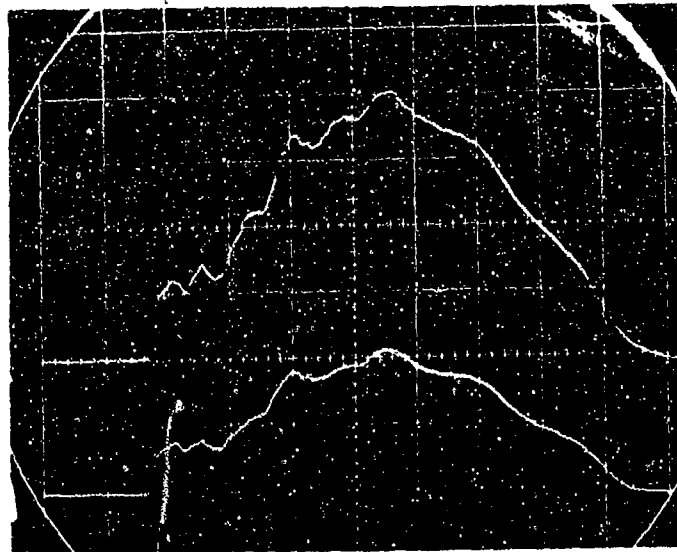
Scale:

4000 $\mu \frac{\text{mm}}{\text{mm}}/\text{div}$
vertical

0.5 msec/major
horizontal

b) Clamped

Figure K53: Impact of Specimen B3, $M = 0.21$, Impact Velocity = 1.73 m/s



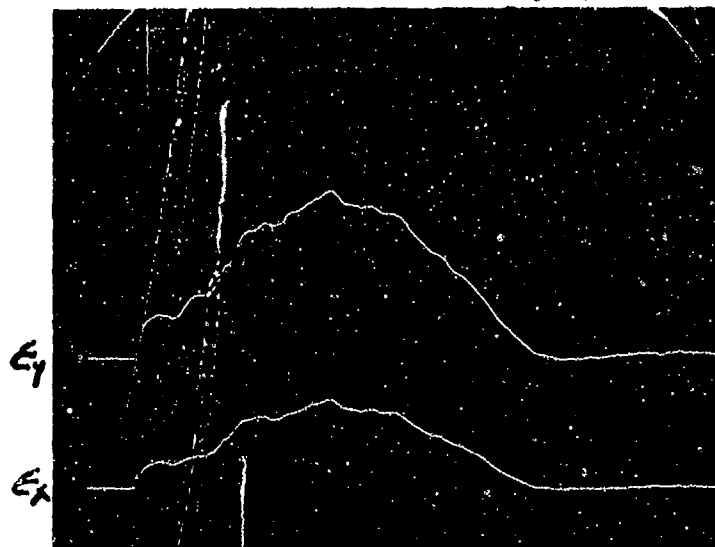
Scale:

2000 $\mu \frac{\text{mm}}{\text{mm}}$ /div
vertical

0.5 msec/div
horizontal

a) Simply Supported

8/16/77 #1



Scale:

4000 $\mu \frac{\text{mm}}{\text{mm}}$ /div
vertical

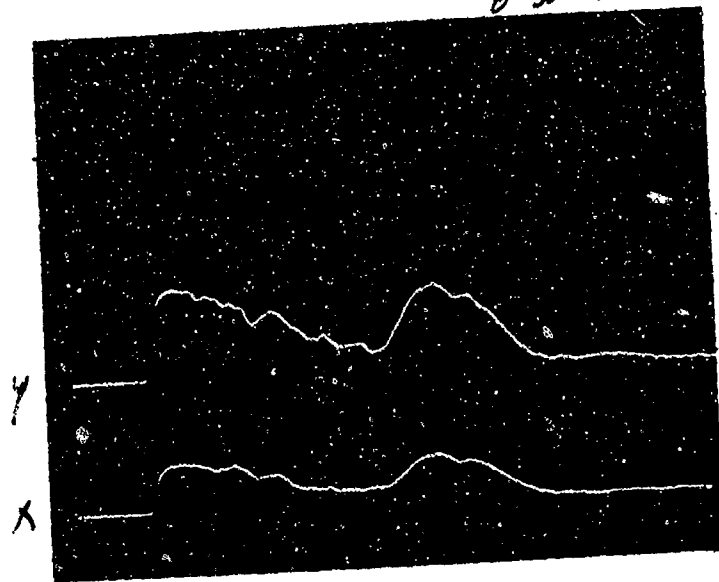
0.5 msec/major
horizontal

b) Clamped

Figure E54: Impact of Specimen B3, $M = 0.21$, Impact Velocity = 2.45 m/sec

NADC-78259-60

8-30-77 #24



Scale:

1000 $\mu \frac{\text{mm}}{\text{mm}}$ /div

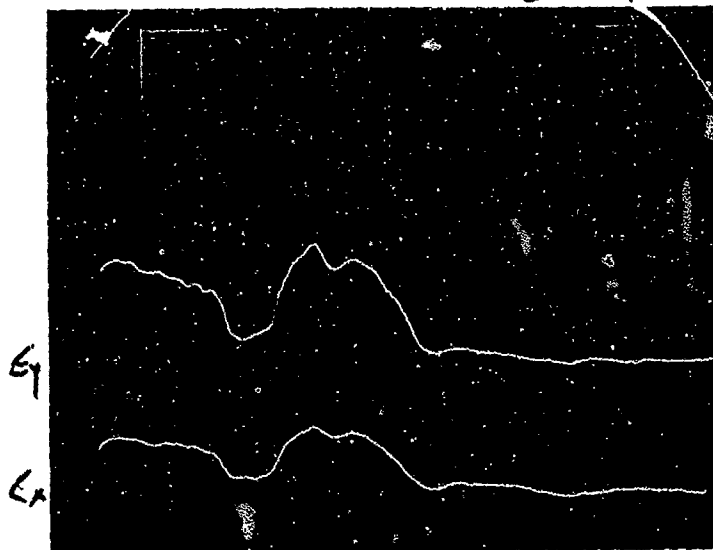
vertical

0.5 msec/div

horizontal

a) Simply Supported

8-30-77 #2



Scale:

1000 $\mu \frac{\text{mm}}{\text{mm}}$ /div

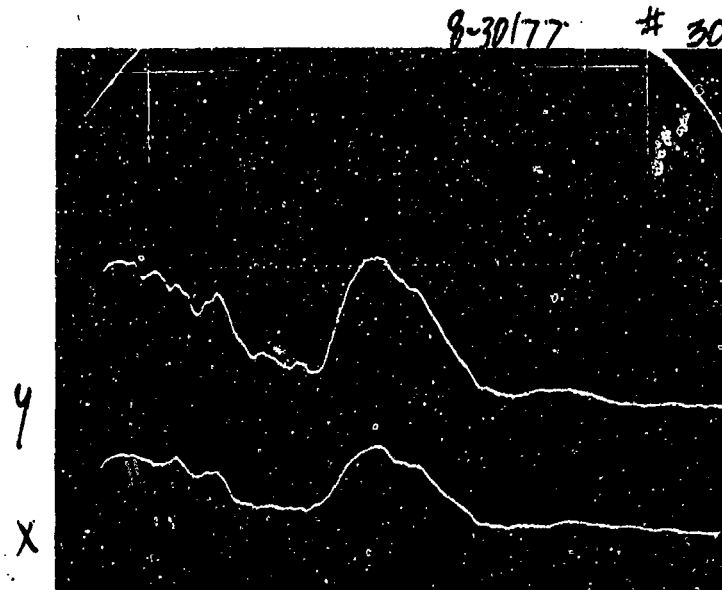
vertical

0.5 msec/major

horizontal

b) Clamped

Figure E55: Impact of Specimen B7, $M = 2.38$, Impact Velocity = 1.73

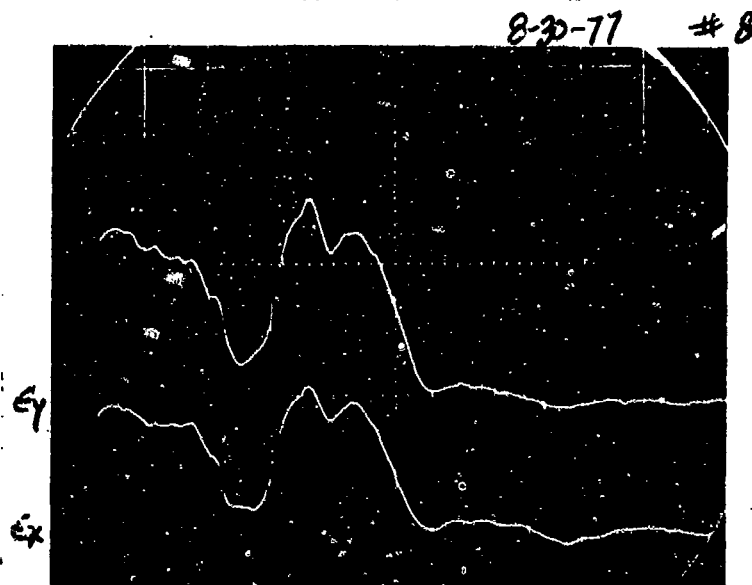


Scale

1000 $\mu \frac{\text{mm}}{\text{mm}}/\text{div}$
vertical

0.5 msec/div
horizontal

a) Simply Supported



Scale

1000 $\mu \frac{\text{mm}}{\text{mm}}/\text{div}$
vertical

0.5 msec/major
horizontal

b) Clamped

Figure E56: Impact of Specimen B7, $M = 2.38$, Impact Velocity = 2.49 m/sec.

Appendix F

The Effect of the Approximation $H = \sqrt{D_{11}D_{22}}$ on the
Predicted Impact Response of an Orthotropic Plate

To simplify the analysis of the bending and vibration of specially orthotropic plates, Timoshenko and Woinowsky-Krieger [13] have suggested the approximation

$$H = \sqrt{D_{11}D_{22}} \quad (F1)$$

where H is defined as

$$H \equiv D_{12} + 2D_{66}$$

An advantage of using this assumption is that the equation governing bending of an orthotropic plate may be transformed, through a simple change in variables, into an equation similar to the equation governing bending of an isotropic plate. By reversing the transformation, a solution for the deflection of an isotropic plate may be converted into the corresponding solution for an orthotropic plate. This is done in Appendix B for a centrally loaded rectangular plate with clamped boundary conditions; the approximation (F1) is instrumental in this instance because no general solution exists for the orthotropic case.

Like all approximations, however, application of Eq. (F1) introduces some error into the solution. In this Appendix, we investigate the influence of this approximation on the strain predicted by the one-degree-of-freedom model of impact of a simply supported rectangular orthotropic plate. This is done by deriving the relationship between the generalized strain $\bar{\epsilon}_x$ and the mass ratio M , both with and without the use of Eq. (F1), and then comparing the results.

The static deflection of a simply supported rectangular orthotropic plate due to a central concentrated load P is [10]

$$w(x,y) = \frac{4P}{ab\pi^4} \sum_m \sum_n \frac{\sin \frac{m\pi x}{a} \sin \frac{n\pi y}{b} \sin \frac{m\pi}{a} \sin \frac{n\pi}{b}}{\frac{m^4}{a^4} D_{11} + 2\frac{m^2 n^2}{a^2 b^2} D_{12} + \frac{n^4}{b^4} D_{22}}$$

where a and b are the plate dimensions in the x and y directions. If we define η as in Eq. (16) and

$$\zeta = \frac{H}{\sqrt{D_{11} D_{22}}}$$

then the maximum deflection, which occurs at the center of the plate, may be expressed as

$$w_{\max} = P/K_1$$

where

$$K_1 = \frac{\pi^4 D_{11} b}{4a^3} \frac{1}{F_1(\zeta, \eta)} \quad (F2)$$

$$F_1(\zeta, \eta) = \sum_m \sum_n \frac{1}{B_{mn}} \quad m, n \text{ odd}$$

$$B_{mn} = m^4 + 2m^2 n^2 \eta \zeta + n^4 \eta^2$$

Similarly, the maximum x -direction bending strain, which also occurs at the plate center, may be expressed as

$$\begin{aligned} \epsilon_{x, \max} &= \frac{2 P h a}{\pi^2 D_{11} b} F_2(\zeta, \eta) \\ &= \frac{2 h a K_1}{\pi^2 D_{11} b} F_2(\zeta, \eta) w_{\max} \end{aligned}$$

where

$$F_2(\zeta, \eta) = \sum_m \sum_n \frac{m^2}{B_{mn}} \quad m, n \text{ odd.}$$

Therefore, the strain-deflection constant, defined in Eq. (6), is

$$d_{12} = \frac{\pi^2 D_{11} b}{2h a K_1} \frac{1}{F_2(\zeta, \eta)} \quad (F3)$$

To apply the one-degree-of-freedom impact model to this case, we substitute Eqs. (F2) and (F3) into Eq. (8) with $e = 0$ and define the generalized strain $\bar{\epsilon}_x$ as in Eq. (21) to obtain

$$\bar{\epsilon}_x = \frac{G_1(\zeta, \eta)}{\sqrt{M}} \quad (F4)$$

where

$$G_1(\zeta, \eta) = \frac{F_2(\zeta, \eta)}{\sqrt{F_1(\zeta, \eta)}}$$

Note that the approximation (F1) corresponds to setting $\zeta = 1$. Thus, if this assumption is used, then the approximate relation between $\bar{\epsilon}_x$ and M , corresponding to Eq. (22), is

$$\bar{\epsilon}_x = \frac{G_1(1, \eta)}{\sqrt{M}} \quad (F5)$$

Therefore, the correction required to adjust the approximate generalized strain $\bar{\epsilon}_x$ given by Eq. (F5) to the exact value given by Eq. (F4) is

$$E(\bar{\epsilon}_x) = \frac{G_1(\zeta, \eta)}{G_1(1, \eta)} - 1$$

This error is plotted vs. ζ for a few values of η in Fig. F1. Note that the magnitude of this error does not exceed 17% for the range of ζ values calculated and is less than 9% for most lay-ups commonly used in actual aircraft structures, which lie in the range $0.60 < \zeta < 1.6$. (Lay-ups having ζ values outside this range [e.g., $\zeta = 0.31$ for unidirectional AS/3501-6] rarely have practical application as plate structures.) Further, for the range of ζ values of the plate specimens used in the impact experiments, this error is always less than 6.5%.

In Table F1, the actual values of ζ , η , and the error in predicted generalized strain $E(\bar{\epsilon}_x)$ for the plate specimens are summarized. The largest value of error among all of the plates is only 5.4%. Therefore, we conclude that the approximation of Eq. (F1) does not contribute a significant error to the design curve for impact of simply supported plates by large impactors. We may infer that a similarly small correction is required for orthotropic plates with other boundary conditions.

Table F1

Error in Predicted Generalized Strain
for the Plate Impact Specimens

Plate Number	$\zeta = \frac{H}{\sqrt{D_{11}D_{22}}}$	$\eta = \left(\frac{a}{b}\right)^2 \sqrt{\frac{D_{22}}{D_{11}}}$	$E(\bar{\epsilon}_x)$
B1	1.430	0.625	-3.6%
B2		0.164	-4.2
B3		2.39	-3.7
B4		0.625	-3.6
B5		0.074	-4.0
B6		5.29	-5.4
B7		1.38	-3.2
B8		0.282	-4.1
B9		0.625	-3.6
F1	1.252	0.641	-2.2
F2		0.168	-2.6
F3		2.45	-2.3
F4		0.641	-2.2
H1	1.270	1.150	-2.1
H2		0.302	-2.7
H3		4.41	-3.3
H4		1.150	-2.1

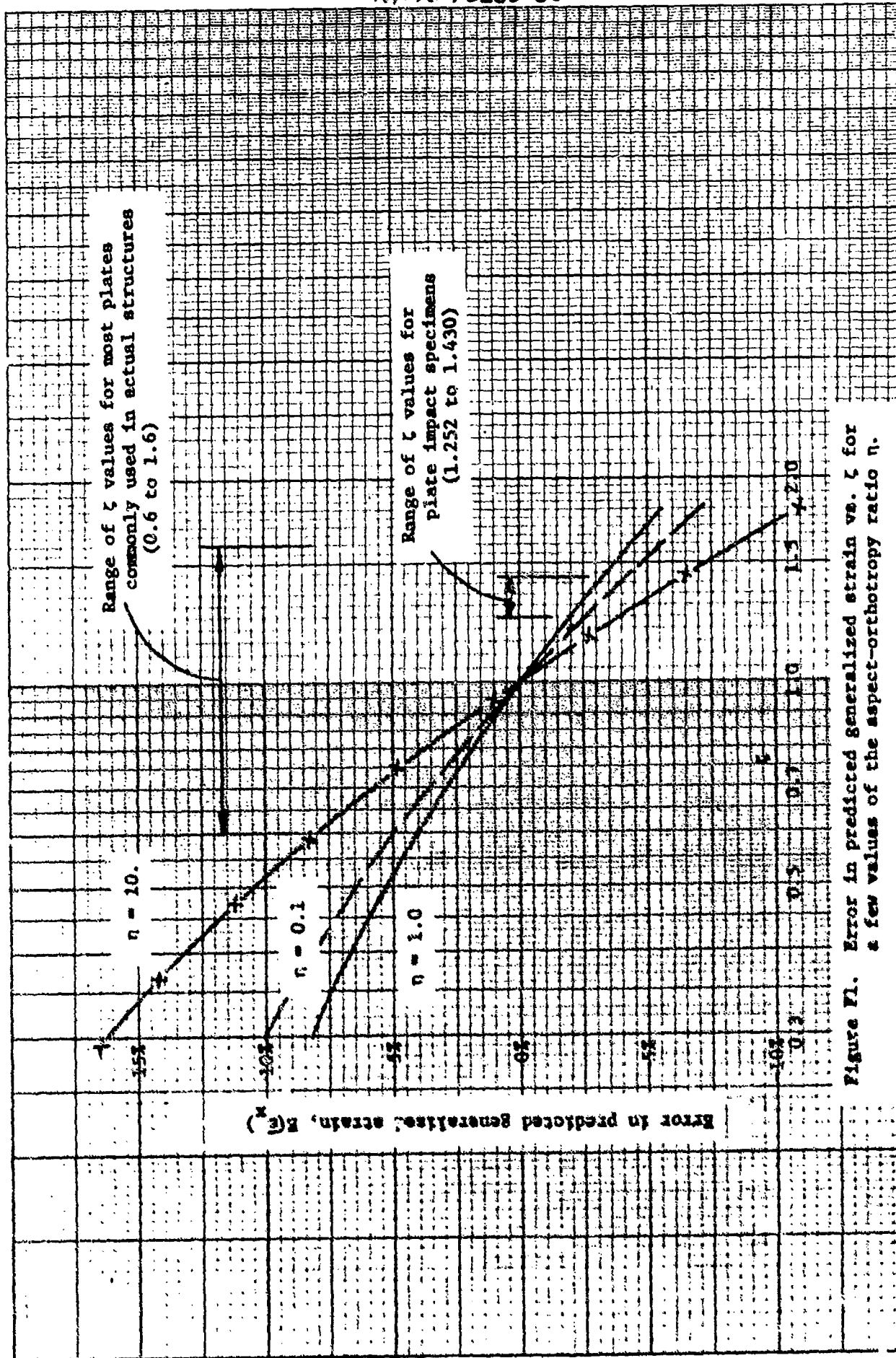


Figure F1. Error in predicted generalized strain vs. ζ for a few values of the aspect-orthotropy ratio η .

DISTRIBUTION LIST

Government Activities

	<u>No. of Copies</u>
NAVAIRSYSCOM, AIR-954 (2 for retention), 2 for AIR-530, 1 for AIR-370B, AIR-52032D, AIR-5302, AIR-53021, AIR-530215).	9
AFFDL, WPAFB, OH 45433.	
(Attn: FB/Mr. P. A. Parmley)	2
(Attn: FBC/Mr. C. Wallace)	1
(Attn: FBC/Mr. E. E. Zink)	1
AFML, WPAFB, OH 45433	
(Attn: LAM (Technical Library))	1
(Attn: LT-1/Mr. W. R. Johnston)	1
(Attn: LTF/Mr. T. Cordell)	1
(Attn: FBSC/Mr. L. Kelly)	1
(Attn: MAC/Mr. G. P. Peterson)	1
(Attn: MKA/Mr. F. J. Fechek)	1
(Attn: MBC/Mr. T. G. Reinhard, Jr.)	1
AFOSR, Washington, D.C. 20333	
(Attn: Mr. J. Pomerantz)	1
DDC.	12
FAA, Airframes Branch, ES-120, Washington, D.C. 20553	
(Attn: Mr. J. Dougherty)	1
NASA (ADM), Washington, D.C. 20546	
(Attn: Secretary)	1
NASA, George C. Marshall Space Flight Center, Huntsville, AL 35812	
(Attn: S&E-ASTN-ES/Mr. E. E. Engler)	1
(Attn: S&E-ASTN-M/Mr. R. Schwinghammer)	1
(Attn: S&E-ASTN-MRM/Dr. J. H. Stuckey)	1
NASA, Langley Research Center, Hampton, VA 23365	
(Attn: Mr. J. P. Peterson, Mr. R. Fride, and Dr. M. Card) . .	3
NASA, Lewis Research Center, Cleveland, OH 44153	
(Attn: Technical Library, and M. Hershberg)	2
NAVPCSCRL, Monterey, CA 95940	
(Attn: Prof. R. Ball, Prof. H. H. Bank)	2
NAVSEASYSOM, Washington, D.C. 20352	
(Attn: Code 035, Mr. C. Pohler)	1
NAVSEC, Hyattsville, MD 20782	
(Attn: Code 6101E03, Mr. W. Graner)	1
NAVSHIPRANDCEN, Bethesda, MD 20034	
(Attn: Code 173.2, Mr. W. P. Cauch)	1
NAVSHIPRANDCEN, Annapolis, MD 21402	
(Attn: Code 2870, Mr. H. Edelstein)	1
NEL, White Oak, MD 20910	
(Attn: Mr. F. R. Barnett)	1
NEL, Washington, D.C. 20375	
(Attn: Dr. I. Wolock)	1
ONR, Washington, D.C. 20362	
(Attn: Dr. H. Ferrona)	1

Government Activities (Cont.)

PLASTEC, Picatinny Arsenal, Dover, NJ 07801
 (Attn: Librarian, Bldg. 176, SARPA-FR-M-D and Mr. H. Febly). . . 2
 Scientific & Technical Information Facility, College Park, MD
 (Attn: NASA Representative). 1
 USAAVMATLAB, Fort Eustis, VA 23603
 (Attn: Mr. R. Beresford) 1
 USAMATRESAG, Watertown, MA
 (Attn: Dr. E. Lence) 1
 USABRSOFC, Durham, NC 27701 1

Non-Government Agencies

Avco Aero Structures Division, Nashville, TN 37202
 (Attn: Mr. W. Ottenville). 1
 Battelle Columbus Laboratories, Metals and Ceramics Information
 Center, 505 King Avenue, OH 43201. 1
 Bell Aerospace Company, Buffalo, NY 14240
 (Attn: Zona I-85, Mr. F. M. Anthony) 1
 Bell Helicopter Company, Fort Worth, TX 76100
 (Attn: Mr. Charles Harvey) 1
 Bendix Products Aerospace Division, South Bend, IN 46619
 (Attn: Mr. R. V. Cervelli) 1
 Boeing Aerospace Company, P.O. Box 3999, Seattle, WA 98124
 (Attn: Code 206, Mr. R. E. Horton) 1
 Boeing Company, Renton, Washington 98055
 (Attn: Dr. R. June) 1
 Boeing Company, Vertol Division, Phila., PA 19142
 (Attn: Mr. R. L. Pinckney, Mr. D. Hoffstedt) 2
 Boeing Company, Wichita, KS 67210
 (Attn: Mr. V. Raneau/MS 18-39) 1
 Cabot Corporation, Billerica Research Center, Billerica, MA
 01821 1
 Drexel University, Phila., PA 19106
 (Attn: Dr. F. C. Chou) 1
 E.I. DuPont Company, Wilmington, DE 19898
 (Attn: Dr. Carl Zweben) Bldg. 262/Room 316 1
 Fairchild Industries, Hagerstown, MD 21740
 (Attn: Mr. D. Buck). 1
 Georgia Institute of Technology, Atlanta, GA
 (Attn: Prof. W. H. Horton) 1
 General Dynamics/Convair, San Diego, CA 92138
 (Attn: Mr. D. R. Dunbar, W. G. Scheck) 2
 General Dynamics, Fort Worth, TX 76101
 (Attn: Mr. P. D. Shockey, Dept. 23, Mail Zone F-46). 1
 General Electric Company, Phila., PA 19101
 (Attn: Mr. L. McCreight) 1
 Great Lakes Carbon Corp., N.Y., NY 10017
 (Attn: Mr. W. R. Benn, Mgr., Markey Development) 1
 Grumman Aerospace Corporation, Bethpage, L.I., NY 11714
 (Attn: Mr. R. Radcock, Mr. S. Dastin). 2

Non-Government Agencies (Cont.)

Hercules Powder Company, Inc., Cumberland, MD 21501
 (Attn: Mr. D. Eug) 1
 H. I. Thompson Fiber Glass Company, Gardena, CA 90249
 (Attn: Mr. N. Myers) 1
 ITT Research Institute, Chicago, IL 60616
 (Attn: Mr. K. Hofar) 1
 J. P. Stevens & Co., Inc., N.Y., NY 10036
 (Attn: Mr. H. I. Shulock) 1
 Kaman Aircraft Corporation, Bloomfield, CT 06002
 (Attn: Tech. Library) 1
 Lehigh University, Bethlehem, PA 18015
 (Attn: Dr. G. C. Sih) 1
 Lockheed-California Company, Burbank, CA 91520
 (Attn: Mr. E. K. Walker, R. L. Vaughn) 2
 Lockheed-Georgia Company, Marietta, GA
 (Attn: Advanced Composites Information Center, Dept. 72-14,
 Zone 42) 1
 LTV Aerospace Corporation, Dallas, TX 75222
 (Attn: Mr. O. E. Dhonau/2-53442, C. R. Foreman) 2
 Martin Company, Baltimore, MD 21203
 (Attn: Mr. J. E. Pawken) 1
 Materials Sciences Corp., Blue Bell, PA 19422 1
 McDonnell Douglas Corporation, St. Louis, MO 63166
 (Attn: Mr. R. C. Goran, O. B. McBee, C. Stenberg) 3
 McDonnell Douglas Corporation, Long Beach, CA 90801
 (Attn: H. C. Schjulderup, G. Lehman) 2
 Minnesota Mining and Manufacturing Company, St. Paul, MN 55104
 (Attn: Mr. W. Davis) 1
 Northrop Aircraft Corp., Norair Div., Hawthorne, CA 90250
 (Attn: Mr. R. D. Hayes, J. V. Noyes, R. C. Isemann) 3
 Rockwell International, Columbus, OH 43216
 (Attn: Mr. O. G. Acker, K. Clayton) 2
 Rockwell International, Los Angeles, CA 90053
 (Attn: Dr. L. Lackman) 1
 Rockwell International, Tulsa, OK 74151
 (Attn: Mr. E. Sanders, Mr. J. H. Powell) 2
 Owens Corning Fiberglass, Granville, OH 43023
 (Attn: Mr. D. Mettes) 1
 Rohr Corporation, Riverside, CA 92503
 (Attn: Dr. F. Riel and Mr. R. Elkin) 2
 Ryan Aeronautical Company, San Diego, CA 92112
 (Attn: Mr. R. Long) 1
 Sikorsky Aircraft, Stratford, CT 06497
 (Attn: Mr. J. Ray) 1
 University of Oklahoma, Norman, OK 93069
 (Attn: Dr. G. M. Nordby) 1
 Union Carbide Corporation, Cleveland, OH 44101
 (Attn: Dr. H. F. Volk) 1